Assessment of Antarctic sea ice by surface validated satellite measurements

---

A thesis submitted in partial fulfilment of the requirements for the Degree

of

Doctor of Philosophy

by

Daniel Price

Gateway Antarctica

University of Canterbury

2014

Table of contents

List of Figures

List of Tables		
#		Page

Abstract

Satellite investigations have documented Antarctic sea ice area, but are restricted in their ability to provide volume, as the procedure to derive thickness is still under development. This procedure requires the measurement of sea ice freeboard, the segment of ice held above the ocean surface by buoyancy. This measurement can be made by satellite altimeters and in conjunction with density and snow depth information; sea ice thickness can be estimated via the hydrostatic equilibrium assumption. The ability to monitor the spatial and temporal characteristics of the thickness distribution must be improved as we strive to understand the linkages between the glaciological, atmospheric and oceanic components of the Antarctic climate system. A key sector in which these components interact is the Antarctic coast. There, offshore winds drive coastal polynyas creating vast amounts of sea ice, and ice shelf interaction modifies ocean properties. Together they condition the ocean for downwelling, driving the global oceanic circulation. In light of this, the coastal Antarctic is a fundamental region in regard to Antarctic sea ice processes and the Earth climate system. McMurdo Sound occupies a coastal area in proximity to an ice shelf in the south-western corner of the Ross Sea. The sound has witnessed scientific investigation for over a century with a fully established research programme since the 1960s. However, the sea ice research in this region is spatially restricted. This thesis aims to expand the knowledge of sea ice in McMurdo Sound to a larger area using space-borne remote sensing instrumentation and design of in situ measurement campaigns. In doing so, this work evaluates the capabilities of satellite platforms to record sea ice freeboard in the coastal Antarctic, whilst developing knowledge of ice shelf-sea ice interaction. This work provides the first satellite altimeter based investigation of sea ice freeboard in McMurdo Sound using ICESat over the period 2003-2009. No observable trend was observed for first-year sea ice freeboard in the region in line with larger scale assessments in the Ross Sea. However, there was significant increase in the freeboard of a temporary multiyear sea ice regime, the segment of the largest increase linked to the outflow of supercooled Ice Shelf Water (ISW) from the McMurdo and Ross Ice Shelf cavities. This remote sensing assessment supports the in situ and modelling work of many others who have identified the influence of ISW on sea ice processes in this region, in particular, that it is thicker than it would otherwise be. The influence of ISW on altimetric sea ice thickness retrievals was also quantified using a Global Navigation Satellite System (GNSS) evaluation of freeboard to thickness conversion. This revealed that a sub-ice platelet layer, created by supercooled ISW and with an estimated solid fraction of 0.16, accumulates beneath the sea ice cover and influences the thickness estimates from the GNSS-derived surface elevation. A cautionary conclusion is reached that within 100 km of ice shelves this buoyant influence should be considered, and in close proximity (< 50 km) can result in overestimations of sea ice thickness of ~ 12 %. It is also suggested that the sea ice freeboard anomalies that result from enhanced growth, driven by supercooled water advection could be used to map the presence of ISW in the coastal Antarctic. Looking to future ability to monitor Southern Ocean sea ice thickness from space, the first comprehensive evaluation of CryoSat-2 (CS-2) over Antarctic sea ice is provided. Using three separate retracking procedures, CS-2 is shown to be capable of detecting the development of a fast ice cover in McMurdo Sound. The role played by a snow cover with layering typical of the Antarctic appears to cause a positive bias in the ice freeboard for a waveform fitting procedure currently used over Arctic sea ice. The identification of open water and the establishment of accurate sea surface heights are also indicated as causing errors (in the order of cms) in the study region. CS-2 is shown to be capable of recording sea ice growth over two growth cycles in McMurdo Sound. This work has advanced the application of satellite investigative techniques to Antarctic sea ice, providing hope that such techniques may be capable of revealing larger scale connections between sea ice and ice shelves.

Deputy Vice-Chancellor's Office
Postgraduate Office

UNIVERSITY OF CANTERBURY
Te Whare Wānanga o Waitaha
CHRISTCHURCH NEW ZEALAND

Co-authorship Form

This form is to accompany the submission of any PhD thesis that contains research reported in co-authored work that has been published, accepted for publication, or submitted for publication. A copy of this form should be included for each co-authored work that is included in the PhD thesis. Completed forms should be included at the front (after the thesis abstract) of each copy of the thesis submitted for examination and library deposit (including electronic copy).

Please indicate the chapter/section/pages of this thesis that are extracted from co-authored work and provide details of the publication or submission from which the extract comes: *Chapter 3 is derived from* **Price, D., W. Rack, C. Haas, P. J. Langhorne, and O. Marsh (2013), Sea ice freeboard in McMurdo Sound, Antarctica, derived by surface-validated ICESat laser altimeter data, *J. Geophys. Res. Oceans*, 118, doi:10.1002/jgrc.20266.**

Please detail the nature and extent (%) of contribution by the PhD candidate:
The candidate has performed all ICESat data analysis, developed the methods and written the text. W. Rack, C. Hass and P.J. Langhorne provided supervisory guidance and proof read *while O. Marsh provided processing assistance.*
Candidate contribution: 85 %

Certification by co-authors:

If there is more than one co-author then a single co-author can sign on behalf of all. The undersigned certifies that:

The above statement correctly reflects the nature and extent of the PhD candidate's contribution to this co-authored work

In cases where the PhD candidate was the lead author of the co-authored work he or she wrote the text.

Name: *Wolfgang Rack* Signature:

Deputy Vice-Chancellor's Office
Postgraduate Office

UNIVERSITY OF CANTERBURY
Te Whare Wānanga o Waitaha
CHRISTCHURCH NEW ZEALAND

Co-authorship Form

This form is to accompany the submission of any PhD thesis that contains research reported in co-authored work that has been published, accepted for publication, or submitted for publication. A copy of this form should be included for each co-authored work that is included in the PhD thesis. Completed forms should be included at the front (after the thesis abstract) of each copy of the thesis submitted for examination and library deposit (including electronic copy).

Please indicate the chapter/section/pages of this thesis that are extracted from co-authored work and provide details of the publication or submission from which the extract comes:
Chapter 4 is derived from **Price, D., W. Rack., P.J. Langhorne., C. Haas., G. Leonard and K. Barnsdale. 2014. The sub-ice platelet layer and its influence on freeboard to thickness conversion of Antarctic sea ice, *The Cryosphere*, 8, 1031-1039, doi:10.5194/tc-8-1031-2014.**

Please detail the nature and extent (%) of contribution by the PhD candidate:
The candidate has performed the analysis of processed GNSS and in situ data, developed the method, written the text and contributed to the fieldwork. W. Rack provided supervisory support and participated in discussions developing the method and scope of the work. All authors partook in the collection of in situ information and provided comments and suggestions to improve the paper.
Candidate contribution: 90 %

Certification by co-authors:

If there is more than one co-author then a single co-author can sign on behalf of all. The undersigned certifies that:

The above statement correctly reflects the nature and extent of the PhD candidate's contribution to this co-authored work

In cases where the PhD candidate was the lead author of the co-authored work he or she wrote the text.

Name: *Wolfgang Rack* Signature:

Deputy Vice-Chancellor's Office
Postgraduate Office

UNIVERSITY OF CANTERBURY
Te Whare Wānanga o Waitaha
CHRISTCHURCH NEW ZEALAND

Co-authorship Form

This form is to accompany the submission of any PhD thesis that contains research reported in co-authored work that has been published, accepted for publication, or submitted for publication. A copy of this form should be included for each co-authored work that is included in the PhD thesis. Completed forms should be included at the front (after the thesis abstract) of each copy of the thesis submitted for examination and library deposit (including electronic copy).

Please indicate the chapter/section/pages of this thesis that are extracted from co-authored work and provide details of the publication or submission from which the extract comes: *Chapter 5 is derived from* **Price, D., J. Beckers., R. Ricker., N. Kurtz., W. Rack., V. Helm., C. Haas., S. Hendricks., P.J. Langhorne., and G. Leonard. 2014. Evaluation of CryoSat-2 derived sea ice freeboard over fast-ice in McMurdo Sound, Antarctica, *Journal of Glaciology*, under review.**

Please detail the nature and extent (%) of contribution by the PhD candidate:
The candidate has written the text and developed and processed the CryoSat-2 Level 2 freeboard method in collaboration with J. Beckers during a research stay at the University of Alberta. The candidate has conceived and overseen the international collaboration between UC, AWI and NASA who provided additional CryoSat-2 data. A major component of the in situ validation campaign for CryoSat-2 was designed and executed by the candidate. W. Rack participated in extensive discussions and all authors provided suggestions and comments to improve the paper.
Candidate contribution: 80 %

Certification by co-authors:

If there is more than one co-author then a single co-author can sign on behalf of all. The undersigned certifies that:

The above statement correctly reflects the nature and extent of the PhD candidate's contribution to this co-authored work

In cases where the PhD candidate was the lead author of the co-authored work he or she wrote the text.

Name: *Wolfgang Rack* Signature:

Acknowledgements

This work would not have been possible were if not for the efforts of many individuals and groups. I will attempt here to share my gratitude for such efforts and acknowledge the guidance and support I have been fortunate enough to receive. I would firstly and chiefly like to thank my senior supervisor, Wolfgang Rack, for his exceptional supervisory guidance and continual availability for discussion. My associate supervisors Patricia Langhorne and Christian Haas are profound sources of knowledge on the topic of sea ice and consistently provided support throughout the duration of this work. I acknowledge the proof reading and assistance of my co-supervisor Adrian McDonald and early conversations with Chris Gomez. The dedicated, relaxed and friendly working environment of Gateway Antarctica provided an ideal base from which to conduct my studies. I would like to thank Bryan Storey, Michelle Rogan-Finnemore and Katrina Hall for their efforts to maintain this environment, and the friendships and support given by the students, staff and visitors of the research centre are greatly appreciated. I would particularly like to thank Oliver Marsh for his input to our academic and technical discussions over the years and greatly acknowledge the value of his friendship. Thank you to Ursula Rack for her kindness and hospitability over the last four years. I am grateful for the receipt of a University of Canterbury Doctoral Scholarship, and would like to highlight the tireless effort that the University has made to endure through a difficult period in the wake of the February 2011 Christchurch Earthquake. I am also appreciative of research funding from Gateway Antarctica and NIWA. I am thankful for the efforts of Nick Key and Justin Harrison who provided assistance in the preparation of equipment for Antarctic fieldwork campaigns in 2011 and 2013. I recognize the boundless efforts of Scott Base and Antarctica New Zealand staff, without which this work would not be possible. I am grateful to have been part of two excellent fieldwork teams in 2011 and 2013. The hard work of Greg Leonard, Wolfgang Rack, Pat Langhorne, Christian Haas, Justin Beckers, Kelvin Barnsdale, Alex Gough and Ken Hughes made a direct contribution to the findings of this work. I would like to further my thanks to Justin Beckers for his generosity and support during a research stay at the University of Alberta, during which significant advancements were made toward the findings of this thesis. The publication of the results presented here was only achievable with the input of the co-authors, and I am grateful for discussions held, suggestions made, and comments placed. Thank you to all my friends, ‘The Retirement Village’, ‘The Ludus’ and everyone I have met through UC Snowsports with whom I have had unforgettable experiences. The incredible Southern Alps of New Zealand provided a haven for adventure and escape during this work. I again thank my friends, and fellow alpine wanderers for these experiences, in particularly I would like to thank Bethany Jane Ward for her invaluable friendship. I thank my parents for their unwavering support, interest, kindness and patience from the other side of the world. I acknowledge how fortunate I am to be able to pursue my interests, and embark on journeys to regions few are privileged enough to reach. I hope this work can contribute to the international scientific effort of countless individuals, who strive to further the understanding of our planet, and in doing so, provide the knowledge we require to progress into a stable future for all.

1 Introduction

1.1 Rationale

The advancement of satellite technology has permitted near-continuous monitoring of the Earth's land, ocean, cryosphere and atmosphere via many differing techniques. This ability has improved our knowledge of the Earth system and led to the development of a more holistic understanding of Earth's governing processes. This global monitoring ability has revolutionized the scientific approach to Earth Sciences and has revealed a complex, interconnected Earth system, which is now understood to be sensitive to relatively small changes. Never before has it been more important to advance our understanding of this system faced with the potential consequences of anthropogenic climatic change.

The cryosphere presents a prime example by which such insight would be impossible without satellite observation. Sea ice, an integral part of the cryosphere, dominates processes in the polar oceans and is an intrinsic part of the climate system. Its growth and melt regimes influence global oceanic circulation (Brandon et al., 2010; Siedler et al., 2013) and once present at the sea surface it acts as a barrier between the ocean and atmosphere altering physical, chemical and biological fluxes between the two media (Dieckmann and Hellmer, 2010). At its maximum annual extent, sea ice covers around 10 % of the Earth's ocean surface (Comiso, 2010) comparable to that of the continental land masses of Russia and Canada combined. Yet, it is only over the last forty years, with the availability of satellite information, that we have been able to routinely monitor the polar oceans and their coverage of sea ice.

In September, Antarctic sea ice extent reaches approximately 19 million km^2 but is reduced to only 4 million km^2 at its minima in February (Parkinson and Cavalieri, 2012; Dieckmann and Hellmer, 2010). This makes the annual advance and retreat of the Antarctic sea ice cover one of the most profound seasonal changes on the Earth's surface. Passive microwave investigations, which began in 1978, have revealed an increasing Antarctic sea ice extent of 1.5 (± 0.3) % per decade (Vaughan et al., 2013 and see Figure 1.1). It should be noted here that recent evidence suggests that this increase may not be significant, and

that inter-algorithm biases could be responsible for the statistical significance indicated over the latter segment of the satellite observational period (Eisenman et al., 2014). However, even in light of this evidence, a paradox is presented; why in a warming world, is the Antarctic sea ice cover stable or undergoing slight expansion? This question is at the forefront of geophysical investigation in the Antarctic and providing explanations is fundamental to developing our understanding of the Earth's climate system and our ability to forecast future changes. The situation in the Antarctic is in stark contrast to the accelerating decline recorded in the Arctic over the same time period (Cavalieri and Parkinson, 2012; Comiso et al., 2008; Stroeve et al., 2007; Comiso, 2002).

The comparison between the two polar sea ice covers is limited by their very different geographical settings and data availability (Maksym et al., 2012). Due to a longer time series and better spatial distribution of information, the understanding of the Arctic system is better developed. Sea ice demise in the Arctic is likely linked to larger scale climatic change and surface air temperature increases (Vinnikov et al., 1999). In the Antarctic, such linkages are not as apparent, except in the vicinity of the Antarctic Peninsula where significant surface air temperature increases have been recorded (Bromwich et al., 2013; Steig et al., 2009; Vaughan et al., 2003). Two dominant geographical characteristics make the Antarctic very different from the Arctic.

(i) The open oceanic setting of the Southern Ocean provides an unimpeded medium upon which atmospheric and oceanic forces can act. Wind, a significant player in resultant sea ice characteristics, is shown to dominate the Antarctic sea ice regime (Holland and Kwok, 2012). Further, the indications are that intensifying wind stress leads to increased volumes of sea ice in the Southern Ocean (Zhang, 2013), again contrary to what would be expected in a warming environment. In regard to what is forcing such changes, the situation is complicated by the disruption of the ozone layer which has been shown to be responsible for Southern Hemisphere tropospheric circulation changes, principally in the summer season (Polvani et al., 2010). Further linkages to changes in larger scale climate phenomena such as the Southern Annular Mode (SAM) and El-Nino Southern Oscillation (ENSO), are key areas of research (Comiso et al., 2011; Stammerjohn et al., 2008). Directly related to wind stress is significant wave height which has recently been linked to sea ice breakup and stability (Kohout et al., 2014). How these processes are changing, what is forcing them, and ultimately how they affect the Antarctic sea ice cover is yet to be fully understood.

(ii) The presence of the Antarctic Ice Sheet and in particular its ice shelves is the second distinction to be made between the two polar regions. The input of freshwater to the Southern Ocean from the Antarctic continent is regulated by basal melting and iceberg calving. Recently, it has become clearer that ice shelf basal melting is the dominant contributor to these freshwater fluxes (Depoorter et al., 2013; Rignot et al., 2013). The interaction of a warming ocean (Schmidtko and Johnson, 2011; Gille, 2008) with ice shelves, and particularly the penetration of warmer waters to their grounding lines is thought to be forcing a negative mass balance for the West Antarctic Ice Sheet (Rignot et al., 2014; Joughin et al., 2014; Shepherd et al., 2004). Such ocean-ward motion of glacial mass will contribute to eustatic sea level rise and alter the physical properties of the Southern Ocean. The common wisdom is that increased freshwater input will aid sea ice growth as it freshens the surface ocean, establishing a more stratified surface ocean more comparable to the Arctic basin (Thomas, 2004). This hypothesis is supported by certain modelling studies (Bintanja et al., 2013) but refuted by others (Swart and Fyfe, 2013). The complexity of these atmospheric, oceanic and glaciological interactions and the inability to draw generalised conclusions is perhaps supported by the regional diversity of trends in sea ice extent around the Antarctic (Figure 1.1). This regional diversity is highlighted by the Ross Sea sector which displays a major advance of the sea ice cover, while the neighbouring Bellingshausen and Amundsen seas sector has undergone continued decline.

The Intergovernmental Panel on Climate Change's Fifth Assessment Report (Vaughan et al., 2013) only draws strong conclusions on the observed trends in sea ice extent. However, model runs do not simulate this overall increase in sea ice coverage (Turner et al., 2014), which is an indication that a lack of knowledge surrounds the link between these observations and the larger climate system. More information is needed to reconcile the drivers of observed change. In order to advance our insight, one of the research areas requiring development is the investigation of sea ice thickness. With adequate monitoring of sea ice thickness, and its combination with already monitored areal data, sea ice volume can be deduced. Sea ice volume provides a more robust quantification of the state of a sea ice cover, particularly with regard to oceanic, atmospheric or more collectively, climatic conditions. Sea ice thickness investigations are hampered by a scarcity of measurements, both temporally and spatially and the inability of current techniques to provide estimates within acceptable error margins.

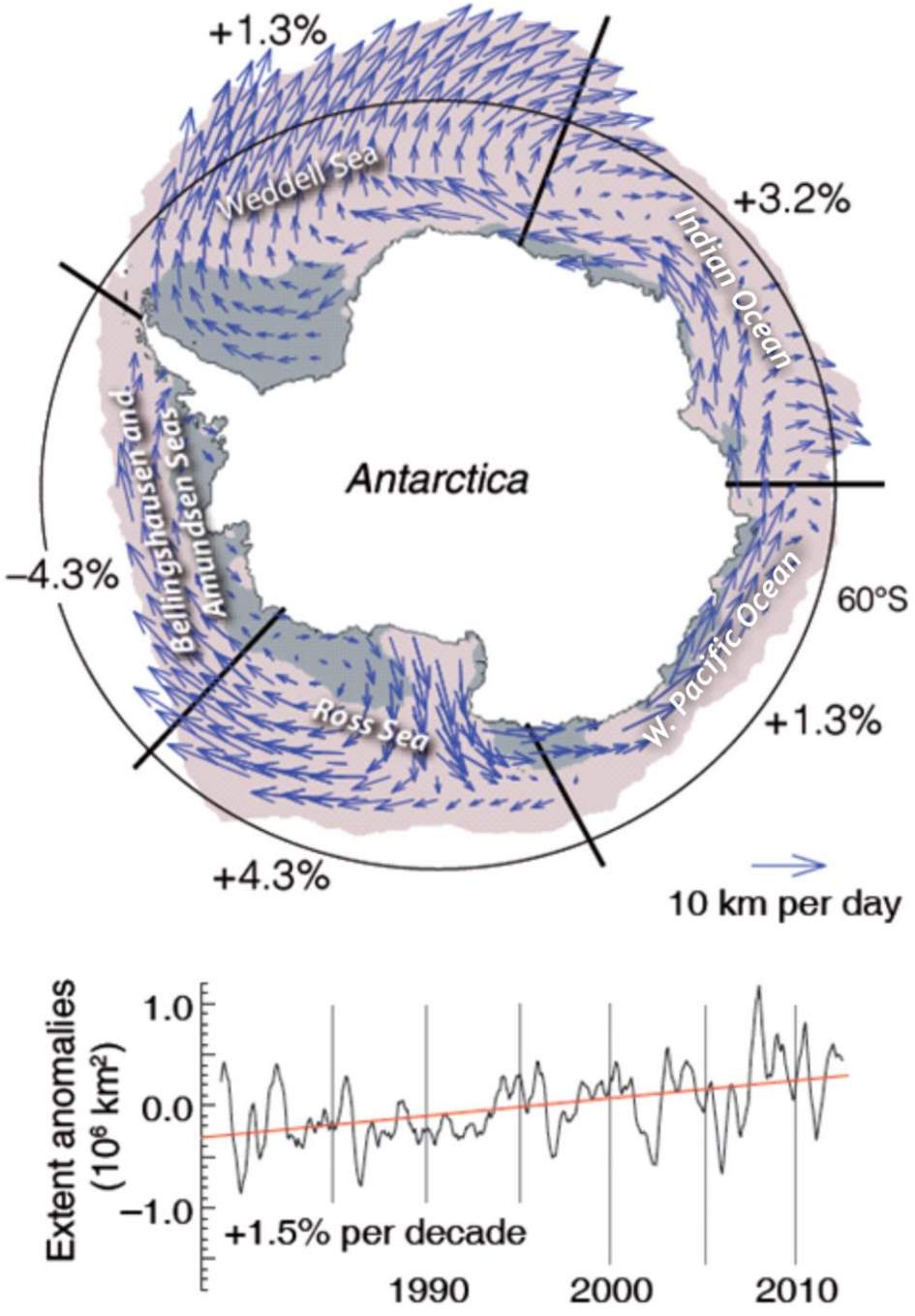

Figure 1.1. Decadal trends of Antarctic sea ice extent in annual anomalies (%) for each sector; Weddell Sea, Bellingshausen and Amundsen seas, Ross Sea, Western Pacific Ocean and Indian Ocean after Vaughan et al. (2013). The mean drift patterns and their magnitude of Antarctic sea ice (arrows) are shown, along with the mean maximum (pink shading) and minimum extents (dark purple shading) as deduced by satellite observations for the period 1979-2012. The graph shows the linear regression of extent anomalies and the observed positive trend for the entire Antarctic sea ice extent.

1.2 Aims and objectives

The aim of this research is to advance the knowledge of Antarctic sea ice processes in close proximity to ice shelves, whilst developing techniques for the remote assessment of Antarctic sea ice thickness. These aims are dictated by the access to a suitable satellite validation site which is in close proximity to an ice shelf. This site, McMurdo Sound, is located in the southwestern Ross Sea. With the use of extensive in situ validation campaigns, along with the strong sea ice research history in this region, this work will contribute to the following objectives:

1. design and conduct extensive in situ measurements of sea ice properties in McMurdo Sound to contribute to the existing temporal series and provide a basis for satellite validation;
2. provide the first satellite derived assessment of freeboard and thickness in McMurdo Sound;
3. validate satellite altimeter methods for sea ice freeboard retrieval to better constrain errors in resultant thickness estimates;
4. quantify errors in the estimation of sea ice thickness using altimetry techniques in close proximity to an ice shelf;
5. investigate the role played by an ice shelf on sea ice thickness distributions using remote sensing platforms.

The completion of these objectives will aid the development of satellite freeboard retrieval algorithms in the Antarctic. Expected errors in such methods driven by the influence of ice shelves will be further explored, while geophysical conclusions on sea ice conditions in close proximity to ice shelves will be drawn.

The annual growth of a fast ice area in McMurdo Sound offers a relatively stable and safe environment in which to undertake in situ investigations. The available, but spatially confined in situ information measured over the last fifty years is one of the cardinal data sets of its kind. This presents an opportunity to place the findings of this work in temporal context and expand measurement capabilities to a larger regional area using remote sensing techniques.

1.3 Antarctic sea ice thickness

Sea ice thickness is perhaps one of the simplest geophysical parameters to measure at the small scale (meters to kilometers). Given access, and with suitable drilling equipment and a modified tape measure, a sea ice thickness measurement can be carried out in a matter of minutes. However, information at such small scales is of limited use when the area of the Antarctic sea ice cover is considered.

The large scale knowledge of sea ice thickness permits:

1. in combination with areal information, quantification of sea ice volume, the key variable that determines sea ice mass and the energy tied up in formation and decay;
2. quantification of seasonal and interannual volume flux of fresh and saltwater to the ocean, further ascertaining its role in the global climate system;
3. a method of evaluating atmospheric and oceanic processes as ice structure and thickness are related to dynamic forcing by wind and currents;
4. further information to be gained on the contribution of sea ice to planetary albedo as thicker ice has a higher albedo;
5. a direct way of assessing climate change in the polar oceans as a volumetric assessment is a more robust measure of detecting whether a sea ice cover is shrinking or growing in its entirety.

Studies on the Antarctic sea ice thickness are temporally and spatially restricted. Only one investigation using direct observations exists for the entire Antarctic. Worby et al. (2008) compiled 23,373 ship based and aircraft observations from two decades of research and find mean sea ice thicknesses of 0.87 m and 0.62 m for ridged and level sea ice respectively. This publication aimed to address some of the goals of the Antarctic Sea Ice Processes and Climate (ASPeCt) program established by the Scientific Committee on Antarctic Research (SCAR) in 1996. In essence this program aimed to broaden our understanding of Antarctic sea ice processes. Although this investigation provides a unique insight to the Antarctic sea ice thickness distribution, it lacks both the spatial resolution required to assess it in detail and the temporal resolution to develop trends. Recent

modelling investigations have suggested a small increase in Antarctic sea ice thickness of 1.55 mmy^{-1} for the period 1992-2010 (Holland et al., 2014) and are also indicative of large regional variability in thickness trends (Massonnet et al., 2013).

Due to the vast area of the Antarctic sea ice cover and the timescales over which such investigations are required, satellite missions provide the only feasible mechanism for large scale assessment of sea ice thickness. The success of passive microwave radiometry and imaging technologies on-board satellites to monitor sea ice concentration, area and extent support such feasibility (Parkinson and Cavalieri, 2012; Comiso et al., 2011; Comiso et al., 2003; Zwally et al., 2002a; Zwally et al., 1983). It became clear that in addition to the above a spaceborne technology to assess both the seasonal and interannual temporal evolution of sea ice thickness was required. The spatial coverage permitted by these platforms also provides an opportunity to fill the gaps between very sparse in situ information. However, due to the inability of current technologies to detect both the top and bottom of the sea ice cover from orbital ranges, no remote sensing system is capable of detecting sea ice thickness directly from space. This situation will persist for the foreseeable future. To circumvent this issue, over the last fifteen years, international efforts have been made to advance the science of satellite altimetry - an indirect method to monitor sea ice thickness. Satellite altimetry provides a range estimate from the satellite to the surface and if precise enough, can discern the elevation difference between the local sea surface height and the height of the surface of a nearby ice floe (Figure 1.2). This measured quantity is termed freeboard. Freeboard, typically only of the order of 0.01-0.25 m requires highly advanced instrumentation to measure and robust error quantification to attain acceptable levels of uncertainty. Freeboard is a relative measure and therefore provides improved accuracy, as the errors associated with spacecraft orbit, atmospheric geophysical considerations, geoid and sea surface height are minimized. It is therefore, the precision of the technique (consistency of measurements along-track) that is key to obtain useful sea ice freeboard data. Two altimetry techniques exist, the first technique, laser altimetry identifies the snow freeboard or ice freeboard in the absence of snow. Using the second, radar altimetry, the identified surface is more ambiguous due to the surfaces influence on the incident radar energy. The measured freeboard can be the snow or ice freeboard, or a layer in the snowpack between the two interfaces.

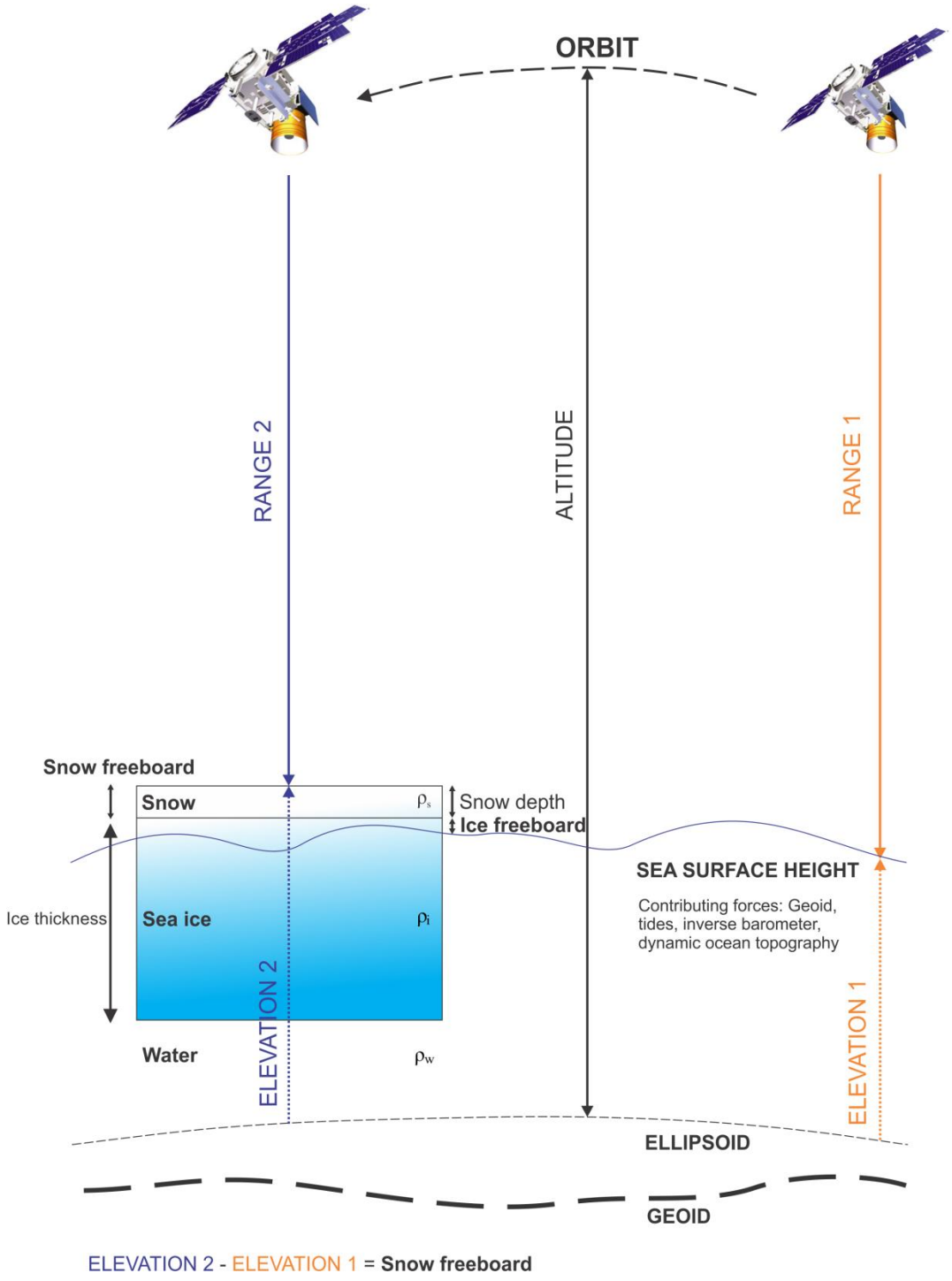

Figure 1.2. Simplified schematic exhibiting the principles of satellite laser altimetry for sea ice freeboard retrieval. With a freeboard measurement and snow depth information sea ice thickness can be estimated using the hydrostatic equilibrium assumption with the addition of the densities of snow (ρ_s), ice (ρ_i) and water (ρ_w). Using radar altimetry the situation is complicated by inadequate knowledge of the surface that is referenced be it the ice freeboard, snow freeboard or somewhere in between the two interfaces.

Upon measurement of freeboard, sea ice thickness can be estimated under the hydrostatic equilibrium assumption. With this assumption, freely floating ice is expected to be in balance when it is at rest, that is, that the buoyant force equals the weight of the sea ice. To infer sea ice thickness (T) freeboard must be used in conjunction with snow (ρ_s), ice (ρ_i) and water (ρ_w) density and snow depth (T_s). Upon the collation of such information this can easily be achieved with:

$$T = \frac{\rho_w}{\rho_w - \rho_i} Fb - \frac{\rho_w - \rho_s}{\rho_w - \rho_i} T_s \tag{1.1}$$

assuming the snow freeboard is measured, and with:

$$T = \frac{\rho_w}{\rho_w - \rho_i} Fb + \frac{\rho_s}{\rho_w - \rho_i} T_s \tag{1.2}$$

assuming the ice freeboard is measured.

Approximately a nine fold multiplication of the freeboard value is required to derive sea ice thickness. Given this mathematical situation, as expressed by equations 1.1 and 1.2 it is clear that any errors in the input factors will result in magnified errors in the resultant thickness estimation. This situation requires excellent information about the input factors to be available to accurately derive sea ice thickness. Currently due to the lack of knowledge about the varying input factors, estimated values must be included which all have associated uncertainties. The freeboard measurement is the most influential variable, especially when the freeboard is small, with snow depth information and sea ice density estimates also being large sources of error (Forsstrom et al., 2011; Alexandrov et al., 2010). Snow loading on the sea ice presents a particular problem on young, thin, sea ice. Firstly it suppresses the ice freeboard to zero, or negative values, and secondly it can force flooding from surrounding seawater, driven by ice freeboard suppression. These processes make it difficult or near-impossible to obtain the ice freeboard from any altimetry technique, and restrict the ability of passive microwave techniques to measure snow depth (Zwally et al., 2008; Markus and Cavalieri, 1998). Given suitable conditions a remote sensing platform that can measure both the ice freeboard and snow freeboard concurrently is highly desirable. Further, concern is expressed over the accuracy of using the hydrostatic

equilibrium assumption over varying spatial scales and in areas of dynamically deformed ice (Hutchings et al., 2014; Forsstrom et al., 2011). The uncertainties in this relationship are further explored in relation to complications introduced by the presence of an accumulating ice layer beneath the sea ice cover, driven by the sea ice's proximity to an ice shelf (Chapter 4).

Originally utilised for physical oceanography and ocean forecasting, advancements using satellite altimetry for sea ice research began in the Arctic with the development of the ability to discriminate between sea ice and open water radar returns using ERS (Peacock and Laxon, 2004; Laxon et al., 2003). The launch of the Ice Cloud and land Elevation Satellite (ICESat) in 2003 further advanced the topic with its much increased precision utilising laser ranging. This led to the rapid development of algorithms and landmark publications upon the state of Arctic sea ice volume (Kwok et al., 2009; Farrell et al., 2009; Kwok et al., 2007; Kwok et al., 2004). In conjunction with thickness measurements obtained using upward looking sonar, available via declassified military submarine records (Rothrock et al., 1999), the thinning and subsequent reduction of the Arctic sea volume has been established through these satellite observations (Kwok and Rothrock, 2009).

In light of the success of investigations in the Arctic which have dominated the research focus (Kern et al., 2014), attempts to assess the state of the Antarctic sea ice thickness distribution have been made. The assessment of Antarctic sea ice freeboard from satellite altimetry is complicated by the more dynamic nature of the Antarctic sea ice pack, a thicker snow cover, more complex snow morphology and scarcity of in situ validation. Regional assessments of sea ice thickness using ICESat (Yi et al., 2011; Xie et al., 2011; Zwally et al., 2008) highlight problems with regard to inaccurate snow depth information. Snow depth is needed as an auxiliary data set when using laser altimetry to attribute the amount of snow represented in the measured freeboard. Inaccurate portrayal of this snow/ice ratio will lead to significant errors in the resultant sea ice thickness estimation. Snow depth information at the large scale is currently only available using passive microwave data (Markus and Cavalieri, 1998), and given the varying spatial resolution of these sensors and altimetry, it is difficult to combine such data sets to produce reliable thickness estimates (Kurtz et al., 2009).

Snow loading on sea ice likely results in widespread suppression of the ice freeboard below sea level, resulting in negative freeboards (Massom et al., 2001). It is suggested that though snow loading certainly suppresses the freeboard, the formation of snow-ice after flooding re-establishes hydrostatic equilibrium, and a near zero ice freeboard situation is maintained (Sturm et al., 1998). The first ICESat, Antarctic-wide assessment incorporated an assumption of zero ice freeboard and found no significant trends in Antarctic sea ice thickness for the period 2003-2008 (Kurtz and Markus, 2012). Radar altimetry investigations are also restricted by limited snow depth information and are further hampered by the inability to constrain the dominant backscattering surface over sea ice (Kwok, 2014; Willatt et al., 2011; Hendricks et al., 2010). This results in even greater uncertainties in the estimated freeboards. One investigation has provided an insight, reporting reasonable agreement between freeboard measurements from ERS-2 and available in situ validation and expected seasonal changes in freeboard (Giles et al., 2008b). It is worth pointing out that radar methods have an advantage over laser techniques as they are not affected by cloud coverage which can be a significant restriction in the Antarctic. In situ validation of sea ice properties related to the conversion of freeboard to thickness, including, the freeboard itself, snow depth, sea ice density and snow density are crucial to attribution of errors and the development of algorithms.

1.4 Sea ice in the Southern Ocean

Within the Southern Ocean, sea ice experiences significant annual variation in its extent and therefore, nearly all sea ice present is firstyear (FY) sea ice as opposed to multiyear (MY) sea ice. Ice growth is impossible without low air temperatures to initiate the substantial heat flux from the ocean to the atmosphere. Fresh water freezes at 0°C, but the freezing point of seawater varies as it is saline. The upper surface layer of Antarctic seawater cools to a temperature of about -1.86°C, at which temperature *frazil* ice formation occurs (Thomas, 2004). Due to turbulent growth conditions, Antarctic sea ice has a relatively high amount of *frazil* ice incorporated into the structure (Lubin and Massom, 2006; Thomas, 2004). The characteristics of the resultant ice cover are determined by the surface conditions of the ocean. In calm seas, *frazil* consolidation at the surface eventually produces a level ice cover. This cover will develop through stages of increasing thickness from *grease* ice to *nilas*. However, in Antarctic waters, it is seldom the case that surface atmospheric conditions are stagnant and sea conditions are calm (Dieckmann and Hellmer, 2010). Therefore, wind plays a crucial role in sea ice formation. At the smallest scale, and in early development, *frazil* ice will coalesce to form *pancake* ice, which is decimeter to meter sized plates of ice, subject to extensive collisions in excited sea states (Thomas, 2004). Upon formation of this initial ice cover, *congelation* ice grows at the ice-ocean interface at a rate that is dependent on the heat flux from the ocean, via the ice into the atmosphere. Of particular interest is the fact that thermal energy exchange is highly dependent upon the sea ice thickness, implying that a description of thickness distributions is of great importance to accurately portray energy exchange at the Earth's surface in the marine polar environment. Further, sea ice cover affects the properties of the surface mixed layer (Duffy et al., 1999; Martinson, 1990; Lake and Lewis, 1970) and rates of gaseous exchange are altered (Rutgers van der Loeff et al., 2014; Parmentier et al., 2013; Stephens and Keeling, 2000).

As sea ice can be considered as mobile on the ocean surface, it is subject to displacement by any force that exerts drag upon its surfaces. The primary source of this drag is wind stress. Other forces play a role including ocean currents, Coriolis force, internal ice stress and sea surface tilt, and all accumulate to give an ice pack, or ice floe momentum in a particular direction. This results in convergence and compressive shear causing rafting and the production of thicker ridges of sea ice, or divergence and shear which may cause the

opening of leads, partitions in the ice where the sea surface is exposed to the atmosphere (Thomas, 2004; Haas, 2010). This dynamic growth of sea ice is primarily responsible for the heterogeneity of sea ice thickness across a given area (Haas, 2010).

Perhaps the most important property of sea ice is that its density is less than that of the water from which it formed (Dieckmann and Hellmer, 2010). Therefore, it floats at the ocean surface acting as a barrier, shielding the ocean from direct solar radiation. Albedo describes the reflectivity of a surface, typically the ratio of short wave radiation reflected from the surface in question to the radiation incident upon it. It is a dimensionless unit which may be expressed as a percentage (Figure 1.3). The variation in surface conditions and optical properties of the sea ice can greatly alter the ratios of reflection, absorption and transmission of incident solar energy (Perovich et al., 1998). The different albedo of a sea ice cover and open ocean result in alterations in the amount of solar radiation absorbed at the surface if the coverage of either of these surface types changes. In a warming scenario this mechanism will drive a decrease in the areal coverage of ice and snow and a corresponding increase in the air and ocean surface temperature, in turn further decreasing the areal coverage of ice and snow (Curry et al., 1994). This process, termed the 'ice albedo feedback mechanism' is indicated as being a positive feedback mechanism. It has likely accelerated change in the Arctic, with the loss of ice and its resultant replacement by water during the summer, increasing the global radiative forcing (Hudson, 2011). Its influence on the large scale Antarctic sea ice system is likely to be less significant given the already existent natural seasonality of the Antarctic sea ice pack (i.e. almost the entirety of the Southern Ocean is exposed to solar radiation in the annual cycle).

The relationship between sea ice and oceanic circulation is potentially of greater influence in the Antarctic. The Global Thermohaline Circulation (or Great Ocean Conveyor Belt) is a fundamental part of the global climate system as it redistributes heat around the Earth at the surface and at depth in the ocean (Siedler et al., 2013; Ganachaud and Wunsch, 2000). At higher latitudes the thermohaline circulation is driven by the cooling of surface waters as they move poleward (Rahmstorf, 2006). The colder surface waters sink as they become denser than that of the underlying water. Salt rejection during the sea ice growth phase and freshwater input during the melt phase also alter surface buoyancy. This in turn influences the rates of downwelling at deep water formation sites. The main bottom water formation sites in the Antarctic are located in the Weddell and Ross seas and along the Adelie Land

Coast (Williams et al., 2010; Whitworth and Orsi, 2006; Gordon et al., 1993; Rintoul, 1985; Foster and Carmack, 1976; Jacobs et al., 1970) with recent identification of an additional contributing site near the Amery Ice Shelf (Ohshima et al., 2013). These sites are responsible for the formation of dense shelf water which collectively forms Antarctic Bottom Water (AABW). AABW dominates the contribution to global bottom water formation and is estimated to account for approximately 30-40 % of the global ocean mass (Johnson, 2008).

Out of the open sea areas of the Antarctic, the coastal regions harbour extensive areas of fast ice (Fraser et al., 2012). Fast ice is sea ice that is fastened to a more permanent feature of the surrounding seascape, typically ice shelves, icebergs or land. Sea ice fastened to land is termed landfast ice and is an important feature of the Southern Ocean sea ice regime. With its inherent need for a fastening surface, fast ice is typically limited to a coastal band around the Antarctic continent of varying width, often dependent on bathymetry. No Antarctic wide assessment of fast ice coverage and trends exists though the East Antarctic region has been investigated (Fraser et al., 2012; Giles et al., 2008a; Fedotov et al., 1998). The role of fast ice in the Southern Ocean is yet to be fully understood, however its location near coastal regions indicates it may act to limit the formation of coastal polynyas and also plays a role in the stabilization of glacier tongues and ice shelves (Massom et al., 2010).

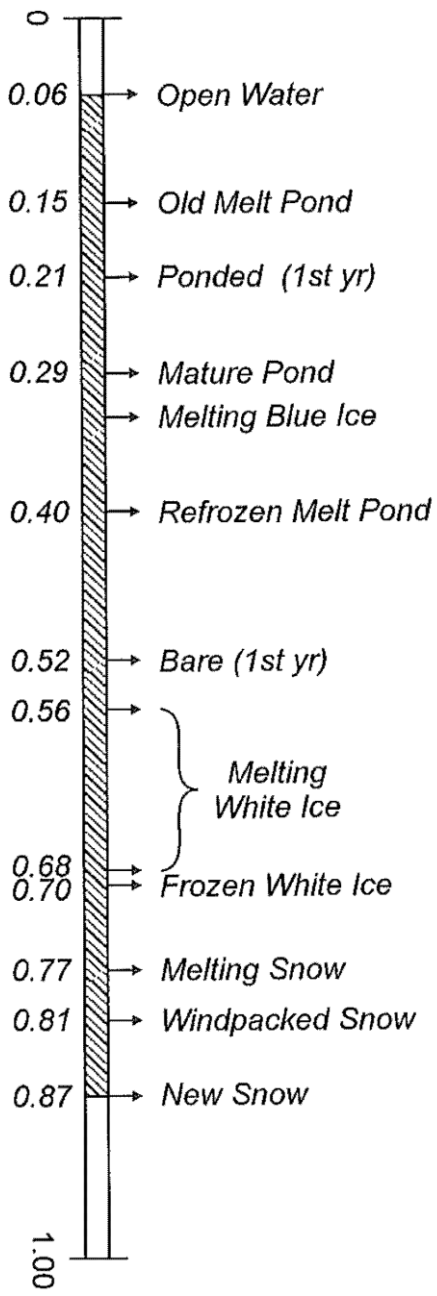

Figure 1.3. Albedo range over varying sea ice surface conditions (Eicken, 2010). An established sea ice cover with snow loading is capable of reflecting > 80% of incident solar radiation as opposed to < 6 % for open water.

1.5 Sea ice in the vicinity of ice shelves

Apart from the opposite land-ocean distribution, perhaps the most striking difference between the two polar regions is the abundance of ice shelves that fringe the Antarctic coastline. The presence of ice shelves cause drastic changes to the oceanographic environment in which they develop an example being abrupt alteration of the thickness of the water column. Approximately 40 % of the Antarctic coastline exists as ice shelves (Bindschadler et al., 2011), their distribution shown in Figure 1.4. Ice shelf-ocean interaction influences coastal fast ice thickness distributions (Gough et al., 2012; Mahoney et al., 2011; Leonard et al., 2011; Dempsey et al., 2010) and is postulated to influence larger scale oceanic properties driving change to the Antarctic sea ice system (Robinson et al., 2014; Bintanja et al., 2013; Hellmer, 2004). It is suggested that the presence of these ice shelves contributes to the observed increase in sea ice extent. The interaction of the ice shelf bases and high salinity shelf water (HSSW) results in the outflow of relatively cool meltwater to the Southern Ocean (Robinson et al., 2010) which accumulates in a surface layer restricting the interaction of relatively warmer deeper water and sea ice (Bintanja et al., 2013; Hellmer, 2004). This process may therefore influence the future trends in Antarctic sea ice extent and thickness, as meltwater volume from Antarctic glaciers and ice shelves is expected to increase under a warming climate (Joughin et al., 2012; Wang and Wang, 2012). A more localised effect associated with the presence of ice shelves is the occurrence of platelet ice (Figure 1.5). Platelet ice formation results from the availability of supercooled water from beneath ice shelf cavities (Gow et al., 1998; Jeffries et al., 1993). Platelet ice attaches itself to the bottom of the existing sea ice cover, where it may be incorporated into the solid structure of the ice cover or accumulate below as a sub-ice platelet layer. Platelet and sub-ice platelet layer formation is therefore linked to ice shelf proximity (Gough et al., 2012; Mahoney et al., 2011; Dempsey et al., 2010; Leonard et al., 2006). This layer is a porous mix of ice and sea water with solid fractions in the range of 0.2 to 0.5 (Gough et al., 2012). Platelet ice may make a significant contribution to fast ice thickness around Antarctica (Langhorne et al., 2006) in close proximity to ice shelves, and observations of accumulations underlying pack ice have been made (Thomas, 2004). However, due to the spatial scarcity of in situ measurements the occurrence of platelet ice is yet to be investigated at the large scale.

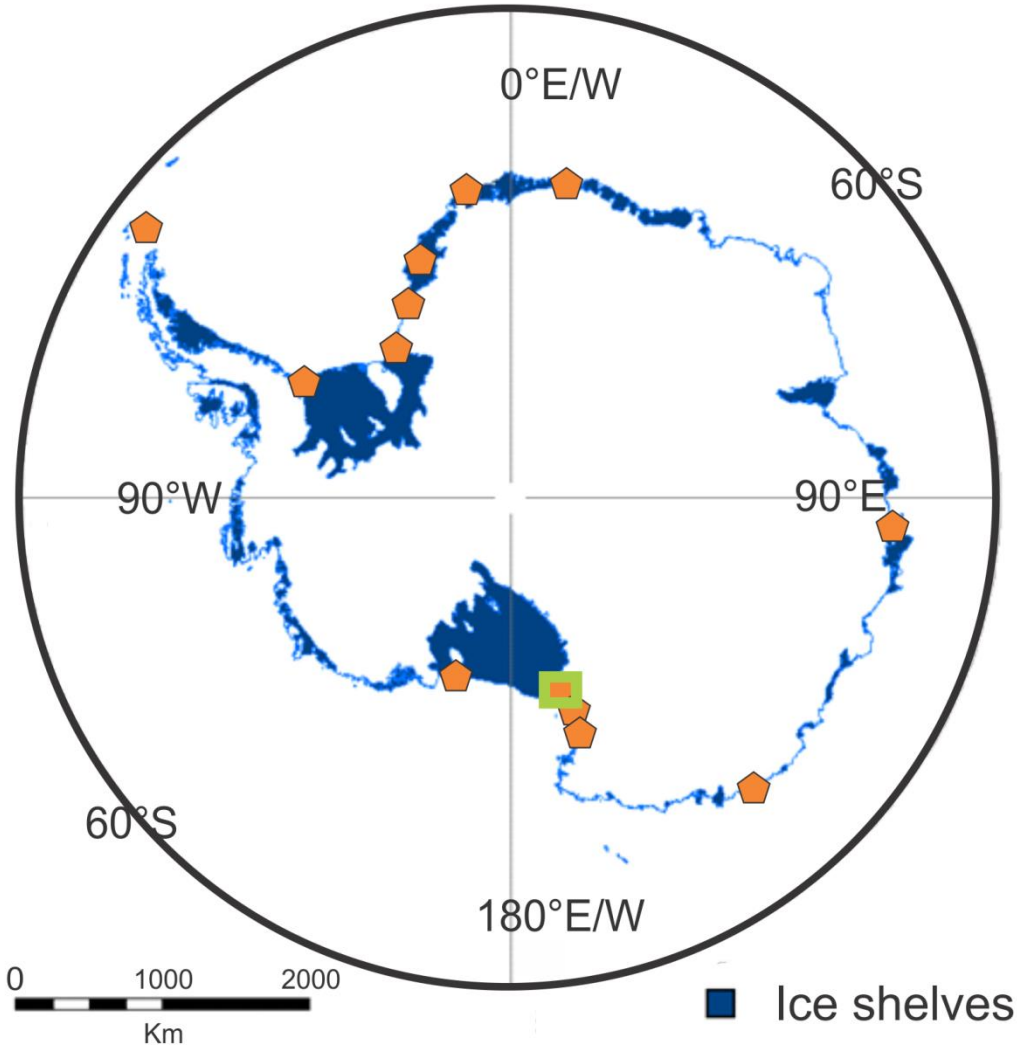

Figure 1.4. The distribution of ice shelves around the Antarctic continent with the study area used in this work; McMurdo Sound highlighted in the green box. Regions in which positive observations of platelet or sub-ice platelet layers have been made are identified with orange pentagons simplified from (Gough, 2012).

(a)

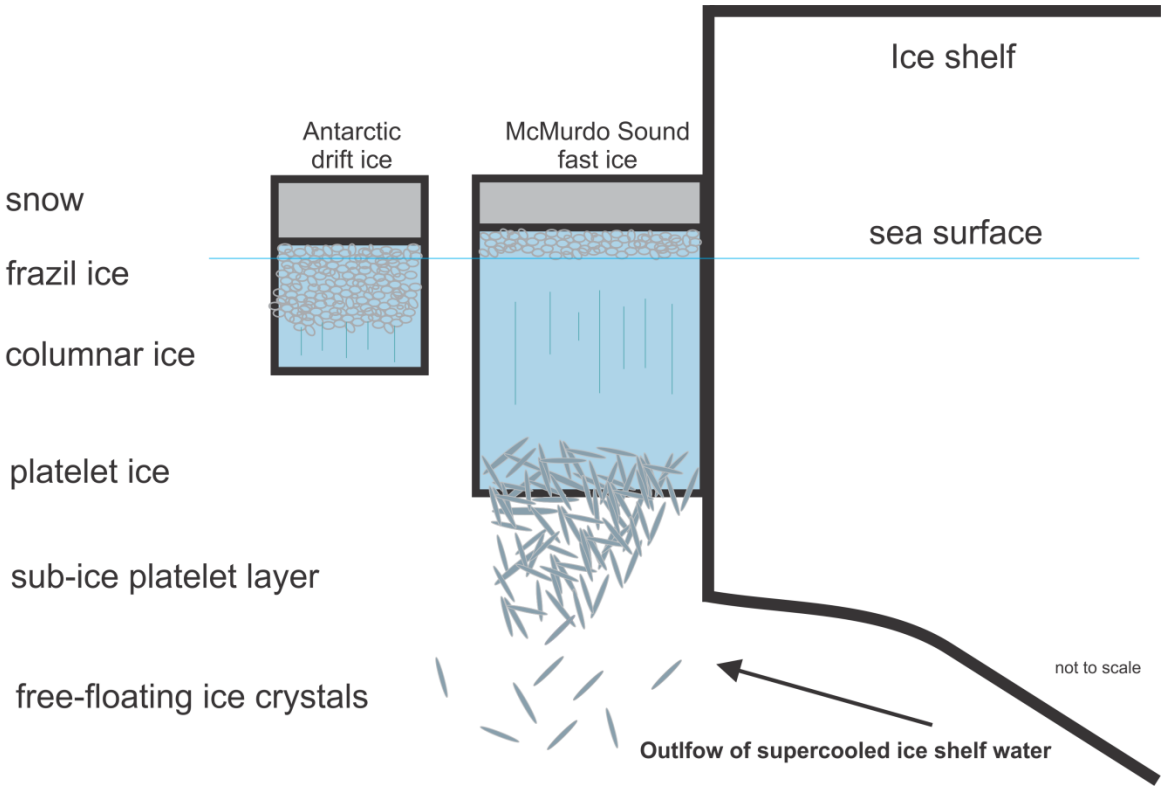

(b)

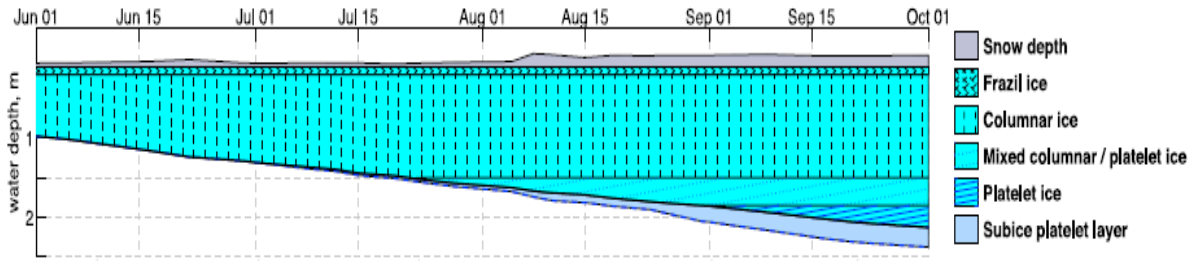

Figure 1.5. (a) The typical structure of fast ice in McMurdo Sound in proximity to supercooled ice shelf water exiting the ice shelf cavity after Gough et al. (2012). Antarctic drift ice which accounts for the majority of the Antarctic sea ice pack is typically thinner, has a higher percentage of frazil ice and a thicker snow cover. **(b)** The growth of McMurdo Sound fast ice from June until October is also displayed after Mahoney et al. (2011).

1.6 Coastal polynyas

Polynyas, areas of reduced or zero ice concentration where it would be expected, are driven by two separate processes. Open ocean polynyas develop because of the upwelling of warmer deep water into the surface ocean, which maintains the temperature above the freezing point and inhibits sea ice growth. Of concern to this work are coastal polynyas, which are forced by wind action, the strength and persistence of which will determine the size and duration of the polynya. Coastal polynyas produce ice as the surface ocean is exposed to the cold polar atmosphere. Thin ice is formed and is immediately pushed away due to wind stress, re-exposing the surface ocean, and initiating an ice production chain. These areas, relatively small in size when compared to the maximum sea ice coverage, have been estimated to be responsible for 10 % of Southern Ocean sea ice production (Tamura et al., 2008). They are also key areas of AABW formation establishing a key link between Antarctic sea ice production rates and global ocean circulation (Ohshima et al., 2013; Comiso et al., 2011).

1.7 A regional perspective – The Ross Sea

The Ross Sea embayment is fringed on its southern flank entirely by the Ross Ice Shelf (RIS), this 1000 km long boundary is the most expansive of its kind in the Southern Ocean. Processes which provide links between key components of the climate system are in operation in these regions and are only beginning to be understood. Ice shelf-ocean interaction is of interest here with regard to its influential role on sea ice processes.

Furthermore, the increasing sea ice extent in the Southern Ocean is the aggregate of its contributing sectors. This extent signal is dominated by a positive anomaly in the Ross Sea which has increased in extent by around 5.0 % per decade since the late 1970s (Comiso et al., 2011; Parkinson and Cavalieri, 2012). The Ross Sea has experienced positive trends in extent for every month, the highest seasonal increase being in spring (Parkinson and Cavalieri, 2012). This increase in the Ross Sea is accompanied by a negative trend in sea surface temperature (Comiso, 2010). Explanations on the change of atmospheric surface temperature in the Ross Sea are restricted due to the severe paucity of measurements. No significant annual trends are reported, although a spring/summer warming is recorded in the

south-western Ross Sea (Sinclair et al., 2012; Turner et al., 2005), and via ice core analysis a decrease in cold season temperature is reported since 1979 (Sinclair et al., 2012). Increases in sea ice production and export from the Ross Ice Shelf Polynya do not appear to have resulted in increased salinity in the Ross Sea, it has actually undergone freshening (Jacobs et al., 2002). Salt input is likely offset from freshwater input from precipitation and glacial melt from the Amundsen and Ross Seas sectors (Comiso et al., 2011; Martin et al., 2007). It is also emphasized by Comiso et al. (2011) that due to the lack of natural barriers between the Ross Sea and adjacent sea ice areas, that increases or decreases in one sector cannot strictly be attributed to changes in that sector alone; but that free advection of ice between regions, could influence the observed trends in extent. These relationships again reflect the complexity of the atmospheric/oceanic interaction in the Antarctic and that simple force-response relationships may not dominate in a particular region. Links to extra-polar climate phenomenon, such as the ENSO and the more localised cycling of SAM are noted. During their different phases both of these teleconnection patterns result in alterations of atmospheric pressure cells. This in turn forces change in surface winds, which drive sea surface conditions and ocean column heat distribution.

A central component of the Ross Sea sea ice regime is the occurrence of polynyas. Three regularly-occurring polynyas are noteworthy within the region, the first of which being the Ross Ice Shelf Polynya (RISP) which is adjacent to the Ross Ice Shelf front (see Figure 1.6b). The RISP is the largest of the Antarctic coastal polynyas with a mean winter area of approximately 25,000 km^2 (Martin et al., 2007) and its ice production rates correlate well with observed sea ice advection from the Ross Sea embayment into the open oceanic area to the north (Comiso et al., 2011). This study, along with Drucker et al. (2011) finds an entirely opposite trend in RISP sea ice production compared to an earlier study (Tamura et al., 2008). The authors attribute this disagreement to different treatment of iceberg interference with the sea ice production algorithms. In spite of this discrepancy, it is appropriate to conclude that the RISP is a prime candidate for a controlling mechanism upon sea ice extent in the region. The RISP provides a significant contribution to high salinity shelf water (HSSW) in the Ross Sea as a result of high sea ice production rates and expulsion of brine to the underlying water column (Mathiot et al., 2012; Assmann and Timmermann, 2005) . HSSW is permitted to build up in this region due to the extensive ocean shelf area in the Ross Sea embayment (Comiso et al., 2011). The Terra Nova Bay Polynya and McMurdo Sound Polynya (see Figure 1.6b) are the remaining two persistent

polynyas in the Ross Sea, but their contributions to sea ice production are far less significant than that of the RISP (Comiso et al., 2011).

Direct sea ice thickness observations in this region are again limited to the spatially sparse and temporally separated investigations of Worby et al. (2008). An ICESat investigation provided by Kurtz and Markus (2012) from 2003-2008 found a negligible negative trend in sea ice thickness in the Ross Sea of 0.01 myr^{-1}, though volume exhibited a positive trend due to increases in sea ice area. It is not correct to presume sea ice extent and thickness are directly related in their response to forcing. It is even indicated that their responses could be opposite (DeLiberty et al., 2011). Therefore the addition of improved sea ice thickness products will complement the developed knowledge of sea ice extent, area, concentration and production in the Ross Sea.

1.8 McMurdo Sound

McMurdo Sound occupies the south western corner of the Ross Sea. The sound is bound by the Victoria Land coast in the west, Ross Island in the east and McMurdo Ice Shelf (MIS) in the south (Figure 1.6c). This geographical setting makes McMurdo Sound highly suitable for the investigation of the interaction of ice shelves, with the ocean and sea ice. Such processes have been investigated in great detail with regard to the ice shelf's influence on the growth of sea ice (Smith et al., 2012; Gough et al., 2012; Mahoney et al., 2011; Leonard et al., 2011; Dempsey et al., 2010; Langhorne et al., 2006; Trodahl et al., 2000; Gow et al., 1998; Jeffries et al., 1993), and the oceanographic details of ice shelf water advection into the wider sea area (Hughes et al., submitted; Robinson et al., 2014; Robinson, 2004). McMurdo Sound harbours a relatively undeformed fast ice regime where fast ice areas are also able to develop dependent upon oceanic and atmospheric conditions (MacAyeal et al., 2008; Brunt et al., 2006). This fast ice regime occupies an area of approximately 3,000 km^2 in austral spring within the geographical bounds of the sound itself, but extends north along the Scott Coast for hundreds of kilometers. The fast ice area is accompanied by a more dynamic sea ice regime in the central and northern area of the sound in the form of the McMurdo Sound Polynya (MSP). Multiple aspects were considered in the selection of a research area. In the first instance, due to the inhospitable environment of Antarctica, access is of primary concern. Secondly, in this case it must be ensured that the region is representative of the larger area in question. McMurdo Sound offers a unique opportunity for such considerations. The support centres of Scott Base and McMurdo Station provide a centre from which to carry out in situ investigations.

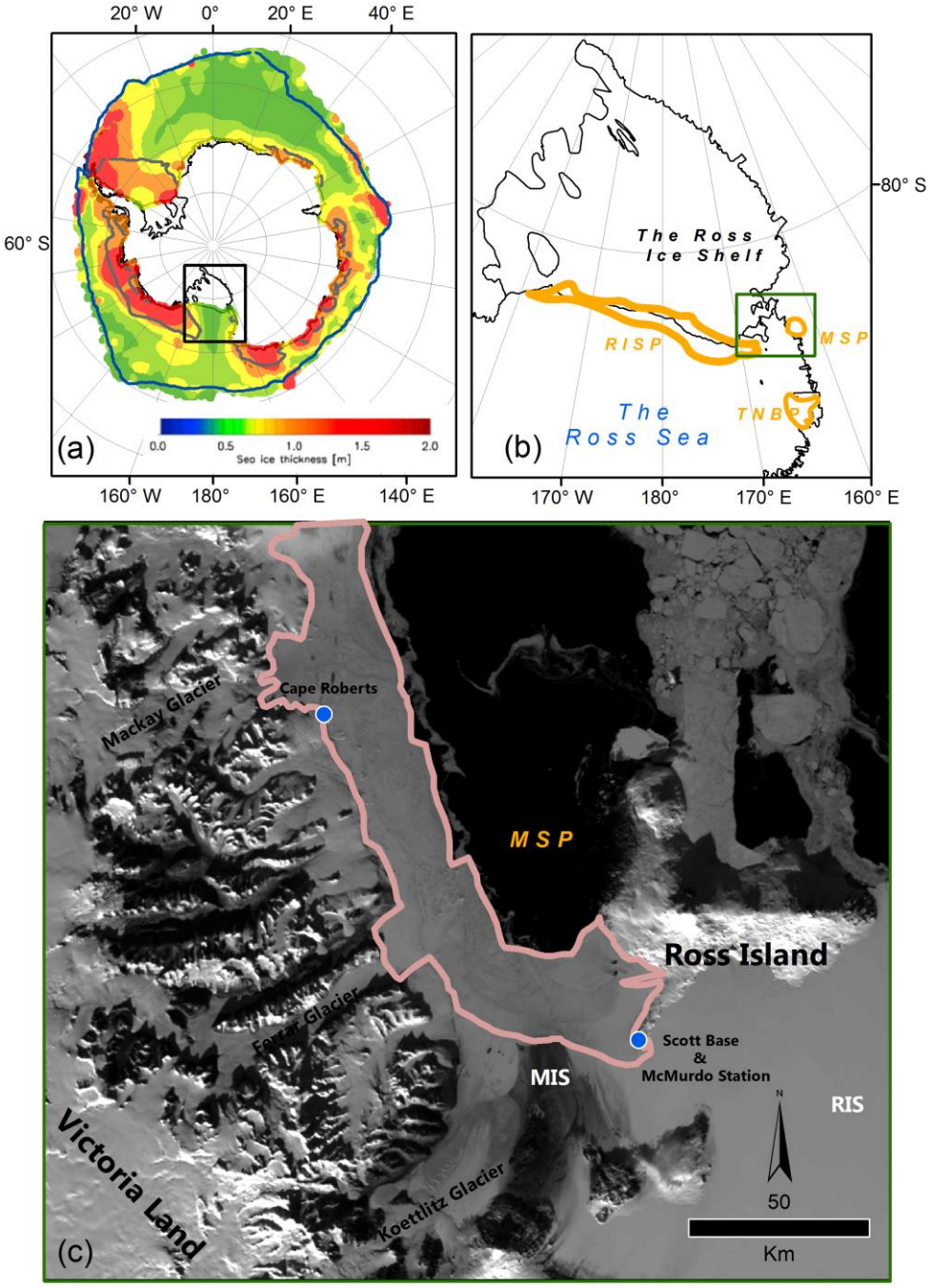

Figure 1.6. (a) Antarctic sea ice area displaying median lines for minimum (grey) and maximum (blue) sea ice extent 1981-2010 and mean spring sea ice thickness from 2003-2008 (Kurtz and Markus, 2012). (b) The area identified by the black box in (a) showing the Ross Sea region with the approximate boundaries of the three main polynyas; the Ross Ice Shelf Polynya (RISP), Terra Nova Bay Polynya (TNBP) and McMurdo Sound Polynya (MSP). (c) The study area of McMurdo Sound as indicated by the green box in (b) imaged with MODIS in November 2011 with its main geographic features including the McMurdo (MIS) and Ross Ice Shelves (RIS). The typical fast first-year sea ice area in austral spring is outlined in pink. Note the reciprocal orientation of (c) from (a) and (b).

1.9 Outline and structure of the thesis

This PhD builds on the unique knowledge of sea ice processes in the McMurdo Sound area of the south-western Ross Sea to advance our understanding of sea ice processes near an ice shelf in the coastal Antarctic, and to develop techniques to investigate Antarctic sea ice thickness. Specifically, remote sensing platforms are utilised to expand in situ measurement information on sea ice freeboard and thickness and draw conclusions on sea ice processes in this region. The structure of this thesis is framed around three separate pieces of work which form the three central research chapters. These three chapters have been written for publication as peer-reviewed journal articles and are presented as such in Chapters 3 to 5. These chapters will aim to achieve the following:

1. provide an improved understanding of spatial characteristics and temporal trends of sea ice in McMurdo Sound in close proximity to an ice shelf (Chapter 3);

2. support the development of satellite altimetry techniques for retrieval of sea ice freeboard in the coastal Antarctic, in particular close to ice shelves and advance efforts to improve remote sensing techniques to monitor the relationship between ice shelves and sea ice (Chapter 4);

3. provide data to derive error budgets for satellite altimetry investigations of Antarctic sea ice thickness, in particular contributing to the validation effort of the European Space Agency's CryoSat-2 (Chapters 4 and 5);

4. continue the development of satellite altimetry techniques to assess Antarctic sea ice thickness by using in situ measurement data to validate and evaluate current operational satellite altimetry missions (Chapter 5).

In this chapter an overview of Antarctic sea ice processes has been provided to put the research chapters into context. Chapter 2 describes the remote sensing tools and validation techniques used in this work, followed by Chapters 3, 4 and 5 which employ these tools to complete the aims outlined above. The findings of these chapters are synthesized and a research outlook is provided in Chapter 6. Full citations and publication status as of August 2014, abstracts, acknowledgements and addenda are given below for Chapters 3 to 5. Equations and variables described in each chapter may be specific to that chapter and therefore caution is advised in comparisons between chapters.

Chapter 3

Citation: Price, D., W. Rack, C. Haas, P. J. Langhorne, and O. Marsh (2013), Sea ice freeboard in McMurdo Sound, Antarctica, derived by surface-validated ICESat laser altimeter data, *J. Geophys. Res*, 118, doi:10.1002/jgrc.20266.

Publication status: received 12/02/2013; revised 29/05/2013; published 04/06/2013.

Abstract: Previous investigations have linked changes in the multiyear sea ice area of McMurdo Sound, Antarctica, from 1,213 km^2 in 2003 to 4,923 km^2 in 2005, to the passage of large tabular icebergs preventing the annual sea ice breakout. This maximum coverage then gradually diminished, by 2009 covering 1,453 km^2. This investigation employs the use of the Ice, Cloud, and land Elevation Satellite (ICESat) laser altimeter to derive freeboard of sea ice in McMurdo Sound from 2003 to 2009 and hence infer thickness changes over this time period. Two techniques for freeboard retrieval are compared. Method-1 (M-1) follows those previously presented in the literature using the lowest elevations to construct an estimate of sea surface height. However, the lack of leads in the study area motivated the development of Method-2 (M-2) which utilizes tide models. Each year is divided into two investigation periods from September to December and February to June, and these investigations were further segmented by sea ice type, first-year (FY), and multiyear (MY). Both applied methods reveal a statistically significant linear increase in multiyear sea ice freeboard. For M-1, the mean freeboard increased over the study period from 0.53 to 1.00 m and for M-2 from 0.46 to 0.95 m. Evidence is presented that the multiyear sea ice freeboard increase is strongly linked to the development and incorporation of a sub-ice platelet layer. No statistically significant trends were observed for first-year sea ice. ICESat derived freeboards over first-year and multiyear sea ice areas compare within one standard deviation of airborne measured freeboard in November 2009.

Acknowledgements: ICESat data were provided by the National Snow and Ice Data Centre, Boulder, Colorado. Envisat ASAR data were received through CryoSat cal/val project 4512. MODIS data were obtained through NASA Earth Observing System Data and Information System. This research was partly supported by NIWA under project CO1X1226 (Ross Sea Climate and Ecosystem). Gratitude is given to participants in the 2009 EM-Bird field work measurements. The field work was supported by Antarctica New Zealand as events K053 and K063. Thanks are given to the two anonymous reviewers and journal editor Andrey Proshutinsky for their comments and suggestions which greatly improved the paper.

Addenda: Post publication, an error in equation 5 (equation 3.5 here) was noted and the relevant corrections have been applied in this work. These corrections were minor, notably the equation was corrected, Figure 12 in the published manuscript (Figure 3.12 here) was edited and relevant referrals to results in the text revised. A corrigendum has been filed to the editor of the *Journal of Geophysical Research – Oceans* to pursue amendment of the error.

Chapter 4

Citation: Price, D., W. Rack., P.J. Langhorne., C. Haas., G. Leonard and K. Barnsdale. 2014. The sub-ice platelet layer and its influence on freeboard to thickness conversion of Antarctic sea ice, *The Cryosphere*, 8, 1031-1039, doi:10.5194/tc-8-1031-2014.

Publication status: received 17/01/2014; published in *The Cryosphere Discuss* 06/02/2014; revised; 07/04/2014; published 11/06/2014.

Abstract: This is an investigation to quantify the influence of the sub-ice platelet layer on satellite measurements of total freeboard and their conversion to thickness of Antarctic sea ice. The sub-ice platelet layer forms as a result of the seaward advection of supercooled ice shelf water from beneath ice shelves. This ice shelf water provides an oceanic heat sink promoting the formation of platelet crystals which accumulate at the sea ice–ocean interface. The build-up of this porous layer increases sea ice freeboard, and if not accounted for, leads to overestimates of sea ice thickness from surface elevation measurements. In order to quantify this buoyant effect, the solid fraction of the sub-ice platelet layer must be estimated. An extensive in situ data set measured in 2011 in McMurdo Sound in the southwestern Ross Sea is used to achieve this. We use drill-hole measurements and the hydrostatic equilibrium assumption to estimate a mean value for the solid fraction of this sub-ice platelet layer of 0.16. This is highly dependent upon the uncertainty in sea ice density. We test this value with independent Global Navigation Satellite System (GNSS) surface elevation data to estimate sea ice thickness. We find that sea ice thickness can be overestimated by up to 19 %, with a mean deviation of 12% as a result of the influence of the sub-ice platelet layer. It is concluded that within 100 km of an ice shelf this influence might need to be considered when undertaking sea ice thickness investigations using remote sensing surface elevation measurements.

Acknowledgements: Acknowledgement is given to the K063 2011 fieldwork team including J. Beckers, A. Gough and K. Hughes and further the Scott Base staff of 2011. Thanks are given to thank J-F. Baure of Icam School of Engineering, Toulouse, France for processing GNSS data during a University of Canterbury supported internship. Gratitude is given for the logistics support of Antarctica New Zealand. Envisat ASAR data were received through CryoSat cal/val project 4512.

Addenda: Two additional tables are provided in the appendices as appendix I and II displaying the in situ measured variables and calculated solid fractions for fieldwork carried out in 2011 and 2013.

Chapter 5

Citation: Price, D., J. Beckers., R. Ricker., N. Kurtz., W. Rack., V. Helm., C. Haas., S. Hendricks., P.J. Langhorne., and G. Leonard. 2014. Evaluation of CryoSat-2 derived sea ice freeboard over fast-ice in McMurdo Sound, Antarctica, *Journal of Glaciology.*

Publication status: in press, received 19/08/2014, accepted 14/10/2014.

Abstract: Using in situ data we evaluate the ability of Crysoat-2 (CS-2) to retrieve sea ice freeboard over fast ice in McMurdo Sound. This provides the first comprehensive validation of CS-2 in the Antarctic and offers insight into the assumptions currently used to process CS-2 data. ESA Level 2 (*ESAL2*) data is compared with results of a waveform fitting procedure (*WfF*) and a Threshold-First-Maximum-Retracker-Algorithm employed at 40 % (*TFMRA40*). A supervised freeboard retrieval procedure is used to reduce errors associated with sea surface height identification and radar velocity in snow. We find *ESAL2* freeboard largely located between ice and snow freeboards. *WfF* is likely influenced by thicker and more complex snow covers which cause a positive bias away from the ice freeboard. *TFMRA40* freeboards are close to the snow freeboard. The separation of freeboard estimates is driven by the different assumptions of each retracker, although waveform alteration by variations in snow depth and surface roughness is evident. Techniques are amended where necessary and automatic freeboard retrieval procedures applied. CS-2 detects annual fast ice freeboard trends using all three automatic procedures in the two years assessed that are in line with known sea ice growth rates in the region.

Acknowledgements: The authors would like to thank all participants in the 2011 and 2013 Antarctic sea ice validation campaigns as members of K063. Gratitude is given to Antarctica New Zealand for logistical support and Scott Base staff for all their efforts. We thank ESA for the processing and provision of CryoSat-2 data, this investigation forming part of the ESA CS-2 calibration and validation activities for project AOCRY2CAL-4512. The Terra-SAR-*X* image was provided by DLR for project OCE1592. The work of V. Helm and S. Hendricks was funded by the German Ministry of Economics and Technology (Grant 50EE1008). We appreciate the efforts of Alec Casey for providing technical assistance in data processing. A research stay from which CS-2 data analysis was achieved was supported by Antarctica New Zealand/Air New Zealand. Further research support was provided by NIWA under contract CO1X1226 (Ross Sea Climate and Ecosystem). This work was collated at Gateway Antarctica, University of Canterbury, New Zealand.

Addenda: None.

2 Satellite and in situ observation

The objectives of this PhD research can only be achieved by the accurate measurement of sea ice properties. Satellites are well suited for investigation of sea ice with proven abilities and experimental applications (Table 2.1). They provide users with a plethora of information and permit data to be retrieved from regions that would be arduous or near impossible to reach otherwise. This work uses satellites operated by the National Aeronautics and Space Administration (NASA), European Space Agency (ESA) and the German Aerospace Center (DLR). Validation is a key component of satellite analysis which gives confidence in the data provided by the satellite instrumentation. Satellite platforms and validation techniques used in this work are described in this chapter. In order to give a data point meaning spatially and temporally, it must first be positioned in space and time. With regard to temporal assessment times reported in this investigation are Universal Time Coordinated (UTC) unless otherwise stated. Spatial components of this work require more specific descriptions and an overview is provided in 2.1.

To complete many of its aims, this work is concerned with the accurate spaceborne retrieval of sea ice freeboard. As freeboard is simply a distance, to obtain such information, instrumentation with a ranging ability must be utilised. Such a ranging ability is offered by satellite altimeters. Satellite altimeters for Earth observation were developed in the 1960s and operational by the 1970s (Fu and Cazenave, 2001) with initial interest in oceanographic applications. They have since become a fundamental tool for assessment of many parts of the Earth system from terrestrial topographic mapping to marine geodesy. Measuring the time interval between transmission and reception of an electromagnetic signal, the distance of the Earth's surface from a reference ellipsoid can be calculated by subtracting its range estimate from its altitude. This is achieved by interrogating the returning signal as a waveform and estimating the position representative of the Earth's surface corresponding to a value selected on the waveform. This procedure is termed retracking and is more simplistic for the first type of altimeter, laser, than the second, radar. Laser and radar systems are separated by their distinctive wavelengths within the electromagnetic spectrum. Laser altimeters typically operate between 400 nm (visible violet) and 1100 nm (near-infrared) while radars between 0.02 m (*Ku*-band) and 0.3 m (*L*-band). These different physical characteristics, resultant of the use of differing wavelengths, makes consideration

of the interaction of the signal with the atmosphere and surface a key consideration upon employment of the instrumentation (Jensen, 2000 and Figure 2.1). With regard to sea ice monitoring in the polar regions, of particular interest is the fact that radar cannot provide the precision that is achievable with laser ranging. However, it has a significant advantage over lasers as cloud interference does not significantly influence the elevation measurement. Energy incident at the Earth's surface from altimeters is distorted. Such distortions manifest themselves as alterations to the recorded waveforms and hold information on surface characteristics such as surface roughness, slope and reflectivity. The two satellite altimeters and their on-board ranging instrumentation used in this work are described in the following sections. However, we first discuss the influence of ocean topography on sea ice freeboard retrieval.

2.1 Ocean topography

Satellite altimeters provide an elevation profile of the Earth's surface along the sub-satellite track. The final procedure for sea ice freeboard retrieval, discerning the elevation of a sea ice floe above the local sea level requires the removal of additional sources of elevation variation within the elevation profile.

The true physical surface of the Earth is highly complex and it has been of much interest to Geodesy to develop ways of representing it. A common approach has been to use mean sea level (MSL) as a reference for heights. This however was not universal as countries developed referenced heights related to the average sea level height in their region. The development of universal terrestrial reference surfaces has been of great importance given the global monitoring capacity of satellites. One approach is the use of the geoid, the shape of the Earth that is given by its gravitational influence (Lowrie, 2007; Fowler, 2005) . The most simplistic description of the geoid surface is the vertical position the surface of the Earth would adopt if it were entirely ocean and under the influence of gravity alone (Lowrie, 2007; Fowler, 2005). This surface in reality closely approximates MSL, but due to the influences of dynamic ocean topography and atmospheric pressure these surfaces differ by around ± 1 m. The geoid therefore is a unique surface which closely follows MSL, but undergoes undulations due to the changing influence of gravity driven by changes in the local Earth's mass (Grafarend, 1994). For sea ice freeboard retrieval, consideration of the

geoid is of great importance. Given the oceanic response to the force of gravity, the surface of the ocean develops slopes. These slopes occur between areas where water bulges and troughs driven by the varying gravitational attraction of the lithosphere below. When a large area is considered, these long wavelength trends in the ocean surface height must be accounted for in order to retrieve relative elevation measurements referenced to sea level. The geoid surface has been modelled and in this work, the Earth Gravitational Model 2008 (NGA, 2014; Pavlis et al., 2012) is used to represent it. In addition to the geoid, the sea surface is also under the influence of atmospheric and tidal forces. The atmosphere changes local sea surface height over short term timeframes (minutes-daily) by two processes, the first by variations in surface air pressure and the second by wind forcing. Local surface air pressure can alter the local sea level typically by around ± 1 m which is termed 'the inverse barometer effect'. Wind can cause changes in significant wave height and drive dynamic ocean topography causing water to pile up in certain regions while it can be moved away from others. These processes all contribute to what is called 'the sea surface height anomaly' (SSHA), i.e. the variation of sea surface height around mean sea level. Each of the components responsible for the SSHA are typically modelled and in this work these models are named where appropriate.

The geoid, or the surface, can also be represented as a positive or negative deviation around what is known as an 'ellipsoid'. The ellipsoid is a further simplification of the Earth's surface, a mathematical approximation which allows for longitudinal (*x*), latitudinal (*y*) and vertical (*z*) positioning from the relevant zero marks of each axis. In this work the World Geodetic System 1984 (WGS-84) is used universally. The coordinate centre of WGS-84 is at the Earth's centre of mass, such a reference frame being termed geocentric. The ellipsoidal sphere is an oblate spheroid with an equatorial radius of 6,378,137 m and flattening of 1/298.257 (Iliffe and Lott, 2008). The origin of the *x* ordinate in the WGS-84 system is 0° E/W and is located at Greenwich in London, U.K. Positions in the eastern hemisphere are typically given positive values, those in the western hemisphere given negative values. The origin of the *y* ordinate is 0° N/S and is located at the equator. Positions in the northern hemisphere are given positive values, and those in the southern negative values. All positions are defined as angles from the respective origin plane and a point on the Earth's surface. For *x* this is the angle from the prime meridian at Greenwich and for *y* the angle from the equatorial plane. The origin of the *z* ordinate is the ellipsoidal surface, elevations above are given positive values and elevations below are given negative

values. The simplistic nature of the system with regards to the actual surface of the Earth results in large deviations of the actual Earth surface from the zero defined by the reference ellipsoid. This is why negative vertical values or elevations are common over sea areas using WGS-84. Geoid undulations around the ellipsoid are typically ± 100 m.

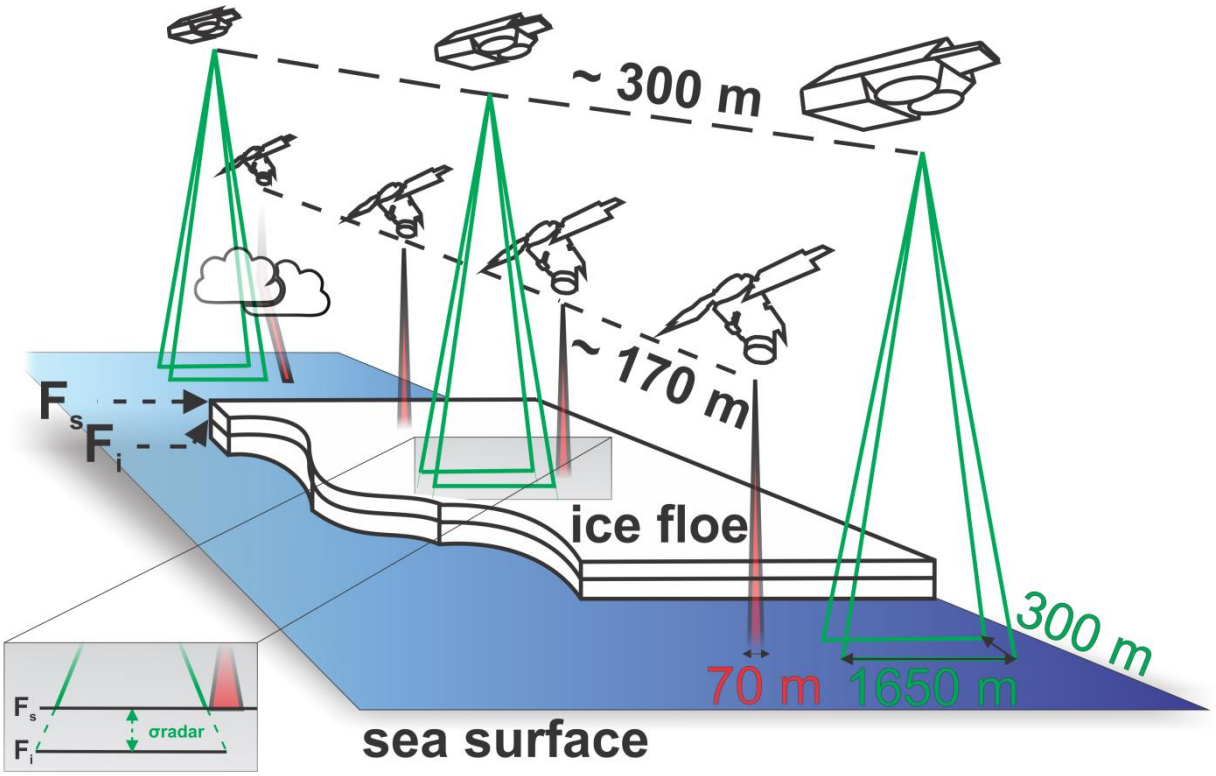

Figure 2.1. Measurement characteristics of ICESat and CryoSat-2. ICESat unambiguously records the snow freeboard (F_s) but suffers from forward scattering by cloud cover. CryoSat-2 is unaffected by cloud but gives uncertainty (σradar) with regard to the surface interface it records, the interface variable and established as a function of surface conditions between the ice freeboard (F_i) and F_s. Satellite footprint separation along-track is given in black writing on each respective satellite track while the dimensions of the footprints are given in red (ICESat) and green (CryoSat-2).

Table 2.1. Satellite sensors utilised for sea ice investigation as provided by Lubin & Massom (2006) with research developments made since its publication highlighted in orange. It can now be argued that altimeters are the most capable tool for the retrieval of large-scale Antarctic sea ice thickness.

Parameter	*Passive Microwave*	*SAR*	*Low-res. Vis-TIR#*	*Hi-res. Vis-TIR#*	*Radar Scatt*	*Radar Alt*	*Laser Alt#*
Sea ice conc.	**P**	**S**	**S**	**S**	**-**	**-**	**-**
Sea (pack) ice extent	**P**	**S**	**S**	**S**	**P**	**S**	**R**
Fast ice extent	**-**	**P**	**P**	**P**	**-**	**-**	**-**
Polynya size	**P**	**P**	**P**	**P**	**-**	**-**	**-**
Iceberg size/tracking	**-**	**P**	**P**	**P**	**-**	**-**	**-**
Ocean colour (prim. prod)	**-**	**-**	**P**	**-**	**-**	**-**	**-**
Sea ice motion	**P**	**P**	**P**	**S**	**P**	**-**	**-**
Ice dynamic kinematic	**S**	**P**	**S**	**-**	**S**	**-**	**-**
Sea ice thickness	**R**	**R**	**R**	**-**	**-**	**P/R**	**P/R**
Sea ice classification	**P**	**P**	**S**	**S**	**S**	**R**	**-**
Snow cover thickness	**P/R**	**R**	**-**	**-**	**-**	**R**	**-**
Surface roughness	**-**	**R**	**-**	**R**	**-**	**R**	**R**
Floe size statistics	**-**	**P**	**S**	**P**	**-**	**-**	**-**
Surface "skin" temp.	**-**	**-**	**P**	**S**	**-**	**-**	**-**
Snow/ice interface temp.	**P/R**	**-**	**-**	**-**	**-**	**-**	**-**
Broadband albedo	**-**	**R**	**P**	**S**	**-**	**-**	**-**
Snow grain size	**-**	**-**	**P**	**-**	**-**	**-**	**-**
Snow impurity content	**-**	**-**	**P**	**-**	**-**	**-**	**-**
Annual melt onset and freeze-up	**P**	**P**	**S**	**S**	**R**	**-**	**-**
Meltpond coverage	**-**	**R**	**-**	**R**	**-**	**-**	**-**
Wave-ice interaction	**-**	**P**	**-**	**-**	**R**	**-**	**-**
Ice edge characteristics	**-**	**P**	**P**	**P**	**R**	**-**	**-**

Vis - visible to near-infrared, TIR - thermal infrared, Scatt – scatterometer, Alt – altimeter, # - cloud-affected (visible to near-infrared sensors are also darkness-affected), P - primary data source, S - secondary data source, R - research and development.

2.2 Ice, Cloud, and land Elevation Satellite

The Ice, Cloud and land Elevation Satellite (ICESat) was launched by NASA in January 2003 with its mission ending in February 2010 after failure of its primary instrument (Dewitt, 2010). The mission was commissioned in order to measure ice sheet mass balance, cloud and aerosol heights and land topography and was the first satellite of its kind with continuous global observation ability to a latitude of 86° N/S (Zwally et al., 2002b). The on-board laser instrument, the Geoscience Laser Altimeter System (GLAS) has documented its ability for the investigation of sea ice freeboard and thickness in the Arctic (Kwok and Rothrock, 2009; Kwok et al., 2009; Farrell et al., 2009; Kwok and Cunningham, 2008; Kwok et al., 2007; Spreen et al., 2006; Kwok et al., 2006; Kwok et al., 2004) and Antarctic (Xie et al., 2013; Kurtz and Markus, 2012; Xie et al., 2011; Yi et al., 2011; Zwally et al., 2008). The system operated three lasers which transmitted at two wavelengths, one in the infrared (1064 nm) for surface investigation and one in the visible green (532 nm) for atmospheric analysis (Schutz et al., 2005). Problems stemming from laser lifetime issues resulted in early amendment of continual surface monitoring to the implementation of 33-day operational periods. ICESat's GLAS instrument operated at 40 Hz resulting in a footprint separation of approximately ~ 170 m with a footprint diameter of ~ 70 m on the Earth's surface (Figure 2.1). These elevation retrievals provide range precision to flat surfaces of 2 cm and accuracies of ~ 10 cm (1σ) (Zwally et al., 2008). The major disadvantage of the system was forward scattering of the laser beam from cloud interference which could significantly affect the accuracy of the surface elevation retrieval (Fricker et al., 2005). Analysis of certain waveform based parameters allowed for removal of data likely to be affected by cloud.

2.3 CryoSat-2

CryoSat-2 (CS-2) was launched by ESA in April 2010 and is dedicated to the quantification of fluctuations in the Earth's major land and marine ice fields (Wingham et al., 2006). Launched as a replacement for CryoSat which was lost in launch failure in October 2005, CS-2 operates in a near-circular polar orbit with an inclination of 92° and aims to achieve high density orbit cross-overs at high latitudes while maintaining near complete coverage of the Arctic Ocean and Antarctic continent (Labroue et al., 2012). The satellite has a repeat cycle of 369 days with a sub-cycle of 30 days (Bouzinac, 2013). The Synthetic aperture radar Interferometric Radar ALtimeter (SIRAL) aboard CS-2 is a 13.6 GHz (*Ku*-band) normal incidence radar altimeter with two receiver chains and three modes: Low Resolution Mode (LRM) over open ocean and the continental ice sheet interiors, Synthetic Aperture Radar (SAR) over sea ice areas and Synthetic Interferometric (SIN) mode over mountainous regions and the continental ice sheet margins (Wingham et al., 2006). In SIN mode, interferometry makes use of the phase information from the returning radar signal by employing two receiver chains. Using the baseline difference between the chains upon reception reflections off nadir can be correctly positioned on the Earth's surface. Full specifications on the SIRAL parameters are given in (Table 2.2).

Table 2.2. SIRAL parameters (Bouzinac, 2013, Scagliola, 2013).

Parameter	*Value*
Satellite Altitude (*h*)	~ 730 km
Satellite velocity (*v*)	~ 7520 m/s
Radio Frequency (RF)	13.575 GHz (*Ku*-band)
Pulse bandwidth (*B*)	320 MHz (40 MHz for tracking only in SIN)
Pulse Repetition Frequency (PRF)	1.97 kHz in LRM, 18.181 kHz in SAR and in SIN; coherent pulse transmission for Doppler processing
Burst Mode PRF **Pulses/burst**	1970 Hz in LRM, 85.7 Hz in SAR and 21.4 Hz in SIN n/a in LRM, 64 in SAR and in SIN
Compressed pulse length (τ)	3.125 ns (1/*B*)
Timing	Regular PRF in LRM, burst mode in SAR/SIN
Samples/pulse	128 in LRM and SAR, 512 in SIN
RF peak power	25 W
Antenna size	2 reflectors, 1.2 m x 1.1 m, side-by-side
Antenna beamwidth (3 dB)	1.06° (along-track) x 1.1992° (across-track)
Antenna footprint	~ 15 km
Range resolution	0.47 m
Along-track resolution	~ 300 m (SAR/SIN)
Data rate	60 kbits/s for LRM,12 Mbit/s SAR,2 x 12 Mbit/s SIN
Instrument mass (with antennas)	90 kg redundant
Instrument power	149 W
Antenna baseline length	1167.6 mm
Speed of light (*c*)	299792458 m/s
RF wavelength (λ)	0.0221 m

The radar geometry and the expected horizontal and vertical resolution of SIRAL can be estimated by using the information provided in Table 2.2 and equations 2.1-2.3. The pulse-limited illuminated area, which defines the across-track width of the CS-2 footprint can be envisaged as a circle on the Earth's surface with radius, *r* as defined by Bouzinac (2013):

$$r = \sqrt{hc\tau} = \sqrt{h\frac{c}{B}} \tag{2.1}$$

with a resultant area of approximately 2.15 km^2 and a subsequent across-track footprint width of 1,650 m. Using Doppler beam formation in the along-track direction, the sharpened beam-limited width (Δx) is defined by:

$$\Delta x = h \frac{\lambda}{2v} \frac{PRF}{64} \quad (2.2)$$

resulting in an along-track footprint length of approximately 305 m. These definitions provide a pulse-doppler-limited footprint for the SIRAL instrument of approximately 0.5 km^2.

SIRAL acquires data in a range window and attempts to maintain the peak power at its centre. This range window is amended for each operating mode; 60 m in LRM covered by 128 samples, 30 m in SAR again covered by 128 samples and increased to 120 m in SIN mode over 512 samples to account for slope variation over complex terrain (Bouzinac, 2013). The range resolution (Δrr) is determined by the pulse bandwidth and is calculated as:

$$\Delta rr = \frac{c}{2B} = 0.47\ m \quad (2.3)$$

To avoid aliasing (Jensen, 1999) SAR and SIN echoes are oversampled by a factor of two which gives a range sampling of 0.234 m. Each range bin of the returned radar echoes amounts to this range sampling (i.e. 120 m/512 range bins = 0.234 m).

The more ambiguous nature of radar interaction over sea ice as opposed to laser methods (Figure 2.1) meant it was clear from the outset that CS-2 would require intense validation to meet the accuracy requirements of the mission. One key variable must be constrained to gain confidence in the expected dominant backscattering surface over sea ice; the penetration depth of the incident radar signal into snow of varying properties. The penetration depth is defined as the depth at which the energy of the incident radiation is reduced to 33 %. Given a dry snow cover, a significant penetration of the radar energy is expected (Hofer and Mätzler, 1980), but this is significantly reduced in wet snow (Mätzler, 1987; Stiles and Ulaby, 1982). This along with other variables including salinity, density, grain size and temperature (Barber et al., 1995; Hallikainen et al., 1986; Ulaby et al., 1986) mean the penetration of the incident SIRAL radar signal will be inconstant and dictated by surface conditions. It was predicted that CS-2 would be capable of measuring Arctic sea ice thickness to an accuracy of 0.068 m in a one month period, over a 100,000 km^2 region at 70° N (Wingham et al., 2006). The CryoSat Validation Experiment (CryoVEx) was implemented by ESA to attempt to quantify the sea ice thickness retrieval uncertainties of

the CS-2 mission. This resulted in an international effort to coordinate surface and airborne validation measurements which Chapter 5 of this work is a part. To date no investigations of Antarctic sea ice properties using CS-2 are available.

2.4 Imaging platforms

An ability to visualize the environment under investigation is also highly desirable. Such ability allows for further interpretation of altimetry information with regard to ice-ocean discrimination and identification of differing ice types.

2.4.1 Environment satellite

Environmental Satellite (Envisat) was launched in March 2002, its mission formally ending on 9 May 2012 after ESA announcing it had lost contact with the satellite. Envisat operated in a sun-synchronous orbit with a repeat cycle of 35 days (ESA, 2014a). However, as most of its instruments are wide swath it could provide full global coverage within 3 days (ESA, 2014a). The satellite carried ten separate instruments for differing Earth Observation investigations. The instrument of primary interest to this work was the Advanced Synthetic Aperture Radar (ASAR). ASAR was an imaging microwave radar operating at 4-8 GHz (*C*-band) with multiple modes (Table 2.3). The system also offered five polarisation modes VV, HH, VV/HH, HV/HH and VH/VV (ESA, 2014a). The system could operate in the presence of cloud cover and allows discrimination of sea ice of different ages.

2.4.2 Terra & Aqua

Terra and Aqua were launched in 1999 and 2002 respectively with multiple sensors for an extensive Earth Observation capability. The orbit configuration between the two satellites allows viewing of the entire Earth's surface every 1 to 2 days. The MODerate-resolution Imaging Spectroradiometer (MODIS) instrument captures data in 36 spectral bands and at varying spatial resolutions (Table 2.3). This study uses high resolution bands 1 and 2 to provide auxiliary information for interpretation of altimetric freeboard information. MODIS use is restricted to daylight hours making it unusable during polar winter (restricted in our study area from late March to late September). Surface observation is also unachievable if even a light cloud cover is present.

2.4.3 TerraSAR-X

TerraSAR-X operated by DLR is a radar imaging satellite employing a 9.65 GHz (*X*-band) SAR instrument. Launched in June 2007, unlike aforementioned platforms it has commercial as well as scientific applications. The system provides high geometric and radiometric resolution along with interferometric capabilities and an ability to tilt the radar beam within a range of 20 to 60 degrees perpendicular to flight direction. The instrument delivers radar imagery in three main imaging modes; SpotLight (1 m resolution, 50 km^2 scene), StripMap (3 m resolution, 1,500 km^2 scene) and ScanSAR (18 m resolution, 15,000 km^2 scene). This work uses TerraSAR-X ScanSAR mode for identification of sea ice types and retrieval of sea ice roughness.

Table 2.3. ICESat, CryoSat-2, Envisat, Terra/Aqua and TerraSAR-X orbital elements and characteristics. The entire Antarctic sea ice area is covered by all five satellites.

Satellite	*Orbit type*	*Mean altitude*	*Inclination*	*Repeat orbit*	*Spatial resolution*
ICESat (De-commissioned)	Near polar, LEO	600 km	94.00°	91 days (33 day sub-cycle)	70 m footprint 170 m separation
CS-2 (Operational)	Near polar, LEO	717.242 km	92.00°	369 days (30 day sub-cycle)	~ 1650 m x 300 m
Envisat ASAR (De-commissioned)	Near polar, LEO	799.8 km	98.55°	35 days	30 m (Image mode) 150 m (Wide Swath) 1000 m (Global Monitoring)
Terra/Aqua (Operational)	Near polar, LEO	715/700 km	98.20°/98.14°	16 days	250 m (bands 1-2) 500 m (bands 3-7) 1000 m (bands 8-36)
TerraSAR-X (Operational)	Near polar, LEO	514 km	97.44°	11 days (View angle capability provides global imaging capacity within 2 to 4 days)	Up to 1 m 18 m for this work

2.5 In situ and near-surface measurements

On site measurements described as ‘in situ’ are the most accurate way to measure sea ice properties. They are however very restrictive spatially and difficult to maintain temporally. Extensive in situ validation campaigns were carried out in November 2009, November and December 2011 and November and December 2013 in support of this work. The 2011 and 2013 campaigns were dedicated to validation of CryoSat-2 while the 2009 campaign provided unintentional validation of ICESat. Overviews of the surface and near-surface validation techniques are provided below.

2.5.1 In situ measurements of sea ice properties

The most reliable technique for sea ice freeboard and thickness retrieval is drilling. The margin for error is greatly reduced as no remote sensing system is in use. The technique simply involves drilling into the sea ice cover and measuring the thickness of the sea ice cover with a tape measure. This technique is labour intensive and time consuming and is therefore aided by the use of an electric drill which employs 1 to 3 auger flights with an ice drilling bit (5 cm diameter). The tape measure system was amended by adding a metal bar to the end of the reel. Upon emerging from the drill hole into open water the bar falls from a vertical position into a horizontal one and gives resistance when the ice/water interface is met. Freeboard was simply measured as the distance from the water surface to the ice surface in the drill-hole. Snow depth was measured in a cross profile around the drill-hole using a ruler and is the distance between the ice/snow interface and the air/snow interface. The usefulness of such a technique is entirely dependent upon the size of the sea ice area in question and the availability of personnel to conduct extensive drilling. In this case the relatively small fast ice region in McMurdo Sound can be sampled at a suitable spatial resolution for satellite validation using a 4-5 man team, with skidoo support in several days. All in situ measurements from the two field seasons undertaken for this work are presented in the appendix.

2.5.2 Global Navigation Satellite System

The Global Navigation Satellite System (GNSS) is provided by a constellation of 20-30 Medium Earth Orbit satellites. These satellites are comprised of the United States Global Positioning System (GPS) and the Russian Global Navigation Satellite System (GLONASS) which provide x, y and z positioning ability in reference to the WGS-84 ellipsoid. This work uses this positioning ability to derive surface elevation using mobile and static GNSS stations for the assessment of freeboard and tidal information. Measurement accuracy was improved using the Precise Relative GNSS technique (Uren and Price, 2010) given the proximity of the study area to a base station at Scott Base.

2.5.3 Helicopter-borne electromagnetic induction sounding

Helicopter-borne electromagnetic induction sounding (EM-Bird) measurements were carried out in November 2009, December 2011 and December 2013, recording approximately 1000 km of sea ice thickness profiles in each year. EM-Bird sounding allows for the determination of sea ice thickness at close range with accuracies of ± 0.1 m over level sea ice (Haas et al., 2010). Making use of the strong electrical conductivity contrast between ice and seawater, the ice-ocean interface is identified. At this location, eddy currents are generated when the EM field interacts with the seawater. These eddy currents generate a secondary EM field which is received by the EM system (Haas et al., 2009). The strength of the returning secondary field is directly related to the distance from source to receiver, i.e. the distance from the ice underside to the EM receiver coil (Haas et al., 2009). Using a single beam lidar (HL) on the instrument the air-snow interface is also identified, the difference between the two distances giving total thickness (ice-plus-snow) measurements. The EM-Bird method encounters footprint issues when the ice is deformed (Haas et al., 2009). The level ice in McMurdo Sound is optimal for assessment under EM sounding methods due to the absence of rough deformed ice. The capabilities of this system in the study area are demonstrated by Rack et al. (2013). In addition, the EM-Bird's HL was used for freeboard retrieval. The nadir pointing laser produces a footprint of a few centimeters from the optimal flying altitude of 20 m. GNSS base stations in close proximity to the study area were used to differentially correct the EM-Bird position. This positioning ability was utilised with HL to obtain surface elevation. From this the freeboard could be measured after calibration of surface elevation measurements using coincident in situ drill-hole measurements.

3 Sea ice freeboard derived by ICESat laser altimeter data

3.1 Introduction

The formation of sea ice near the Antarctic coast is significantly influenced by the existence of ice shelves and presence of polynyas. Almost three quarters of the grounded ice boundary of the Antarctic ice sheet abuts floating ice shelves (Bindschadler et al., 2011) and it is estimated from model simulations that, close to larger ice shelves, approximately 10-25 % of total sea ice thickness is attributed to the outflow of cold water from the ice shelf cavities (Hellmer, 2004). The sea ice cover in the Ross Sea sector is of particular interest as it has experienced a significant increase in extent during the satellite observation period of 5.0 ± 0.6 % per decade (Comiso et al., 2011). However, information on sea ice thickness over this period is very limited. Investigations that are spatially sparse and exhibit extended periods of temporal separation provide some insight indicating that sea ice thickness and extent do not co-vary (DeLiberty et al., 2011) and that the Ross Sea has thicker sea ice in comparison to other sectors, but is highly influenced by the opening of the Ross Sea polynya in spring and the advection of thicker ice from adjacent sea areas (Worby et al., 2008). A recent study based on satellite derived freeboard suggests a small decreasing trend in thickness of 0.01 m from 2003 to 2008, but due to the observed increasing extent, an increasing trend in volume over the whole Ross Sea sector for the period (Kurtz and Markus, 2012).

A major limitation of satellite based sea ice thickness studies in general is the temporal and spatial scarcity of freeboard, snow depth and thickness measured in situ for validation. McMurdo Sound, located in the south-western Ross Sea, provides a unique opportunity to address this issue. The sea ice formation process is comparatively well studied in McMurdo Sound and its suitability for assessment by satellite is bolstered by a developed understanding of local processes from in situ investigations (Gough et al., 2012; Smith et al., 2012; Dempsey et al., 2010; Leonard et al., 2006; Jeffries et al., 1993). In our study we concentrate on temporal and spatial trends of sea ice freeboard in McMurdo Sound from satellite laser altimetry and draw some conclusions on sea ice thickness in 2009 with the use of surface and airborne investigations.

The quantification of sea ice mass balance requires information on both its extent and thickness (Haas, 2010). The latter is particularly difficult to assess from satellites as it is indirectly determined from sea ice freeboard, which itself is estimated from an altimetric measurement of sea ice elevation. Freeboard is strictly the elevation of the sea ice surface above the ocean surface. However, accumulation of snow on top of the sea ice inhibits the direct measurement of the sea ice surface from laser altimetry methods. Therefore, a total freeboard (ice-plus-snow) is obtained, from here referred to as freeboard.

Our study is based on data from NASA's Geoscience Laser Altimeter System (GLAS) onboard of the Ice, Cloud, and land Elevation Satellite (ICESat), which has been used for freeboard retrieval in the Antarctic (Kurtz and Markus, 2012) and Arctic (Kwok and Rothrock, 2009; Farrell et al., 2009; Kwok et al., 2004). As Antarctic sea ice is largely young and thin and therefore its freeboard relatively small (Worby et al., 2008), the required accuracy in the altimeter measurement is very high. Any errors in the initial freeboard estimation will be amplified in the later thickness calculation (Kwok and Cunningham, 2008).

To derive freeboard the local sea surface height must be identified as a reference surface. This task is complicated by natural undulations in this reference surface. Our current inability to represent this variation to the required accuracy hinders freeboard estimation. Inaccuracies are dominated by erroneous heights of the geoid and the tides provided by models. Unless the sea surface height can be established in time and space by independent information, open water must be available nadir to ICESat to produce a local sea surface height for the relative estimation of freeboard. The accuracy of this freeboard measurement will decrease as a function of distance from the sea surface height measurement until another open water area is available for referencing. McMurdo Sound harbors areas of fast ice creating an immediate challenge. The geoid dominates the trend in surface elevation and even over short distances of 10 km poor geoid knowledge can cause errors in estimated freeboard.

Taking account of buoyancy principles, converting freeboard to sea ice thickness involves inclusion of density information and snow depth. This is a complex relationship as density values and snow depth exhibit large temporal and spatial variability. If snow depth

information is not available, no information can be gained for sea ice mass balance alone. Zwally et al. (2008) suggest that interannual changes in estimated thickness are mainly representative of snow depth changes. Efforts to correct for snow depth may be hindered by the difficulty of achieving temporal coincidence of the altimetry and snow depth information and their differing spatial resolution (Weissling and Ackley, 2011). This is especially the case for smaller scale assessments in coastal areas where low resolution passive microwave techniques provide inadequate information on snow depth. Further errors introduced in the estimation of thickness by inclusion of nominal information on snow, ice and water density can also be quite significant (Yi et al., 2011). Other studies have made use of in situ information to support satellite data (Markus et al., 2011; Worby et al., 2011; Xie et al., 2011) allowing assessment of method accuracy.

For our study we derive the sea ice freeboard in an area where good temporal (Gough et al., 2012; Purdie et al., 2006) and spatial (Dempsey et al., 2010) in situ information is available and sea ice conditions are well understood. During the investigation from 2003 to 2009 the area hosted three, approximately level, sea ice types: multiyear (MY) sea ice persisted in the southern portion of the Sound, held fast by the McMurdo Ice Shelf in the south, Hut Point Peninsula in the east and the Victoria Land coast in the west (Figure 3.1). The MY sea ice was partly bordered by seasonal first-year (FY) landfast sea ice. The remainder of the study area was covered by variable FY pack ice.

We present two freeboard retrieval methods, Method-1 (M-1) utilizing ICESat information alone, variants of which have been well documented in the literature (Yi et al., 2011; Zwally et al., 2008). Our results show that we do not require more sophisticated approaches as described in Farrell et al. (2009) and Kwok et al. (2006) as our investigation area, characteristic of level thermodynamically grown sea ice, is void of leads, with a single open water area in the north. Method-2 (M-2) is a novel approach involving the development of sea surface height from a mean sea surface grid, tidal heights and atmospheric pressure data. The satellite analysis is validated by in situ and airborne measurements in 2009. These include near-coincident drill-hole measurement of freeboard and ice thickness and helicopter-borne electromagnetic induction sounding thickness (EM) and helicopter lidar (HL) freeboard measurements.

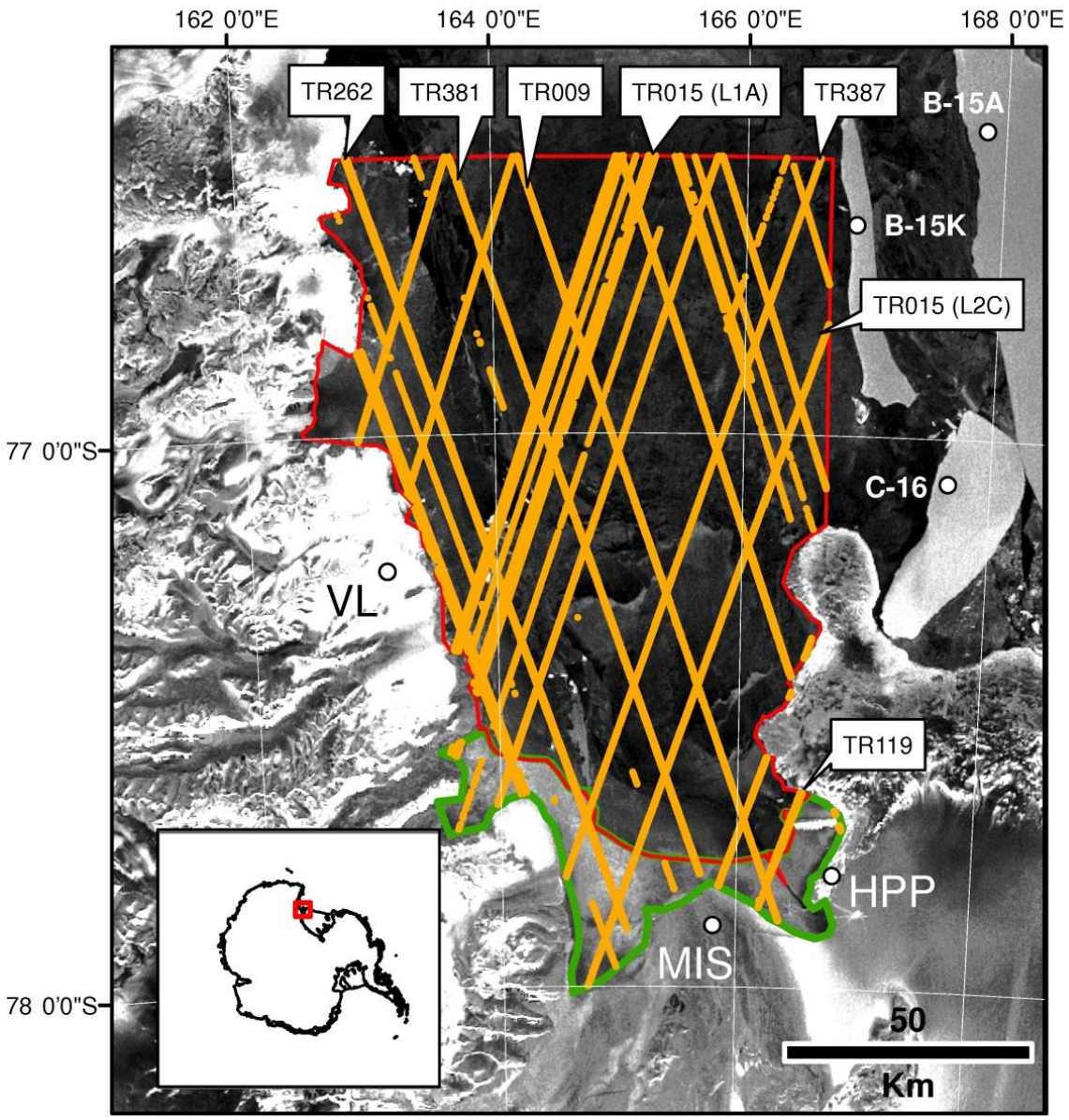

Figure 3.1. Location of the study area and satellite map (Envisat ASAR, 12 October 2004) with all used ICESat measurement points (orange) and track numbers mentioned in the text. Sectors of multiyear and first-year sea ice are outlined in green and red, respectively. The first-year-multiyear transition was variable throughout the study period but the study area remained fixed within the displayed bounds. VL: Victoria Land, MIS: McMurdo Ice Shelf, HPP: Hut Point Peninsula, large icebergs: B-15A, B-15K and C-16.

This research chapter is organised as follows: section 3.2 provides an overview of sea ice conditions in the study area. Section 3.3 explains M-1 with data quality and method quality checks provided separately in section 3.1. Section 3.4 outlines M-2 freeboard retrieval. Section 3.5 provides ICESat recorded freeboard information and section 3.6 describes the EM induction sounding and HL investigations and comparison of remote sensing techniques with in situ information. Sections 3.7 and 3.8 follow with discussion and conclusions.

3.2 Sea ice types in the study area

During the investigation sea ice was highly variable with regard to the distribution of differing sea ice types. Sea ice development in the sound is dominated by thermodynamic growth resulting in the establishment of a relatively flat land-fast regime. From historical information, most commonly, conditions in the region result in a sea ice regime where fast ice breaks out one of every two years (Heine, 1963). Prior to the study the last time at which open water was abutting the ice shelf was 1998. The passage of large tabular icebergs B-15A, B15-K and C16 (Figure 3.1), which were grounded near Ross Island and restricted the local ocean circulation from mid 2002 to mid 2005 (Robinson and Williams, 2012; MacAyeal et al., 2008) played a role in the observed sea ice conditions during the study period (Remy et al., 2008). Brunt et al. (2006) report that the influence of the iceberg passages was insufficient to cause the change in fast ice distribution alone and that increased storm activity was also influential. However the key role played by the icebergs was to prevent FY sea ice from being flushed out into the wider Ross Sea region (Brunt et al., 2006). The development of large areas of MY sea ice in the region is of particular interest because of the partially understood relationship between the outflow of ice shelf water and development of the sub-ice platelet layer (Gough et al., 2012). Sporadic measurements and word of mouth offer the only information on the changes in the MY sea ice regime. Satellite altimeter information is therefore invaluable for extension of the investigation.

The starting point of our analysis involves a manual ice classification for separating different sea ice types. The sea ice area was first masked for land and ice shelf by comparison with Envisat Advanced Synthetic Aperture Radar (ASAR) imagery yielding a

total size of 12,350 km^2 (Figure 3.1). This was fixed in size for the study. This area was then separated into MY and FY sectors for each year from 2003 to 2009. The MY sectors were defined by the landfast MY sea ice area in mid October of each year as indicated by ASAR imagery. The FY sector simply covered the remainder of the study area. This sector consisted of a FY landfast sea ice area and an area of FY drift ice to the north in which open water was common. The northern boundary of the study area was established at -76.5° (Figure 3.1). This location is north of McMurdo Sound itself but this step was undertaken to maximize the open water availability in the study area. ASAR Wide Swath imagery from mid October of each year shows that the MY landfast sea ice extent experienced a very large increase in area from 2004 to 2005 (Figure 3.2). A large area of FY fast ice attached to the western coastline of the study area persisted through the 2004 melt season into 2005 increasing the initial area of MY fast ice in 2003 from 1213 km^2 to 4293 km^2. In the following years this MY fast ice area experienced a gradual decline and by 2009 the area was 20 % greater than the original 2003 area. The classified FY and MY sectors were used to put the observed ICESat derived freeboard changes into perspective.

An additional component of the sea ice regime in the study area is the sub-ice platelet layer driven by the outflow of supercooled water from beneath the McMurdo Ice Shelf (Dempsey et al., 2010). The sub-ice platelet layer is a very porous mix of ice and sea water with solid fractions in the range of 0.2 to 0.5 (Gough et al., 2012). The appearance of a plume of ice crystals from underneath the McMurdo Ice Shelf progresses northward into McMurdo Sound with the eventual development of a sub-ice platelet layer later in the sea ice growth season (Gough et al., 2012; Mahoney et al., 2011). The sub-ice platelet layer is highly influential on sea ice formation processes in this area which is revealed by findings that up to 13 % of sea ice growth during winter in McMurdo Sound cannot be accounted for by conduction of heat from the ocean to the atmosphere (Purdie et al., 2006).

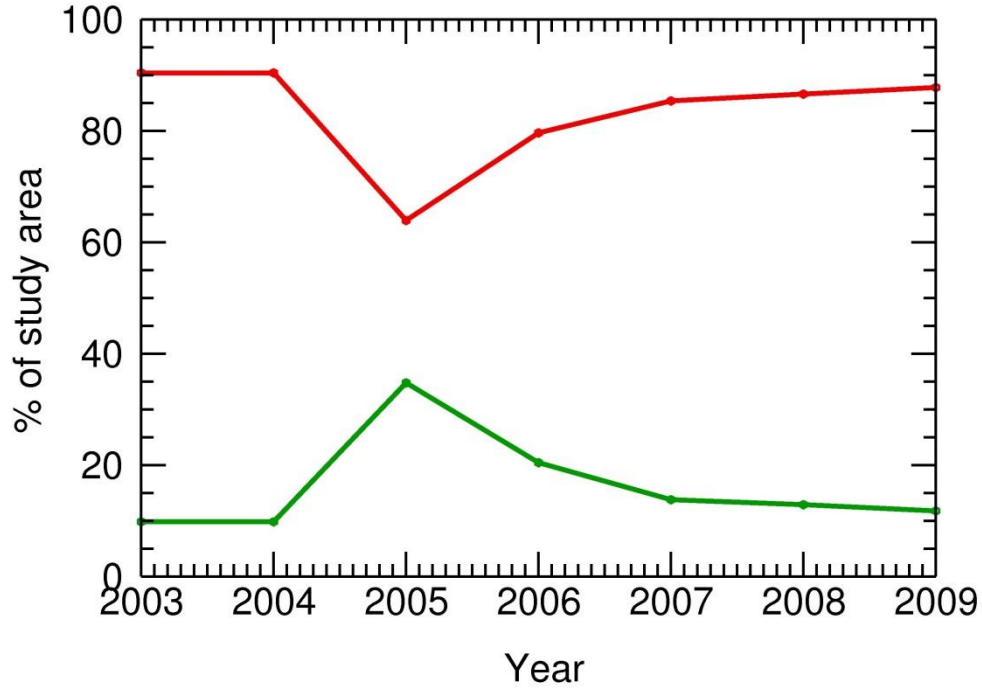

Figure 3.2. Percentage of study area covered by multiyear fast ice (green) and maximum possible cover of first-year sea ice (red) for the mid October period. The size of this total area is 12,350 km^2.

The snow cover on sea ice in McMurdo Sound is variable but decreases in general from the south-east to the north and west. Relatively high accumulation rates of snow in the eastern part of McMurdo Sound forced by local topographic features result in heavy snow loading atop of the sea ice cover. This forces negative sea ice freeboard. Interannual variations in snow depth add further uncertainty to the snow distribution. These factors restrict the ability to discern information about the sea ice unless good snow depth information is available.

3.3 Method-1 ICESat freeboard retrieval

ICESat's GLAS instrument operated at 40 Hz resulting in a footprint separation of approximately 172 m. The laser footprint size and shape exhibited variation during the mission with a mean major axis range between 51 m and 100 m and a range in eccentricity between 0.48 and 0.88 (Kurtz and Markus, 2012). General details of ICESat's operational information are presented in Yi et al. (2011). Of further interest, two additional sources of error have been announced by the ICESat Science Team, the Inter-Campaign Elevation Biases (I-CEB) and Error in the Range Determination from Transmit-Pulse Reference-Point

Selection (Centroid vs. Gaussian) termed G-C. No corrections are available on a shot-to-shot basis for either identified source of error at the time of writing. The I-CEB error is addressed by the relative measurement of Method-1 employed in this study. The comparison of our data set with the available information on campaign mean error values for G-C indicates that they are of little consequence to the findings of this study.

The following analysis is based on GLA 13 Records, Release 33 of the ICESat/GLAS data product, the latest data release at the time of writing. To extend the satellites operational period after the failure of Laser 1 in March of 2003 the two remaining lasers of the GLAS instrument were utilized in turn under 33-day to 56-day campaigns. Here, these campaigns are binned into September to December (S-D) and February to June (F-J) investigation periods.

Before any method for freeboard retrieval is applied, the success of the investigation is dependent upon the accuracy of the ICESat surface elevation retrieval. Scattering of the laser beam by clouds may introduce an elevation error which results in the sea surface appearing lower (Zwally et al., 2008). Corrections are applied in the literature (Kurtz and Markus, 2012; Zwally et al., 2008), notably the application of detector gain (*i_gval_rcv*) thresholds to remove data with a high likelihood of atmospheric scattering and a low signal-to-noise ratio (Kurtz and Markus, 2012). We find that we are able to obtain good comparison with in situ validation while using a less stringent criterion for removal of cloud affected data. However, to ensure the findings of this study were not biased by atmospheric influence, results under our less stringent criteria were compared to more conservative approaches. Upon application of filtering criteria where *i_gval_rcv* is less than 30 counts (60 counts for the low laser energy May-June 2004 period) 34 % of the data set is discarded. When the results are compared we find the linear trends in freeboard remain the same with r^2 values of 0.82 and 0.96 for the FY and MY assessments respectively. A single test case is also presented in Section 3.1 where usable data are lost under the more stringent criteria. These findings support excluding conservative cloud filtering methods for this study as they reduce the data that can be compared with in situ measurements and result in no change to the conclusions.

Thus, only the following corrections were applied to the ICESat data in this study to produce the ICESat derived elevation; (i) a pre-defined saturation correction

(*i_satElevCorr*) was applied to account for saturated waveforms – waveforms with very high energy causing low elevation estimates; (ii) all laser shots with reflectivity values (*i_reflctUncorr*) lower than 0.05 and higher than 1 were discarded because low and high reflectivity values are indicative of forward scattering and saturated signals, respectively (Yi et al., 2011). Using these criteria discards 19 % of ICESat data in the study region. Tidal corrections which are applied to GLA 13 Records are removed producing the true elevation profiles. This provides an ICESat derived elevation value (h_{ELEV}) which has been referenced to the WGS-84 ellipsoid.

As mentioned, the freeboard is relative to the local sea surface height. In this case the spaceborne retrieval of freeboard is hampered by the complexity of identifying the sea surface reference level over large ice covered areas void of leads.

The general equation for generating elevation above sea level (h_{asl}) from the ICESat derived surface elevation (h_{ELEV}) which takes account of environmental variables is given by:

$$h_{asl}(\lambda,\varphi,t) = h_{ELEV} - h_T - h_{IB} - h_{DOT} - h_G \quad (3.1)$$

where h_G is the geoidal height in reference to the WGS-84 ellipsoid which is represented here by the Earth Gravitational Model 2008 (h_{EGM08}). By assuming that the geoid represents the mean sea level, h_{asl} is given by taking account of the tide level (h_T) and by correcting for both the inverse barometric effect (h_{IB}) and the water level change due to dynamic ocean topography (h_{DOT}). In general, the sum of h_G, h_T, h_{IB}, and h_{DOT} is a variable function of geographic longitude (λ), geographic latitude (φ), and time (t) and not known at the required accuracy to retrieve sea ice freeboard. This can be circumvented by establishing the local sea level at tie points along-track identifying the ice free sea surface for each track individually. The steps used in this investigation to generate a sea surface reference level for the relative determination of freeboard closely follow Zwally et al. (2008), who use open water leads in the sea ice for this purpose. However, some amendments must be made because of the shape of the geoid and lack of open water in the southern part of the study area. h_{EGM08} depicts the general shape of the sea surface well (Figure 3.3) and produces a slight positive absolute bias in the region. The mean deviation of h_{EGM08} from h_{ELEV} is + 1.81 m. The range of h_T in McMurdo Sound is approximately 1 m. The contribution from h_{IB} and h_{DOT} does not account for the remaining observed deviation and therefore the

h_{EGM08} does not provide the required accuracy to be used directly as a mean sea surface reference. However, a first approximation of the sea surface, h, is given by subtracting h_{EGM08} from h_{ELEV}.

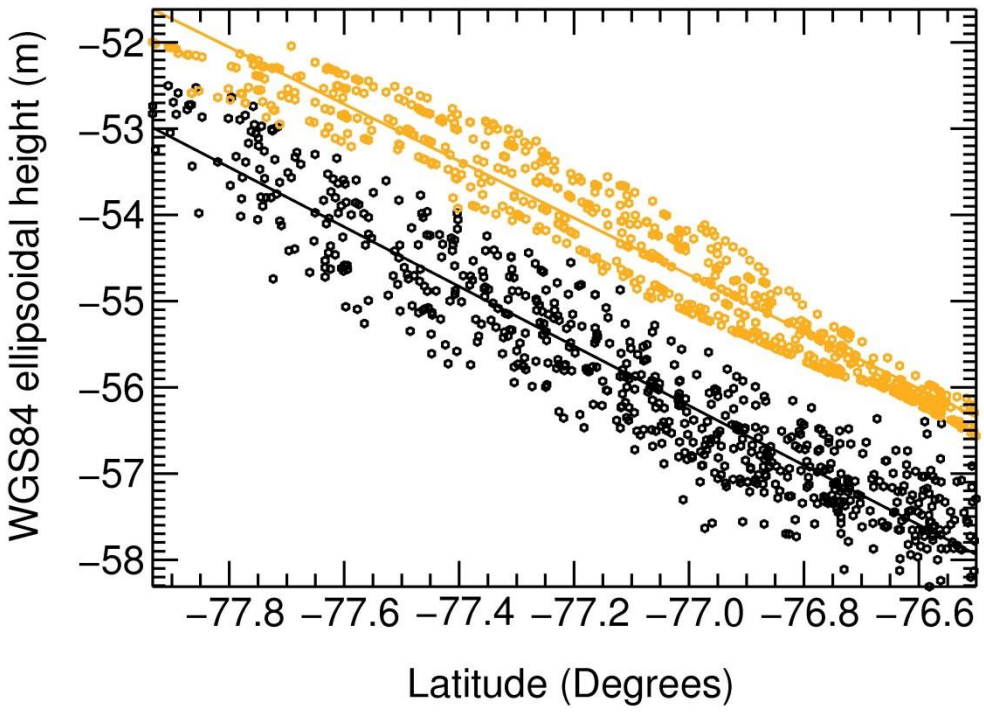

Figure 3.3. Systematic sampling of every 100th h_{ELEV} (WGS84 referenced ICESat surface elevation) value (black) and Earth Gravitational Model 2008 value referenced to WGS84 (orange) in the study area 2003-2009.

Expected elevation changes are present at the southern end of the elevation profiles from the FY-MY sea ice transition. However, many tracks exhibit a large positive deviation in h in the north, a direct consequence of residual errors from usage of h_{EGM08}. This is addressed by application of a polynomial fit to the FY sea ice section (Figure 3.4b). The fit was halted at the FY-MY sea ice transition and the coefficients of the closest FY value were maintained for the MY retrievals which avoided disrupting the ice type transition. If the fit was applied to complete tracks the MY sea ice freeboard would be underestimated. The fit is then subtracted from each elevation track giving a corrected surface elevation (h_c).

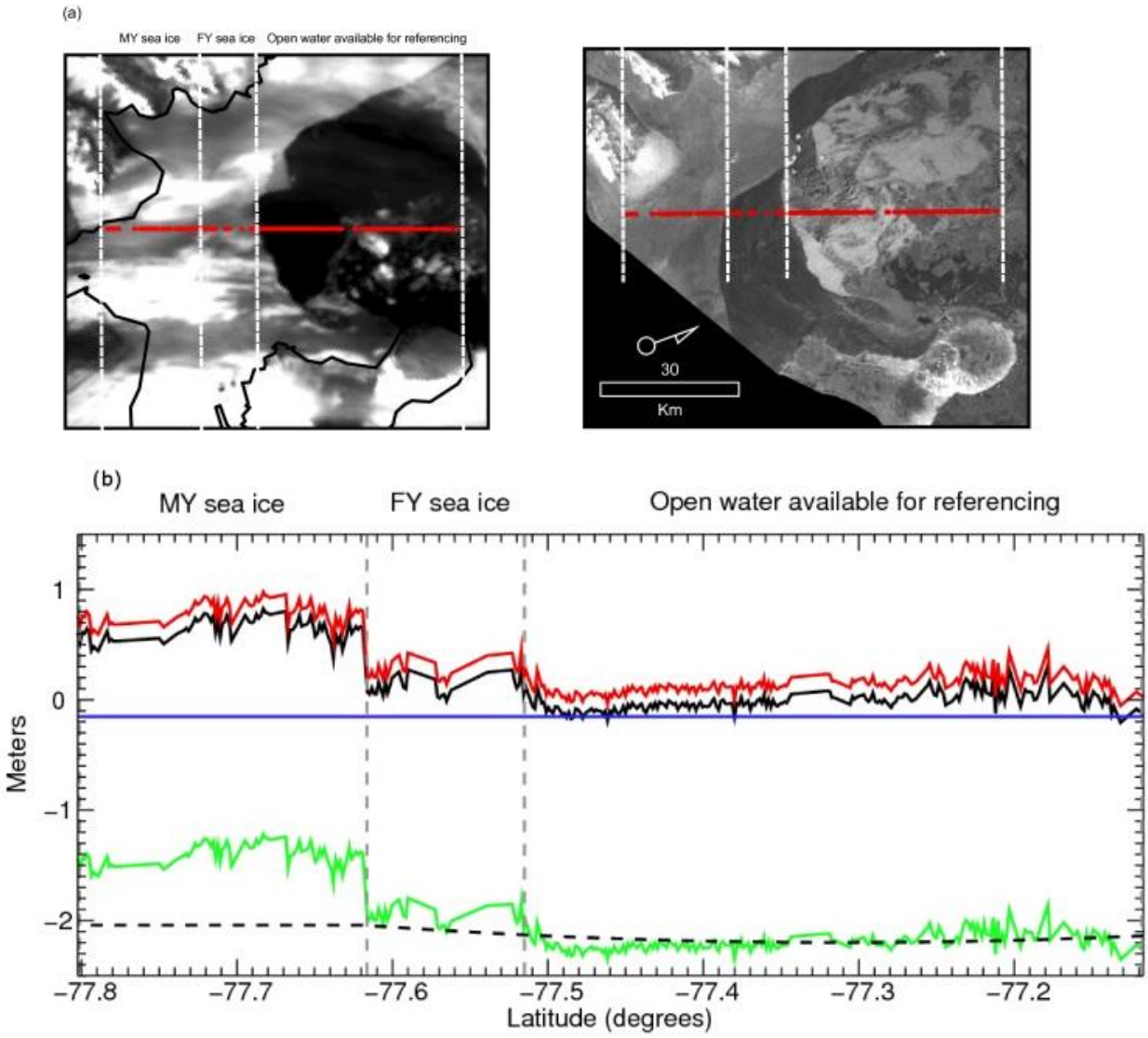

Figure 3.4. Illustration of typical processing steps for Method-1. (a) Near coincident ICESat track (red line) at T = 25/11/2006 0722 UTC with MODIS at T - 19 hours (upper left) and Envisat ASAR at T - 12 hours (lower left) imagery. (b) Initial estimation of the sea surface (h, green) with 2nd order polynomial fit overlaid (dotted black), fitted estimate of the sea surface (h_c, black), 5 % sea surface reference value (h_s, blue), and freeboard (Fb, red). MODIS (partly cloud covered) shows open water to the north of the fast ice area, confirmed by high backscatter in the ASAR image as a result of increased surface roughness driven by wind, successfully identified as reference sea surface height. The ASAR image also allows discrimination of first-year and multiyear sea ice.

For obtaining surface elevation above sea level, h_c still needs to be referenced to the sea surface (Kwok et al., 2006; Kwok et al., 2004). This step of the method relies on the assumption that the lowest elevation retrieval along an ICESat track represents the sea surface. The elevation profile h_c is therefore sampled for its lowest elevation retrievals. We assumed the sea surface to be represented by the mean of the lowest 5 % of elevation measurements along each track. The selection of a percentage value for this purpose may be case dependent as a value that is too low will result in insufficient samples producing reference values with large error. High values increase the risk of including sea ice. Zwally et al. (2008) used a 2 % value and reported that an optimized value will be presented as our knowledge of the distribution of leads in the Southern Ocean improves. 5 % has been selected here as the data count was much lower than available in large scale assessments. In our small scale study it is critical to ensure that tracks with small numbers of elevation retrievals may be kept rather than discarded. This methodology filters out any tracks which are unable to produce at least 3 lowest elevation retrievals i.e. tracks that have less than 60 individual elevation retrievals. Other percentage thresholds were trialed, however the value of 5 % produces the best agreement between ICESat derived freeboards and in situ measurements in 2009.

Using the mean of the lowest 5 % of elevation retrievals, this value (h_S) is then subtracted from h_c giving a freeboard (Fb) value:

$$Fb = h_c - h_s \tag{3.2}$$

The method is displayed graphically in Figure 3.4 overlaid upon near coincident ASAR and MODIS imagery.

3.4 Evaluation of ICESat freeboard retrieval

In March 2003 an ICESat repeat pass on track 119 (Figure 3.1) were able to clearly identify the icebreaker channel cut into the sea ice to reach the United States Antarctic Program's McMurdo Station. The repeat pass is separated by 16 days and 400 m, and the surface elevation profile and the laser reflectivity is shown in Figure 3.5. The passage of a fuel tanker on 03/03/2003 and in situ observations on the same day (Purdie et al., 2006) as the

first overpass on 04/03/2003 ensured open water or very thin ice was present in the icebreaker channel. A drop in ICESat derived surface reflectivity from approximately 0.65 to 0.30 also indicates a well-defined change at the surface (Figure 3.5a).

The second profile's reflectivity, 16 days later on the 20/03/2003 gives little indication of such change, indicating the surface has become more homogeneous (Figure 3.5b). Visible MODIS imagery indicates a slight whitening of the icebreaker channel at this time indicative of ice growth and potentially a thin snow cover. From measurements of Purdie et al. (2006) we know that the FY sea ice in the ice breaker channel grew by 0.5 m between 04/03/2003 and 20/03/2003. This ice would be expected to have a freeboard of approximately 0.04-0.05 m for densities typical of the region.

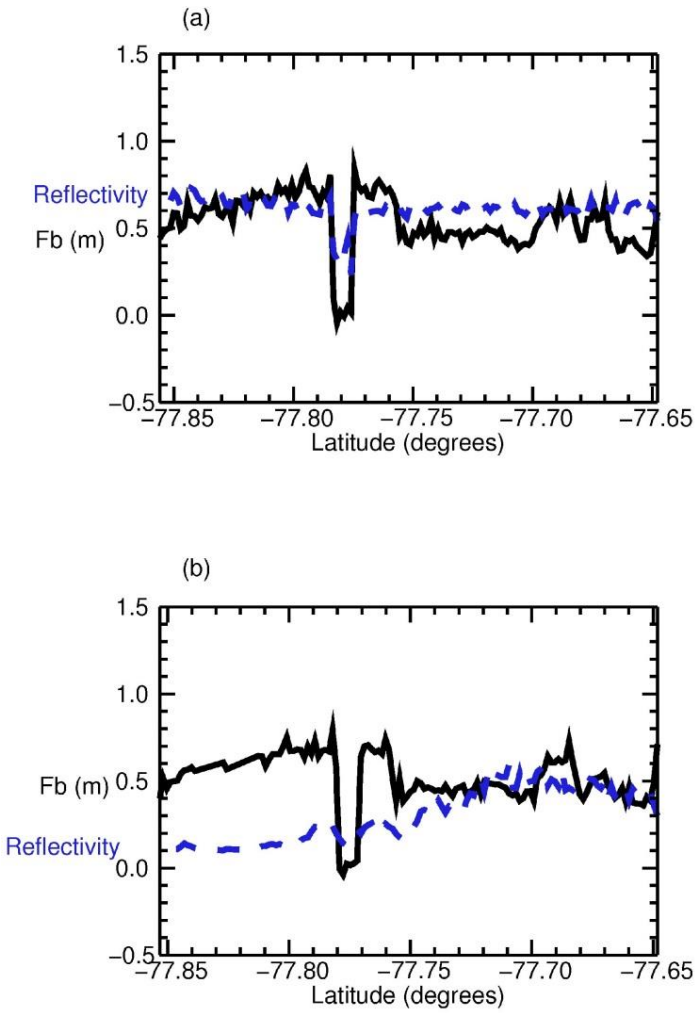

Figure 3.5. ICESat freeboard and reflectivity at (a) 04/03/2003 0239 UTC and (b) 20/03/2003 0209 UTC. The icebreaker channel is clearly identifiable as the decrease in the multiyear sea ice freeboard.

Weather records at McMurdo Station about 2 hours before each ICESat overpass indicate that cloud cover was far greater with 7/8 on the 20/03/2003 than on the 04/03/2003 with 1/8, no information is provided on cloud type. With regard to the ICESat cloud correction criteria mentioned previously, upon application of more stringent correction criteria half of the profile on 20/03/2003 (significant cloud cover) is discarded. Using the mean of the h_{ELEV} values for each track the remaining difference in elevation after accounting for tide and the inverse barometer effect is 0.10 m, which is at least in part attributed to atmospheric forward scattering due to clouds (Fricker et al., 2005). The interference from cloud in this example track, with appreciation of the 400 m spatial separation is considered small. It is clearly shown in Figure 3.5 that ICESat can still perform well with the chosen moderate cloud filtering approach. Useable data would be lost if more stringent correction criteria were to be applied.

The freeboard at the MY ice boundary with the icebreaker channel as calculated from the mean of the 5 nearest h_{ELEV} retrievals to open water is 0.75 m on the 04/03/2003 and 0.70 m on the 20/03/2003. The decrease in freeboard is attributed to the fact the open water reference level had become ice covered giving a lower apparent freeboard on the 20/03/2003. Thus the icebreaker channel, which was ice covered but still representative of the lowest 5 % of elevation retrievals causes a false decrease in freeboard of the surrounding MY sea ice of 0.05 m.

ICESat repeat passes and crossover points were compared to assess the methods' freeboard retrieval accuracy. As each track generates its freeboard independently, comparison at designated points allows an assessment of the accuracy of the method. At comparison points where the temporal separation is less than 50 days, the mean freeboard retrieval within a radius of 850 m is derived. The repeat pass tracks and crossover points are displayed with the end of summer fast ice edges for each year (Figure 3.6a and Gough 2012). Values for repeat pass and crossover tracks are displayed as pairs in Figure 3.6b. A separation of points indicates a change in freeboard at that location within the 50 day time segment and/or an error in freeboard retrieval. It is possible that changes in freeboard are caused by environmental variables as opposed to method error. In an attempt to reduce this possibility, the crossover and repeat pass locations were selected at sites with established ice covers where change was expected to be minimal. Indicated by the crossover and repeat pass analysis is a mean freeboard error of 0.13 m.

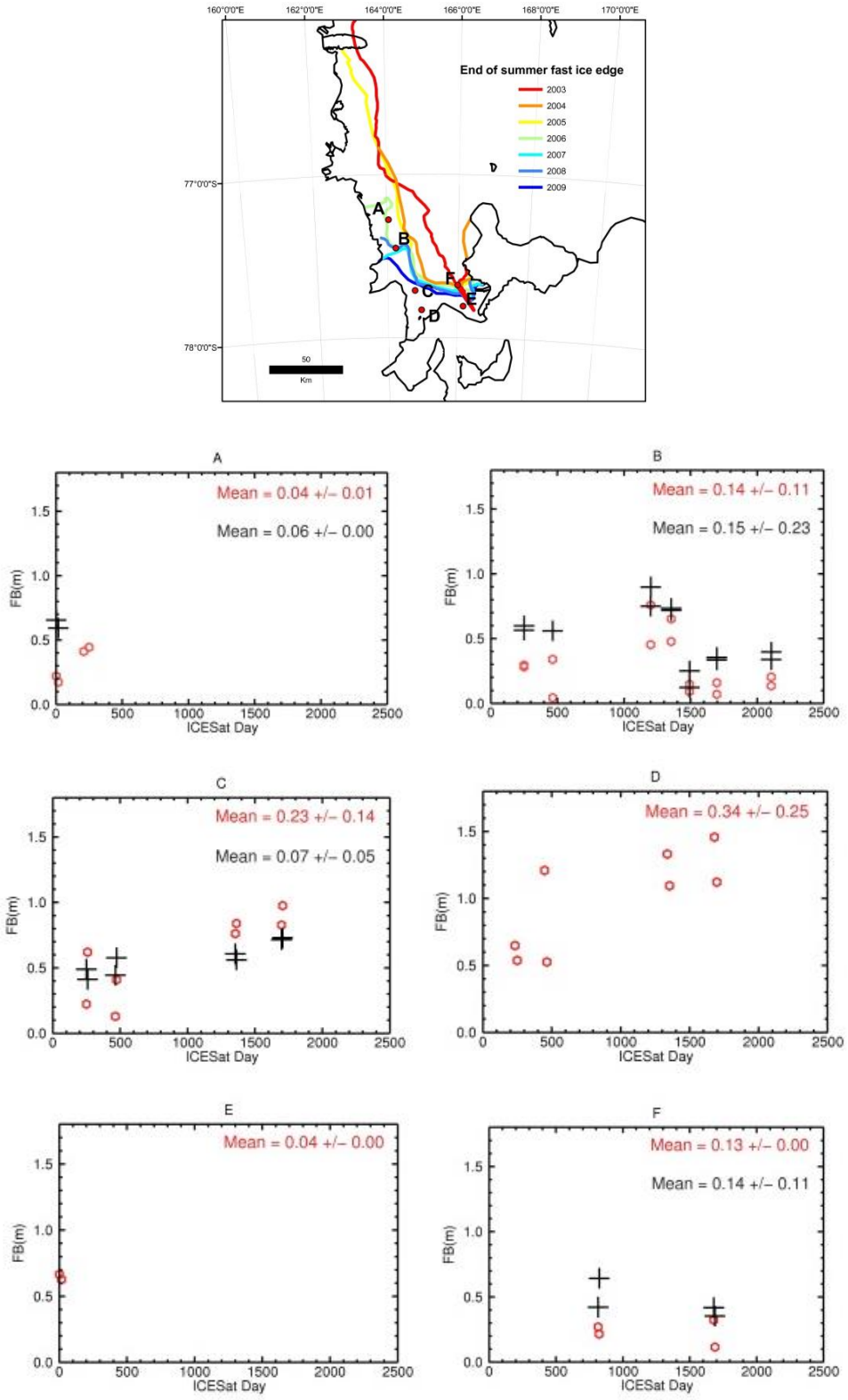

Figure 3.6. Repeat pass and crossover analysis for points A-F from ICESat Day 1 (3/03/2003) - 2500 (06/10/2009). The freeboard difference at each comparison point for Method-1 (red circles) and Method-2 (black crosses) are displayed. Statistics describe the mean and standard deviations of the separation for the crossover/repeat pass for each method. No data for Method-2 are available at crossover and repeat pass sites D and E due to unavailability of tide data.

3.5 Method-2 ICESat freeboard retrieval

Method-2 was developed for measurement of sea ice freeboard in McMurdo Sound for comparative purposes. The same filtering criteria for atmospheric influences were applied to this method as described for M-1 (see Section 3.3). This method attempts to construct a sea surface reference level for each ICESat h_{ELEV} value from auxiliary information without usage of the ICESat elevations along each track. However as a first step, a mean sea surface (MSS) height was constructed which was achieved by using ICESat elevation retrievals over open water areas identified by manual comparison with near-coincident MODIS imagery. 19 points were identified evenly distributed across the sound from 2003-2009. Ice floes were sometimes present in the areas of interest and potential interference would cause false open water retrievals. To reduce the possibility of inclusion of sea ice, ICESat reflectivity was also taken into consideration. Since reflectivity values of less than 0.5 were observed over areas where we are confident there was sea ice (see Figure 3.5b), potential open water retrievals were documented only if ICESat reflectivity was less than a conservative 0.3.

Given the variation of the shot-to-shot ICESat elevation measurement can be considerable (mean variation here recorded as 0.09 m) it is insufficient to use a single elevation measurement to represent the sea surface height. Using the mean of three ICESat elevation retrievals over the open water area reduced the noise in the elevation measurement and smoothed the SSH variations for each point.

This mean value was then adjusted for tide (h_T) and the inverse barometer effect (h_{IB}). The Circum-Antarctic Tide Simulation (CATS2008a_opt) (pers. comm. L. Padman, 2008) and Load Tide Model (Egbert and Erofeeva, 2002) heights were applied to account for the tidal variation around the MSS. Variation due to atmospheric pressure loading was corrected using available data from the New Zealand Scott Base (SCTB) Automatic Weather Station (-77.85°, 166.75°). A mean sea level pressure of 989.48 hPa was calculated by averaging the hourly recorded sea level pressure at this station during the ICESat investigation (03/03/2003-06/10/2009). The difference between the mean sea level pressure and the

observed sea level pressure at the time of the ICESat recorded elevation was then used for applying a correction to the MSS of 0.01 m hPa^{-1} (Padman et al., 2003). A MSS height was also established at SCTB and Cape Roberts (CPRB) by averaging the tidal height from tide gauges at those locations over the study period.

The 19 corrected ICESat elevation retrievals and 2 tide gauge data sets were then interpolated with a second order polynomial trend. Upon establishment of a MSS grid, SSH was then estimated in temporal and spatial coincidence for each ICESat elevation retrieval using the same source of modelled tidal and measured atmospheric information as described above. The resolution of CATS2008a_opt (4 km) resulted in certain ICESat elevation retrievals being lost as ICESat retrievals near the coast were incorrectly identified as land providing no tidal components. 6 % of elevation retrievals were therefore discarded. The ocean tide component provided by CATS2008a_opt is the largest source of error. The tidal simulation was compared to the measured tide height at SCTB with inclusion of Load Tide and the inverse barometer correction (Figure 3.7). The mean tidal height difference over the one month of October 2003 was 0.01 m. However the error on an individual measurement was as high as 0.14 m. The actual SSH is therefore provided by:

$$SSH = MSS + h_T + h_{IB}, \tag{3.3}$$

and the freeboard is calculated by

$$Fb = h_{ELEV} - SSH, \tag{3.4}$$

where h_{ELEV} is the previously discussed ICESat measured surface elevation.

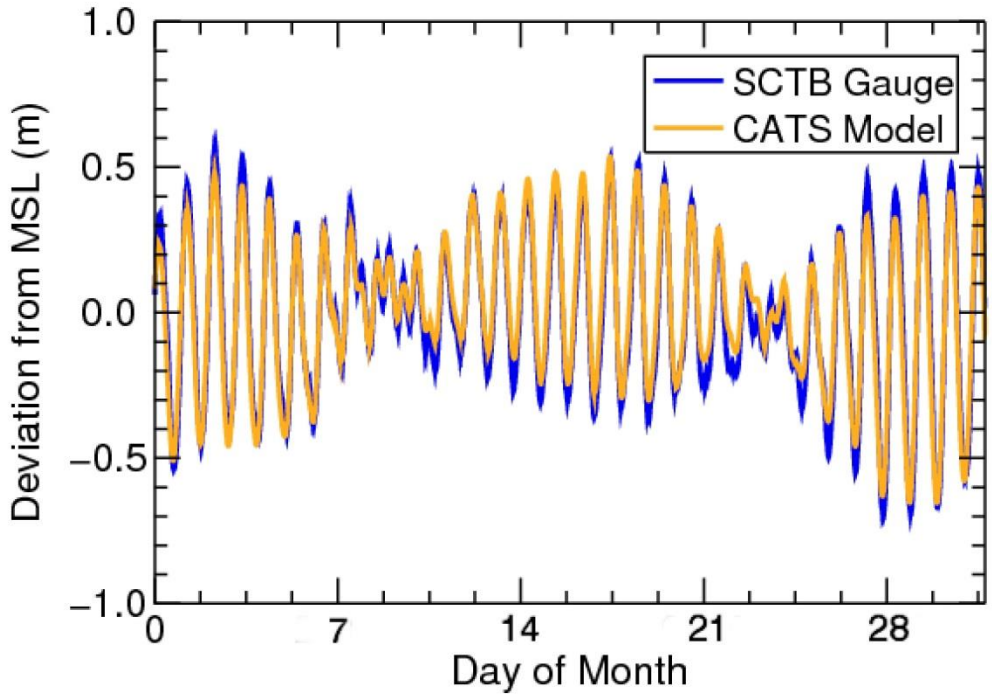

Figure 3.7. Comparison of measured tidal height around mean sea level at the Scott Base tide gauge with Circum-Antarctic Tidal Simulation CATS2008a_opt (Load Tide TPX06.2 and inverse barometer correction applied) for October 2003. The mean difference between the two data sets is 0.01 m with a maximum error of 0.14 m.

3.6 Freeboard in McMurdo Sound 2003-2009

The two investigation periods, September to December (S-D) and February to June (F-J) had two spatial components with regard to freeboard. First the sea ice was assessed for FY only and second for MY only. Results are reported by sea ice type in each investigation period and for each method, M-1 (black) and M-2 (grey) (Table 3.1 and Table 3.2). Data availability was far less in 2009 due to a decrease in the operational days of the laser on-board ICESat. Helicopter lidar data from the 2009 fieldwork campaign, as described in Section 6 are provided in support of the ICESat observed trends.

Table 3.1. Mean September-December (S-D), first-year and multiyear freeboard with standard deviations (1σ) and the number of individual ICESat h_{ELEV} values (N) used to derive the mean. Method-1 freeboard retrieval results are shown in black and Method-2 in grey. Helicopter lidar (HL) measurements (blue) are also displayed for comparison.

September-December Freeboard				
Year	MeanFY (m)	N(h_{ELEV})	Mean MY (m)	N(h_{ELEV})
2003	0.27 (±0.17)	6890	0.53 (±0.32)	674
	0.07 (±0.31)	6465	0.39 (±0.18)	513
2004	0.19 (±0.14)	4679	0.40 (±0.21)	209
	0.39 (±0.34)	4490	0.62 (±0.05)	159
2005	0.20 (±0.15)	3697	0.55 (±0.35)	702
	0.30 (±0.26)	3686	0.73 (±0.25)	643
2006	0.19 (±0.12)	4299	0.85 (±0.28)	969
	0.09 (±0.30)	4226	0.71 (±0.27)	815
2007	0.20 (±0.13)	5082	0.93 (±0.30)	951
	0.09 (±0.27)	4994	0.75 (±0.23)	871
2008	0.25 (±0.14)	3755	0.91 (±0.34)	585
	0.13 (±0.32)	3707	0.71 (±0.20)	501
2009	0.25 (±0.13)	1464	1.00 (±0.30)	135
	0.13 (±0.15)	1074	0.95 (±0.32)	135
	HL = 0.18 (±0.25)		*HL = 1.39 (±0.79)*	
	Lidar samples = 2234		*Lidar samples = 3383*	

Table 3.2. Mean February-June (F-J), first-year and multiyear freeboard with standard deviations (1σ) and the number of individual ICESat h_{ELEV} values (N) used to derive the mean. Method-1 freeboard retrieval results are shown in black and Method-2 in grey. Helicopter lidar (HL) measurements (blue) are also displayed for comparison.

February-June Freeboard				
Year	Mean FY (m)	N(h_{ELEV})	Mean MY (m)	N(h_{ELEV})
2003	0.18 (±0.12)	4412	0.56 (±0.44)	353
	0.11 (±0.38)	3144	0.46 (±0.26)	297
2004	0.25 (±0.15)	6149	0.70 (±0.40)	525
	0.14 (±0.33)	6026	0.49 (±0.18)	452
2005	0.20 (±0.13)	5771	0.47 (±0.33)	1483
	0.27 (±0.31)	5694	0.57 (±0.25)	1374
2006	0.19 (±0.12)	5198	0.81 (±0.19)	850
	0.12 (±0.30)	5121	0.70 (±0.21)	768
2007	0.19 (±0.11)	3969	0.93 (±0.18)	599
	0.13 (±0.29)	3904	0.78 (±0.37)	550
2008	0.18 (±0.10)	892	1.36 (±0.06)	28
	0.06 (±0.38)	851	0.48 (±0.26)	26
2009	0.28 (±0.15)	1611	1.16 (±0.51)	3
	-0.01 (±0.29)	1577	1.06 (±0.00)	1
	HL = 0.18 (±0.25)		*HL=1.39 (±0.79)*	
	Lidar samples = 2234		*Lidar samples = 3383*	

Analysis was carried out on the FY and MY sea ice sectors separately because of differences in thickness and behaviour. The two freeboard retrieval methods show good agreement with respect to the MY freeboard linear trend (Figure 3.8). The mean MY freeboard from 2003-2009 increased from 0.53 m to 1.00 m for the S-D period and from 0.56 m to 1.16 m for the F-J period under M-1. M-2 showed mean MY freeboard increasing from 0.39 m to 0.95 m for the S-D period and 0.46 m to 1.06 m for the F-J period (Figure 3.8). The standard deviations (from 0.18-0.51 m) are listed together with mean values in Tables 3.1 and 3.2. Using the Mann-Kendall trend test with a significance value (α) of 0.05, significant positive trends of 0.108 my^{-1} are identified for the linear regression of the MY time series under M-1 (p value = 0.000) and 0.069 my^{-1} under M-2 (p value = 0.003). A bias between the mean values of ICESat derived freeboard and HL derived freeboard is expected as neither temporal nor spatial coincidence was achieved. However, the ICESat derived mean freeboard for FY and MY sea ice in 2009 falls within one standard deviation of the HL data set for both methods (Figure 3.8). No statistically significant trends are identified for FY sea ice for either method.

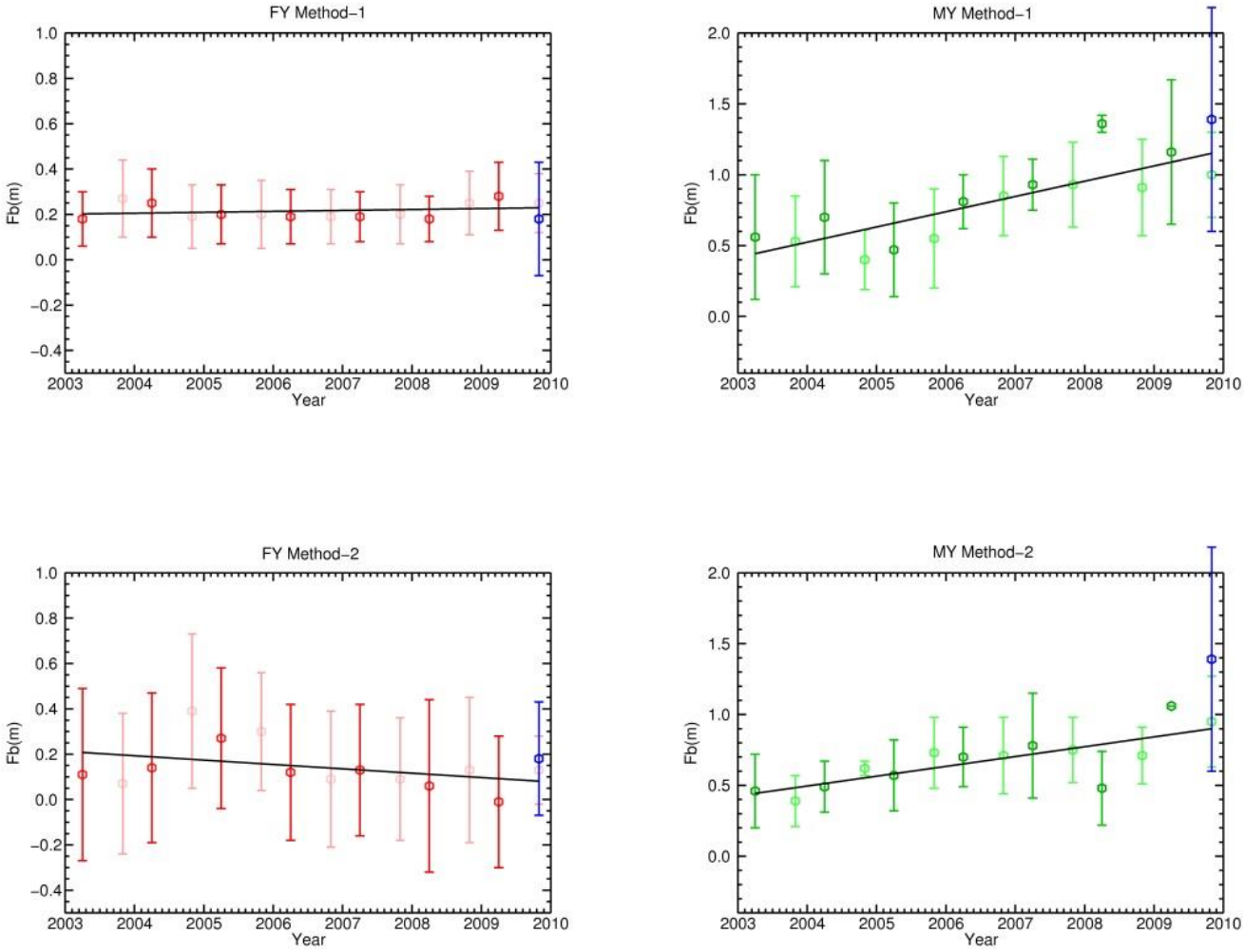

Figure 3.8. First-year (red) and multiyear (green) freeboard for Method-1 and Method-2 with complementary helicopter lidar data (blue) for 2009.

To remove any influence of a changing MY sea ice area during the study, the initial 2003 MY sea ice area (shown in Figure 3.11) was segmented and assessed alone for each year (Figure 3.9). M-1 indicates a significant positive trend in the linear regression of 0.135 my^{-1} in MY freeboard from 0.52 ± 0.44 m to 1.10 ± 0.18 m (p value = 0.000) and M-2 also indicates a significant positive trend of 0.068 my^{-1}, MY freeboard increasing from 0.45 ± 0.26 m to 1.12 ± 0.17 m (p value = 0.020).

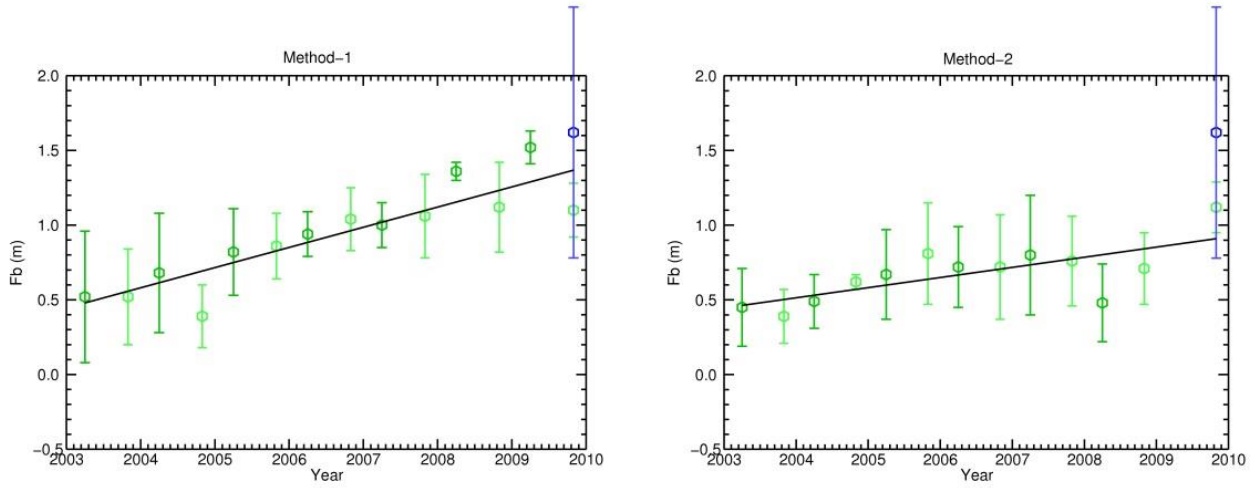

Figure 3.9. Method-1 and Method-2 freeboard trends for 2003-2009 for the 2003 multiyear sea ice area only. The 2009 helicopter lidar data (blue) are also displayed. No data were available for the 2009 February to June Method-2 investigation.

The temporal and spatial variation of freeboard across McMurdo Sound is plotted against geographic longitudinal degrees in the scatter plot in Figure 3.10. A FY sea ice freeboard (black dots) of around 0.21 m is typical for all years. The freeboard of MY sea ice (coloured dots) increases with time and shows a peak in the freeboard distribution around the geographic longitude of 165° east. This peak is centered upon the area of the sound exhibiting the greatest abundance of platelet ice (Dempsey et al., 2010).

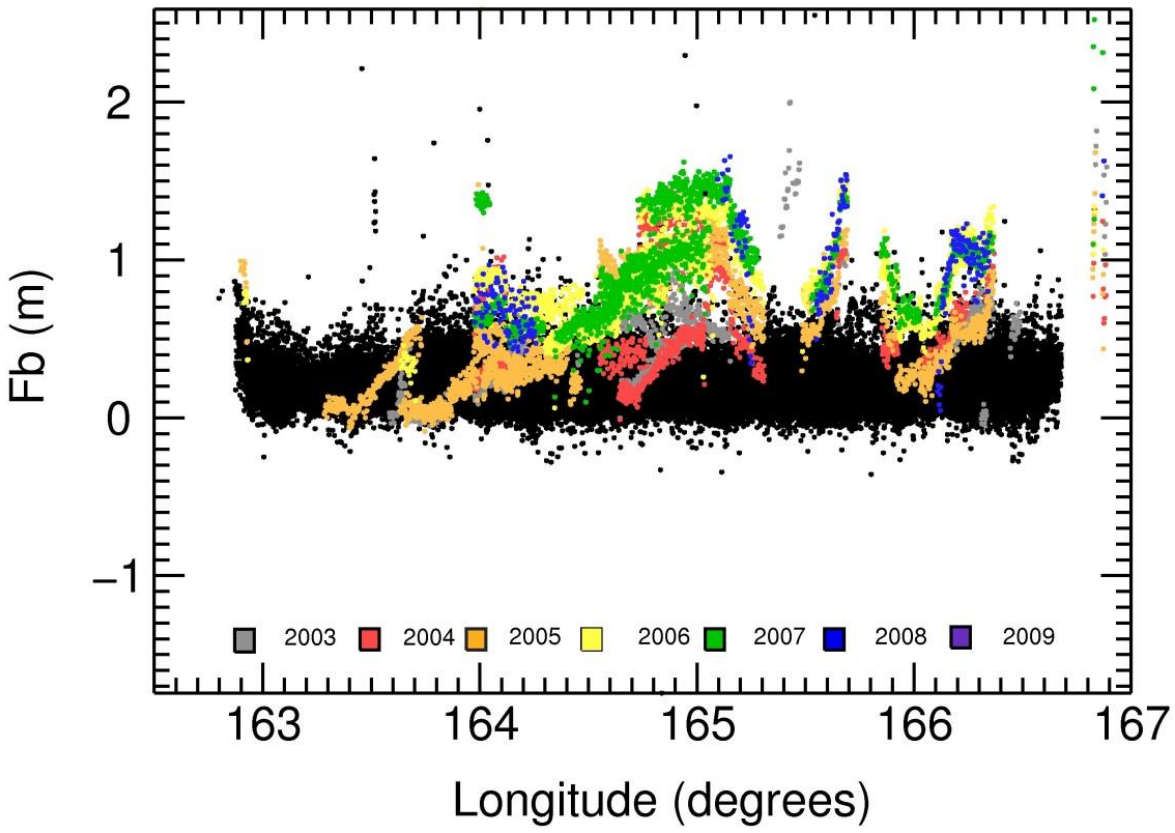

Figure 3.10. Freeboard as a function of geographic longitude across McMurdo Sound using Method-1. Colored data represent multiyear sea ice for each year, the black data first-year sea ice. A distinct peak in multiyear freeboard and its change is identified centered around 165°.

Along-track analysis provides a good overview of freeboard trends but sampling is restricted aerially. To extend our insight of the total area under investigation we aim to generate information between tracks. Here we fill in these gaps using a Natural Neighbour interpolation method to generate freeboard maps of the MY sea ice areas for each year for M-1 (Figure 3.11). The typical inter-track spacing is 10 km with a maximum interpolation distance of 30 km. This analysis provides a good overview of MY sea ice freeboard and distribution for each year and permits visualization of the changes during the study. An example is provided by the large increase in MY sea ice area in 2005. The expansion of the MY sea ice area resulted in the development of a younger MY sea ice cover in the western sound with a mean freeboard lower than that of the older MY ice in the south (Figure 3.11).

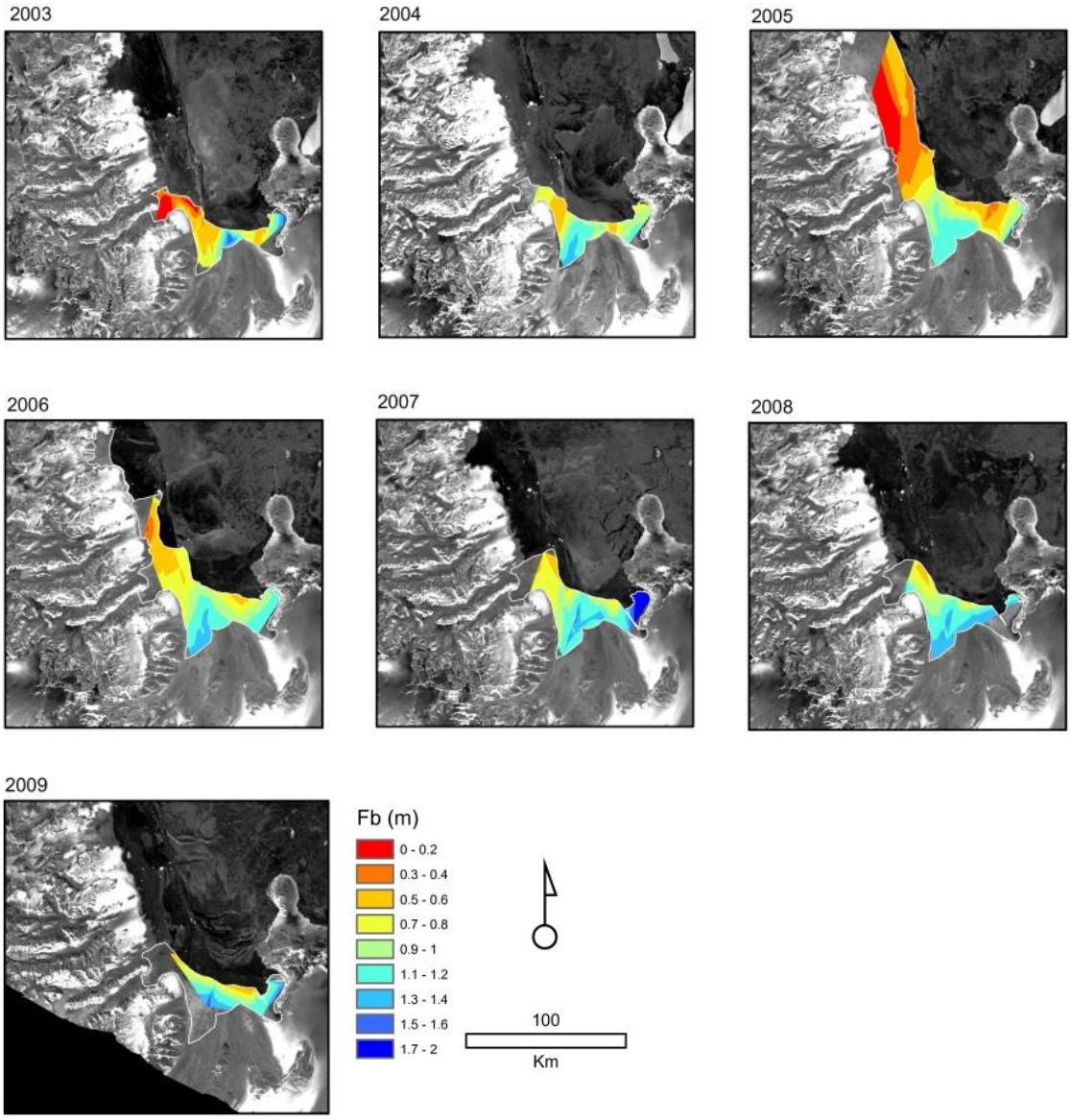

Figure 3.11. The multiyear sea ice areas with interpolated freeboard maps for 2003-2009 for Method-1 displayed upon a mid October Envisat ASAR image. The multiyear areas (white line) without colour coding were outside the interpolation area.

3.7 Comparison with airborne measurements and in situ information

Helicopter-borne electromagnetic induction sounding (EM) measurements were carried out in November 2009 recording approximately 1000 km of sea ice thickness profiles. EM sounding allows for the determination of sea ice thickness at close range with accuracies of ± 0.1 m over level sea ice (Haas et al., 2010). Making use of the strong electrical conductivity contrast between ice and seawater, the ice-ocean interface is identified. Using a lidar on the instrument the air-snow interface is also identified, the difference between the two distances giving total thickness (ice-plus-snow) measurements. Fixed to a cable and mounted below a helicopter, and termed the EM-Bird, spatial sampling can be greatly increased. The EM method encounters footprint issues when the ice is deformed (Haas et al., 2009). The level ice of McMurdo Sound is optimal for assessment under EM sounding methods due to the absence of rough deformed ice.

In addition, the EM-Bird's single beam lidar (HL) was used for freeboard retrieval. The nadir pointing laser produces a footprint of a few centimeters from the optimal flying altitude of 20 m. The nearby SCTB GPS base station was used to differentially correct the EM-Bird position. This positioning ability was utilised with the lidar to obtain surface elevation. HL elevations were acquired at 100 Hz and sampled by averaging to the 1 Hz GPS time. The 1 Hz freeboard was calibrated using the nearest in situ drill-hole measurements which were located within about 100 m of the flight tracks. This permitted two laser based methods to be compared with regard to freeboard retrieval as this field information was obtained during the last ICESat campaign in the region.

Freeboard distributions from ICESat and the HL have two peaks under all methods which are caused by the presence of FY and MY sea ice (Figure 3.12a). The HL derived freeboard is considered more accurate than the ICESat derived freeboard as it has been calibrated with drill-holes along the helicopter flight path. Results show that in general ICESat overestimates FY freeboard and underestimates MY freeboard for both methods. Respectively, for the ICESat M-1, M-2 and HL investigations over the FY sea ice area mean freeboard values of 0.31 ± 0.10 m, 0.27 ± 0.17 m and 0.18 ± 0.25 m are recorded and over the MY sea ice 0.99 ± 0.30 m, 0.95 ± 0.32 m and 1.39 ± 0.79 m. HL data acquired in November 2009, with drill-hole freeboard measurements and ICESat data recorded

approximately 5 weeks earlier are displayed in Figure 3.13. ICESat measured freeboard is then converted to sea ice thickness (*T*) following Zwally et al. (2008) and using measured and estimated densities for snow (ρ_s), water (ρ_w), and ice (ρ_i) typical of the study region:

$$T = \frac{\rho_w}{\rho_w - \rho_i} Fb + \frac{\rho_w - \rho_s}{\rho_w - \rho_i} T_s \quad (3.5)$$

ρ_s = 380 kg m^{-3}
ρ_w = 1027 kg m^{-3} (Mahoney et al., 2011)
FYρ_i = 920 kg m^{-3}
MYρ_i = 900 kg m^{-3}

Sea ice and snow density values were defined from multiple field measurements. Taking the reported ρ_i from Gough et al. (2012) of 934 kg m^{-3} and multiple ρ_i measurements in McMurdo Sound from the 1990s (unpublished data) a mean value is rounded to 920 kg m^{-3} for FYρ_i. Timco and Frederking (1996) report that the MY sea ice density below the water line is similar to that of FY sea ice, but above the waterline densities vary from 720 kg m^{-3} to 910 kg m^{-3}. We take a lower estimate of 750 kg m^{-3} MYρ_i above the waterline given the MY sea ice had existed through multiple melt seasons (see Section 3.7). Splitting the ice thickness at a ratio of 0.1 above to 0.9 below the waterline gives a rounded MYρ_i of 900 kg m^{-3}. Snow depth (T_s) information was available from the 2009 in situ measurements. For the application of T_s to the ICESat derived freeboard the mean percentage of the freeboard (Fb) that was snow for the 2009 in situ measurements was applied to the ICESat freeboard. The mean value for snow depth for FY freeboard was calculated as 26 % and 57 % for MY ice. These values were taken as representative of snow depth on the two ice types in McMurdo Sound for austral spring 2009.

We conducted an error analysis to estimate the expected error for the sea ice thickness determination. Following Spreen et al. (2006) equation number 6 we used the same density values provided above with uncertainties of 2 % and 15 % for ρ_i and ρ_s, respectively. The uncertainties for ρ_i are given by the standard deviation of ρ_i measurements in the 1990s and those for ρ_s by field measurements in November of 2011. We assume the uncertainty in ρ_w to be negligible and the uncertainty in T_s to be 50 %. The uncertainty in T_s is derived from a snow variability assessment in the same area in 2011. Assuming independent and random

errors, the main contributor to the total error in the resulting thickness is the freeboard. The ICESat surface elevation accuracy from shot-to-shot should be reduced using our crossover and repeat pass analysis which uses between 5 and 10 individual shots to derive each mean. We expect a large component of the reported standard deviations to be a result of natural variability in the surface elevation. This is supported by the in situ measurements in 2009 (Figure 3.13) which confirm changes in freeboard of 0.10 m over distances of 5 km. We expect any errors to be reduced upon consideration of the entire ICESat data set. A prime example is provided by the comparison of in situ measurements and ICESat for the S-D 2009. The mean freeboard for FY sea ice from each method falls within one standard deviation of the average for FY sea ice freeboard from 12 in situ measurements in November 2009 of 0.25 m. Under M-1, mean freeboards agree within 0.01 m. The crossover and repeat pass analysis along with our in situ comparison offer the only information on the freeboard retrieval accuracy. For the estimated error we report the crossover and repeat pass analysis freeboard separation for a worst case error estimate. The crossover and repeat pass analysis indicates that the combined mean separation at comparison points for both methods is 0.13 m. Given a typical FY freeboard of 0.25 m this introduces an error of 1.31 m for sea ice thickness. For a typical MY freeboard of 0.66 m an error of 1.52 m is expected.

Upon comparison of EM thickness and ICESat derived thickness (Figure 3.12b) for the same campaign as the HL-ICESat comparison, the large range in sea ice thickness within McMurdo Sound from thin FY sea ice (2 m) to very thick MY sea ice (10 m) is identified by the EM-Bird. Thicker ice is also identified between 10-15 m thick which is not detected by either ICESat method. The ICESat methods both identify two sea ice distributions around 2 and 6 m in thickness in agreement with expected FY and MY thicknesses respectively. Respectively, for the ICESat M-1, M-2 and EM investigations over the FY sea ice area mean thickness values of 2.46 ± 0.78 m, 2.14 ± 1.38 m and 2.98 ± 0.88 m are recorded and over the MY sea ice 6.12 ± 1.85 m, 5.86 ± 1.95 m and 9.21 ± 2.87 m. The higher mean value for the EM investigation over FY sea ice is attributed to the peak in the distribution around 4 m in thickness (Figure 3.12b). Direct comparison with our in situ data showed that this peak is likely caused by interference from the sub-ice platelet layer causing an overestimation of the total EM derived thickness using standard processing (Haas et al., in prep). The FY sea ice thickness peaks from the ICESat methods and EM methods fall within ± 0.5 m of one another. The two independent methods can be used here as a measure

of the thickness retrieval capability of ICESat. With regard to the MY sea ice cover the thicker distribution identified by the EM investigation, which is indicated by the higher mean thickness of the MY area is attributed to the larger area sampled under this investigation including regions of much thicker ice in the south-western sound.

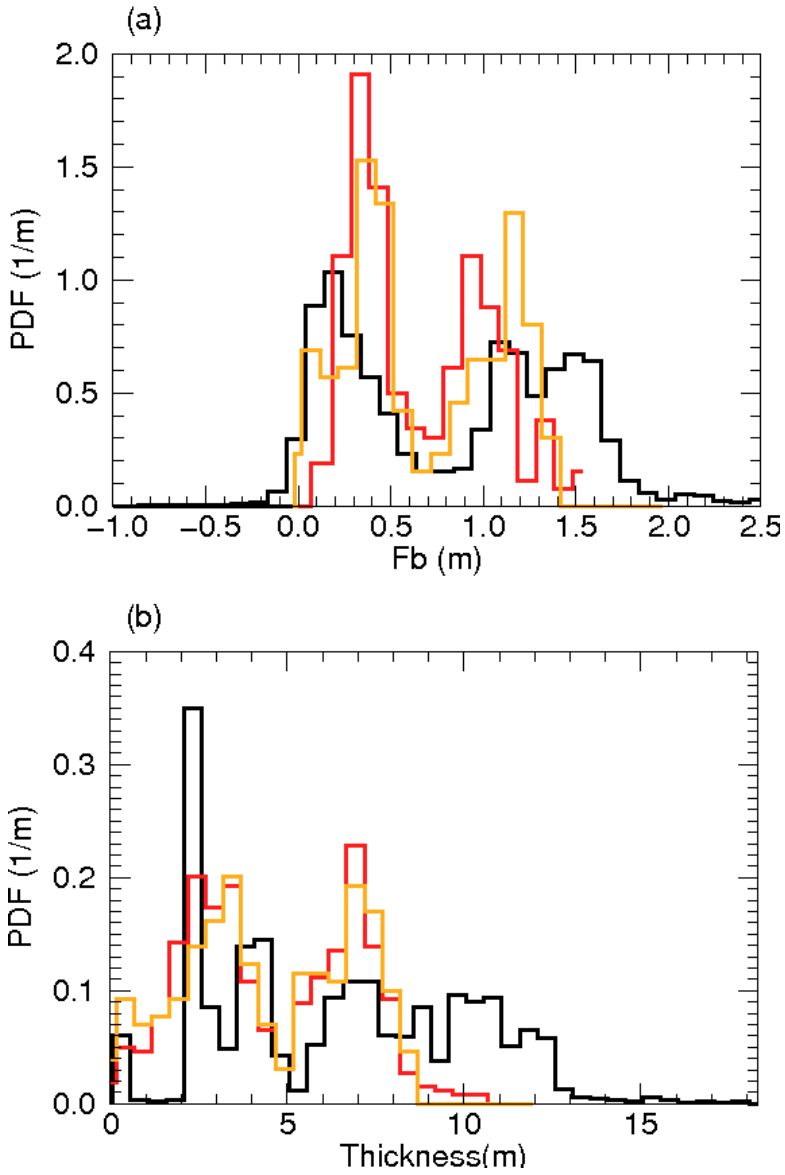

Figure 3.12. Probability Density Functions (PDF) for (a) freeboard and (b) sea ice thickness of ICESat Method-1 (red), Method-2 (orange) and helicopter lidar/electromagnetic induction sounding (black) for October/November 2009.

Two field sites from the 2009 EM Bird in situ (IS) campaign were within 2 km and 0.5 km of two ICESat tracks 15 and 9, respectively (Figure 3.13). IS1 and IS2 are both temporally separated from their respective ICESat acquisitions by 5 weeks. Taking the mean of the 10 nearest ICESat shots to the IS measurements, M-1 derived freeboard at IS1 of 0.26 m is within one standard deviation of track 15 with a mean value of 0.34 ± 0.10 m. The mean freeboard on track 9 of 1.07 ± 0.08 m shows a larger deviation from freeboard measured at IS2 of 0.51 m. With application of the same principles for thickness determination as above, track 15 ice thickness is determined as 2.73 ± 0.79 m with a IS of 2.36 m and track 9 determined as 6.76 ± 0.44 m with thickness at IS2 measured as 7.04 m. M-2 underestimates freeboard on track 15 with a mean value of 0.06 ± 0.09 m and a resultant thickness value of 0.50 ± 0.77 m. M-2 overestimates freeboard on track 9 with a mean value of 1.20 ± 0.08 m and a thickness value of 7.51 ± 0.46 m.

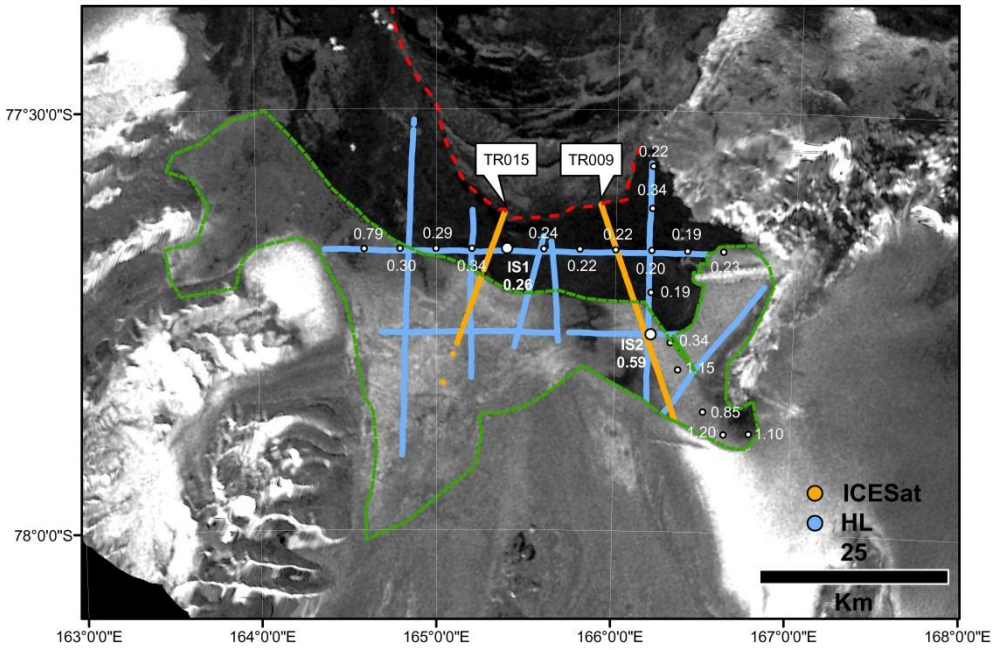

Figure 3.13. Helicopter lidar tracks (blue), ICESat tracks (orange) and in situ measurements of total freeboard (ice-plus-snow) in October and November 2009. Sites IS1 and IS2 are mentioned in the text. Green: multiyear sea ice boundary; red: first-year fast-dynamic sea ice boundary. Image: Envisat ASAR October 2009.

A further in situ measurement data set from 2007 (Dempsey et al., 2010) consists of two sites that are less than 500 m from two ICESat tracks and are temporally coincident by 7 weeks. No freeboard measurements were taken. Dempsey et al. (2010) report a light snow cover with a maximum of 0.07 m. Taking account of this snow depth information ICESat converted thicknesses for M-1 of 1.50 ± 0.19 m and 3.13 ± 0.40 m compare to measured thicknesses of 1.15 m and 2.1 m respectively. M-2 compares poorly with these in situ measurements. In the first case it produces an erroneous thickness from a negative freeboard value and for the second example a thickness that is double the in situ measurement. This in situ comparison is an example of the error for single tracks if the tide information produced by the model is potentially inaccurate. The maximum error suggested by the Scott Base tide gauge comparison (Figure 3.7) is 0.14 m and allowing for this, M-2 thickness would fall within one standard deviation of the in situ measurements.

3.8 Discussion

Here we discuss results in terms of their significance to sea ice characteristics in the area and our confidence in these. Statistically significant positive trends are identified for MY sea ice under M-1 and M-2. While this is an interesting demonstration of the ability of ICESat to monitor a thickening MY ice cover, the various contributions to the increasing MY freeboard are difficult to quantify. Freeboard would be expected to increase upon the establishment of a MY sea ice cover due to the accumulation of snow, as a consequence of decreasing density by continuing brine drainage to the ocean, and growth of new ice from below. Linear extrapolation of the MY trend for M-1 gives a mean freeboard of 0.20 m in 2001 suggesting that FY sea ice was present over most of McMurdo Sound at this time and MY sea ice developed thereafter. Assuming an upper estimate of annual snow accumulation of 300 mm y^{-1} water equivalent as indicated by in situ and satellite measurements (Kruetzmann et al., 2011; Arthern et al., 2006) suggests that only half of the observed increase in freeboard can be attributed to snowfall. The remainder of the observed growth in MY sea ice can be attributed to two separate processes. The first is the winter freezing at the base of the sea ice cover by conductive heat flux from the ocean to the atmosphere, and the second is the attachment and incorporation of the sub-ice platelet layer to the MY sea ice. The role of this second process is strongly supported by Figure 3.10, which identifies the area of greatest freeboard growth along longitude 165° in agreement

with the platelet ice distribution described by Dempsey et al. (2010). The important role of the ocean in sea ice growth in this region is highlighted by this finding. Assessment of the sub-ice platelet layer itself from satellite altimetry is however difficult. The influence of the sub-ice platelet layer on freeboard is dependent upon not only its thickness, but also on the fraction of solid in this porous layer. With a thickness of 1 m and a typical solid fraction of 0.25 (Gough et al., 2012) the sub-ice platelet layer will only force an increase of approximately 1-2 cm in freeboard for a typical FY sea ice cover in McMurdo Sound. Detection of such a change would be at the limit of ICESat's capabilities. However, within McMurdo Sound the sub-ice platelet layer has been measured exceeding 6 m, permitting a change in freeboard to be documented by satellite altimetry. Even so, attributing the change in freeboard to an increase, or on the contrary a decrease in the sub-ice platelet layer thickness would need higher temporal and spatial resolution of in situ measurements.

With regard to the FY sea ice assessment no statistically significant trends in freeboard were identified for the 2003-2009 period with M-1 or M-2. This is in agreement with larger scale assessments of the Ross Sea region (Kurtz and Markus, 2012). However the methods exhibited differences in the annual variation of freeboard. FY freeboard is expected to be near its annual maximum in November and its annual minimum in early February. As the majority of ICESat measurements are within the first two months of each of the S-D and F-J investigations, we expect a seasonal signal to be recorded by ICESat. A change of approximately 0.20 m in FY freeboard is expected from February to November in McMurdo Sound (Gough et al., 2012). M-1 gives little indication of this with a mean F-J freeboard of 0.21 m and a S-D mean of 0.22 m, representing only 5 % of the expected change. M-2 has recorded a change with a mean F-J freeboard value of 0.12 m and a mean S-D freeboard of 0.17 m, but still 75 % of the seasonal signal is not observed.

The accuracy of the methods was assessed by using repeat pass and crossover analysis (Figure 3.6). With regard to M-1 comparison points C and D show the largest separations in recorded freeboard. The largest, 0.68 m, is found around ICESat Day 500 at point D. This is due to the fact that ICESat track 262 running down the western side of the sound (Figure 3.1) was recorded at a time when no sea surface was visible. Therefore freeboard is underestimated on this track. Track 15 completing this comparison point (Figure 3.1) as a crossover track has been able to sample open water to the north-east and recorded freeboard accurately. This source of error causes minimal variation to the mean of that year (< 0.02

m). As its measurements are not influenced by inclusion of sea ice, M-2 shows less separation at comparison point C, the mean separation between measurements decreasing by 30 % (Figure 3.6). This would likely be the case at comparison point D. However, data are removed under M-2 at this site as the resolution of the tide model restricts the availability of tide data due to the site's proximity to land. The analysis indicates that M-1 and M-2 are capable of producing independent coincident mean freeboard measurements to an accuracy of up to 0.01 m. However, in certain cases when error sources associated with misidentification of sea surface height and inaccurate tidal information are at their largest, discrepancies can exceed 0.50 m. This results in a mean separation at crossover and repeat pass comparison points for both methods of 0.13 m.

The decision to maintain a fixed percentage threshold for the identification of open water using M-1 was made due to our inability to accurately monitor the changing open water area in the north during the ICESat mission. The agreement between freeboard measured in situ in 2009 and the 5 % threshold used to generate the ICESat derived freeboards in that year gives us confidence in the results. M-2 was developed to provide a reference sea level independent of ICESat measurements. The dominant uncertainties introduced are from two sources; first the development of the MSS grid itself and second the application of modelled tide data. The MSS grid was developed from independent ICESat elevation retrievals with a good distribution across McMurdo Sound. Care was taken to avoid the inclusion of sea ice in the ICESat elevation measurements to derive the MSS grid. We are confident this was achieved but cannot account for the influence of waves and DOT on the resulting MSS. Also, as areas in the far south-west were covered by MY sea ice for the duration of the study, no information could be gained on the MSS in this region. The application of tidal heights from models in order to correct MSS to SSH further increased the error as indicated by comparison with SCTB tide gauge measurements (Figure 3.7). Attempting to measure a typical FY freeboard of 0.20 m means that a tidal error of 0.14 m, which has been indicated by the SCTB tide gauge comparison will result in 70 % error in freeboard measurements. Some individual tracks exhibit these large errors when compared with in situ measurements. We also expect a large component of the standard deviations to be attributed to natural variation in the surface elevation measurement. However, as the same ICESat h_{ELEV} values were used for M-1 and M-2 an increasing standard deviation is an indicator of larger sources of error. Examples are provided by the larger standard deviations (mean standard deviation increase of 0.17 m) for M-2 over the large FY sea ice

area attributed to the higher inaccuracies in the SSH for M-2 (Tables 3.1 and 3.2). On the contrary the standard deviation decreases using M-2 over the MY sea ice area. This likely reveals the magnitude of the error as a result of increasing distance from the open water area, directly influential on the accuracy of M-1. The trends using M-1 and M-2 concur. These independent techniques have entirely separate sources of error giving us confidence in the results.

Data availability decreased through the study period with 2009 having only 23 % of data that was available in 2003. Interannual comparison of freeboard is therefore slightly hindered. Due to its smaller size the 2009 ICESat data set would have been discarded, but the coincidence with in situ validation (Gough et al., 2012; Mahoney et al., 2011) made it very valuable. The F-J MY dataset for 2009 was a prime example of such data scarcity. The ICESat recorded mean freeboard of 1.16 ± 0.51 m under M-1 was derived from only 3 elevation retrievals. Inclusion of the November 2009 HL data set provided support. The HL and ICESat comparison (Figure 3.12a) gives further insight to the accuracy of the methods. Derived mean freeboards from HL and the two ICESat methods fall within one standard deviation of the other (see Section 3.6). Discrepancies between the data sets may be due to the sampling differences as there was neither temporal nor spatial coincidence between ICESat and the HL. This is likely the case for the MY comparison as areas of thicker MY sea ice were covered by the HL. The EM-Bird and ICESat derived thicknesses all indicate the same sea ice distribution, though the EM-Bird identifies areas of thicker ice (Figure 3.12b). This is also indicated by the mean values, especially in the MY sea ice assessment, the EM-Bird derived mean thickness deviating from the other two means by 3.22 m (see Section 3.6). The EM-Bird measured over extensive areas of thicker ice where ICESat tracks were not available. The inability to achieve complete coincidence in spatial sampling has resulted in a spatial bias. Further, interference from the sub-ice platelet layer causes overestimation of thickness under the EM-Bird technique. Errors associated with assumptions on snow depth and ice density also play a role in the total error. However, these errors are negligible when compared to the influence of freeboard error. The thickness determination was not a principal objective of this investigation but was undertaken to assess ICESat's capability in a small scale assessment to obtain such information. Though our reported errors are large, we have been able to provide thickness measurements from three independent methods (ICESat M-1, ICESat M-2 and EM) which all compare within ±

0.5 m as described by the peaks in sea the ice distribution (Figure 3.12b). Mean values show larger separation due to the spatial bias.

The role played by large tabular icebergs grounded by Ross Island during the study has been well documented (Robinson and Williams, 2012; MacAyeal et al., 2008; Remy et al., 2008; Brunt et al., 2006). Generally, sea ice breakout conditions in McMurdo Sound are driven by the gradual decay of the fast ice integrity over spring with the eventual complete breakout of sea ice from the McMurdo Ice Shelf front forced by storm activity in late summer. The conditions in McMurdo Sound from 2003-2009 were influenced by other sources. Thinning of the sea ice cover in McMurdo Sound is primarily driven by basal melting from warmer oceanic currents from the north (Remy et al., 2008). Surface water is reported as being colder by the end of summer than it had been during non-iceberg years (Robinson and Williams, 2012). Not only altering oceanic conditions, the physical barrier created by the icebergs resulted in a limited capacity for expulsion of sea ice from McMurdo Sound (Gough et al., 2013; Remy et al., 2008) permitting it to persist. We observed an increase in MY freeboard through the study period together with the large 2005 increase in area. These events were coincident with the passage of icebergs B-15A, B-15K and C16 which changed the ocean circulation in McMurdo Sound (Robinson and Williams, 2012). Therefore the sea ice regime in McMurdo Sound likely falls into two distinct modes dependent upon the larger scale situation in the western Ross Sea. A normal mode persists in the absence of large tabular icebergs where FY sea ice dominates with regular breakout events exposing the McMurdo Ice Shelf to open water. A deviant mode develops in the presence of large tabular icebergs calving from the Ross Ice Shelf and grounding off Ross Island disrupting oceanic and atmospheric interaction with the sea ice cover. During this time conditions are favourable for the development of MY sea ice and larger areas of fast FY sea ice. The appearance of icebergs in this region is thought to occur every 30-50 years (Robinson and Williams, 2012) giving an insight to the frequency of this deviant mode.

3.9 Conclusions

In this study ICESat data over a relatively small geographical region have been used to derive freeboard information of sea ice close to an ice shelf and draw conclusions upon the driving mechanisms of the sea ice regime at this time. Using a combination of ICESat elevation data and auxiliary satellite imagery M-1 and M-2 ICESat freeboard retrieval methods show that the freeboard of landfast MY sea ice in McMurdo Sound steadily increased from 2003-2009. The distribution of this increase was variable, the largest increase documented in the region of the sound in which the sub-ice platelet layer is most abundant. This suggests a strong connection between MY sea ice growth and the ocean. The limited temporal and spatial resolution of the available ICESat data set and discontinuous in situ information during the study did not allow conclusions to be drawn on the thickness changes of the sub-ice platelet layer. No significant trends in freeboard were detected for FY sea ice using either method. The FY sea ice investigation did not record the expected seasonal change in freeboard, however, with improvement of the mean sea surface grid and tide models it may be possible to record this signal. Satellite repeat passes and crossovers allowed continued assessment of sea ice freeboard and analysis shows agreement with knowledge obtained from previous in situ studies. Information on inter-track sea ice characteristics are necessary to further advance our knowledge from satellite altimetry methods. In a first attempt the interpolation presented in Figure 3.11 accurately portrays the dominant sea ice freeboard characteristics identified by ICESat.

Satellite derived freeboard under both methods fall within one standard deviation of the helicopter laser recorded freeboard. After conversion from freeboard, ICESat derived thickness for FY sea ice falls within one standard deviation of the thickness derived from helicopter-borne electromagnetic induction (EM-Bird) techniques. However over MY sea ice a mean difference of 3.22 m exists between the two ICESat methods and the EM-Bird technique. This discrepancy is attributed to a larger sampling area under the helicopter campaign over areas of thicker ice. Interference from the sub-ice platelet layer also produces higher thickness estimates from the EM-Bird. Errors associated with freeboard and snow depth estimation from satellite remote sensing platforms mean that in situ information is crucial in the development and validation of retrieval methods in McMurdo Sound. A more representative application of snow depth, as opposed to a generic

percentage of the freeboard value will be taken when a better knowledge of snow distribution across the sound is gained.

We conclude that M-1 should be regarded as a primary method and M-2 used as a secondary method which gives further confidence in the observed trends. This conclusion is primarily driven by the large errors associated with current tide models which currently do not have the required accuracy for retrieval of thin FY sea ice.

The derived freeboard trends and characteristics fit well into the general picture of sea ice and oceanographic conditions during the observations. The passage and grounding of large tabular icebergs at the entrance of McMurdo Sound favoured the growth of fast MY sea ice in line with our observations of an increasing freeboard and thickness. However, further analysis is needed to separate the contribution to freeboard and thickness growth from oceanic and atmospheric heat fluxes.

4 The sub-ice platelet layers and freeboard to thickness conversion

4.1 Introduction

The increasing sea ice extent in the Ross Sea is the main contributor to the overall positive trend in the Antarctic sea ice cover as recorded over the satellite observational record (Parkinson and Cavalieri, 2012). The causes of this increase are unclear, but are likely linked to enhanced sea ice production in areas such as the Ross Sea Polynya and regional sea surface cooling (Comiso et al., 2011). The southern Ross Sea is also characterised by the presence of ice shelf margins which are zones of abrupt physical change, in particular with regard to water mass interaction. At the large scale, the interaction of water sourced from ice shelf basal melting, which freshens the surface ocean, has been suggested as a potential contributor to increasing sea ice extent in the Southern Ocean (Bintanja et al., 2013). Of further interest, it is well known that the outflow of supercooled water from the ice shelf cavity creates an additional heat sink to the ocean promoting sea ice growth (Gough et al., 2012; Purdie et al., 2006; Hellmer, 2004; Trodahl et al., 2000), which increases sea ice thickness in close proximity to ice shelves (Hughes et al., submitted; Purdie et al., 2006; Hellmer, 2004,). This additional ice that forms as a direct result of oceanic heat flux driven by the availability of supercooled water can be split into three components; platelet (or frazil) crystals suspended in the water column, an unconsolidated porous layer of sub-ice platelets directly beneath the sea ice and a layer of consolidated platelet ice incorporated into the sea ice (Dempsey et al., 2010). The sub-ice platelet layer, which does not contribute to the mechanical integrity of the sea ice cover, and has a very different density than consolidated ice, creates an additional source of buoyancy resulting in an increase in sea ice freeboard. Currently the use of sea ice freeboard measurements from satellite altimetry is the only method to derive large-scale sea ice thickness estimates in the Antarctic (Kurtz and Markus, 2012). Using a freeboard measurement alone to estimate sea ice thickness under the hydrostatic equilibrium assumption could result in an overestimation of sea ice thickness – if the influence of the unknown sub-ice platelet layer thickness turns out to be significant. Further, spatial anomalies in sea ice thickness may be

interpreted as indictors of the presence of a sub-ice platelet layer, which in turn may infer the presence of supercooled ice shelf water (ISW) (Hughes et al., submitted). As it is very common for sea ice to abut ice shelves in the Antarctic (Bindschadler et al., 2011), and the extent and persistence of the sub-ice platelet layer is substantially unknown, we consider here the effects of this layer on estimates of sea ice thickness.

The estimation of remotely sensed sea ice thickness from freeboard information is based on altimetric methods. In the simplest sense the difference between altimetric measurements of the local sea surface height and the sea ice elevation provides the freeboard, which can be used in conjunction with snow depth and the densities of ice and snow to estimate sea ice thickness (Price et al., 2013; Kurtz and Markus, 2012; Zwally et al., 2008). The additional influence of the sub-ice platelet layer has not yet been considered. In order to assess this influence the solid fraction (*sf*) of the sub-ice platelet layer must be derived. Here *sf* defines the solid volume of ice per total volume and hence can be calculated from the buoyancy contribution of this layer to the sea ice cover above. The direct measurement of *sf* is complicated by the inaccessible environment beneath sea ice and the immediate alteration of its properties upon disturbance by drilling due to the unconsolidated nature of the layer. Previous investigations have provided values from 0.2 to 0.5 for *sf* of the sub-ice platelet layer (Gough et al., 2012).

Here we firstly discuss deriving *sf* under the hydrostatic equilibrium assumption and the influential components which must be considered. We then describe our in situ data set from McMurdo Sound in the south-western Ross Sea (Figure 4.1) and briefly describe the sea ice conditions (Figures 4.2 and 4.3). Using this information we estimate a *sf* value (Figure 4.4). We then focus on total freeboard (ice-plus-snow) measurements using Global Navigation Satellite System (GNSS) to estimate sea ice thickness and given our estimate of the *sf*, demonstrate how these GNSS based estimates are influenced by the presence of a sub-ice platelet layer. Given that GNSS based estimates of sea ice thickness follow the same principles of surface elevation to thickness conversion as satellite altimeter measurements, we consider the observed affects to be applicable to both techniques. Equally, although we use a localized region to constrain our values, we expect the formation of the sub ice platelet layer to be similar in comparable areas of coastal Antarctic sea ice that abut an ice shelf. Therefore, conclusions about its influence may be considered at the larger scale.

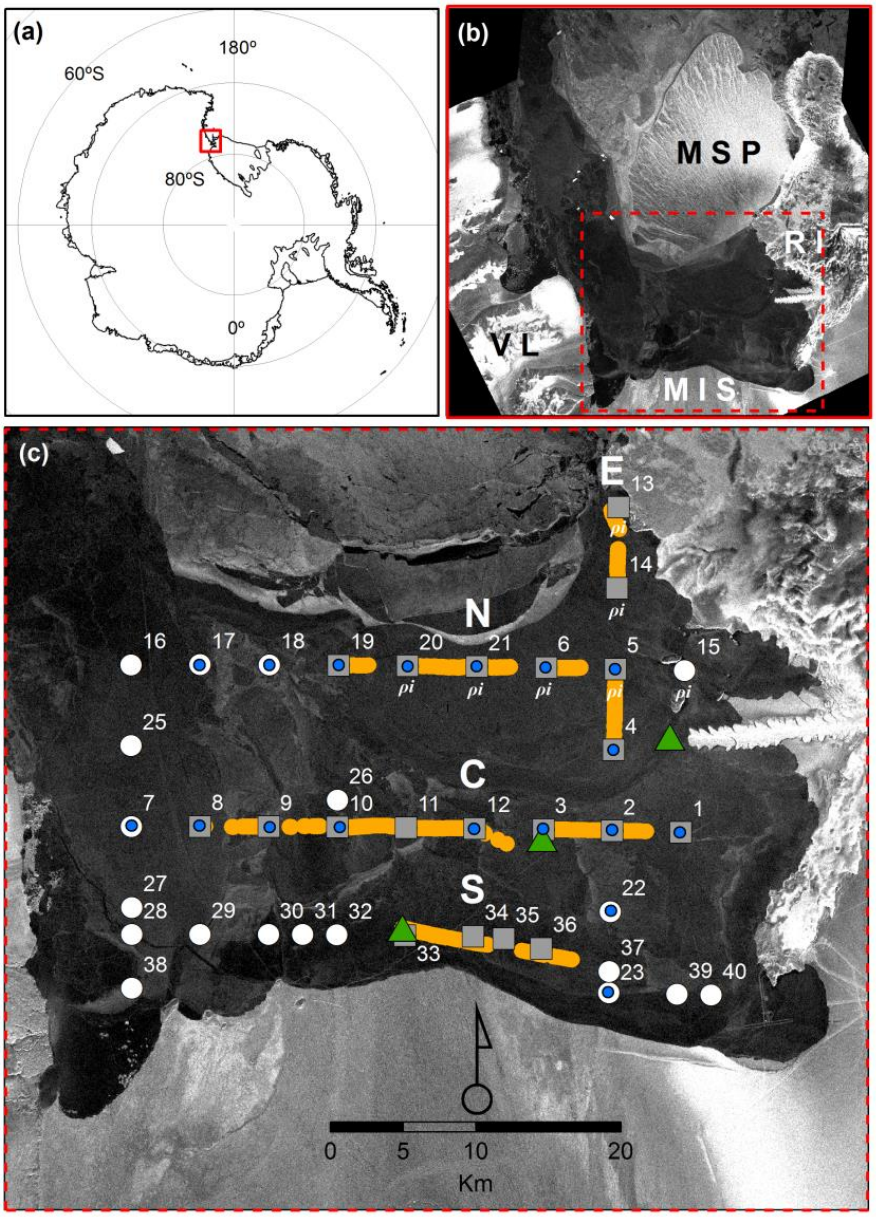

Figure 4.1. (a) Location of the study area (b) Envisat Wide Swath Advanced Synthetic Aperture Radar (ASAR) image (31.08.2011) of McMurdo Sound showing the first-year fast ice area. The McMurdo Sound Polynya (MSP) is driven by offshore winds from Ross Island (RI) in the east. Victoria Land (VL) and the McMurdo Ice Shelf (MIS) are also identified. (c) Magnified view of red box in (b) with an ASAR image from 28.09.2011. Drill-hole measurement sites are indicated by white dots, those used for comparison with the GNSS surveys by grey squares. The GNSS survey lines, Northern, Central, Southern and Eastern are indicated by the orange lines and tidal GNSS stations for tide correction by the green triangles. The 18 sites at which snow density was measured are indicated with blue circles. The 7 sites at which sea ice density was estimated using the hydrostatic equilibrium assumption are makred with 'ρi' underneath the measurement site.

4.2 Estimating solid fraction under the hydrostatic equilibrium assumption

To calculate the buoyant influence of the sub-ice platelet layer upon the sea ice cover above, *sf* must first be derived. Assuming hydrostatic equilibrium *sf* may be calculated as;

$$sf = \frac{-(\rho_w - \rho_i)T_i + (\rho_w SE) - (\rho_w - \rho_s)T_s}{(\rho_w - \rho_i)T_p} \quad (4.1)$$

where ρ_w, ρ_i and ρ_s are the densities of water, sea ice and snow respectively and T_i, T_p and T_s are sea ice thickness, sub ice platelet layer thickness and snow depth respectively (see illustration Figure 4.2). Surface elevation (*SE*) is the elevation of the snow/air interface (or ice/air interface if T_s = 0) relative to sea level. For our study all values were measured simultaneously at drill holes (see section 4.3) for the derivation of *sf* apart from ρ_w, ρ_s and ρ_i. We use a constant value of 1027 kg m^{-3} for ρ_w as there is little variability in observed sea water density (0.1%) in this area . Uncertainty in ρ_w is therefore ignored. For ρ_s we use the values measured in the field at 18 sites in McMurdo Sound in November and December 2011 (Figure 4.1) ranging between 281 and 461 kg m^{-3}. At sites where no data are available we use the mean value of all the measurements of 385 kg m^{-3}.

The selection of a value for ρ_i is complicated by the range in measurements from different techniques and the fact that sea ice density exhibits large natural variability. Timco and Frederking (1996) report mean ρ_i values for first-year (FY) sea ice are likely in the range of 900 to 920 kg m^{-3}. Previous unpublished direct measurements of ρ_i in McMurdo Sound from one co-author (Langhorne) have been obtained via the displacement method in 1992, 1994 and 1996. The 160 measurements of ρ_i ranged between 900 and 925 kg m^{-3}, the mean of these previously unpublished data being 915 kg m^{-3}. ρ_i can also be estimated using the hydrostatic equilibrium assumption. However this must be carried out in areas where no sub-ice platelet layer is present. Using this method in McMurdo Sound, Gough et al. (2012) report ρ_i as 934 kg m^{-3}. Using an amended method at seven of our measurement sites in 2011 (where ρ_i estimate for each site is the mean of ρ_i derived from 5 drill-hole measurements - see Figure 4.2b) where no sub-ice platelet layer was measured we obtain a mean value of 927 kg m^{-3}. The locations of these sites are indicated in Figure 4.1. Given this information, and considering the uncertainties we use a value of ρ_i = 925 kg m^{-3} in our

calculations which represents the middle range of expected ρ_i in McMurdo Sound. We evaluate and discuss the density dependent sensitivity of *sf* in the following sections.

The total error for *sf* can be estimated by error propagation from equation (4.1) using Drosg (2009);

$$\sigma_{sf} = \left[\begin{array}{c} \left(\frac{\rho_w SE + \rho_s T_s - \rho_w T_s}{T_p(\rho_w - \rho_i)^2}\sigma_{\rho_i}\right)^2 + \left(-\frac{1}{T_p}\sigma_{T_i}\right)^2 + \left(\frac{\rho_w}{(\rho_w - \rho_i)T_p}\sigma_{SE}\right)^2 + \left(\frac{T_s}{(\rho_w - \rho_i)T_p}\sigma_{\rho_s}\right)^2 \\ + \left(\frac{\rho_s - \rho_w}{(\rho_w - \rho_i)T_p}\sigma_{Ts}\right)^2 + \left(-\frac{1}{{T_p}^2}\left(\frac{\rho_w SE + \rho_s T_s - \rho_w T_s}{(\rho_w - \rho_i)} - T_i\right)\sigma_{Tp}\right)^2 \end{array} \right]^{1/2} \quad (4.2)$$

where we expect random and independent measurement errors for σ_{ρ_i}, σ_{T_i}, σ_{SE}, σ_{ρ_s}, σ_{Ts} and σ_{Tp} to be 10 kg m^{-3}, 0.02 m, 0.01 m, 50 kg m^{-3}, 0.05 m and 0.10 m respectively. All thickness measurement uncertainties are deducted from in situ observations. ρ_i uncertainty is given by the spread of values recorded for ρ_i in McMurdo Sound between 915 and 934 kg m^{-3}. ρ_s uncertainty is indicated by the standard deviation of measurements carried out in 2011.

As we derive *sf* and σ_{sf} from *SE*, T_i, T_p, T_s and ρ_s, the collection of these measurements from a dedicated in situ fieldwork campaign in McMurdo Sound in November and December 2011 is described in the next section.

4.3 In situ investigation

An extensive drill-hole measurement campaign was carried out in November and December 2011 collecting information on freeboard, snow depth and snow density, sea ice thickness and sub-ice platelet layer thickness for FY sea ice in McMurdo Sound (Figure 4.1).

4.3.1 Drill-hole measurements

Measurements were undertaken at 39 sites distributed across an area of approximately 1,000 km^2 in the southern sound. Cross-profiles with 30 m transects were established at each site, and snow depths were measured at 0.5 m intervals with a ruler (Figure 4.2). A mean snow depth for each site was derived from these 120 measurements. Freeboard, ice thickness and sub-ice platelet layer thickness were recorded at five locations at each site, once at the central crossing point and at the end points of each transect (Figure 4.2). The mean of these was then calculated and taken as representative of the site. Ice thicknesses were measured by using a tape measure with a brass T-anchor attached at the zero mark (Haas and Druckenmiller, 2009). This was deployed vertically through the drill-hole and allowed to rotate to a horizontal alignment when exiting the bottom of the drill-hole at the ice ocean interface. From this position, and as described in Gough et al. (2012) the anchor is slowly pulled upward until some resistance is met and the first measurement is taken. This resistance is taken to mark the sub-ice platelet layer/ocean interface. The tape measure is then pulled harder, forcing the bar to pass through the sub-ice platelet layer until it sits flush against the sea ice/sub-ice platelet layer interface where a second measurement is taken. Snow density was measured at half of the drill-hole sites using a density tube and spring balance. Freeboard, ice thickness and sub-ice platelet layer thickness and snow depth were interpolated between sites to produce thickness maps (Figure 4.3) using a natural neighbour interpolation method with a maximum point separation of approximately 11 km.

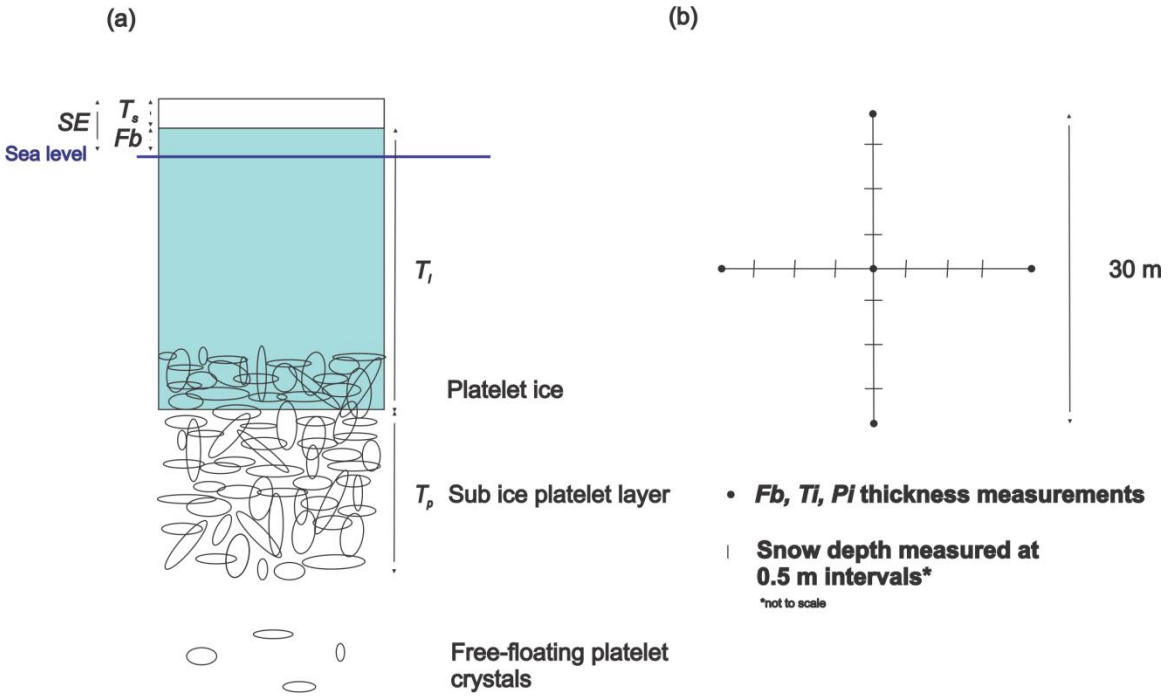

Figure 4.2. (a) Typical vertical profile through first-year sea ice in McMurdo Sound in austral spring, adapted from Gough et al. (2012). Surface elevation (*SE*) describes the combined protrusion of the ice freeboard (*Fb*) and snow cover (T_s) above sea level. Ice thickness (T_i) describes the sea ice formed from heat flux to the atmosphere along with the platelet ice which is the incorporated as the sea ice-ocean interface advances into accumulating platelets below. The sub-ice platelet layer accumulates beneath (T_p). Platelet crystals float freely in the water column below. (b) Graphical display of the drill-hole measurement site set up.

4.3.2 Maps of sea ice and snow cover characteristics

Prior to our measurements in November and December 2011 the fast FY sea ice in McMurdo Sound experienced undisturbed growth for a minimum of 5 months. There is a clear ice thickness gradient from east to west (Figure 4.3). Thinner ice with a typical thickness of 1.5 m is commonplace in the east, particularly in the north east, becoming gradually thicker to the west, where it reaches 2.5 m in thickness. This is significantly higher than the pack ice of the Ross Sea which typically has a thickness of 1 m or less (Worby et al., 2008; Kurtz and Markus, 2012). In comparison to other fast ice areas, McMurdo Sound sea ice thickness is still greater than expected. Uto et al. (2006) report that land-fast FY ice in Eastern Antarctica which had been growing for 4-5 months was

typically up to 1.5 m in thickness. This is comparable to thicknesses in the north-east of McMurdo Sound. The mean sea ice thickness as derived from all 39 drill-hole measurement sites was 2.11 m. In the southwest, sea ice had been growing for approximately 7 months, two months longer than in the northeast. This is the first of three mechanisms likely responsible for the observed sea ice thickness distribution. The ISW plume is the second mechanism. The influence of this plume on sea ice processes has been documented in studies of sea ice structure and growth (Gough et al., 2012, Mahoney et al., 2011, Dempsey et al., 2010, Langhorne et al., 2006). Satellite altimeter observations have indicated that the locations of the largest increases in multiyear sea ice thickness from 2003-2009 during the NASA ICESat mission (Price et al., 2013) were coincident with the greatest abundance of platelet ice (Dempsey et al., 2010). This region has recently been identified as the location of an ISW plume (Robinson et al., 2014). The thickness and density distributions revealed by a localised airborne freeboard and thickness investigation of the MIS margin in 2009 (Rack et al., 2013) are supportive of the emergence of such a plume into McMurdo Sound. In 2011, sea ice in the west was comprised almost entirely of platelet ice (Hughes et al., submitted) as would also be expected from the presence of such a plume. The sub-ice platelet layer has an east-west distribution commensurate with the presence of this plume (Hughes et al, submitted). The layer is thickest where it protrudes from the MIS front between 165° and 165° 30' E, where it has been measured as 7.5 m in thickness (Figures 4.3 and 4.5). As expected, the sub-ice platelet layer distribution closely follows the platelet distribution as described by Dempsey et al. (2010). As it is not a solid structure and may be mobile, the sub-ice platelet layer thickness at a single location may be highly variable over short time scales of hours to days.

The third mechanism which plays a role in the observed sea ice thickness distribution is snow cover. Limited published information is available on the snow depth distribution in McMurdo Sound. Gow et al. (1998) reported very generally that snow thickness was greatest in close proximity to the MIS front decreasing to only trace amounts in remote areas of McMurdo Sound. In 2011, the snow cover in the west and the central parts was patchy, with small scale dune features with thicknesses in the order of decimeters and with exposed sea ice in many places. There is a clear east-west gradient in this pattern, contrary to the sea ice thickness pattern, with deeper snow in the east gradually becoming thinner to the west. In the east, where the snow is thicker, it acts as an insulating layer from the

atmosphere, limiting sea ice growth. In the west where it is thinner or absent, greater heat flux to the atmosphere results, which in turn facilitates the formation of thicker sea ice.

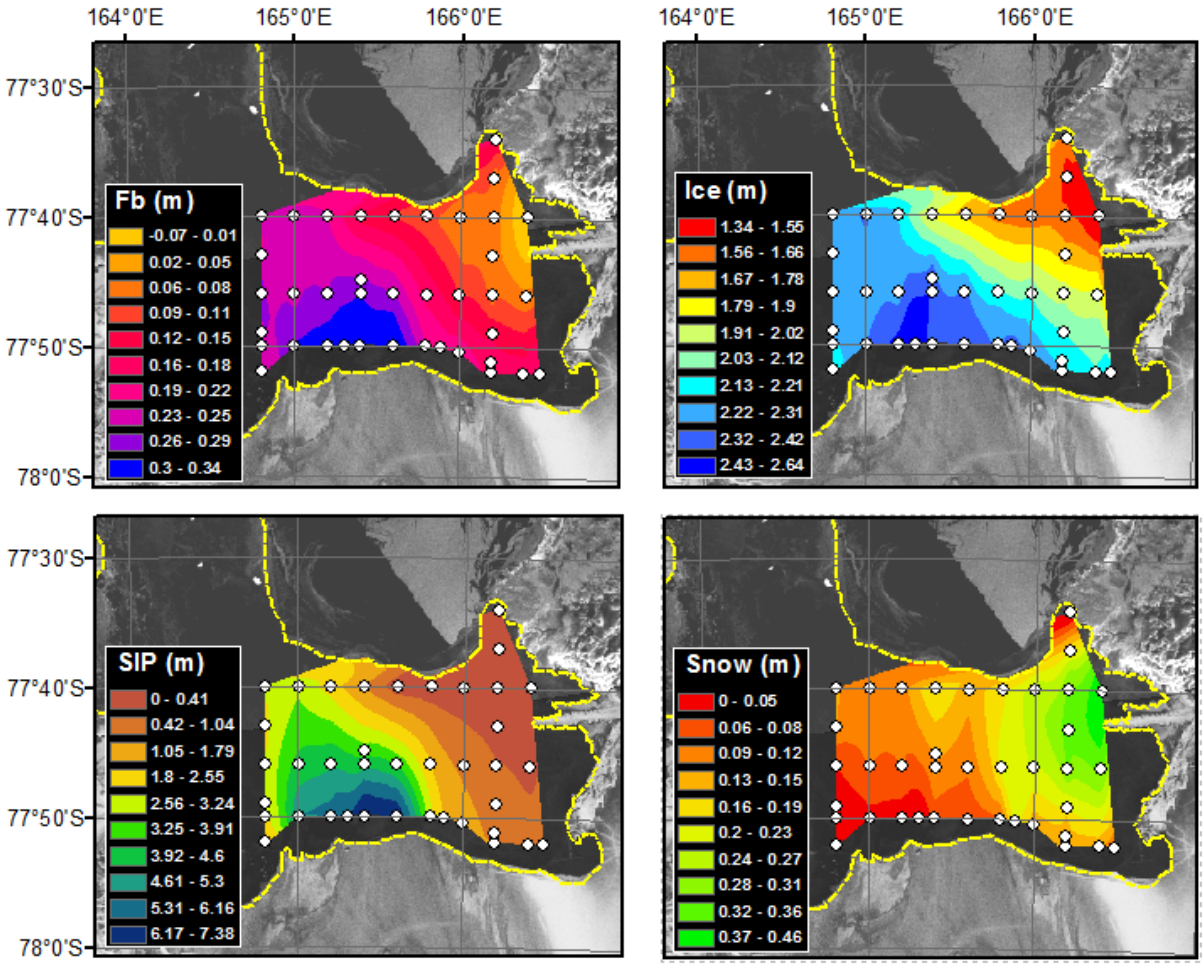

Figure 4.3. Interpolated maps of drill-hole measurements of (a) freeboard (b) ice thickness, (c) sub-ice platelet layer thickness (SIP) and (d) snow thickness of first-year sea ice in McMurdo Sound in November and December 2011. These are overlaid upon an Envisat ASAR mosaic composed of two images from 25 and 28 November. Partitioned yellow line indicates typical first-year fast ice area in spring.

4.4 The solid fraction in McMurdo Sound

Using our drill-hole measurements the derived *sf* values using equation (4.1) and the expected error (σ_{sf}) from equation (4.2) are shown in black in Figure 4.4 with ρ_i = 925 kg m^{-3}. The derivation of *sf* is especially sensitive if the sub-ice platelet layer is less than 2 m

thick. Sites at which the sub-ice platelet layer is thin commonly produce negative *sf* values especially when ρ_i < 920 kg m^{-3}. Using 32 of 39 sites in our investigation where a sub-ice platelet layer is present and with the removal of 9 further sites where the sub-ice platelet layer was less than 1.5 m results in a mean *sf* value of 0.16 ± 0.07. Figure 4.4 displays all sites where a sub-ice platelet layer was present and also linear fits of *sf* with ρ_i = 915 kg m^{-3} (green line) and ρ_i = 935 kg m^{-3} (orange line). This clearly demonstrates firstly the dependence of *sf* estimates on ρ_i and secondly the high sensitivity of the *sf* calculation where the sub-ice platelet layer is thin.

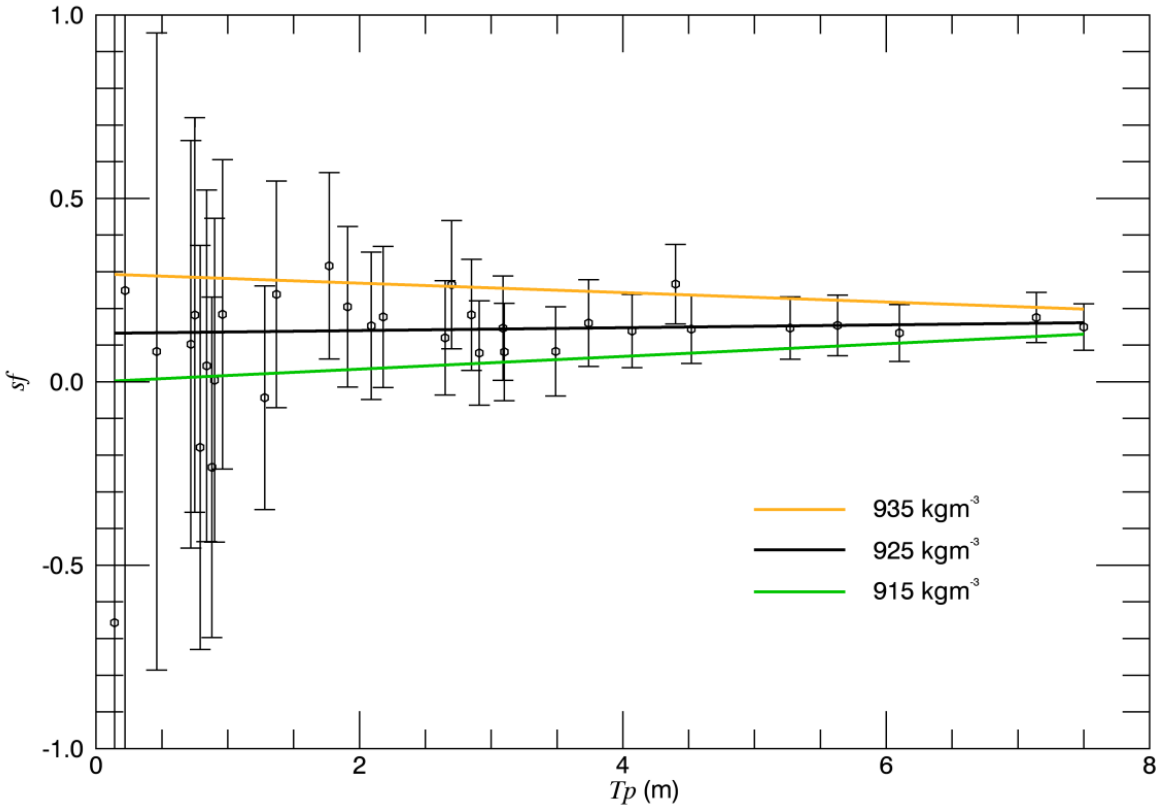

Figure 4.4. Solid fraction (*sf*) derived by equation (4.1) (black circles) and expected errors from equation (4.2) derived for 32 measurement sites. A linear fit is shown in black for this data set. The influence of varying sea ice density (ρ_i) is also displayed as linear fits for higher and lower ρ_i values (no symbols plotted).

4.5 Sea ice thickness from GNSS derived surface elevation

GNSS elevation data were collected for positional and height information across the sound. The GNSS derived ellipsoidal heights, relative to WGS-84, were calibrated to produce total freeboard (ice-plus-snow) measurements, herein described as GNSS surface elevation (SE_{GNSS}). This calibration was achieved by applying a correction value derived from comparison of drill-hole measured surface elevation (SE) and all GNSS height measurements within 0.5 km of the drill-hole measurement. This altered the reference frame of the GNSS height data from the WGS-84 ellipsoid to elevation above local sea level and permitted surface elevation information to be recorded at increased spatial resolution along each of the four profiles; Northern, Central, Southern and Eastern. Initially sampled at 1 Hz, the GNSS observations were averaged along-track resulting in a ground separation of approximately 100 m. GNSS positions were established using the Precise Relative GNSS technique, referenced to the Scott Base base station located on Ross Island's Hutt Point Peninsula at 77.85 °S, 166.76 °E. After processing with Trimble Business Centre, mean horizontal and vertical precision were shown to be 0.04 and 0.09 m respectively. All data where the expected vertical precision was greater than 0.17 m were removed. This value was chosen as it removed erroneous data in the west where GNSS precision was lower due to the larger baseline distance (anything over approximately 40 km). In order to compensate for the tidal influence on the GNSS height and subsequently the SE_{GNSS} retrieval, three separate GNSS stations were deployed on the fast ice (see Figure 4.1 for locations). These tidal stations logged height information at 30 second intervals, which was subsequently down-sampled to 10 minute intervals. As the transit time of the mobile GNSS on the sea ice was hours, this information was used to correct the rover GNSS information for tidal height variation between drill-hole cross-over points. There was no discernible gradient in the tidal signal between the three tidal GNSS stations. Changes in elevation due to tides were taken from the closest tidal GNSS station to the mobile observation to correct SE_{GNSS} at the time of acquisition.

In order to derive sea ice thickness from SE_{GNSS} we need to take into account the effect of the sub-ice platelet layer. Following Zwally et al. (2008) we estimate sea ice thickness without taking account of the sub-ice platelet layer (T_{ip}) in equation (4.3) and then taking account of it (T_i) in equation (4.4):

$$T_{ip} = \frac{\rho_w}{\rho_w - \rho_i} SE_{GNSS} - \frac{\rho_w - \rho_s}{\rho_w - \rho_i} T_s \quad (4.3)$$

$$T_i = \frac{\rho_w}{\rho_w - \rho_i} SE_{GNSS} - \frac{\rho_w - \rho_s}{\rho_w - \rho_i} T_s - T_p sf \quad (4.4)$$

All density values described in section 4.2 are used here with *sf* = 0.16 as described in section 4.4. Taking account of all the information described above, we calculated the sea ice thickness along four continuous GNSS surface elevation profiles using equations (4.3) and (4.4) (Figure 4.5), the mean estimates of which are shown in Table 4.1. These are compared to coincident measured drill-hole thickness. Taking the mean for all of the profiles the deviation from drill-hole measured sea ice thickness improves by 0.28 m when the sub-ice platelet layer is taken into consideration. The Northern, Central and Southern profiles show a shift towards drill-hole sea ice thickness. The Southern profile shows a drastic improvement from a mean deviation of + 0.55 m in thickness neglecting the sub-ice platelet layer to - 0.01 m when accounting for it. The Central profile improves from a mean deviation of + 0.43 m from the drill-hole measurements when estimating T_{ip} to + 0.02 m when estimating T_i. The Northern profile improves by 0.03 m but still deviates from the drill-hole sea ice thickness mean by + 0.24 m. This small change from T_{ip} to T_i is resultant of a negligible mean sub-ice platelet layer thickness of 0.24 m. The Eastern profile shows no change as the platelet layer recorded there was very thin with a mean thickness of 0.04 m. The Northern and Eastern profiles both have a bias toward higher sea ice thickness estimates than measured at the drill-holes. This could be a result of the interpolations inability to capture the small scale variability of the snow cover. This could result in underestimations of snow depth and subsequently high sea ice thickness estimates.

The mean of all drill-hole measurements used along the profiles (n = 20) of 2.00 ± 0.31 corresponds better to a surface elevation derived sea ice thickness accounting for the sub-ice platelet layer (T_i) of 2.11 ± 0.85 m, than one in which it is ignored (T_{ip}) giving 2.39 ± 0.99 m.

Table 4.1. Mean Drill-hole measured, surface elevation derived sea ice thickness (T_{ip}) and surface elevation sub-ice platelet layer corrected thickness (T_i) with standard deviations for each profile. The mean sub-ice platelet layer thickness (T_p) for each profile is also displayed.

Profile	Drill-hole (m)	T_{ip} (m)	T_i (m)	Mean T_p (m)
Northern	1.69 ± 0.13	1.96 ± 0.77	1.93 ± 0.75	0.24 ± 0.42
Central	2.19 ± 0.16	2.62 ± 1.02	2.21 ± 0.90	2.53 ± 1.70
Southern	2.33 ± 0.06	2.88 ± 0.70	2.32 ± 0.56	3.30 ± 2.29
Eastern	1.60 ± 0.10	1.92 ± 1.02	1.92 ± 1.02	0.04 ± 0.06

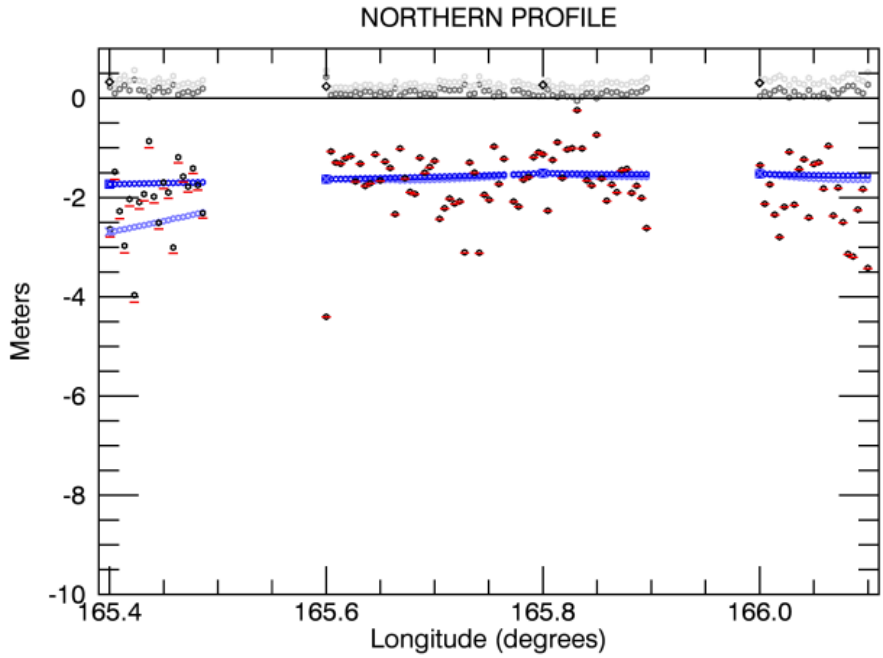
NORTHERN PROFILE
0
-2
-4
-6
-8
-10
Meters
165.4
165.6
165.8
166.0
Longitude (degrees)

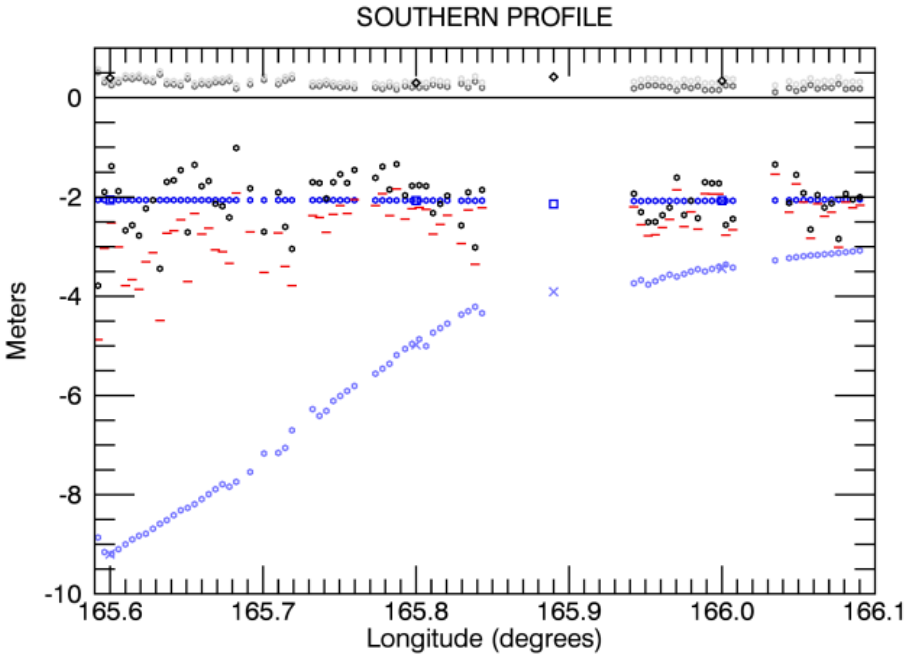
SOUTHERN PROFILE
0
-2
-4
-6
-8
-10
Meters
165.6
165.7
165.8
165.9
166.0
166.1
Longitude (degrees)

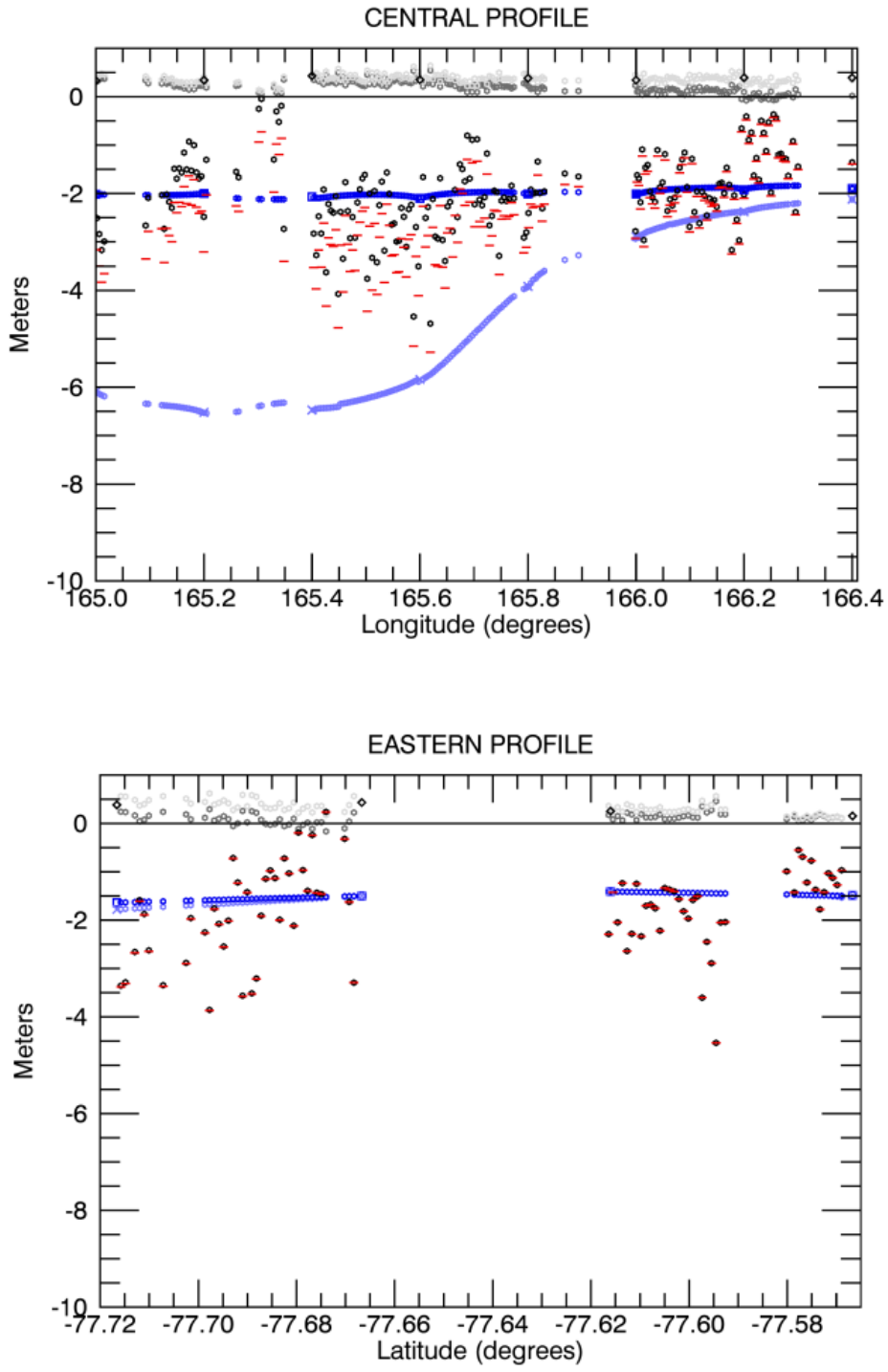

Figure 4.5. The four profiles with GNSS derived surface elevation (light grey), interpolated drill-hole derived sea ice freeboard (dark grey), sea ice draft (dark blue) and sub-ice platelet layer draft (light blue). Red dashes indicate sea ice draft as predicted by equation (4.3) taking no account of the sub-ice platelet layer, black circles indicate the estimated draft with consideration of the sub-ice platelet layer as estimated by equation (4.4). Drill-hole measurements of surface elevation (◊), sea ice draft (□) and sub-ice platelet layer draft (×) are also displayed for comparison with the interpolations.

As the sub-ice platelet layer is not the only source of error when estimating sea ice thickness a full error assessment is shown below. Following Spreen et al. (2006, equation 2) with the additional inclusion of the sub-ice platelet layer uncertainty we estimate our final error in sea ice thickness once accounting for the sub-ice platelet layer (σ_{T_i}) as;

$$\sigma_{T_i} = \left[\begin{array}{c} \left(\frac{\rho_w}{\rho_w-\rho_i}\sigma_{SE_{GNSS}}\right)^2 + \left(\frac{\rho_s-\rho_w}{\rho_w-\rho_i}\sigma_{Ts}\right)^2 + \left(\frac{T_s(\rho_s-\rho_w)+SE_{GNSS}\rho_w}{(\rho_w-\rho_i)^2}\sigma_{\rho_i}\right)^2 + \left(\frac{T_s}{\rho_w-\rho_i}\sigma_{\rho_s}\right)^2 + \\ \left(\sigma_{Tp}sf\right)^2 + \left(\sigma_{sf}T_p\right)^2 \end{array} \right]^{1/2} \quad (4.5)$$

Here we estimate uncertainties in ρ_i and ρ_s to be 10 kg m^{-3} and 60 kg m^{-3} respectively as indicated by the standard deviations of field measurements. T_s and T_p values used in the thickness calculation are from the interpolation of the measurement sites. Leave-one-out cross validation was used with random selection to assess the accuracy of our interpolation method. Eight drill-hole sites were removed in turn and eight separate interpolations run. This procedure indicated a mean absolute deviation between the removed snow thickness measurement and subsequent interpolation of 0.05 m for T_s and 0.23 m for T_p. These values are used for the uncertainties in each thickness. The uncertainty in *sf* is 45 %. The main contributor to the error in sea ice thickness estimation from GNSS measurements is the accuracy of the GNSS surface elevation measurement itself. The mean GNSS vertical elevation uncertainty as indicated by the processing software is 0.09 m. At least 20 measurements are included in our along track averaging to 100 m spacing reducing the random error in surface elevation measurements to 0.02 m i.e. $\sigma SE_{GNSS} = \frac{0.09}{\sqrt{20}}$. For a single GNSS measurement this results in an expected sea ice thickness error of 0.58 m once the sub-ice platelet layer has been taken into account.

4.6 Discussion

Using our drill-hole measurements we have indirectly estimated a mean solid fraction (*sf*) of the sub-ice platelet layer for McMurdo Sound of 0.16 ± 0.07. This is lower than previous estimates, but still within the uncertainty from Gough et al. (2012) of 0.25 ± 0.06, who base their estimate on the measurement of heat fluxes. Our estimate is based on mean freeboard and thickness measurements by applying the hydrostatic equilibrium assumption. The primary systematic uncertainty in the *sf* estimation is sea ice density (ρ_i). Our result uses a mean ρ_i value of 925 kg m^{-3}. Under the same criteria as described in section 4 the mean *sf* varies from 0.03 to 0.36 given ρ_i values ranging from 915 to 935 kg m^{-3} respectively. We used 925 kg m^{-3} for ρ_i as it represents the middle range of expected ρ_i in the study area. With this value an estimate of *sf* is provided, but we reiterate the dependence of the calculation on ρ_i. 915 kg m^{-3} is considered a lower estimate of ρ_i as brine drainage is expected from the base of sea ice cores when undertaking the displacement technique. Assuming hydrostatic equilibrium we derive 927 kg m^{-3} for ρ_i, a higher estimate in better agreement with the 934 kg m^{-3} reported by Gough et al. (2012). We suggest 934 kg m^{-3} as an upper bound to ρ_i (Timco and Frederking, 1996) in McMurdo Sound. Furthermore, under a simple measurement set up surface elevation could be slightly suppressed due to the loading of personnel and equipment near the drill-hole site. We found after testing this, that the sea ice surface may be suppressed by up to 0.01 m when such loading is present in close proximity to the drill-holes resulting in ρ_i overestimates of approximately 5 kg m^{-3}. We also suggest that a large number of measurements using our method are necessary as sea ice is not necessarily in hydrostatic equilibrium over very short spatial scales. We do not expect this to have significantly influenced the mean of our freeboard values, and subsequently our ρ_i estimate as most of our drill-holes were drilled at least 15 m away from such loading, and our estimate is based on an average of 35 separate drill-hole measurements (5 measurements at each site, 7 in total).

Though we have confidence that other sources of error play a smaller role, their influence cannot be entirely ignored. A 0.1 % uncertainty in water density (ρ_w) has been reported by Albrecht et al. (2006). This results in a ± 1 kg m^{-3} variation in reported mean ρ_i. Any larger variations in ρ_w would result in a larger range in calculated ρ_i.

The estimate of *sf* for the sub-ice platelet layer has permitted the influence of the sub-ice platelet layer to be removed from sea ice thickness derived from GNSS measurements of surface elevation. Without accounting for the sub-ice platelet layer, the mean deviation of estimated level ice thickness from drill-hole measured sea ice thickness is 0.39 m. Taking account of the sub-ice platelet layer the mean deviation is reduced to 0.11 m. Therefore in areas of sea ice in close proximity to ice shelves it can be expected that thicknesses derived from freeboard or surface elevation may deviate from actual thickness by 12 %, with maximum deviations in the order of 19 % as a direct result of not accounting for a sub-ice platelet layer. In our study results may be improved along certain GNSS profiles with better snow depth information.

Platelet ice and sub-ice platelet layers have been documented in many coastal Antarctic regions (Gough, 2012) making this link a key component of the Antarctic coastal sea ice regime. As the GNSS surface elevation sea ice thickness estimation operates under the same fundamental principles as satellite altimetry, this establishes an uncertainty in estimating sea ice thickness from satellite altimetry in proximity to ice shelves from the presence of a sub-ice platelet layer. Given that our estimate of *sf* is low in the range of reported values, the influence of the sub-ice platelet layer on sea ice thickness estimation from *SE* measurements could be even more significant. The variability of *sf*, both vertically through the sub-ice platelet layer and horizontally in a larger spatial sense could not be quantified. This will also play a role in the error of the estimation of sea ice thickness.

4.7 Conclusions

We have used an extensive drill-hole measurement campaign to estimate a solid fraction value of 0.16 for the sub-ice platelet layer found under land fast sea ice in McMurdo Sound. Using this information we were able to quantify the error associated with using satellite surface elevation measurements to estimate sea ice thickness. Sea ice thickness was overestimated on average by 12 % in southern McMurdo Sound as a result of the buoyant influence of the sub-ice platelet layer on the sea ice cover above. The influence of the ice shelf is expected to extend beyond 200 km from the edge of the McMurdo Ice Shelf (Stevens et al., 2009). Platelet ice observations partly confirm this and have been recorded

in sea ice cores 80 km north of the ice shelf edge (Dempsey et al., 2010). During fieldwork in 2013 the authors also measured a sub-ice platelet layer of 0.20 m in thickness at approximately the same distance. Though ice shelf water may still be influential on sea ice thickness out to and beyond 200 km, the sub-ice platelet layers thickness clearly diminishes at such distances from the ice shelf margin. It is unlikely it still has a buoyant influence on the sea ice cover beyond a distance of 100 km. We conclude that its influence may need to be considered in sea ice thickness investigations using satellite altimetry within 100 km of ice shelves. It should be noted however that ice shelf thickness is likely influential on whether supercooled water and platelet crystals can reach the upper few meters of the ocean and interact with sea ice.

Sub-ice platelet layer formation results from the advection of supercooled ice shelf water from beneath the McMurdo and Ross Ice Shelf cavities providing an oceanic heat sink for sea ice formation. This heat sink contributes to sea ice thicknesses exceeding 2.5 m, at least double that of sea ice in pack ice areas of the Antarctic. Given the prevalence of ice shelves around the Antarctic and the fact that approximately 35 % of the Antarctic coastline is fringed by fast ice in austral spring (Fraser et al., 2012), such interaction could be a primary driver of the sea ice thickness distribution near ice shelves. With adequate information on snow loading and using these anomalies in recorded sea ice thicknesses it may be possible to map ice shelf water presence in coastal Antarctica using satellite altimetry measurements.

5 Evaluation of CryoSat-2 derived sea ice freeboard

5.1 Introduction

Although Antarctic sea ice extent and concentration have been routinely monitored since 1979 (Parkinson and Cavalieri, 2012) the spatial and temporal distribution of sea ice thickness remains one of the least understood physical components of the global cryosphere (Vaughan et al., 2013). Quantification of this thickness is of crucial importance, as when combined with areal data it allows the computation of sea ice volume. Sea ice volume provides insight into the heat budget of the Antarctic sea ice system and quantification of freshwater and saltwater fluxes in the Southern Ocean. Due to the scarcity of in situ measurements of Antarctic sea ice thickness there is great demand for improved temporal and spatial thickness data through satellite altimeter observations (Kurtz and Markus, 2012; Xie et al., 2013; Yi et al., 2011; Zwally et al., 2008). Such observations develop the ability to monitor trends and in turn provide data to improve the capability of models to forecast future Antarctic sea ice properties (Holland et al., 2014; Massonnet et al., 2013).

The use of satellite altimetry for sea ice thickness estimation is entirely reliant upon freeboard measurements and their conversion to thickness based on the assumptions of hydrostatic equilibrium and input of values for the densities of snow, ice, water and snow thickness (Alexandrov et al., 2010). The ability to accurately measure freeboard and to include information on snow morphology is vital as any errors in these input factors are greatly magnified in the eventual sea ice thickness estimation. The European Space Agency's (ESA) SIRAL (Synthetic aperture radar Interferometric Radar ALtimeter system) on-board CryoSat-2 (CS-2) is the most capable radar altimeter instrument for sea ice freeboard retrieval in operation to date (Wingham et al., 2006; Drinkwater et al., 2004) and at the time of writing is improving understanding of the Arctic sea ice thickness distribution (Kurtz et al., 2014; Ricker et al., 2014; Laxon et al., 2013). Given the more heterogeneous and thinner state of Antarctic sea ice, primarily due to its more dynamic nature, and its highly variable snow distribution and morphology (Ozsoy-Cicek et al., 2013; Massom et

al., 2001) the uncertainty in resultant thickness estimates from CS-2 in the Southern Ocean are likely to be higher.

In this study we validate freeboard measurements from CS-2 over fast ice in McMurdo Sound in 2011 and 2013. The fast ice in this area provides a safe platform for the collation of in situ data (Price et al., 2014). Consisting of largely uniform level sea ice, with smooth gradients in thickness and snow cover the complexity in view of satellite validation is significantly reduced compared to the more dynamic pack ice conditions. In common with many other coastal Antarctic regions (Fraser et al., 2012; Fedotov et al., 1998) McMurdo Sound harbours extensive areas of fast ice neighbouring coastal polynyas and ice shelves as regions of significant sea ice production (Tamura et al., 2008; Massom et al., 1998). The performance of radar altimeters for freeboard retrieval in these regions of highly variable ocean conditions are yet to be evaluated, specifically with regard to sea ice/water discrimination over differing water surface types (i.e. leads, polynyas of varying sizes).
Compared to ICESat (infrared laser shots with 70 m footprints every 170 m along track), the CS-2 radar signal penetrates cloud cover but produces a larger footprint of ~ 380 x 1,650 m dependent upon orbit parameters and surface geometry (Bouzinac, 2013). Freeboard retrieval using laser instrumentation is simplified by the fact that the main reflection from the snow surface is well defined whereas in *Ku*-band (SIRAL centre frequency = 13.6 GHz) the backscattered radar energy was initially assumed to originate primarily from the snow/ice interface (Laxon et al., 2013) (Figure 5.1). The limited radar chirp bandwidth of SIRAL (320 MHz) results in a reduced range resolution of 0.47 m which can neither resolve the air/snow, nor the snow/ice interface making the identification of surface height highly dependent on the slope of the leading edge of the returned waveform (Figure 5.2). Recent investigations from airborne *Ku*-band radars operating at higher bandwidths suggest that the influence of snow on sea ice is not negligible as it can broaden the waveform of the returned signal, thus displacing the tracking point (corresponding to the retrieved surface height) toward the altimeter (Kwok, 2014). Previous observations were inconclusive as they showed varying dominant scattering depths in various data sets (Willatt et al., 2011; Hendricks et al., 2010). The influence of snow on the shape of the returned waveform depends on its dielectric properties which are dictated by salinity, liquid water content, density, grain size and temperature (Barber et al., 1995; Hallikainen et al., 1986; Ulaby et al., 1986). Given the complex snow stratigraphy and snow microwave interaction, there is effectively no consensus on a dominant backscattering

surface. For example, no single dominant backscattering surface was found for stratified snow during in situ investigations using a 10-16 GHz band instrument, but returns from the snow/ice interface dominated when layering in the snow cover was absent (Willatt et al., 2010). Surface roughness also influences the freeboard retrieval as it directly affects the shape of the returning radar waveform (Hendricks et al., 2010; Drinkwater, 1991; Beaven et al., 1995). Surface roughness may be separated into radar and geometric roughness, the former is associated with small scale features at length scales comparable to the radar wavelength (in this case 0.02 m) and the latter concerned with large scale surface undulations (e.g. ridging, cracks). These factors exacerbate the accurate localization of a dominant backscattering surface over sea ice, and in turn, the retracking, a procedure which interprets the waveform to accurately estimate the range to surface is complicated (Figures 5.1 and 5.2). There are currently two separate approaches using waveform interpretations to establish retracking points; (i) a waveform fitting approach that takes into account the shape of the returned waveform based on a physical model; (ii) an empirical approach that only considers the leading edge and estimates surface height at a given power threshold. Waveform fitting forms the basis of ESA's Level 2 product (*ESAL2*) and the waveform fitting procedure (*WfF*) as described by Kurtz et al. (2014). The Threshold-First-Maximum-Retracker-Algorithm (*TFMRA40*) is an empirical approach presented by Helm et al. (2014) and employed over sea ice by Ricker et al. (2014). We assess the assumptions behind these techniques against a detailed in situ investigation. We undertake a supervised freeboard retrieval procedure in which sea surface height is manually classified using near-coincident MODIS imagery on a small number of selected CS-2 tracks in 2011 and 2013. Using this optimal data set, and additional CS-2 waveform information, we provide insight into the influence of differing surface conditions (snow properties and surface roughness) on the resultant freeboards from each technique. This supervised analysis also provides information on the expected accuracy of CS-2 freeboard retrievals over the fast ice. With information gained in this initial evaluation we develop automatic freeboard retrieval procedures and assess the sea ice regime in McMurdo Sound for the entirety of 2011 and 2013.

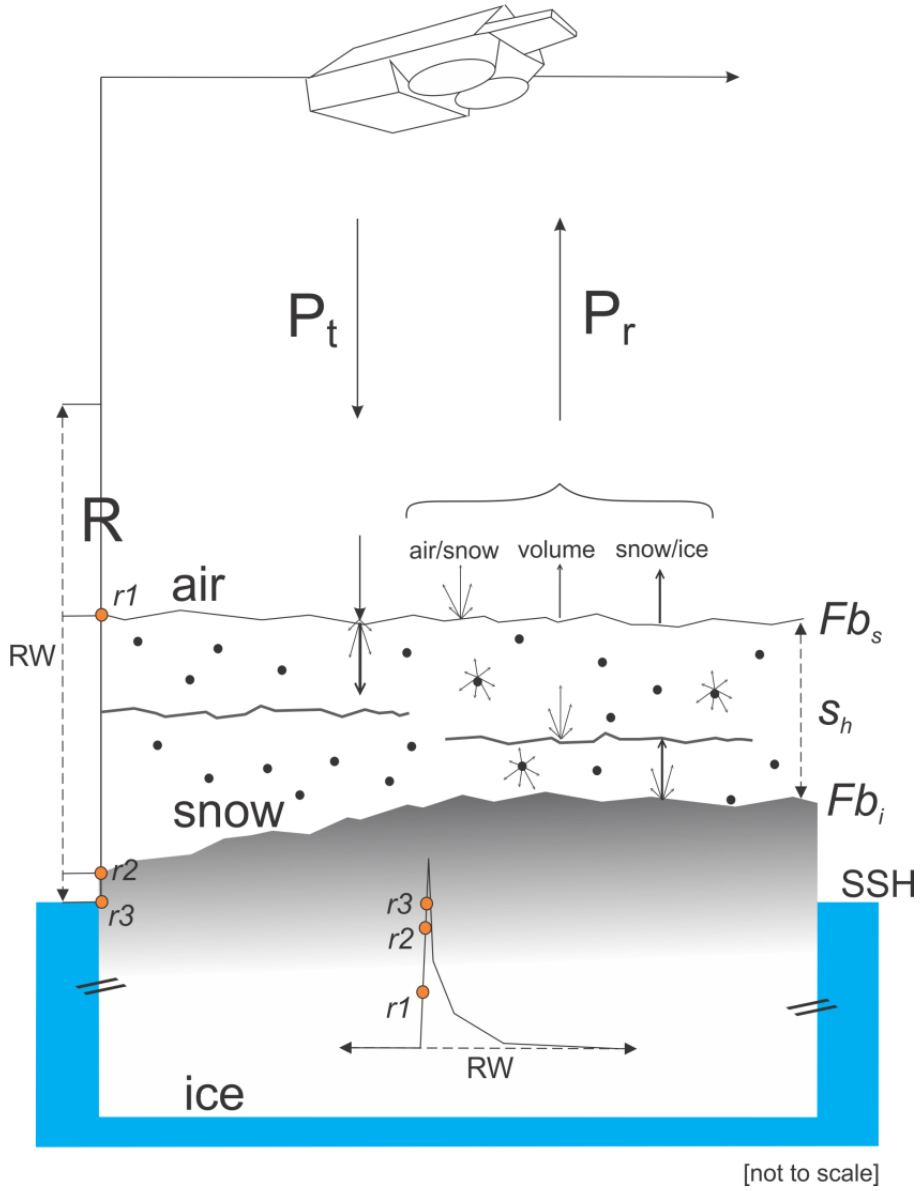

Figure 5.1. Components relating to the interpretation of CryoSat-2 freeboard data. The reception period is maintained by a range window (RW - 120 m in SIN mode) which is constantly adjusted in the vertical dimension to receive echoes from the surface. The transmitted power (P_t) is subject to interaction at the surface from the air/snow interface, volume of the snow cover and snow/ice interface which all influence the power returned to the satellite (P_r). The dominant backscattering surface is variable and is displaced by varying snow depth (s_h), snow layering and snow and ice properties. The retracking procedure is completed which results in a range (R) between *r1* and *r2* over sea ice (*r3* over water) dependent upon the assumptions of the respective retracking technique. This range is subtracted from the satellites altitude above the ellipsoid to provide uncorrected height. After application of geophysical corrections freeboard is obtained by discerning the difference between local sea surface height (SSH) and an interface in the range of the ice freeboard (Fb_i) and the snow freeboard (Fb_s) as measured by the satellite.

We aim to highlight some of the issues associated with CS-2 freeboard retrieval in the coastal Antarctic while gaining an idea of the characteristics and accuracies of the evaluated techniques. First in section 5.2 we describe the study area of McMurdo Sound, in situ information and provide an overview of CS-2. In section 5.3 we describe and discuss the surface height retrieval procedure for CS-2 under each technique. In section 5.4 we manually identify sea surface height and complete a supervised freeboard retrieval investigation providing freeboard estimates for each technique and report the findings of these results and their implications. Following this, in section 5.5, we describe the three automatic algorithms used to assess the years 2011 and 2013 in a larger area of McMurdo Sound. Results from these automated procedures are then reported and discussed in the final sections.

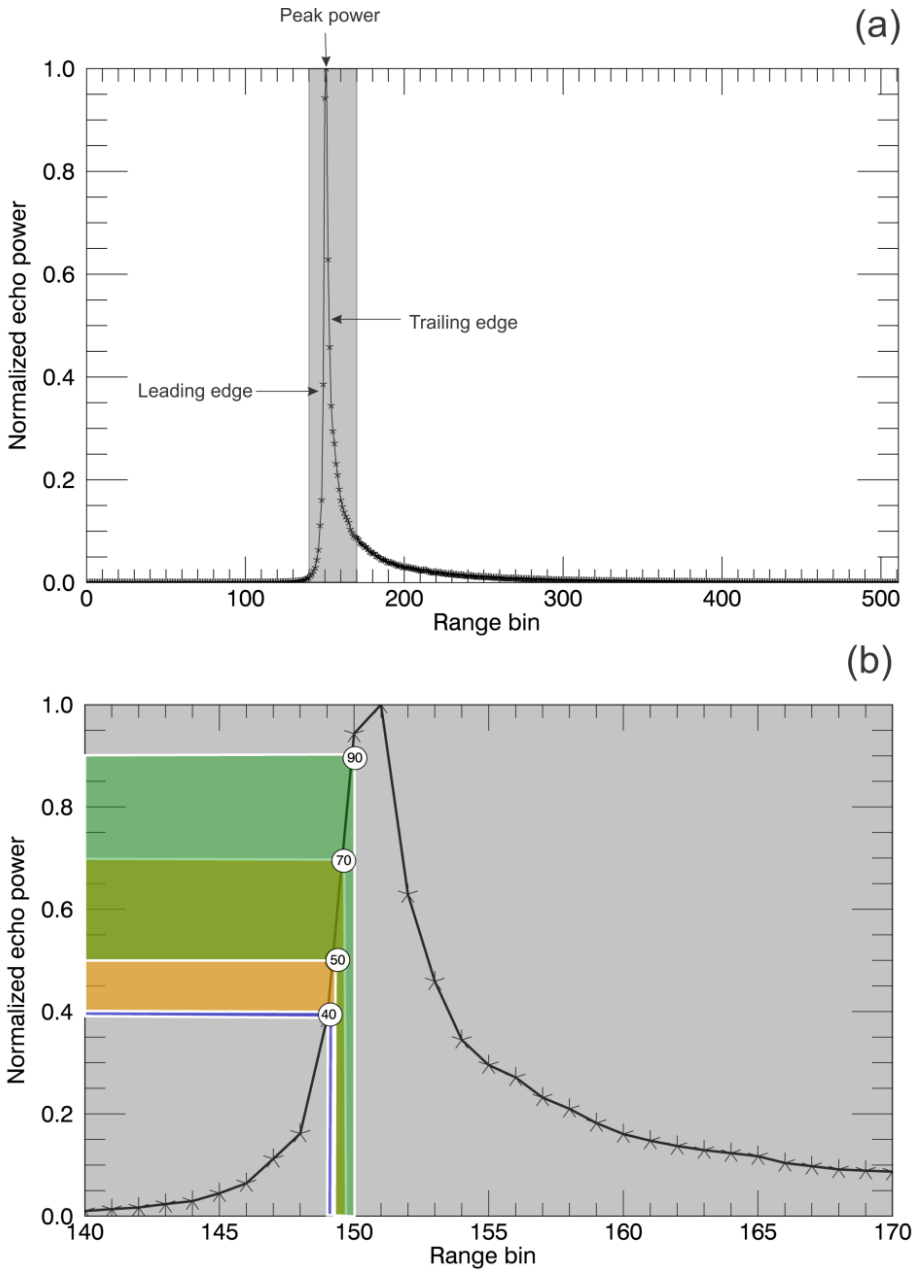

Figure 5.2. Typical CryoSat-2 SIN mode waveform over snow covered sea ice in McMurdo Sound with labelling of characteristics mentioned in the text (a). (b) Displays an expanded view of the outlined grey area in (a) from range bins 140 to 170 (1 bin = 0.234 m) and the expected retracking points on the leading edge for the techniques described here: *ESAL2* (40-70 % orange), *WfF* (50-90 % green) and *TFMRA40* (40 % blue). Note the overlapping of each procedure to avoid confusion.

5.2 CryoSat-2 assessment in McMurdo Sound

The study area indicated in Figure 5.3 covers an area of approximately 6,400 km^2. McMurdo Sound's vicinity to ice shelves and the outflow of cold ice shelf water from the ice shelf cavity contributes to sea ice formation in this area (Price et al., 2014; Gough et al., 2012; Mahoney et al., 2011; Dempsey et al., 2010; Purdie et al., 2006). This influence is hypothesized to be present in similar settings around the Antarctic with potential basin wide implications (Bintanja et al., 2013, Hellmer, 2004). During 2011 and 2013 McMurdo Sound harbours a first-year (FY) sea ice regime with extensive areas of highly homogeneous fast ice in its southern and western extremities and the MSP at its centre. The MSP undergoes complete freeze up and break out events throughout autumn and winter but is typically open water during spring and summer. This open water area can become intermittently inundated with a cover of sea ice floes that have drifted south from the Ross Sea. A detailed description of the study area is provided in (Price et al., 2014).

5.2.1 In situ investigations

During two in situ measurement campaigns in November and December 2011 and 2013 sea ice freeboard, thickness and snow depth/density measurements were made for comparison with CS-2 freeboard retrievals. The sites of in situ measurements are shown in Figure 5.3. The in situ measurement campaign for 2011 is described in detail in Price et al. (2014). These same procedures were followed in 2013. It is important to note that 2011 and 2013 had quite different sea ice conditions. In general the sea ice cover was more deformed in the west in 2013 resulting in higher geometric surface roughness. In 2011 the snow was characterized as wind compacted, with a large variability in hardness, density, and grain size. Grain size was generally large near the ice (around 3 mm), and smaller in the upper layers typically ~ 0.5 mm and smaller. Where snow was 0.20 m in thickness we found 2-3 layers, with densities varying between 330 and 450 kgm^{-3} with no significant correlation between depth and density. In 2013 a similar situation existed but both thickness and layering were reduced. In both years the distribution was highly variable with many different snow types present.

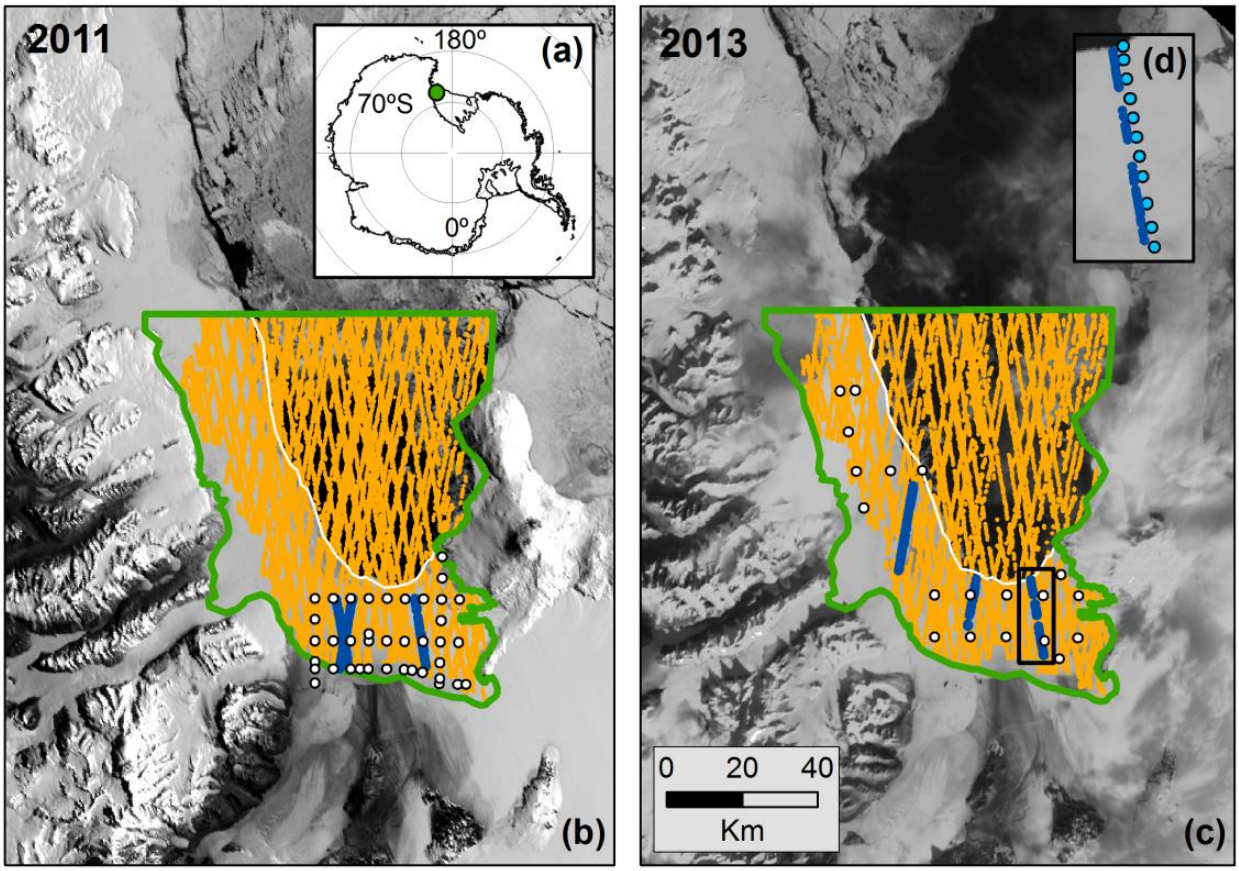

Figure 5.3. Location of the study area within the Antarctic (a). McMurdo Sound and the study area for 2011 (b) and 2013 (c) showing the distribution of CryoSat-2 tracks for each automatic study period (orange lines), those used in the supervised analysis (blue lines) and locations of in situ measurement sites (white dots). The November fast ice edge is displayed for each year (white line). The full study area for each annual automatic analysis is outlined in green. The validation line in Figure 5.4 is highlighted by the black rectangle and expanded in (d) to show each in situ measurement point (light blue dots) along the CryoSat-2 track.

5.2.2 CryoSat-2

Launched in April 2010, CS-2 operates in a near-circular polar orbit with an inclination of 92° and has a repeat cycle of 369 days with a sub-cycle of 30 days. It's on-board altimeter, SIRAL, operates at a centre frequency of 13.6 GHz, is normal incidence, with two receiver chains and operates in two modes over sea ice areas (Bouzinac, 2013). Its dedicated sea ice mode uses synthetic-aperture radar (SAR) to process height retrievals along-track at an improved spatial resolution. In addition, being pulse limited across-track results in a footprint size of approximately 380 x 1650 m with along-track sampling at ~ 300 m intervals permitting enhanced along-track ice-water discrimination and higher sampling (Bouzinac, 2013). In Antarctic coastal regions it switches to SAR interferometric mode (SIN) for ice sheet margin investigation. Interferometric processing discerns the arrival angle of radar returns via phase comparison of the returning signal which permits them to be correctly positioned on the Earth's surface, and therefore off-nadir returns accurately ranged to the surface (Bouzinac, 2013; Wingham et al., 2006). This is a necessity in complex terrain where off-nadir reflections can be received by the satellite before nadir reflections. The SIN mask extends out to a maximum distance of approximately 300 km from the Antarctic coastline and ice shelf margins. Due to the study area's proximity to the Antarctic continental coast it falls within the SIN mask. To account for the increased range over which the surface may be encountered by the incident radar beam in complex terrain, a longer tracking window is permitted in SIN mode. A reduction in burst-repetition frequency also decreases the number of resulting measurements by a factor of four compared to SAR mode (Bouzinac, 2013, Wingham et al., 2006). The measurement range window is segmented into 512 bins providing a range sampling of 1.563 ns (0.234 m in vacuo). A CS-2 SIN mode example waveform with labelling relevant to the text is shown in Figure 5.2. The surface is maintained in a range window along-track, which constantly adjusts to keep the leading edge at a specific point (centrally located at bin 255 in SIN mode) within the window (Bouzinac, 2013). Energy from the surface that is returned to the satellite builds above the noise level and increases along the leading edge to the peak power. This then decays (the trailing edge) to the end of the tracking window. The retracking procedure is then used to identify the point on the waveform that provides the range to the surface. Multiple methods exist to execute this procedure based on different assumptions about the interaction of radar energy and the surface.

5.3 Tracking surface height from CS-2 waveforms

We begin our analysis with a description of the respective retracking procedures for each method. The retracking procedure aims to provide the best estimate of range between the satellite centre of mass and the dominant backscattering horizon on the Earth's surface. This is achieved by interrogating ESA's baseline B Level 1B (*SIR_SIN_L1*) waveforms. Such interrogation provides geolocated surface heights (h^*) with reference to the WGS-84 ellipsoid that can be calculated by subtracting retracked range from the satellite's altitude.

5.3.1 European Space Agency Level 2 data product (*ESAL2*)

We utilize ESA baseline B Level 2 SIN mode (*SIR_SIN_L2*) data which has already undergone a retracking procedure. Using *SIR_SIN_L1* the ESA processor applies a model fit to determine heights from waveforms fitted to the model echo shape (Wingham et al., 2006; Wingham et al., 2004). The ESA waveform retracker is described as a '*customer furnished item*' in the CryoSat Product Handbook (Bouzinac, 2013) but no further information is provided by ESA at the time of writing. From establishing the retracking point using *SIR_SIN_L1*and *SIR_SIN_L2* data in unison, in our study area it is shown that the *ESAL2* heights have been retracked on the leading edge over a range from 40 to 70 % (Figure 5.2). Using phase information, a correction for off-nadir scattering is also applied in this product. We are unable to conclude from the available literature which surface (air/snow or snow/ice) is expected to dominate the backscatter, or what assumptions are made in the model.

5.3.2 Waveform Fitting Procedure data product (*WfF*)

An in depth overview of this product is given by Kurtz et al. (2014). Surface height is estimated by fitting a physical model to the *SIR_SIN_L1* waveforms. The model parameters include the surface roughness, which is assumed to be Gaussian, and the variation of the backscatter with incidence angle.

Dependent upon the parameters described in Kurtz et al. (2014) *WfF* establishes its retracking point at ~ 50-90 % (Figure 5.2) of peak power on the leading edge for non-specular returns and assumes that the dominant backscattering surface is the ice/snow interface. For specular returns, the model converges to the shape of the compressed transmit pulse and the retracking point is near the point of peak power, but can also be beyond the leading edge due to the finite sampling resolution of the waveform.

For the SIN mode data used in this study, the phase information is used to determine the angle to the point of closest arrival determined by the retracking point. A correction for the retracked height due to off-nadir scattering is determined from the phase information using the procedure described in (Armitage and Davidson, 2014).

5.3.3 Threshold-First-Maximum-Retracker-Algorithm 40 (*TFMRA40*)

We use *SIR_SIN_L1* waveforms but discard phase information from the returning echo. The range of the main scattering horizon is obtained by applying a Threshold-First-Maximum retracker to the waveforms. In this study we use a threshold of 40 %. The processing follows Ricker et al. (2014) by:

1. Oversampling of the original waveform by a factor of 10 using linear interpolation.
2. Smoothing of the oversampled waveform by applying a running mean with a width of 10 range bins to reduce noise.
3. The first maximum is determined by the derivative of the interpolated curve.
4. Finally the ellipsoidal elevations are retrieved by tracking the leading edge of the first maximum at 40 % of the peak power (as in Figure 5.2).

The main scattering horizon is assumed to be close to the uppermost surface, whether this is the air/snow interface or in the absence of snow cover the ice/air interface.

5.3.4 Tracking of sea surface height

The sea surface state at the time of the satellite overpass can alter the shape of the returning waveform. Over leads, given their small fetch the surface is typically flat. This provides a uniform surface with a characteristic specular waveform response, an ideal surface for both discrimination of water from sea ice and the use of consistent techniques for tracking the sea surface. However, as the size of the sea surface area being referenced is increased so is its susceptibility to atmospheric disturbance. This is clearly evident over the larger open water areas in McMurdo Sound. This was observed to hamper the identification of sea surface height (SSH). In elevated sea states that produce higher significant wave heights the slope of the leading edge of the radar waveform is flatter, due to increasing off-nadir contributions. In the case of *TFMRA40* this influence resulted in insufficient separation of fast ice elevation retrievals from sea surface retrievals (i.e. SSH was too high relative to the sea ice surface). Such an influence was not observed on the *ESAL2* or *WfF* techniques that retrack 'higher' on the leading edge and attempt to account for physical differences of surface roughness and incidence angle backscatter variations. This emphasized the need for the inclusion of an additional surface type to the *TFMRA40* procedure. The surface type *polynya* has been added to the original three; *ocean*, *lead* and *sea ice* (Ricker et al., 2014) to accurately record SSH for the larger open water area in McMurdo Sound. Over surfaces flagged as *polynya* the surface is tracked at 60 % as opposed to 40 % over *leads* and *sea ice*. This increase in the retracking threshold accommodates for the flatter leading edge forced by a higher significant wave height. This amendment improved agreement between *TFRMA40* freeboard retrievals and in situ measured freeboard data.

Second the occurrence of 'mixed' surface types within the CS-2 footprint produced noisy waveforms. Regions in which larger open water areas are intertwined with sea ice floes and smaller open water areas, more representative of leads, caused complications with the height retrieval procedure. These conditions were more prevalent in 2011 when ice floe conditions were more variable in the regions classified as open water areas. The *WfF* procedure was influenced by this, which led to SSH retrievals being too low. Slight amendments were applied to attempt to discard noisy waveforms that were causing a delay in range. These amendments, which attempted to remove noisy waveforms by assessing the occurrence of early peaks in power before maximum power and altering the initial guess of

the power to be retracked resulted in negligible improvements. Further improvement of this procedure is a current research focus.

Thirdly, as the leading edge is not necessarily affected over its entire height in the same manner, this can result in the influence of such conditions being variable between retrackers that are operating at different positions on the leading edge (Figure 5.2). This introduces an inter-retracker bias given the same sea surface conditions. The quantification of these errors is not within the scope of this study given our inability to confidently establish ocean surface conditions at the time of data acquisition. We do not find significant differences in the noise over open water between the retrackers with standard deviations of 0.14, 0.16 and 0.11 m for *ESAL2, WfF* and *TFMRA40* respectively. These values were obtained over open water areas along three CS-2 tracks covering a distance of approximately 75 km.

5.4 Supervised freeboard retrieval procedure

Upon the construction of a surface height data set, the retrieval of sea ice freeboard from altimetry includes multiple processing steps until all the dominant influences on the height profile are removed and the main variations in surface height are due to freeboard.

At this stage the main uncertainties in the CS-2 freeboard retrieval are driven by:

1. The ability of an algorithm to distinguish between water and sea ice and therefore accurately establish SSH.
2. The availability and accuracy of snow depth information.

Here we minimize the uncertainty under point 1 with the use of MODIS optical imagery to undertake a supervised identification of SSH and establish SSH more accurately. We greatly reduce the uncertainty in point 2 with available in situ snow depth/density information. We use this method on six CS-2 tracks, three from each year, 2011 and 2013 for mid-November to early December (Figure 5.3). This places the in situ validation measurements in near temporal coincidence with the CS-2 data which were acquired between 21st November and 4th December. In this section we use the supervised freeboard

retrieval procedure to yield freeboard data sets (Fb_{sup}) for the six CS-2 tracks mentioned above.

We begin our analysis using h^* estimated for each technique in section 3 which is first corrected for varying influences on the propagating radar wave through the atmosphere (cr_t); dry tropospheric, wet tropospheric and ionospheric corrections (Bouzinac, 2013). The ellipsoidal height is then reduced to a quasi-orthometric height (h) after subtracting geoid height (N) provided by the Earth Gravitational Model 2008 (EGM2008). This approximates mean sea level (MSL). To construct a SSH from this, further information is needed to quantify the sea surface height anomaly, which is the sum of the varying influences of tides (t) and atmospheric pressure and wind (i). No corrections are applied for t at this stage as the tidal gradient was found to be negligible over the spatial area in the supervised assessment. This was determined through the use of Global Navigation Satellite System (GNSS) stations deployed on fast ice in McMurdo Sound which showed no tidal gradient across the assessed distances (Price et al., 2014). Given the ~ 50 km distance we also expect the influence of i to be negligible. We therefore arrive at h with;

$$h = (h^* + cr_t) - N \tag{5.1}$$

We use MODIS imagery to identify open water areas along each CS-2 track and manually prescribe surface types of water or sea ice to each h value. The construction of SSH is highly sensitive to surface height outliers over the water surface type. The mean is largely biased by such outliers, and therefore in this case, where we are confident open water dominates we use the median to establish the supervised SSH (SSH_{sup}). We sample ~ 25 km sections along track which provides approximately 100 individual h values from which to construct SSH_{sup}. Radar freeboard (Fb_{radar}) is then derived by:

$$Fb_{radar} = h - SSH_{sup} \tag{5.2}$$

Given the assumptions about each retracker with regard to snow penetration, we follow Kurtz et al. (2014) and freeboard is then derived with the addition of a correction for the speed of light in snow. This correction (h_c) over sea ice areas is given by:

$$h_c = s_h \left(1 - \frac{c_{snow}}{c}\right) \quad (5.3)$$

Where s_h is the snow depth, c the speed of light in a vacuum, and c_{snow} the speed of light in the snowpack following (Tiuri et al., 1984) parameterized as:

$$c_{snow} = \frac{c}{\sqrt{1+1.7\rho_s+0.7\rho_s^2}} \quad (5.4)$$

where ρ_s is the snow density in gcm^{-3} measured as 385 kgm^{-3} in McMurdo Sound (Price et al., 2014). This value was also measured as the mean snow density from in situ measurements in 2013. s_h is provided by the spatial interpolation of in situ snow depth measurements. With regard to snow pack penetration by the incident radar wave we assume full penetration for *ESAL2* and *WfF* and no penetration for *TFMRA40*. The reduction of c in the snow cover results in an increased range estimate from satellite to surface. This will force a negative bias in the resultant freeboard if uncorrected; we therefore arrive at Fb_{sup} for each respective retracker under the manual assessment over fast ice with:

$$Fb_{sup} = Fb_{radar} + h_c \quad (5.5)$$

We treat Fb_{sup} outliers by removing any retrieval that deviates by more than 3 standard deviations from the mean over the sea ice area. Finally we ensure data sets are comparable with the manual removal of Fb_{sup} values that are not available for all three products.

5.4.1 Supervised freeboard retrieval results

In this section we provide results from the supervised analysis of CS-2 derived freeboards from each retracker. We compare these results to in situ validation and use this in combination with complementary field and satellite data to relate the effect of surface conditions on the resultant Fb_{sup} values. In situ ice freeboard (F_i) and snow freeboard (F_s) are provided from the interpolation of in situ measurements and extracted to be spatially coincident with each individual CS-2 Fb_{sup} retrieval. *Fbsup* which are the mean values of the three CS-2 tracks in each year are shown with in situ means in Table 5.1. The retracking techniques produce Fb_{sup} mean values ranging from 0.17 to 0.36 m which are in line with

the range of in situ measured freeboards in McMurdo Sound of 0.21 to 0.33 m. All retrackers provide higher Fb_{sup} estimates in 2011 than 2013, in agreement with the in situ measured difference in F_s between the years (0.33 to 0.26 m). 2013 Fb_{sup} values for each technique are in agreement with what is expected given the assumption of the relevant retrackers (see Figure 5.2 and difference in range), *WfF* the lowest and *TFMRA40* the highest. *WfF* shows closer agreement with F_i while *TFMRA40* freeboards are closer to F_s. *ESAL2* Fb_{sup} is established between F_i and F_s. Therefore, the trivial relationship between differences in retracked range and resultant freeboard values is maintained in 2013. Whether the comparison is complicated further by the influence of surface conditions on each technique is perhaps better showcased in 2011. It appears that the situation is complicated in 2011 with regards to *WfF* as its Fb_{sup} value is 0.19 m higher than in 2013 with no significant change in F_i recorded in situ. The cause of this discrepancy is either related to alteration of the retracking procedure over the sea ice, driven by surface conditions or by inadequate establishment of SSH_{sup}, or a combination of these factors. It is likely that interference with SSH_{sup} establishment, as alluded to in section 5.3.4, played a part in the high freeboard value for *WfF*, but we also attribute the influence of the snow cover. The full snow cover penetration assumption of the *WfF* method may not be fulfilled given a thick snow cover that can be an effective scatterer of the incident radar energy. When the echo power from the snow/ice and air/snow interfaces have a similar magnitude a positive freeboard bias may be introduced (Kwok, 2014, Kurtz et al., 2014). This bias is estimated to reach a maximum of 0.04 m for homogenous snow conditions (Kurtz et al., 2014). It is likely to have played a more significant role here due to the layering in the snow cover and wind hardening at the surface. From our limited information about the retracking procedure for *ESAL2* we would expect to see a similar relationship. Such a relationship is measured, with *ESAL2* Fb_{sup} 0.05 m higher in 2011 than 2013.

Table 5.1. Mean freeboard values, standard deviations and sample sizes (*n*) derived by each retracker by the supervised procedure in austral spring (November and December) 2011 and 2013 and comparison to interpolated in situ mean ice (F_i) and snow freeboards (F_s).

Re-tracker	**Spring 2011** Fb_{sup} **n = 148**	**Spring 2013** Fb_{sup} **n = 163**
	Meters	Meters
Fb_i	0.22 ± 0.07	0.21 ± 0.04
Fb_s	0.33 ± 0.01	0.26 ± 0.04
ESAL2 Fb_{sup}	0.29 ± 0.14	0.24 ± 0.17
WfF Fb_{sup}	0.36 ± 0.13	0.17 ± 0.13
TFMRA40 Fb_{sup}	0.36 ± 0.15	0.29 ± 0.11

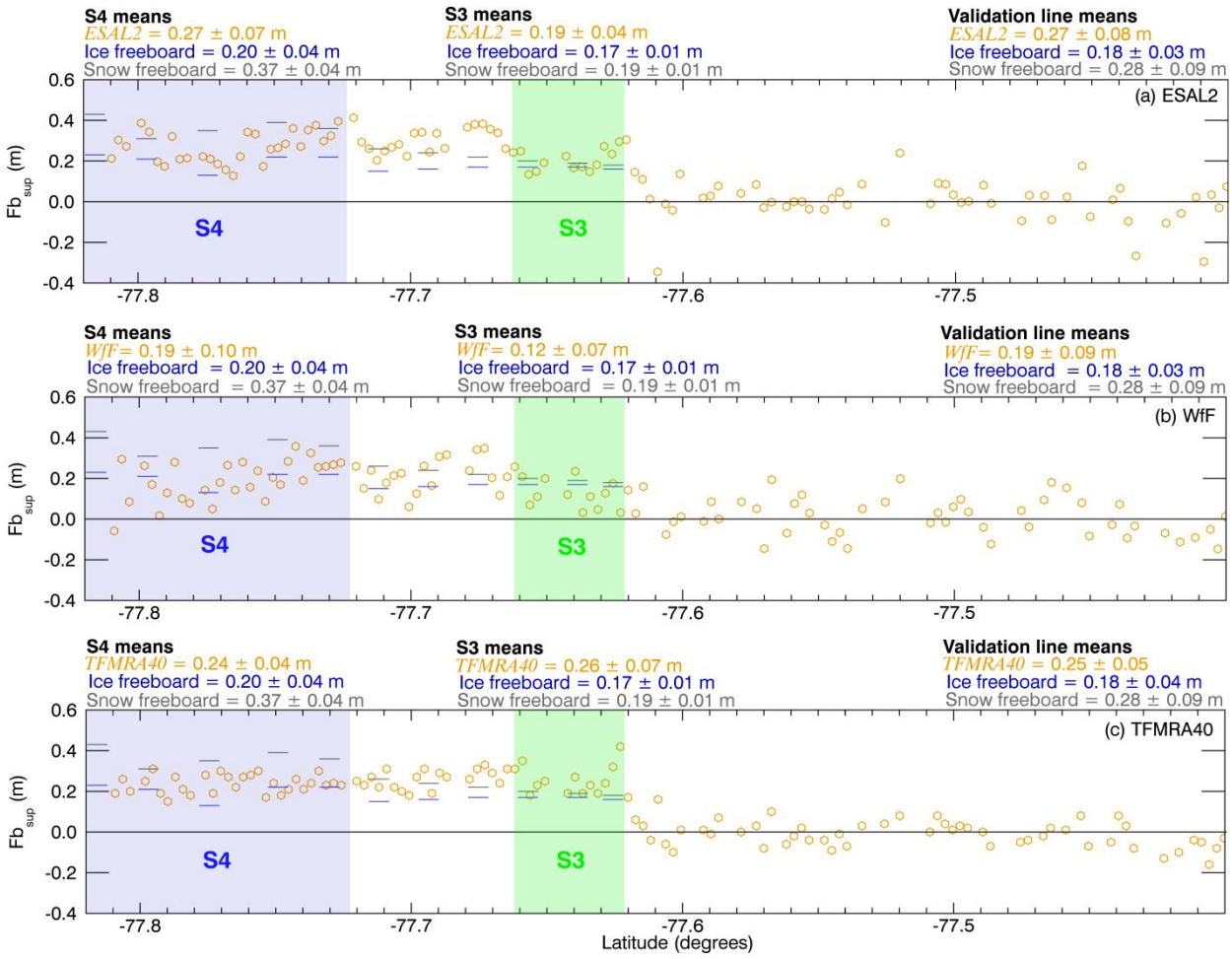

Figure 5.4. Comparison of each method along a validation line coincident with a CryoSat-2 overpass on the 27.11.2013 for (a) *ESAL2*, (b) *WfF* and (c) *TFMRA40*. In situ measured ice and snow freeboards are shown as blue and grey horizontal lines respectively. Segments 3 (S3) and 4 (S4) in Figure 5.5 are also shown. Sea surface height was identified using the supervised procedure. The CryoSat-2 height profile begins in the north over open water and progresses south over the fast ice edge at the beginning of segment 3. The freeboard retrievals for each respective retracker are displayed as orange circles, the validation line statistics describing the sea ice area only. S3 and S4 means are also displayed for each technique, ice freeboard and snow freeboard.

To provide further insight into the influence of snow cover and ice conditions on the radar signal we show *Fbsup* along a coincident in situ validation line on 27.11.2013 (Figure 5.4). The validation measurements along this line were temporally coincident to within 3 hours of the CS-2 overpass. It should be noted that due to a satellite orbit manoeuvre the validation line was ~ 1 km west of the CS-2 groundtrack. Visually we observed no significant changes to the characterized sea ice surface conditions or snow depth over this distance and therefore find the in situ and CS-2 data sets comparable. The surface conditions on the sea ice varied along the validation line from north to south. Clear differences in Fb_{sup} are displayed between the techniques. Mean Fb_{sup} for *WfF* shows good agreement with F_i. *ESAL2* mean Fb_{sup} is in better agreement with F_s but the response of the height retrievals to surface conditions follow a similar pattern as observed for *WfF*. *TFMRA40* has a very consistent Fb_{sup} profile which exhibits minimal response to changing surface conditions producing values that closely agree with F_s across the whole profile. We are able to assess the response of each of the retracking techniques to the presence of a homogenous section of dry snow in segment 4 (Figure 5.4). Fb_{sup} for all techniques appear to track and interface in good agreement with in situ F_i over segment 4, with *ESAL2* and *WfF* measuring the in situ measured decrease in Fb_i in the central part of the segment. Further in support of *WfF* assumptions, its Fb_{sup} appears to exhibit no significant positive bias as CS-2 passes over this area of relatively homogenous snow cover (segment 4 – mean *WfF* Fb_{sup} = 0.19 m, in situ F_i = 0.20 m, in situ F_s = 0.37 m). However in 2011, when the snow cover was thicker, less homogeneous and more layered in comparison to segment 4 in 2013, the mean *WfF* Fb_{sup} value is 0.36 m, even higher than the F_s of 0.33 m.

Both *ESAL2* and *WfF* clearly exhibit a large variability in freeboard retrievals over sea ice in response to either snow or ice conditions. Using near coincident TerraSAR-*X* (*X*-band) imagery and in situ measurements and observations we attempt to separate the influences of snow and sea ice conditions. We provide four segments in McMurdo Sound in 2013 over which sea ice geometric roughness (GR) and radar roughness (RR) varied. Given the similar wavelengths of *X*-band (~ 0.03 m) and *Ku*-band (~ 0.02 m) and assuming the incidence angle dependence of backscattering properties is dominated by surface scattering a near inverse relationship between backscattered power between TerraSAR-*X* (40° incidence angle) and CS-2 (normal incidence) can be expected. The relatively bright areas on level sea ice (bounded by white line in Figure 5.5a) are rough with respect to the radar wavelength and the dark areas are smooth. This is maintained for CS-2, but for its nadir

looking roughness (SAR image brightness) to CS-2 power, the relationship is opposite. For the sea ice area, we assess the differences in waveforms that have been averaged and stacked. The numbers of waveforms averaged to create each representative waveform were between 15 and 28. We identify an area of high GR (segment 1, FY ice that has likely been deformed by storm activity) and low GR (segment 2, older FY ice which was less deformed) over the FY fast ice area. These were established primarily from field observations, with the TerraSAR-*X* image as support. Segment 1 (high GR, variable RR, lowest s_h) causes the largest power return closely followed by segment 2 (low GR, low RR, low s_h). It is clear that other variables also influence the signal return. This is clearly established by comparison of segments 3 and 4. Segment 3 has the lowest power return of the assessed waveforms and exhibits high radar backscatter in the TerraSAR-*X* image. This indicates that RR is high. These observations are supportive of the fact that RR is the dominant influence on the power returned to the satellite and that GR is playing a secondary role. It is difficult to attribute the influence of volume scattering from snow as no areas with the same RR are available with significant differences in snow depth.

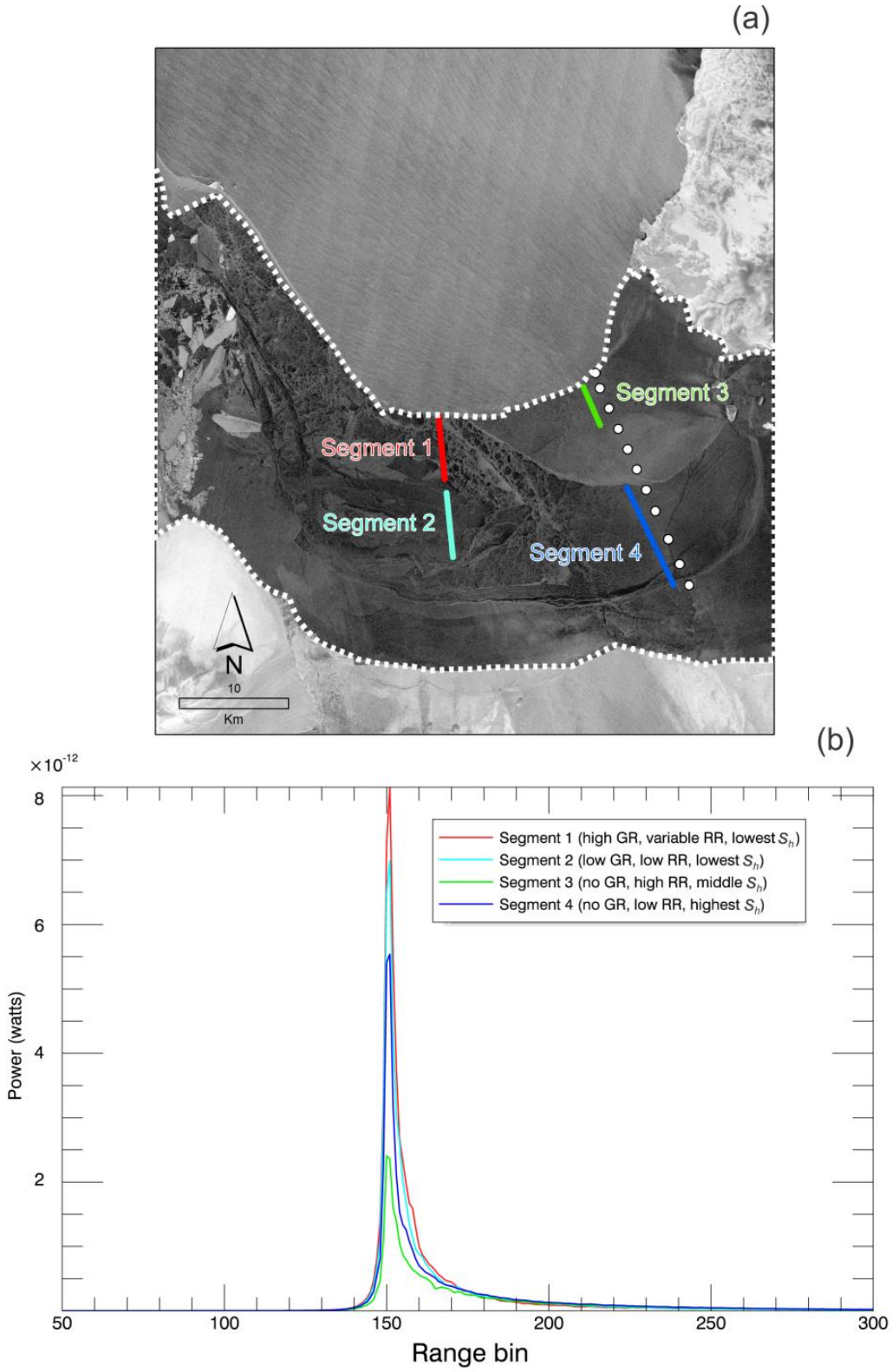

Figure 5.5. Segments 1 to 4 over the first-year sea ice area (bounded by white dotted lines) are overlaid upon a TerraSAR-*X* radar image from 28.11.2013 (c). TerraSAR-*X* image courtesy DLR. Mean waveforms from these segments are plotted as power (watts) for multiple sea ice surface conditions with variable geometric roughness (GR), radar roughness (RR) and snow depth (s_h).

In an attempt to assess the influence of snow depth we look at two tracks in 2011 that exhibited a larger difference in snow depth for which we expect RR to be less variable. These example tracks, snow (mean depth 0.20 m) and reduced snow (mean depth 0.07 m) are displayed in Figure 5.6 with the retracking points for each technique. These waveforms are the mean normalized echo power of ~ 50 waveforms and are aligned by peak power to achieve comparativeness between each technique. The mean retracking point for each waveform for each technique is also displayed. It should be noted here that comparison of their absolute range differences cannot be inferred from the available information, only the inter-example variation in the waveform shape. It is shown that in the presence of a significant snow cover that the slope of the leading edge becomes shallower, and that the power of the trailing edge is increased along with the overall width of the waveform.

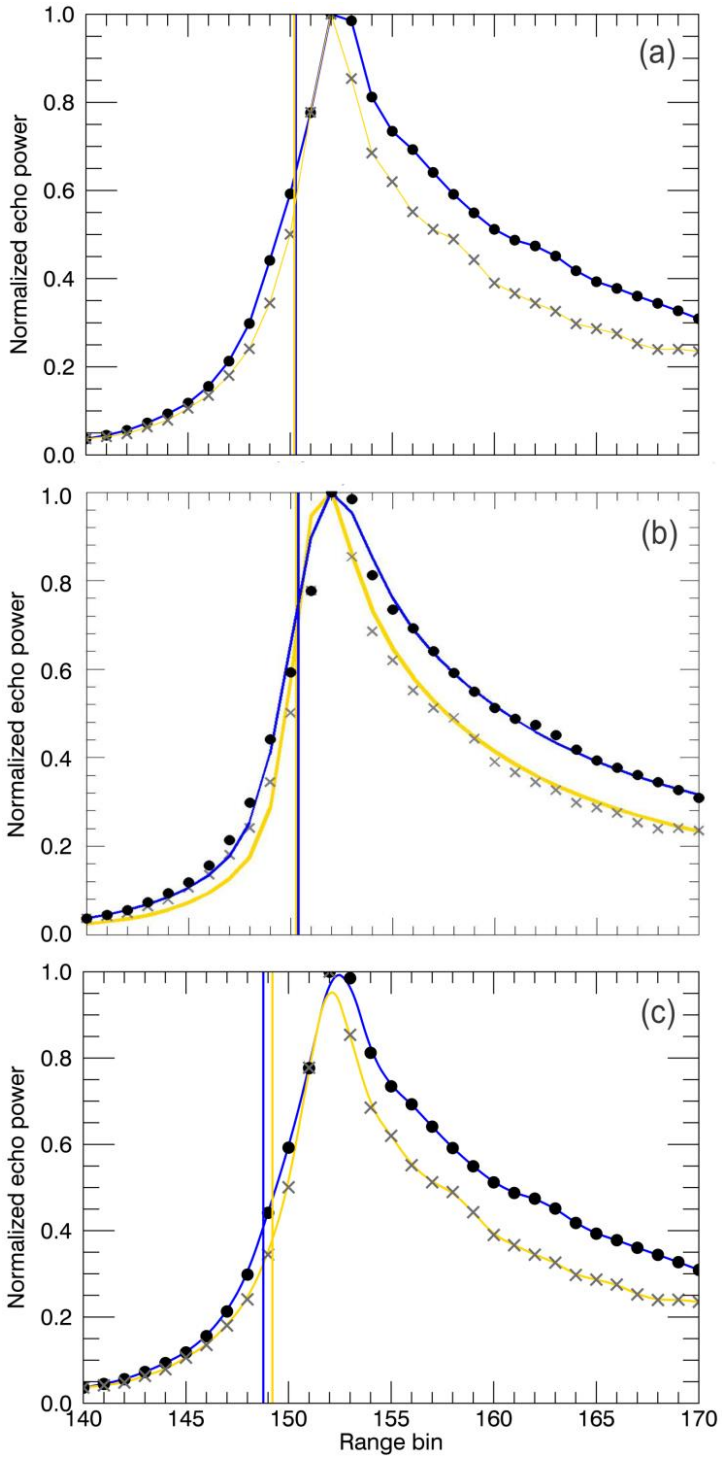

Figure 5.6. Mean waveform examples for sea ice in 2011 with significant snow cover (circles and blue fits) and minimal snow cover (crosses and orange fits). The area with significant snow cover had a mean snow depth of 0.20 m with consistent coverage. Over the minimal area a mean snow depth of 0.07 m was measured with a patchy distribution. (a) Shows the retracking points for *ESAL2* with linear fits between each bin, (b) the retracking points for *WfF* with respective model fits and (c) the retracking points for *TFMRA40* with interpolated curves.

5.5 Automatic freeboard retrieval procedure

The automatic differentiation of sea ice and water is a fundamental requirement for large scale altimetric sea ice freeboard retrieval. Automated methods generally fall into two categories, the first relying on the use of information received in the surface return signal by the instrument and the second on mathematical generalizations that approximate expected surface conditions, or, a combination of the two. In the case of CS-2, methods currently presented in the literature (Kurtz et al., 2014; Ricker et al., 2014; Laxon et al., 2013) fall into the first category following similar investigative procedures initially demonstrated by (Peacock and Laxon, 2004). These contemporary methods make use of the pulse peakiness and stack standard deviation, among other parameters, to differentiate between radar returns from small open water leads in the sea ice cover and sea ice floes. In the second category, the expected amount of water along-track is given a value and the heights of this lowest percentage are averaged for a certain segment of track giving a sea surface height (Zwally et al., 2008; Price et al., 2013). This approach, commonly termed along-track filtering is yet to be examined in the literature with respect to CS-2. The three automatic retrieval techniques used in this study area described below.

Following from h established in section 4 all data undergo the same additional corrections to produce comparable data sets. *h* is further corrected for *t* and *i* to give *H*:

$$H = h + t + i \tag{5.6}$$

The influence of i is accounted for using a dynamic atmosphere correction and compensates for the influence of barometric pressure and winds on the sea surface. *t* is the sum of corrections for ocean tide, long period equilibrium tide, ocean loading tide, solid earth tide and the geocentric pole tide. Further details on the corrections applied for *t* and *i* are given in Bouzinac (2013). These additional corrections accommodate for the larger geographical region (Figure 5.3) under investigation in the automatic procedure over which tidal and atmospheric effects will be influential on the 'flattening' of the height profile. Each method then produces its own automatic SSH (SSH_{auto}) to provide Fb_{auto} as;

$$Fb_{auto} = H - SSH_{auto} \quad (5.7)$$

No adequate snow depth information is available for the two annual test cases assessed under the automatic procedure and therefore no correction is applied for h_c. The procedures for attaining SSH_{auto} for each technique and other relevant amendments are described in the following sub-sections.

5.5.1 *ESAL2* automatic SSH identification

Measurement quality flags provided in the CS-2 Level 2 record structure were used to improve the quality of the data set. *H* values are discarded if the following parameters in the product are flagged as poor; *block degraded*, *orbit error*, *orbit discontinuity*, *height error*, *calibration caveat*, *backscatter error*, *peakiness error*, *SIN cross-track angle error*, *SIN receive channel 1 error*, *SIN receive channel 2 error*, *mispointing error* and *delta time error* which are given in Bouzinac (2013). In SIN mode, the off nadir location of the height retrieval can be determined from phase information of the dominant scattering in the power echo, which over sea ice areas can be significantly off nadir (Armitage and Davidson, 2014). This ability prevents underestimations of ocean elevation as a result of 'snagging' from leads located off nadir providing a reduction in noise over height profiles. According to the across-track offset computed from the phase difference, open water and level sea ice areas also produce echoes geolocated off nadir. From assessment of approximately 800 separate elevation retrievals over open water in McMurdo Sound from two tracks in 2013, identified by comparison with near-coincident MODIS imagery the mean deviation from nadir was 270 ± 70 m. We apply a removal threshold of ± 750 m from nadir simply to limit information to the expected nadir footprint area that we are comparing to validation measurements and to maintain comparativeness to the other methods.

To remove height outliers we apply a vertical threshold of ± 2 standard deviations of the mean to each track. Heights outside this threshold are discarded.

We use the Level 2 parameter peakiness (P) as a means of differentiating between three surface types; open water, leads and fast ice. P is suggestive of how sharply peaked the

returning waveform is, and is defined as the ratio of the highest bin value to the mean of all bins above the retracking point (Bouzinac, 2013). P ranges between 0 and 120 in our investigation area (Figure 5.7). High P values are indicative of leads, which are geometrically of similar size to the radar footprint and typically have specular surfaces. Low P values are indicative of open water areas that are geometrically larger than the radar footprint and are typically diffuse surfaces. Fast ice P values are in between these two extremes but are affected by sea ice surface conditions. We establish thresholds for these surface types after comparison of P values over certain surface types in the study region as indicated by MODIS and TerraSAR-*X* imagery and knowledge of the sea ice regime. P has a large standard deviation even when a certain surface type is completely isolated indicating it is highly sensitive to small changes in surface conditions.

First we assessed the P threshold for leads. It is very challenging to constrain such a value due to the difficulty of achieving coincidence between CS-2 measurements and satellite imagery. Therefore, we investigated P values in March when sea ice begins to freeze on the open water in McMurdo Sound and the surface is dominated by developing floes. At this time leads are abundant and we take the upper quartile of P values as representative of the leads surface type ($P > 90$) for both years.

The two remaining surface types require further scrutiny due to overlaps in their P distributions. McMurdo Sound was assessed in February 2013 when it was dominated by open water. In both 2011 and 2013 the majority (> 95%) of P values were < 15. However, in 2011 the surfaces types open water and fast ice overlapped, whereas in 2013 a clear separation is achievable (Figure 5.7). This is a result fast ice surface conditions differing in 2011 that lowered values in the P distribution over fast ice. We are unable to fully establish the cause of this change. The pulse shape, and thus P are largely determined by variation of backscatter with incidence angle (Wingham et al., 2006). This is related to RR and therefore given the differing conditions over the fast ice between the two years, a change in RR from the dominant backscattering surface was likely the cause. In 2013 it is possible to clearly differentiate and establish open water as $P < 15$ and fast ice $15 < P < 90$. In 2011 we lower the threshold for open water to $P < 7.5$ to reduce the amount of fast ice potentially included in the expected open water retrievals. 2011 fast ice is therefore given thresholds of $5 < P < 90$. We appreciate these thresholds for open water and fast ice overlap, but if a higher bound is taken for the low limit of P for fast ice in 2011 ~ 60 % of fast ice identified

height retrievals will be discarded. The fast ice P distributions were established from assessment of the fast ice area. The sea ice growth season in McMurdo Sound begins in March, but fast ice does not become fully established for some time. We are confident that fast ice is established by August and derive a P value for this surface type by masking the end of growth season fast ice area from August to December. We assume the fast ice area to also be representative of P values for ice floes in McMurdo Sound. Finally due to the discussed overlaps of open water and fast ice (Figure 5.7), and potential inclusion of sea ice in expected open water retrievals it is necessary to filter *H* values with regard to their heights. This approach is altered for each year to account for the expected inclusion of ice in the open water retrievals (Figure 5.7, 40 % in 2011 and 20 % in 2013). We calculate the mean of the lowest 60 % of *H* values in 2011 and 80 % in 2013 that meet the open water and lead criteria and establish SSH_{auto} for each track from this. Though the use of along-track filtering in radar altimetry is avoided, likely due to noise levels and off-nadir scattering, we have confidence in its ability here after attempts to reduce noise using standard deviation thresholds and available phase information which limits the influence of off-nadir returns.

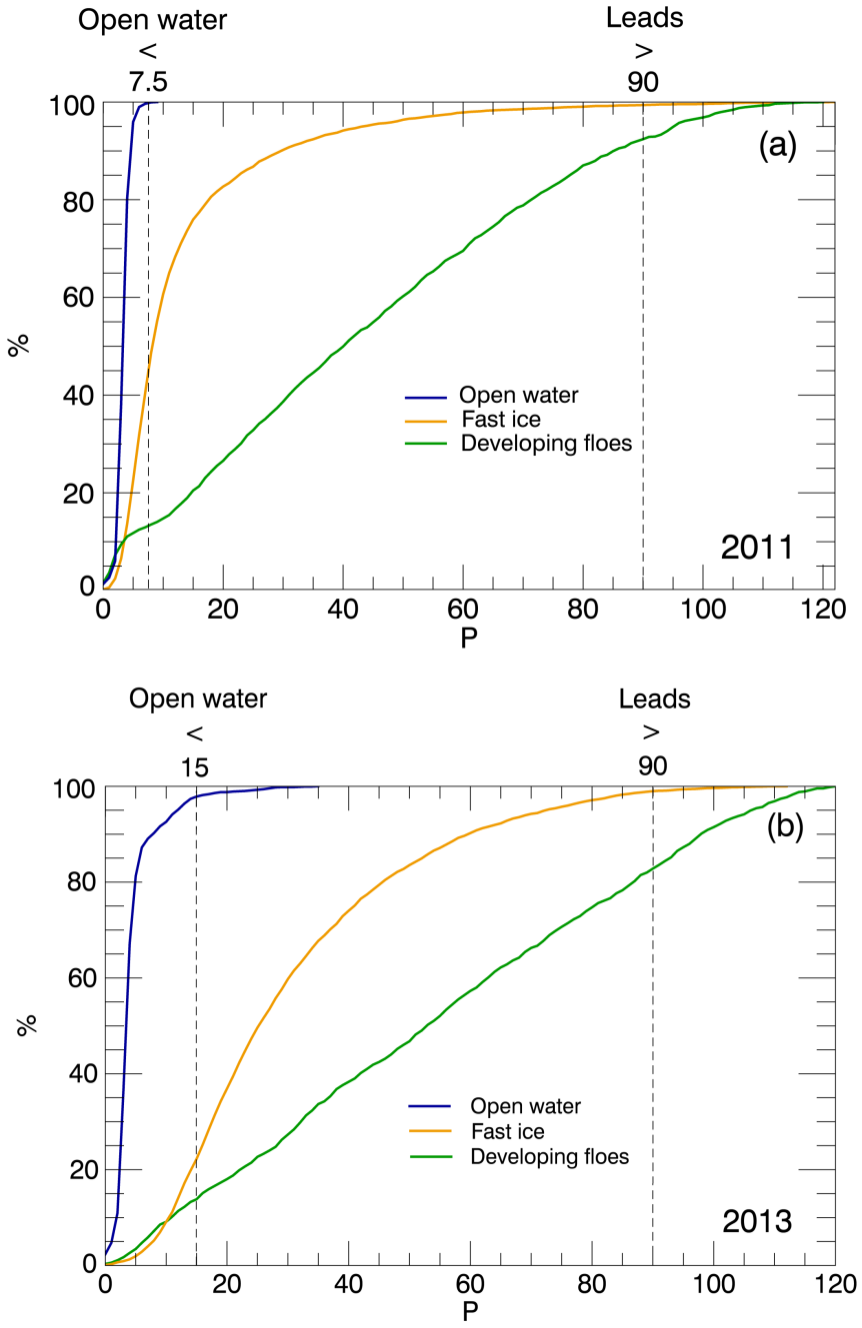

Figure 5.7. Surface type discrimination as indicated by Level 2 parameter peakiness (P) displayed as a cumulative percentage. Surface types, open water, fast ice and developing floes are displayed for 2011 (a) and 2013 (b). In 2011 surface conditions made the discrimination of open water and fast ice more difficult. This resulted in a change in the thresholds between the years. The expected inclusion of sea ice in the open water surface type is indicated by the percentage overlaps.

5.5.2 *WfF* automatic SSH identification

We attain SSHauto by using a similar parameter to Level 2 P, the pulse peakiness (PP) as described by Armitage and Davidson (2014). The assigned values for the discrimination of each surface type were chosen after comparison of PP values over surface types in the study area using the same method as described for *ESAL2* in section 5.1. We flag leads as PP > 0.30 and open water as PP < 0.05. Sea ice is classified as 0.08 < PP < 0.30. Overlaps of sea ice and open water surface types were noted as in section 5.1. To remove this height bias from inclusion of sea ice we establish SSH_{auto} from the mean of the lowest 60 % and 80 % of elevations flagged as leads of open water in 2011 and 2013 respectively. Phase information is also used in this product in the same manner as *ESAL2*. We again remove elevation outliers with application of a vertical threshold of ± 2 standard deviations of the mean to the track.

5.5.3 *TFMRA40* automatic SSH identification

We use the algorithm described in Ricker et al. (2014) but amend the procedure as surface conditions differ in the investigation area from those that the technique has previously been applied. As mentioned in section 3.4 we maintain the inclusion of the additional surface type, *polynya* and its amended 60 % retracking threshold. The elevations retrieved for both leads and polynyas in close proximity should be of the same mean value to construct a consistent SSH_{auto}. We compared the elevations of detected leads that were in close proximity to the *polynya* surface type for several CS-2 tracks and found sufficient agreement using a 60 % and 40 % threshold for each surface type in conjunction. Track sections with a significantly inaccurate SSH_{auto}, as a consequence of sparse lead/open water coverage, have been discarded.

5.5.4 Automatic results

The application of the three retracking techniques produced Fb_{auto} datasets for McMurdo Sound for the years 2011 and 2013 (Table 5.2). All techniques show a decrease in freeboard in McMurdo Sound from 2011 to 2013 over the study area as a whole and the fast ice area when assessed alone. The magnitude of this change varies between methods. *ESAL2* and *TFMRA40* both identify the fast ice area as having a higher freeboard than the mean of the entire study area. *WfF* does not show such a relationship with fast ice mean Fb_{auto} being 0.01 m lower in 2011 and the same value in 2013. A lower mean freeboard is expected for the entire study area as sea ice in the dynamic area inclusive of the MSP is expected to be thinner than the fast ice that has undergone near continuous and stable growth over winter. This discrepancy may be driven by the identified problems with surface type discrimination. Open water areas may have been erroneously included as sea ice, lowering the Fbauto averages. Clearly apparent are the large standard deviations of the CS-2 data.

Table 5.2. Mean automatic procedure freeboard values and standard deviations derived by each technique for each year for the entire study area and fast ice only (bold). The total number of measurements (*n*) for each year are also displayed.

Retracker	2011 Meters	2013 Meters
ESAL2 Fb_{auto}	0.09 ± 0.25	0.08 ± 0.24
	0.11 ± 0.27	**0.09 ± 0.26**
	(*n* = 16611)	(*n* = 12884)
WfF Fb_{auto}	0.12 ± 0.24	0.10 ± 0.23
	0.11 ± 0.25	**0.10 ± 0.22**
	(*n* = 7094)	(*n* = 9439)
TFMRA40 Fb_{auto}	0.16 ± 0.35	0.11 ± 0.38
	0.23 ± 0.36	**0.15 ± 0.46**
	(*n* = 7532)	(*n* = 8244)

To investigate the ability of CS-2 further and to minimize the influence of the MSP sea ice area we assess the fast ice area with regard to its seasonal development. The FY fast sea ice regime in McMurdo Sound typically breaks out in February, and often in one of every two years (Heine, 1963), leaving McMurdo Sound nearly entirely ice free. FY sea ice begins to form in March when air temperatures are low enough to initiate freezing as indicated by field studies (Purdie et al., 2006, Leonard et al., 2006) and MODIS imagery. This was the case in 2011 and 2013. The sea ice develops into a fast ice cover in a coastal band (Figure 5.3) around McMurdo Sound throughout the year, with fast ice establishment intermittently interrupted by storms events (as indicated by radar optical and SAR imagery). Sea ice growth is expected until mid-December (Jeffries et al., 1993). We use the region of McMurdo Sound that is covered by fast ice at the end of the growth season as a mask for the entire year. We expect to observe a signal in the recorded Fb_{auto} data sets indicative of increasing freeboard from March to December. Such findings are displayed in Figure 5.8 where we clearly see this development using all three techniques. All techniques record increasing Fb_{auto} through autumn and winter toward Fb_i and Fb_s in situ measurements in spring. We apply a linear trend from the beginning of March to mid-December to capture the sea ice growth as captured by measured Fb_{auto} for each technique. Using this trend to compare Fb_{auto} results to in situ measurements centered around mid-November (~ day 260 in Figure 5.8) we find *ESAL2* Fb_{auto} underestimates Fb_i in both years by 0.04 m. In 2011 *WfF* Fb_{auto} overestimates in situ measured sea ice freeboard by 0.04 m and in 2013 underestimates it by 0.01 m. *TFMRA40* provides a mean Fb_{auto} value of 0.33 m in 2011 in agreement with Fb_s. In 2013 *TFMRA40* Fb_{auto} underestimates Fb_s by 0.10 m. All techniques also display a decrease in Fb_{auto} after reaching their respective maximums in line with the observed break out of the fast ice area in late February/early March of each year. Mean values and standard deviations for each month are displayed in Table 5.3.

Table 5.3. Mean automatic procedure freeboard values, standard deviations and number of measurements used to derive the statistics for each technique in each year over the fast ice area. The data are binned into calendar month. The day corresponding approximately to the middle of each calendar month from the start of the analysis (day zero = 1st March) are also displayed.

Month	2011 Meters			2013 Meters		
	ESAL2	***WfF***	***TFMRA40***	***ESAL2***	***WfF***	***TFMRA40***
MAR (+15.2)	-0.04 ± 0.16 (494)	0.00 ± 0.35 (232)	0.05 ± 0.29 (105)	-0.01 ± 0.30 (394)	0.01± 0.21 (260)	0.05 ± 0.19 (271)
APR (+45.6)	0.02 ± 0.24 (560)	0.13 ± 0.18 (400)	0.03 ± 0.15 (317)	0.03 ± 0.12 (480)	0.08 ± 0.15 (488)	0.16 ± 0.43 (362)
MAY (+76)	0.06 ± 0.14 (537)	0.12 ± 0.16 (296)	0.14 ± 0.38 (526)	0.05 ± 0.26 (623)	0.13 ± 0.15 (508)	0.08 ± 0.19 (238)
JUN (+106.4)	0.14 ± 0.31 (400)	0.02 ± 0.30 (246)	0.05 ± 0.22 (204)	0.07 ± 0.24 (543)	0.04 ± 0.21 (409)	0.03 ± 0.19 (267)
JUL (+136.8)	0.19 ± 0.25 (859)	0.17 ± 0.18 (395)	0.12 ± 0.12 (221)	0.04 ± 0.22 (732)	0.11 ± 0.17 (531)	0.08 ± 0.32 (266)
AUG (+167.2)	0.05 ± 0.23 (838)	0.16 ± 0.17 (165)	0.31 ± 0.35 (443)	0.08 ± 0.16 (604)	0.16 ± 0.13 (486)	0.26 ± 0.41 (588)
SEP (+197.6)	0.12 ± 0.25 (952)	0.11 ± 0.26 (199)	0.24 ± 0.22 (703)	0.03 ± 0.28 (647)	0.10 ± 0.21 (499)	0.03 ± 0.23 (241)
OCT (+228)	0.11 ± 0.22 (786)	0.24 ± 0.19 (102)	0.21 ± 0.39 (341)	0.14 ± 0.14 (208)	0.36 ± 0.14 (159)	0.14 ± 0.19 (199)
NOV (+258.4)	0.15 ± 0.20 (725)	0.27 ± 0.24 (121)	0.37 ± 0.22 (196)	0.17 ± 0.18 (602)	0.19 ± 0.18 (286)	0.24 ± 0.26 (255)
DEC (+288.8)	0.11 ± 0.29 (847)	0.26 ± 0.21 (136)	0.39 ± 0.43 (527)	0.26 ± 0.34 (910)	0.09 ± 0.26 (705)	0.11 ± 0.35 (453)
JAN (+319.2)	0.19 ± 0.35 (643)	0.10 ± 0.30 (161)	0.37 ± 0.45 (407)	0.18 ± 0.22 (313)	0.01 ± 0.31 (228)	0.46 ± 0.72 (516)
FEB (+349.6)	0.10 ± 0.44 (340)	-0.10 ± 0.18 (119)	0.33 ± 0.70 (72)	0.00 ± 0.34 (325)	-0.14 ± 0.20 (216)	-0.11 ± 0.62 (455)

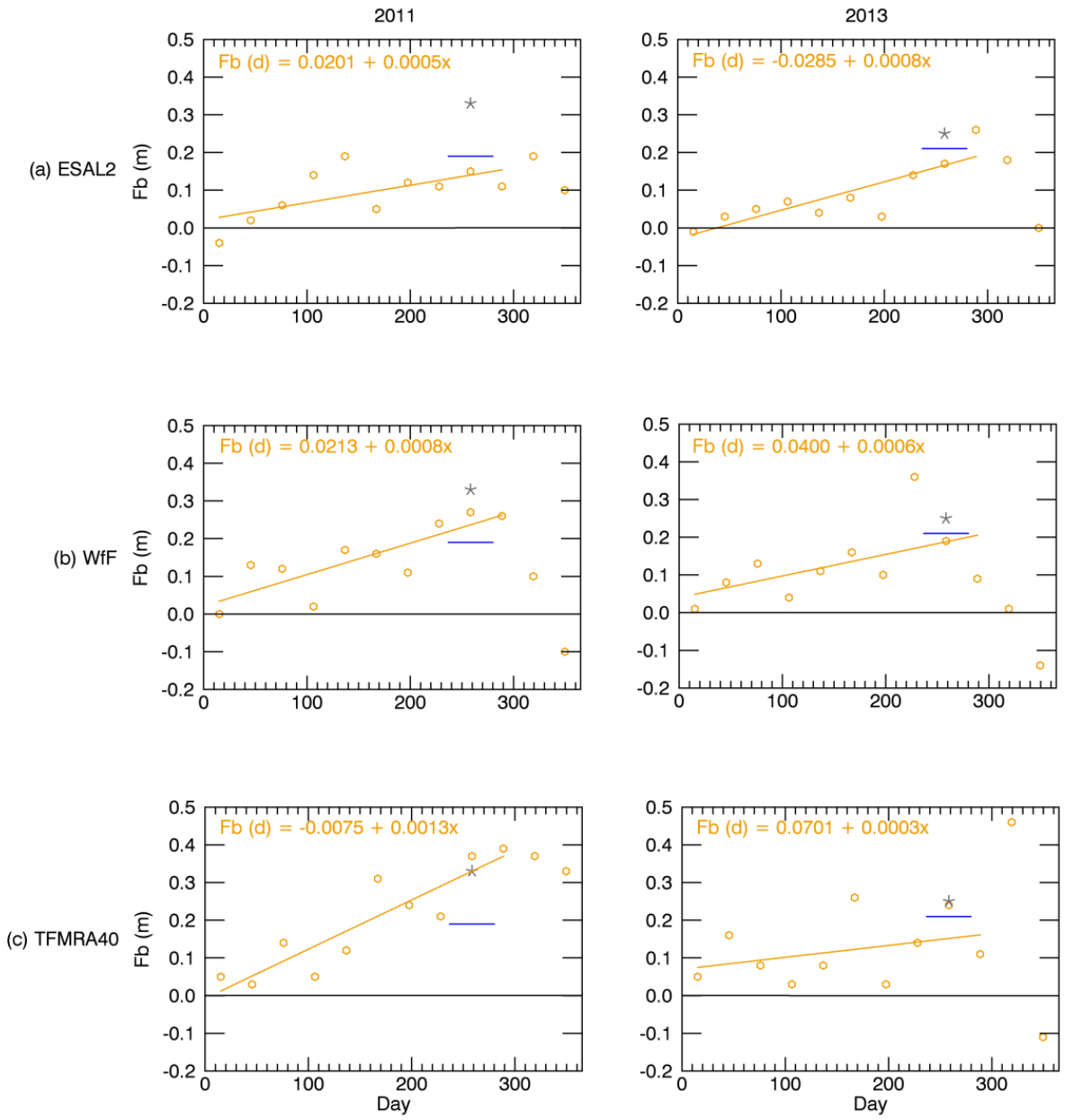

Figure 5.8. The development of the McMurdo Sound fast ice cover from mean automatic procedure freeboard values for each month for 2011 and 2013 (day zero = 1st March) for *ESAL2* (a), *WfF* (b) and *TFMRA40* (c). A linear fit from the beginning of mid-March (~ day 15) to mid-December (~ day 290) defines the expected sea ice growth season. Mean in situ measured ice and snow freeboards measured in November/December of each year are shown by the blue line and the grey asterisk respectively.

We are able to evaluate the performance of the automatic procedure by comparison of the CS-2 mean Fb_{sup} over the validation line (Figure 5.4) against the Fb_{auto} mean over the same track. With the application of a correction for c in snow, Fb_{auto} overestimates Fb_{sup} by 0.07, 0.05 and 0.01 m for *ESAL2*, *WfF* and *TFMRA40* respectively. The overestimation of freeboard by Fb_{auto} for *ESAL2* and *WfF* is driven by the along-track filtering of *H* employed. The filtering assumes a percentage inclusion (40 % for 2011 or 20 % for 2013) of sea ice within the total sampled area along each track. In this case, the open water area to the north has an ice concentration of zero and therefore SSH_{auto} is established too low, and subsequent Fb_{auto} is too high.

5.6 Discussion

We have evaluated the performance of two retracking techniques currently presented in the literature; *WfF* (Kurtz et al., 2014) and *TFMRA40* (Ricker et al., 2014). The first assumes the surface is retracked at Fb_i and the second near Fb_s. We also use *ESAL2*, a product for which we have limited information about its retracking procedure and assumptions therein. Here we discuss the extent to which our in situ observations support the assumptions in view of the mean and standard errors of the measured Fb_{sup} and Fb_{auto} data sets and information provided by the waveform responses to surface conditions.

As expected, the best agreement is found between in situ measurements and CS-2 freeboard retrieval techniques for *ESAL2*, *WfF* and *TFMRA40* using a supervised SSH identification with the exception of *WfF* in 2011. For the latter we attribute the anomalously high freeboard to two sources. The first is a low SSH estimate due to the reduced ability of the technique to establish SSH in the presence of differing surface types over a small segment of the SSH reference area. Secondly the introduction of a positive freeboard bias as supported by Kwok (2014) and Kurtz et al. (2014) is likely observed which is forced by a thicker and morphologically more complex snow cover in 2011. Our findings related to the snow cover influence on the retrieved freeboards for *WfF* are supportive of the fact that a snow cover can introduce a positive bias due to an increase in power returned from above the snow/ice interface (Kurtz et al., 2014). In the presence of a snow cover that is fully transparent to the incident *Ku*-band radar energy, no bias is expected to be observed. In the case of significant contribution from surface scattering (air/snow interface) or volume scattering (snow layers and ice crystals), the resulting ice freeboard will be biased high. Our observations show that the snow in the study area has higher mean densities and exhibits distinct layers with varying hardness, density and crystal size, as when compared with the simplified assumptions in Kurtz et al. (2014). It is speculated that in combination with the larger grain size and higher salinity near the snow/ice interface, the effective point of scattering is shifted even further away from the ice surface. We also observe a higher Fb_{sup} for *ESAL2* in 2011 when compared to 2013, and speculate a similar response to the change in snow properties has influenced the procedure. The role of the heterogeneity of the snow cover on CS-2 freeboard retrieval requires further study as our results suggest a complex snow cover will increase the expected positive bias. However we are unable to fully

separate the influence of SSH identification error even under the supervised assessment. Experiments in which the influence of SSH misidentification is isolated will need to be carried out to completely quantify the positive bias introduced by a snow cover using *WfF*. Direct comparisons between supervised and automatic procedures suggest differences in excess of 0.05 m in the established SSH are apparent. Attaining knowledge of the dominant backscattering surface is crucial to undertake any meaningful time series assessment of sea ice freeboard, permitting thickness estimation. Modification of the radar waveform and variation of penetration depth which are both dependent upon snow properties have been identified here as previously indicated by other studies (Willatt et al., 2010). Such variation in the penetration and response of the radar energy makes the assumptions made for the retracking techniques unrealistic at the large scale.

It was not possible to determine the accuracy of the established SSH_{sup}, and we can only evaluate the resulting freeboards. The SSH_{sup} of all three data products was independently assessed without tuning to in situ measured freeboards. However, the characteristics of the study area made it necessary to modify the processing methods for water surface identification currently used in the Arctic (Kurtz et al., 2014; Ricker et al., 2014). The surface type *polynya* was added to the surface classification for *TFMRA40* to improve ice-water discrimination. This surface type produces similar but more diffuse waveforms than sea ice with a leading edge that is typically flatter. The power threshold for retracking over this surface type was increased to 60 %. The fact that larger open water areas can result in significantly different SSH estimates may introduce a significant inter-retracker difference in SSH establishment due to the inconsistent change along the leading edge. Certain adaptations were made to the *WfF* technique to improve the establishment of SSH_{sup} over areas with a mixture of surface types in close proximity (i.e. leads, open water, sea ice floes within a few hundred meters). These conditions cause noisy waveforms and improvement of our understanding of the influence of this noise on the retracking procedure is a current research focus. It seems that the more sophisticated approach of *WfF* is more sensitive to these conditions than *TFMRA40* and a more stringent data discard procedure may need to be adopted to reject such waveforms. Further, using automatic surface discrimination algorithms resulted in insufficient separation of sea ice and water surface types. It may be of benefit to adopt procedures which account for the seasonal change in sea ice conditions which force alteration of surface discriminatory parameters (e.g. P, PP, SSD). This may

improve the separation of surface types and Fb_{auto} results, both in this investigation area and when larger regions are considered for assessment.

With the aid of information gained in the supervised freeboard retrieval procedure we were able to place in context and develop automatic freeboard retrieval procedures for each technique. Our results have shown the ability of CS-2 to record a developing fast ice cover in the Antarctic. Although our supervised analysis provides insight upon the surface that is tracked with respect to Fb_s and Fb_i we do not have the confidence to estimate sea ice thickness with an acceptable error margin. However, we do find the growth rate as recorded by Fb_{auto} over both years for all techniques of 0.7 mmd^{-1} (mean of all rates displayed in Figure 5.8) is in agreement with other studies of ice growth rates in McMurdo Sound (Gough et al., 2012; Purdie et al., 2006). By April, all retracking techniques identify positive freeboard values. Although we identify the onset and the trend in freeboard growth we note the standard deviations of Fb_{auto}, which are typically twice that found over this area when it was assessed using ICESat from 2003-2009 (Price et al., 2013). There was an extensive multiyear sea ice cover in McMurdo Sound from 2003 to 2009. However, we do not expect any significant change to environmental conditions which could increase the variability of surface conditions over the area covered by FY sea ice in McMurdo Sound between the two satellite observation periods, although the CS-2 assessment area is smaller. We look to instrumental and methodological sources to explain the observed noise. Findings from CS-2 presented here were attained using SIN mode which acquires data at a reduced burst repetition interval (by a factor of four) compared to SAR mode which will be used over the majority of the Antarctic sea ice pack. The ability to average and reduce measurement noise in the SIN mask which occupies the entire coastal Antarctic, a key area of sea ice production is therefore significantly reduced. Assuming normally distributed noise the values for the standard deviations would reduce by a factor of two if data were acquired in SAR mode. Even with this restriction there is no evidence that SIN mode is inadequate for sea ice freeboard retrieval with other studies even providing evidence in support of its usage (Armitage and Davidson, 2014). As SIN mode also provides phase information which can be used to reduce the impact of snagging on height retrievals an opportunity is presented. Such an ability is beneficial as a less stringent data discard is required to remove off-nadir range estimates which exhibit a positive range bias and subsequently height retrievals that are too low. We have used phase information for *ESAL2* and *WfF*. Omitting this information for *TFMRA40* could result in the underestimation of

freeboard if the radar reflection originates from an off-nadir scatterer, which is typically not the case for open water and level sea ice. The standard deviations of Fb_{auto} using *TFMRA40* are higher than those from the other two procedures, perhaps an indication of the noise introduced from the range bias' present without phase information. An additional source of scatter and an increased standard deviation could be introduced to the *TFMRA40* procedure as the slope of the leading edge is typically shallower at 40 % in comparison to higher thresholds. This could force a higher noise if waveforms change significantly from one measurement to the next. The noise in *TFMRA40* heights could also indicate that undulations or roughness of the snow surface was often higher than the ice surface beneath. These factors do not seem to have been influential along the validation line (Figure 5.4) where *TFMRA40* produced the least noisy Fb_{sup} data set of the three techniques.

The surface, or more realistically, the height that is tracked is dependent upon where on the leading edge each processor establishes its retracking point, this point selected on the basis of the dominant backscattering interface that is assumed (e.g. retracking at 40 %, 40-70 % or 50- 90 %). This is a trivial consideration and in the absence of any alteration of the waveform by surface conditions these simple differences in range would cause the resultant differences in measured freeboard. We are able to state that in McMurdo Sound using the supervised analysis in an optimal scenario when there is a thin and homogeneous snow cover (mean = 0.05 m), that *TFMRA40* approximates F_s well, that *WfF* approximates F_i well, and *ESAL2* identifies a horizon in between F_i and F_s. This relationship is not as well maintained in the automatic analysis in 2013 with all documented trends being slightly lower than in situ measurements. Though we have identified that GR, RR and snow are influential on the leading edge, we cannot separate their influence with any certainty. It is evident that from interpretation of the leading edge alone that no separation of the air/snow interface and ice/snow interface is directly achievable, which is expected due to the range resolution of CS-2 (Kwok, 2014; Kurtz et al., 2014; Bouzinac, 2013; Wingham et al., 2006). However, using a comparison of a snow covered sea ice area and an area with significantly less snow, the gradient of the leading edge becomes shallower and the width of the entire waveform is extended in the presence of snow. Based on the model assumptions of *WfF* very small changes in the leading edge are expected as a function of surface roughness, and insufficiencies in the fit of the leading edge as shown in Figure 5.6b indicate a higher than expected influence of roughness and snow cover on the leading edge. This will alter the retracking position on the leading edge for every retracker in a different

way, and it is therefore appropriate to conclude that the difference in surface properties between our two assessment years influenced the eventual freeboard measurements.

Relating our findings to the development of larger scale Antarctic assessments outside the coastal band is hindered by the nature of our study area in comparison to the majority of the Antarctic sea ice pack. However, the dynamic sea ice area in the MSP is more representative of the wider Antarctic sea ice zone. Although this area was not the focus of our assessment, automatic freeboard retrieval procedures have produced freeboards which are considered reasonable for Antarctic pack ice (Table 5.2). We have identified certain issues within our analysis which are applicable at the larger scale which must be addressed in order to develop techniques. Given the abundance of large open water areas in the Antarctic sea ice zone which do not exhibit the typical 'peaky' response from leads, it is necessary to characterize them as suggested. If they are large enough and their sea ice concentration is low, they can be masked using auxiliary satellite information. However in regions of high ice concentration where leads are too large to be discernible, discrimination may be hindered. At what size a lead becomes too large to exhibit a typical waveform would need to be ascertained to conclude whether open water areas may be an issue in the Antarctic sea ice pack. The spatial and temporal heterogeneity of the snow cover, even in our small study area highlights the challenge presented for freeboard retrieval algorithms to assess larger areas in the Antarctic. Further advances in retracking techniques guided by in situ validation will need to be made in order to attain freeboard measurements at higher accuracy. Further complications will be introduced by the significant snow loading which typically suppresses sea ice freeboard resulting in a zero ice freeboard condition in the Antarctic sea ice pack. This issue may be addressed by a combination of different retracking procedures that attempt to identify the air/snow interface as shown to be successful here. In any case, it is clear that data treatment may need to be altered for different regions, in particular retracker algorithms to cater for the variability of the Antarctic sea ice regime.

5.7 Conclusion

Our validation measurements reveal that retracking techniques based on the fitting of waveforms (*ESAL2* and *WfF*) and a threshold retracker (*TFMRA40*) can be used to derive freeboard estimates over Antarctic fast ice from CS-2. In the validation area of McMurdo Sound, which harbours homogenous fast ice, we find these three separate techniques freeboard retrievals fall within the margins of expected freeboards as indicated by in situ measurements in austral spring 2011 and 2013, using both a supervised classification sea surface height and automatic open water identification algorithms. Mean freeboard values from *ESAL2* are shown to be representative of an interface between the air/snow and snow/ice interface. It is indicated that *WfF* is influenced by the presence of a snow cover which causes a positive bias away from the ice freeboard. In the absence of a snow cover, *WfF* is more representative of the ice freeboard. *TFMRA40* identifies freeboards in better agreement with in situ measured snow freeboard. We observe higher standard deviations in automatic retrieval procedures which could be reduced by spatial averaging if data at a higher sampling rate, such as in SAR mode were available. Difficulties in the identification of sea surface height were noted for *TFMRA40* over larger open water areas and for *WfF* over areas inclusive of multiple surface types (e.g. leads, sea ice, open water) within the satellite footprint. Automatic algorithms were tested through 2011 and 2013 and recorded the growth of the FY fast ice cover in McMurdo Sound, the trends from each method in line with sea ice growth rates measured in situ in the region. Automatic surface type discrimination procedures may benefit from spatial and seasonal adjustment to account for heterogeneous conditions and improve ice-water discrimination. It is likely that different approaches with regard to retracker algorithms will need to be region specific given the understood properties of varying snow covers and ice conditions. In situ validation in the Antarctic pack ice will be a fundamental component for the development of CS-2 freeboard retrieval techniques. CS-2 accuracy is expected to be achieved over larger spatial scales than assessed here. We see our results as highly positive in this context as expansion of spatial scales and improvement of height retrieval techniques can only improve results further.

6 Synthesis and Conclusions

This work has aimed to improve the understanding of sea ice properties and processes in the coastal Antarctic using McMurdo Sound as a case study region. Focus was placed on the relationship between ice shelves and sea ice, along with the advancement of techniques to record sea ice freeboard from satellite altimeters. The conclusions of this work fall into two focus areas separated into geophysical implications and methodological advancement.

From a geophysical standpoint an average area of 5,000 km^2 was covered by fast ice within the spatial (Chapter 3 assessment area) and temporal (2003-2013) context of this work. With a mean thickness of 2.15 m provided by in situ measurements and supported by satellite freeboard information, a sea ice volume of approximately 10 km^3 grows and decays in McMurdo Sound every year. With regard to thickness trends, extension of the temporal series using this work gives no indication of any change to the FY sea ice thickness distribution in McMurdo Sound. This is almost certain for the fast ice area. However, it is more difficult to draw conclusions on sea ice in the dynamic area of the sound with the absence of in situ validation, and the uncertainties of automatic freeboard retrieval algorithms. Chapter 3 provides the first space-borne evidence that the sea ice thickness distribution in McMurdo Sound is influenced by the outflow of supercooled Ice Shelf Water (ISW) from beneath the Ross and McMurdo Ice Shelf cavities. These findings play a part in the completion of objectives 2 and 3 stated in section 1.2. Evidence presented prior to this study (Gough et al., 2012; Mahoney et al., 2011; Leonard et al., 2011; Dempsey et al., 2010; Purdie et al., 2006; Hellmer, 2004; Trodahl et al., 2000; Gow et al., 1998; Jeffries et al., 1993) is spatially enhanced here. It confirms that sea ice thickness in this region is much thicker than it would otherwise be due to the influence of the ice shelf. In light of these findings, chapter 4 builds upon this established relationship between sea ice and the ice shelf with regard to remote sensing. The influence of the sub-ice platelet layer upon freeboard to thickness conversion was quantified and found to be significant in the region amounting to a mean overestimation of solid sea ice thickness of 12 %. This highlights, that not only is the ‘solid’ sea ice cover thicker in this region close to an ice shelf, but that an additional mass accumulates, which is also capable of increasing the freeboard. Such findings provide an error estimate for sea ice freeboard to thickness conversion for any technique which is attempting to assess sea ice thickness via freeboard

measurements in close proximity to an ice shelf. This directly addresses objective 4 as given in section 1.2. The findings here also present an opportunity to use sea ice freeboard/thickness anomalies to document the interaction of ISW on coastal sea ice, providing an indirect way to map ISW occurrence in coastal Antarctica. What exactly is considered an 'anomaly' in Antarctic sea ice freeboard/thickness has not been fully established. It is thought of here as the excess mass of ice that forms due solely to the presence of ISW, that forces an increase in freeboard/thickness. Isolation of this influence will be difficult to achieve as many processes play a role in the thickness of a sea ice cover. The dominant drivers of sea ice thickness are the atmospheric conditions and the snow cover on the sea ice. However Gough et al. (2012) have found that an oceanic heat flux, driven by ISW can be responsible for up to 25 % of observed growth. Identification of this more minor influence may be possible by assessing growth rates at certain times of the year to isolate the influence of an oceanic heat flux, and in turn the presence of supercooled ISW. The ability to monitor this via satellite altimetry will require continued development of many remote sensing techniques, the current limitations of which are discussed in section 6.2.

Following the theme of continued development, and focusing more upon methodological advancement, chapter 5 undertook the first comprehensive validation of CryoSat-2 (CS-2) in the Antarctic. This formed part (project AOCRY2CAL-4512) of the international effort to evaluate the performance of this satellite led by ESA. The ability of CS-2 to document the growth of the fast ice sea ice area in McMurdo Sound was proven using three separate retracking techniques. Using extensive in situ validation planned and carried out for this work, it was noted that a waveform fitting procedure (*WfF*) was influenced by the presence of a thick and complex snow cover which caused a positive bias in estimated ice freeboard. A Threshold-First-Maximum-Retracker-Algorithm employed at 40 % (*TFMRA40*) showed close agreement with in situ measured snow freeboard while European Space Agency Level 2 (*ESAL2*) freeboard was commonly between the snow and ice freeboard. The development of such techniques and understanding of what influences the retracking procedures is key to the continuation of Antarctic sea ice thickness monitoring. This adequately addressed objective 1 in section 1.2, while advancing the original scope of objectives 2 and 3. More detail on the findings of this work, and how Chapters 3 to 5 have contributed to the research aims are given in the following sections. Given the conclusions of these sections, lastly, a research outlook is provided.

6.1 ICESat investigation in McMurdo Sound

The objectives of this work were heavily based around satellite altimeter investigation of sea ice, specifically, the measurement of sea ice freeboard. Under assessment by ICESat utilising one method based on techniques previously presented in the literature and a second novel method, sea ice freeboard was assessed over a 7 year period. ICESat-derived freeboards in austral spring 2009 were within one standard deviation of airborne laser measurements of sea ice freeboard and show good overall comparison with in situ measurements. First year sea ice freeboard in McMurdo Sound underwent no significant change from 2003-2009 which concurs with the findings of Kurtz and Markus (2012) who examined the wider Ross Sea region. However, a statistically significant increase in MY sea ice freeboard was documented using both methods. It is suggested that the sea ice regime in McMurdo Sound may switch into a deviant mode, when large tabular icebergs ground in its northern extremities. These icebergs act as barriers to oceanic stresses and accommodate the establishment of a MY sea ice cover. The growth of this MY ice may then be enhanced by the ISW plume in McMurdo Sound. The area of MY sea ice which experienced the greatest growth rate was coincident with this plume of supercooled ISW exiting the McMurdo Ice Shelf cavity as documented by other studies (Robinson et al., 2014; Gough et al., 2012; Mahoney et al., 2011; Leonard et al., 2011; Dempsey et al., 2010). This evidence is further suggestive of a strong link between ocean processes and sea ice growth in McMurdo Sound. Chapter 3 also concluded that a higher spatial resolution of in situ measurements was required, in unison with remote sensing techniques, to attribute the influence of ISW and subsequent platelet ice incorporation or attachment on the observed growth in the MY sea ice cover.

The lack of open water reference points over the fast ice region in the study area caused initial concerns about the ability of satellite altimetry to record sea ice freeboard. This was especially true in the western segment of the sound for ascending satellite passes where no open water was available at certain times of the year. This promoted the development of Method-2 (M-2). M-2 made use of an independently developed mean sea surface (MSS) grid and tidal and atmospheric pressure information to establish local sea surface height (SSH). M-2 supported the conclusions of Method-1, which used along-track filtering to

establish SSH. M-2 exhibited higher standard deviations, due to the noise in the SSH estimates driven by inaccuracies in tide models and the MSS grid. M-2 displayed the potential for alternative approaches to altimetric freeboard retrieval in the Antarctic. Significant advancements in the accuracy of tide models (e.g. CATS) and the establishment of MSS will be required before errors in SSH can be minimised. The results of this research suggest that for improvement of small scale sea ice thickness assessment in McMurdo Sound a robust gravitational survey needs to be carried out to build a higher resolution geoid model. This will provide a basis for improved establishment of a MSS. Using this, with additional information from tide gauges and barometric measurements, it is feasible that SSH could be established constantly. Via satellite altimeters sea ice freeboard could then be continually monitored in McMurdo Sound with little need for in situ validation.

6.2 The influence of a sub-ice platelet layer

Platelet ice accumulates beneath a solid sea ice cover as a result of the oceanic heat flux associated with the outflow of supercooled ISW from ice shelf cavities. This results in the formation of two additional ice types; platelet ice, which becomes part of the mechanical integrity of the solid sea ice cover and a sub-ice platelet layer. This process has been documented in great detail in McMurdo Sound (see Gough et al., 2012 and references there in) and at other locations in the Antarctic (Langhorne et al., in prep). Both ice types originate from the same process but in regard to freeboard conversion to ice thickness require separate treatment. The additional growth of the 'solid' sea ice cover from incorporation of platelet crystals and eventual consolidation causes an increase in freeboard. As this additional mass has a similar density to the overlying ice cover, the ice thickness estimate via freeboard is not erroneous. However, the sub-ice platelet layer still produces a buoyant influence but has a very different density (Gough et al. 2012 and Chapter 4 here). Using in situ measurements of sea ice freeboard, thickness and snow, with their respective densities, a solid fraction of 0.16 ± 0.17 was calculated using the hydrostatic equilibrium assumption. This value was at the lower range of estimates previously presented in the literature and its calculation was highly sensitive to the value used for sea ice density. The spread of measured sea ice density in the area (915 to 935 kgm^{-3}) results in a range of solid fractions from 0.03 to 0.36. Upon application of a GNSS surface elevation survey, it was

noted that sea ice thickness can be overestimated by up to 19 % with a mean deviation of 12 % when converting surface elevation measurements to sea ice thickness when this influence was not accounted for. Such a finding justifies the inclusion of such influences in error budgets for satellite altimetry derived sea ice thickness in the Antarctic. The mean overestimation of 12 % reported here is primarily driven by the study areas proximity to the ice shelf edge. The thickness of the sub-ice platelet layer quickly tails off in the seaward direction, and it is unlikely to influence measurements discussed here beyond 100 km. The separation of the influence of platelet ice and the sub-ice platelet layer is not possible without in situ validation.

The identification of such freeboard/thickness anomalies presents an opportunity to achieve an ambitious, but sought-after geophysical conclusion. Shown here, and in other work, it is clearly established that ice shelf expulsion of supercooled water increases the freeboard of fast sea ice. This can be driven by formation of platelet ice and/or a sub-ice platelet layer. Assuming similar ice shelf margin properties, it is reasonable to suggest that satellite altimeters could provide an insight to the presence of supercooled water via sea ice freeboard/thickness anomalies. This may provide a way of mapping ISW advection into the Southern Ocean. Such advection is indicated as being influential upon larger scale sea ice processes (Bintanja et al., 2013). This ability will only be permitted if certain technical and methodological constraints are overcome. The snow cover must be accurately measured or modelled to reveal the true increases in sea ice freeboard alone. This will require advances in instrumentation or improvement of the accuracy of current techniques which suffer from interference from wet snow and surface roughness (Markus et al., 2011, Zwally et al., 2008, Markus and Cavalieri, 1998). Even then, the measurement of increases in ice freeboard will require highly precise operational instrumentation. Freeboard anomalies associated with increases in sea ice thickness and accumulation of a sub-ice platelet layer are typically less than 0.05 m in the most extreme cases (i.e. within a few kilometers of the ice shelf margin). The measurement of such increases are currently at the limits of contemporary and antecedent satellite altimeter capabilities. Environmental conditions may also restrict such investigations as fast ice areas that are too large (McMurdo Sound is likely at the limit) will be located too far from open water and have insufficient sea surface tie points to retrieve freeboard accurately.

While undertaking in situ measurements for this work, it was proposed that the loading of equipment and personnel near drill-hole sites could suppress the local freeboard. This was checked in a rudimentary fashion during in situ validation in 2013, which indicated such an affect was occurring. This surface suppression can lead to overestimates of sea ice density using in situ measurements and the hydrostatic equilibrium assumption of 5 kgm^{-3}. It is recommended that loading is not permitted in the immediate vicinity of measurements and that multiple measurements are carried out over an area with a radius of at least 15 m. A larger survey area will also reduce the effect of surface undulations on sea ice density estimates using the hydrostatic equilibrium assumption. Such undulations can lead to the inclusion of freeboard and thickness measurements that are not representative of the local hydrostatic balance and cause a spread in the estimated sea ice density. Whether the hydrostatic equilibrium assumption is fulfilled in sea ice investigations has become a topic of debate. There is no doubt that a sea ice floe, or fast ice cover is in hydrostatic equilibrium, however, disturbance from loading of personnel and equipment as described here, and interference from ships (Hutchings et al., 2014) are cause for concern. In addition the spatial scales that are assessed will also be influential as surface conditions are variable. There is a particular need for improved comparison between satellite sensors, airborne instruments and in situ validation which all represent different spatial scales.

6.3 CryoSat-2 over Antarctic sea ice

Although the Antarctic sea ice system has been evaluated in its entirety by laser (Kurtz and Markus, 2012) and radar (Giles et al., 2008b) altimeter systems, the technique is still under development. Many sources of error contribute to large uncertainties in sea ice thickness estimation. As the initial freeboard value that is recorded is multiplied by ~ 9 to infer thickness, it is imperative that this measurement is as accurate as possible. This requires techniques to be evaluated against in situ validation campaigns and the assumptions behind techniques tested.

At the time of writing, no published CS-2 investigations of Antarctic sea ice are available. The complex interaction of *Ku*-band radar altimeter energy and the sea ice environment result in increased uncertainty in the eventual sea ice thickness estimation. As a result, multiple approaches to the treatment and interpretation of CS-2 data have been pursued.

This work has attempted to test the assumptions of these approaches in the Antarctic. Three separate approaches to Antarctic freeboard retrieval have been examined, the first using European Space Agency Level 2 data (*ESAL2*), the second using a waveform fitting procedure (*WfF*) and the third a Threshold-First-Maximum-Retracker-Algorithm employed at 40 % (*TFMRA40*). First a supervised freeboard retrieval procedure was applied. The sea surface was identified manually using MODIS imagery and in situ information was used to correct for the speed of the propagating radar wave in the snow cover. This procedure indicated that *WfF* records the ice freeboard in the absence of a deep and complex snow cover, but in the presence of such snow a positive bias, away from the ice freeboard was observed. *TFMRA40* freeboards showed close agreement with in situ measured snow freeboard, while *ESAL2* measured a freeboard in between the snow and ice freeboard. The influence of the snow cover on *WfF* supports the findings of Kwok (2014) and Kurtz et al. (2014) and highlights a major issue faced for CS-2 assessment of Antarctic sea ice freeboard. Difficulties were also noted which were forced by the retrieval of sea surface height as certain methods were subject to complications from certain surface conditions. The *TFMRA40* procedure was amended to a 60 % threshold over larger open water areas which were flagged under a new surface type *polynya*. The more sophisticated approach of *WfF* appeared to be hindered when surface types were mixed over small areas (i.e. leads, open water, sea ice over areas comparable to the satellite footprint) producing noisy waveforms. The development of this technique to deal with such complications is a current research focus. The clear separation in recorded freeboards using the techniques justifies a statement which considers the potential for snow depth retrieval using CS-2. Although findings here indicate there is a relationship between snow depth and retrieved freeboards, further work is required to support the above statement. With knowledge gained in the supervised assessment, an automatic procedure was employed which provided annual data sets for 2011 and 2013. CS-2 provided a time series assessment of the development of a fast ice sea ice cover for these years in McMurdo Sound. The mean observed rate in freeboard increase of 0.007 md^{-1} was in line with the known sea ice growth rate in the region, and the end of growth season freeboard values were consistent with in situ measurements. Poor discrimination of open water and sea ice was documented in automatic retrieval algorithms. This problem will require more attention in order to develop larger scale freeboard retrieval procedures. A large data discard may need to be adopted to address the surface discrimination issues and the occurrence of noisy waveforms which hinder sea surface height retrieval. The automatic method exhibited high standard deviations of freeboard

measurements, which is attributed, at least in part to the reduced sampling capability of SIN mode in the Antarctic coastal band. The use of SAR mode in the pack ice areas of the Antarctic may reduce this noise, but the impact of snagging on sea surface height retrievals cannot be circumvented in the absence of an interferometric capability. While primarily validating CS-2 in a coastal Antarctic environment, this work has taken a step towards the development of larger scale assessments of Antarctic sea ice thickness using CS-2. This is crucial to monitor the state of the Antarctic sea ice thickness distribution both spatially and temporally into the future.

In reference to the conclusions of Chapter 4, the current knowledge gap in the interpretation of CS-2 waveform information, and subsequently freeboard heights makes using CS-2 to detect freeboard/thickness anomalies around the Antarctic a very difficult task. Therefore, with acknowledgement of the early research phase of CS-2 it was not possible to directly tie Chapter 5 to the previous chapters with respect to satellite altimetry investigations of sea ice thickness anomalies.

6.4 Research outlook

This work was heavily concerned with the measurement of Antarctic sea ice freeboard via satellite altimetry. In Chapters 3 and 5 this was explored in detail in McMurdo Sound where such measurements were validated against extensive in situ information. With regard to the concept of Antarctic sea ice freeboard retrieval itself, a significant problem is presented by a thick snow cover on a thin sea ice cover, and a large ratio of snow to ice above the waterline. This firstly reduces the amount of ice discernible by the satellite altimetric measurement, and secondly adds complexity to the eventual thickness conversion given no adequate snow depth information. Improved treatment of snow on sea ice will greatly reduce uncertainties in the eventual thickness estimation. This is especially true over the thinner pack ice areas where the errors in the snow depth and freeboard measurements are most influential on the total error in thickness. As the ice thickens the uncertainty in the sea ice density begins to dominate the expected thickness error. The availability of accurate snow depth data is an Antarctic sea ice research priority to improve the current paucity of information (Vaughan et al., 2013). Kurtz and Markus (2012) and Giles et al. (2008b) have provided the only Antarctic wide sea ice thickness investigations to date. Both show

promise but are certainly limited by the contemporary treatment of snow. Kern et al. (2015) have indicated that large differences (up to 50%) in thickness result when the zero freeboard assumption is used as opposed to auxiliary snow depth information. It is clear that a 'one shoe fits all' approach is not sufficient to retrieve sea ice thickness in the Antarctic. Assessments will need to take account of expected regional differences in snow cover from available in situ and auxiliary satellite information. Even within McMurdo Sound its unavailability in periods outside of in situ validation meant it had to be ignored, and only total freeboard trends identified (Chapter 5). This makes the accurate estimation of sea ice thickness impossible. In Chapter 3 the issue was addressed by applying a percentage threshold of the total freeboard measured and assuming this to be representative of the snow depth. Techniques will have to be much improved to reduce the errors in eventual thickness estimation. Work was undertaken to advance the knowledge of the snow distribution via atmospheric modelling approaches outside the work presented in this thesis (Soltanzedeh et al., in prep). This may provide another avenue for the application of snow depth information to sea ice freeboard estimates in McMurdo Sound as model results show good agreement with in situ measured snow depth. In Chapter 5 there are indications that the differences in retracking techniques for CS-2, that claim to identify sea ice and snow freeboard could be used as a way to discern snow depth. Further work is needed to progress this research to a useful stage. The launch of the Advanced Topographic Laser Altimeter System (ATLAS) instrument on-board ICESat-2 scheduled for launch in 2017 (NASA, 2014), in conjunction with CryoSat-2 (if still operational) and Sentinel-3 (scheduled for launch in mid-2015 (ESA, 2014)) will provide the best opportunity to date to improve the spatial and temporal variability of the Antarctic snow cover for sea ice thickness estimation. Operational overlap of these instruments for at least one year will allow a complete annual comparison of data sets. This opportunity will also provide the first information upon the differences in measured freeboard from different space-borne altimeter systems. In addition, Sentinel-3 will operate an Ocean and Land Colour Imager (OLCI) permitting imagery to be acquired in complete coincidence with altimeter information. This is a first for sea ice investigation and will likely improve sea ice freeboard retrieval algorithms and error analysis. The present study planned to undertake measurements in coincidence with NASA's Operation Ice Bridge (OIB) in November 2013 to further explore the validation opportunities presented in McMurdo Sound. However, United States Antarctic Program logistical constraints prevented this. Future OIB operations in McMurdo Sound should be coordinated with the planned EM-Bird and in situ investigations in the region over the

coming years. This will further complement the efforts of New Zealand and United States researchers to expand the efforts of sea ice research from McMurdo Sound into the key region of the Ross Sea. Future pan-Antarctic satellite sea ice investigations will require robust validation. In situ measurements, alongside airborne campaigns like OIB will play a pivotal role in providing validation data sets. This linkage between surface, airborne and spaceborne sea ice freeboard measurements will require development as the spatial scales greatly vary.

Given the relatively small size of the study area presented here data availability was reduced. The increased data sampling of ICESat-2 over ICESat from 40 Hz to 10 kHz means along-track resolution will be increased to < 1 m (McGill et al., 2013; Abdalati et al., 2010). Given the expected performance of the system, temporal sampling will also be improved over the unplanned campaign-based approach of ICESat. There is no change from ICESat in the orbital placement of ICESat-2, therefore similar track spacing can be expected which results in the exclusion of sea ice areas within the inter-track spacing.

With the development of sea ice freeboard retrieval, the opportunity to assess the linkages between ice shelf and sea ice in the coastal Antarctic is greatly enhanced. The influence of ice shelf basal melting and the outflow of ISW on the physical condition of the Southern Ocean is a topic of intense investigation. Its presence certainly influences sea ice thickness distributions in close proximity to ice shelves (Langhorne et al., in prep; Gough et al., 2012; Smith et al., 2012; Mahoney et al., 2011; Dempsey et al., 2010). Further it may contribute to sea ice formation in the wider oceanic area as it accumulates in the surface ocean and subsequently stabilizes and freshens it (Bintanja et al., 2013; Hellmer, 2004). This work has shown that the mapping of sea ice freeboard and thickness anomalies driven by the outflow of ISW is achievable using satellites with a ranging ability (Chapters 3 and 4). Application of these methodologies to the wider Antarctic could reveal for the first time the occurrence of ISW at the large scale, providing information on its sites of expulsion and potentially its abundance in the surface ocean. This information could reinforce data provided by modelling and mass balance investigations of the Antarctic Ice Sheet to increase the accuracy of estimates of the volume of ISW entering the Southern Ocean. As the first larger scale investigation of sea ice-ice shelf linkages is presented in Langhorne et al. (in prep.) the ability of remote sensing platforms should not be overlooked for future research. To begin this process, in addition to the required advancements in satellite altimetry techniques

and snow depth retrieval, as described above, two preliminary investigations will provide a basis for progress (i) a study to map pan-Antarctic fast ice distribution following the efforts of Fraser et al. (2012) (ii) documentation of ice shelf thickness at the margin to confirm whether ISW could reach the surface ocean and interact with sea ice. The work of Griggs and Bamber (2011) provides the basis for such an investigation. This information will narrow down areas of interest for further research.

Currently the freeboard to thickness conversion approach offers the only way of assessing the Antarctic sea ice thickness distribution. This will be the case for the foreseeable future. This work has contributed to the understanding of the complex relationship between sea ice freeboard and thickness in the Antarctic, while providing further insight upon the relationship between sea ice and ice shelves. Knowledge gained has improved our ability to undertake the monumental task of routinely monitoring Antarctic sea ice thickness accurately from space. This monitoring ability will permit the volume of sea ice in the Southern Ocean to be quantified and provide a far more informative measure of the current and future state of Antarctic sea ice in the global climate system. This is identified as a key question in the recent SCAR Antarctic and Southern Ocean Science Horizon Scan and is pursued as an international research priority given the paucity of information provided in the Intergovernmental Panel on Climate Change's Fifth Assessment Report.

7 Appendices

Appendix I. In situ measurement locations, dates and values for sea ice freeboard (*Fb*), ice thickness (T_i), sub ice platelet layer thickness (T_p), snow depth (T_s) and surface elevation (*SE*) for 2011 campaign. Site 24 was a repeat site and is not included.

Site	*Lat*	*Lon*	*Date*	*Fb*	T_i	T_p	T_s	*SE*
1	**-77° 40'**	**166° 24'**	**22.11.2011**	**0.06**	**1.96**	**0.22**	**0.33**	**0.39**
2	-77° 40'	166° 12'	23.11.2011	0.06	1.98	0.46	0.33	0.39
3	**-77° 40'**	**166° 00'**	**23.11.2011**	**0.11**	**2.12**	**0.88**	**0.23**	**0.34**
4	-77° 43'	166° 12'	23.11.2011	0.06	1.70	0.14	0.32	0.38
5	**-77° 40'**	**166° 12'**	**23.11.2011**	**0.09**	**1.59**	**0.00**	**0.34**	**0.43**
6	-77° 40'	166° 00'	24.11.2011	0.05	1.57	0.00	0.26	0.31
7	**-77° 46'**	**164° 48'**	**25.11.2011**	**0.28**	**2.22**	**2.70**	**0.04**	**0.32**
8	-77° 46'	165° 00'	25.11.2011	0.24	2.26	4.07	0.09	0.33
9	**-77° 46'**	**165° 12'**	**26.11.2011**	**0.25**	**2.25**	**4.52**	**0.09**	**0.34**
10	-77° 46'	165° 24'	26.11.2011	0.30	2.37	4.40	0.13	0.43
11	**-77° 46'**	**165° 36'**	**26.11.2011**	**0.26**	**2.36**	**3.74**	**0.09**	**0.35**
12	-77° 46'	165° 48'	26.11.2011	0.17	2.18	1.91	0.21	0.38
13	**-77° 34'**	**160° 12'**	**27.11.2011**	**0.15**	**1.64**	**0.00**	**0.00**	**0.15**
14	-77° 37'	166° 12'	27.11.2011	0.06	1.47	0.00	0.19	0.25
15	**-77° 40'**	**166° 24'**	**27.11.2011**	**-0.07**	**1.34**	**0.00**	**0.46**	**0.39**
16	-77° 40'	164° 48'	28.11.2011	0.23	2.25	2.85	0.12	0.35
17	**-77° 40'**	**165° 00'**	**29.11.2011**	**0.24**	**2.32**	**3.09**	**0.10**	**0.34**
18	-77° 40'	165° 12'	29.11.2011	0.22	2.21	2.18	0.10	0.32
19	**-77° 40'**	**165° 24'**	**29.11.2011**	**0.13**	**1.86**	**0.96**	**0.20**	**0.33**
20	-77° 40'	165° 36'	29.11.2011	0.11	1.74	0.00	0.13	0.24
21	**-77° 40'**	**165° 48'**	**29.11.2011**	**0.09**	**1.60**	**0.00**	**0.18**	**0.27**
22	-77° 49'	166° 12'	01.12.2011	0.15	2.12	0.79	0.17	0.32
23	**-77° 52'**	**166° 12'**	**02.12.2011**	**0.17**	**2.21**	**0.90**	**0.13**	**0.30**
25	-77° 43'	164° 48'	29.11.2011	0.21	2.25	2.09	0.12	0.33
26	**-77° 40'**	**165° 24'**	**01.12.2011**	**0.27**	**2.43**	**3.49**	**0.00**	**0.27**
27	-77° 49'	164° 48'	29.11.2011	0.24	2.24	3.10	0.02	0.26
28	**-77° 50'**	**164° 48'**	**29.11.2011**	**0.25**	**2.20**	**2.65**	**0.00**	**0.25**
29	-77° 50'	165° 00'	29.11.2011	0.29	2.30	5.27	0.04	0.33
30	**-77° 50'**	**165° 12'**	**29.11.2011**	**0.32**	**2.47**	**5.63**	**0.03**	**0.35**
31	-77° 50'	165° 18'	28.11.2011	0.34	2.65	6.10	0.01	0.35
32	**-77° 50'**	**165° 24'**	**28.11.2011**	**0.32**	**2.33**	**7.50**	**0.06**	**0.38**
33	-77° 50'	165° 36'	04.12.2011	0.34	2.40	7.14	0.06	0.40
34	**-77° 50'**	**165° 48'**	**04.12.2011**	**0.22**	**2.29**	**2.91**	**0.08**	**0.30**
35	-77° 50'	165° 53'	04.12.2011	0.21	2.35	1.77	0.21	0.42
36	**-77° 50'**	**166° 00'**	**04.12.2011**	**0.21**	**2.28**	**1.37**	**0.13**	**0.34**
37	-77° 51'	166° 12'	01.12.2011	0.18	2.23	0.84	0.12	0.30
38	**-77° 52'**	**164° 48'**	**29.11.2011**	**0.21**	**2.17**	**1.28**	**0.00**	**0.21**
39	-77° 52'	166° 24'	02.12.2011	0.17	2.13	0.72	0.13	0.30
40	**-77° 52'**	**166° 30'**	**04.12.2011**	**0.20**	**2.18**	**0.75**	**0.08**	**0.28**

Appendix II. In situ measurement locations, dates and values for sea ice freeboard (*Fb*), ice thickness (T_i), sub ice platelet layer thickness (T_p), snow depth (T_s) and surface elevation (*SE*) for 2013 campaign.

Site	***Lat***	***Lon***	***Date***	***Fb***	T_i	T_p	T_s	***SE***
1	**-77° 46'**	**166° 24'**	**01.12.2013**	**0.21**	**2.16**	**0.4**	**0.06**	**0.27**
2	-77° 49'	166° 12'	01.12.2013	0.27	2.70	0.72	0.07	0.34
3	**-77° 47'**	**166° 02'**	**01.12.2013**	**0.13**	**2.01**	**0.86**	**0.22**	**0.35**
4	-77° 46'	165° 36'	26.11.2013	0.26	2.26	2.43	0.02	0.28
5	**-77° 46'**	**165° 12'**	**26.11.2013**	**0.28**	**2.31**	**4.08**	**0.00**	**0.28**
6	-77° 46'	164° 48'	26.11.2013	0.24	2.36	2.43	0.08	0.32
7	**-77° 40'**	**166° 24'**	**29.11.2013**	**0.21**	**2.11**	**0.00**	**0.01**	**0.22**
8	-77° 37'	166° 12'	29.11.2013	0.15	1.51	0.00	0.02	0.17
9	**-77° 40'**	**166° 00'**	**29.11.2013**	**0.15**	**1.64**	**0.04**	**0.05**	**0.20**
10	-77° 40'	165° 36'	30.11.2013	0.16	1.64	0.16	0.00	0.16
11	**-77° 40'**	**165° 12'**	**30.11.2013**	**0.25**	**2.29**	**1.26**	**0.00**	**0.25**
12	-77° 40'	164° 48'	30.11.2013	0.26	2.29	2.68	0.03	0.29
13	**-77° 28'**	**164° 02'**	**20.11.2013**	**0.21**	**2.35**	**0.28**	**0.04**	**0.25**
14	-77° 22'	163° 57'	21.11.2013	0.20	2.23	0.32	0.07	0.27
15	**-77° 22'**	**164° 20'**	**21.11.2013**	**0.21**	**2.28**	**0.17**	**0.04**	**0.25**
16	-77° 22'	164° 40'	21.11.2013	0.17	1.69	0.74	0.00	0.17
17	**-77° 17'**	**163° 53'**	**21.11.2013**	**0.22**	**2.37**	**0.19**	**0.04**	**0.26**
18	-77° 11'	163° 58'	22.11.2013	0.19	2.29	0.12	0.07	0.26
19	**-77° 11'**	**163° 48'**	**23.11.2013**	**0.22**	**2.36**	**0.20**	**0.03**	**0.25**

8 Bibliography

Abdalati, W., Zwally, H.J., Bindschadler, R., Csatho, B., Farrell, S.L., Fricker, H.A., Harding, D., Kwok, R., Lefsky, M., Markus, T., Marshak, A., Neumann, T., Palm, S., Schutz, B., Smith, B., Spinhirne, J and Webb C. **2010**. The ICESat-2 laser altimetry mission, *Proceedings of the IEEE*, 98(5), 735-751. doi:10.1109/JPROC.2009.2034765.

Alexandrov, V., Sandven, S., Wahlin, J and Johannessen, O.M. **2010**. The relation between sea ice thickness and freeboard in the Arctic. *The Cryosphere*, 4, 373-380, doi:10.5194/tc-4-373-2010, 2010.

Armitage, T.W.K and Davidson, M.W.J. **2014**. Using the Interferometric Capabilities of the ESA CryoSat-2 Mission to Improve the Accuracy of Sea Ice Freeboard Retrievals. *IEEE Trans.on Geo. and Rem. Sens*, 52, 529-536, doi: 10.1109/TGRS.2013.2242082.

Arrigo, K.R. **2010**, Primary Production in Sea Ice, in D. Thomas & G.S Dieckmann (eds), *Sea Ice*, 2nd ed, Wiley-Blackwell, Oxford.

Arthern, R.J., Winebrenner, D.P and Vaughan, D.G. **2006**. Antarctic snow accumulation mapped using polarization of 4.3-cm wavelength microwave emission. *J. Geophys. Res*, 111, D06107, doi:10.1029/2004JD005667.

Assmann, K and **Timmermann**, R. **2005**. Variability of dense water formation in the Ross Sea. *Ocean Dynamics*, vol. 55, no. 2, pp. 68-87, doi:10.1007/s10236-004-0106-7.

Barber, D.G., Reddan, S.P and LeDrew, E.F. **1995**. Statistical characterization of the geophysical and electrical properties of snow on Landfast first-year sea ice. *J. Geophys. Res*, 100 (C2), pp. 2673-2686, doi:10.1029/94JC02200.

Bindschadler, R., Choi, H., Wichlacz, A., Bingham, R., Bohlander, J., Brunt, K., Corr, H., Drews, R., Fricker, H., Hall, M., Hindmarsh, R., Kohler, J., Padman, L., Rack, W., Rotschky, G., Urbini, S., Vornberger, P and Young, N. **2011**. Getting around Antarctica: new high-resolution mappings of the grounded and freely-floating boundaries of the Antarctic ice sheet created for the International Polar Year. *The Cryosphere.*, 5, 569-588, doi:10.5194/tc-5-569-2011.

Bintanja, R., van Oldenborgh, G.J., Drijfhout, S.S., Wouters, B and Katsman, C.A. **2013**. Important role for ocean warming and increased ice-shelf melt in Antarctic sea-ice expansion. *Nature Geosci*, 6, 376-379, doi: 10.1038/ngeo1767.

Bouzinac C. **2013**. CryoSat Product Handbook. Accessed August 2014, available at: https://earth.esa.int/documents/10174/125272/CryoSat_Product_Handbook.

Brandon, M.A., Cottier, F.R and Nilsen, F. **2010**. Sea Ice and Oceanography, in D. Thomas & G.S Dieckmann (eds), *Sea Ice*, 2nd ed, Wiley-Blackwell, Oxford.

Bromwich, D.H., Nicolas, J.P., Monaghan, A.J., Lazzara, M.A., Keller, L.M., Weidner, G.A and Wilson, A.B. **2013**. Central West Antarctica among the most rapidly warming regions on Earth. *Nature Geosci,* 6, 2, pp. 139-145, doi:10.1038/ngeo1671.

Brunt, K.M., Sergienko, O and MacAyeal, D.R. **2006**. Observations of unusual fast-ice conditions in the southwest Ross Sea, Antarctica: Preliminary analysis of iceberg and storminess effects. *Annals of Glaciology*, 44, pp. 183-187, doi: 10.3189/172756406781811754.

Cavalieri, D.J and Parkinson, C.L. **2012**. Arctic sea ice variability and trends, 1979-2010. *The Cryosphere,* 6, 4, pp. 881-889, doi:10.5194/tc-6-881-2012.

Comiso, J.C., Kwok, R., Martin, S and Gordon, A.L. **2011**. Variability and trends in sea ice extent and ice producution in the Ross Sea. *J. Geophys. Res*, 116, C04021, doi:10.1029/2010JC006391.

Comiso, J. **2010**. *Polar Oceans From Space*, Springer, New York.

Comiso, J.C. **2010**. Large-scale Characteristics and Variability of the Global Sea Ice Cover, in D. Thomas & G.S Dieckmann (eds), *Sea Ice*, 2nd ed, Wiley-Blackwell, Oxford.

Comiso, J., Parkinson, C.L., Gersten, R and Stock, L. **2008**. Accelerated decline in the Arctic sea ice cover. *Geophys. Res. Lett*, 35, L01703, doi:10.1029/2007GL031972.

Comiso, J.C., Cavalieri, D.J and Markus, T. **2003**. Sea ice concentration, ice temperature, and snow depth using AMSR-E data , *Transactions on Geoscience & Remote Sensing*, 41, 2, pp. 243-252.

Comiso, J.C. **2002**. A rapidly declining perennial sea ice cover in the Arctic. *Geophys. Res. Lett*, 29, 29(20), 1956, doi:10.1029/2002GL015650.

Curry, J.A., Schramm, J.L and Ebert, E.E. **1994**. Sea Ice-Albedo Climate Feedback Mechanism. *Journal of Climate,* 8, pp. 240-247.

DeLiberty, T.L., Geiger, C.A., Ackley, S.F., Worby, A.P and Van Woert, M.L. **2011**. Estimating the annual cycle of sea-ice thickness and volume in the Ross Sea. *Deep-Sea Research Part II-Topical Studies in Oceanography*. 58, 9-10, pp. 1250-1260.

Dempsey, D.E., Langhorne, P.J., Robinson, N.J., Williams, M.J.M., Haskell, T.G and Frew, R.D. **2010**. Observation and modeling of platelet ice fabric in McMurdo Sound, Antarctica. *J. Geophys. Res.,* vol. 115, C01007, doi:10.1029/2008JC005264.

Depoorter, M.A., Bamber, J.L., Griggs, J.A., Lenaerts, J.T.M., Ligtenberg, S.R.M., van den Broeke, M.R and Moholdt, G. **2013**. Calving fluxes and basal melt rates of Antarctic ice shelves. *Nature*, 502, 89-92, doi:10.1038/nature12567.

Dewitt, S. **2010**. *NASA's Successful Ice Cloud and Land Elevation Mission Comes to and End*. Accessed January 2011, available at: http://www.nasa.gov/mission_pages/icesat/icesat-end.html

Dieckmann, G.S and **Hellmer**, H.H. **2010**. The Importance of Sea Ice: An Overview, in D. Thomas & G.S Dieckmann (eds), *Sea Ice*, 2nd ed, Wiley-Blackwell, Oxford.

Drinkwater, M.R., Francis, R., Ratier, G and Wingham, D.J. **2004**. The European Space Agency's Earth Explorer Mission CryoSat: measuring variability in the cryosphere. *Annals of Glaciology*, 39, 1, pp. 313-320.

Drucker, R., Martin, S and Kwok, R. **2011**. Sea ice production and export from coastal polynyas in the Weddell and Ross Seas. *Geophys. Res. Lett*, 38, L17502, doi: 10.1029/2011GL048668.

Duffy, P.B, Eby, M and Weaver, A.J. **1999**. Effects of sinking of salt rejected during formation of sea ice on results of an ocean-atmosphere-sea ice climate model. *Geophys. Res. Lett*, 26, 12, pp. 1739-1742, doi:10.1029/1999GL900286.

Egbert, G.D and **Erofeeva**, S.Y. **2002**. Efficient inverse Modeling of barotropic ocean tides. *Journal of Atmospheric and Oceanic Technology*, 19, 2, pp. 183-204.

Eicken, H. **2010**. From the Microscopic, to the Macroscopic, to the Regional Scale: Growth, Microstructure and Properties of Sea Ice, in D. Thomas & G.S Dieckmann (eds), *Sea Ice*, 2nd ed, Wiley-Blackwell, Oxford.

Eisenman, I., Meier, W.N and Norris, J.R. **2014**. A spurious jump in the satellite record: has Antarctic sea ice expansion been overestimated? *The Cryosphere*, 8, 4, pp. 1289-1296, doi:10.5194/tc-8-1289-2014.

ESA. **2014**. *Missions: Sentinel 3*. Accessed August 2014, available at: https://earth.esa.int/web/guest/missions/esa-future-missions/sentinel-3.

ESA. **2002**. *Missions, Envisat, Instruments, ASAR*. Accessed February 2011, available at: https://earth.esa.int/web/guest/missions/esa-operational-eo-missions/envisat.

Farrell, S.L., Laxon, S.W., McAdoo, D.C., Yi, D and Zwally, H.J. **2009**. Five years of Arctic sea ice freeboard measurements from the Ice, Cloud and land Elevation Satellite. *J. Geophys. Res*, 114, C04008, doi:10.1029/2008JC005074.

Fedotov, V.I., Cherepanov, N.V and Tyshko, K.P. **1998**. Some Features of the Growth, Structure and Metamorphism of East Antarctic Landfast Sea Ice, in *Antarctic Sea Ice: Physical Processes, Interactions and Variability*, American Geophysical Union, pp. 343-354.

Forsstrom, S., Gerland, S and Pedersen, C.A. **2011**. Thickness and density of snow-covered sea ice and hydrostatic equilibrium assumption from in situ measurements in Fram Strait, the Barents Sea and the Svalbard coast. *Annals of Glaciology*, 52, 57, pp. 261-270.

Foster, T.D and Carmack, E.C. **1976**. Frontal zone mixing and Antarctic Bottom water formation in the southern Weddell Sea. *Deep Sea Research and Oceanographic Abstracts*, 23, 4, pp. 301-317.

Fowler, C.M.R. **2005**. *The Solid Earth: An introduction to Global Geophysics*, 2nd ed, Cambridge University Press, Cambridge.

Fraser, A.D., Massom, R.A., Michael, K.J., Galton-Fenzi, B.K and Lieser, J.L. **2012**. East Antarctic Landfast Sea Ice Distribution and Variability, 2000-08. *Journal of Climate*, 25, 4, pp. 1137-1156, doi:dx.doi.org/10.1175/JCLI-D-10-05032.1.

Fricker, H.A., Borsa, A., Minster, B., Carabajal, C., Quinn, K and Bills, B. **2005**. Assessment of ICESat performance at the Salar de Uyuni, Bolivia. *Geophys. Res. Lett*, 32, L21S06, doi:10.1029/2005GL023423.

Fu, L-L and Cazenave, A. **2001**. Preface, in L-L Fu and A Cazenave (eds), *Satellite Altimetry and Earth Sciences: A handbook of techniques and applications*, Academic Press, San Diego.

Ganachaud, A and Wunsch, C. **2000**. Improved estimates of global ocean circulation, heat transport and mixing from hydrographic data. *Nature*, 408, 6811, pp. 453-457, doi: 10.1038/35044048.

Giles, A.B., Massom, R.A and Lytle, V.I. **2008a**. Fast-ice distribution in East Antarctica during 1997 and 1999 determined using RADARSAT data. *J. Geophys. Res*, 113,. C02S14, doi: 10.1029/2007JC004139.

Giles, K.A., Laxon, S.W and Worby, A.P. **2008b**. Antarctic sea ice elevation from satellite radar altimetry. *Geophys. Res. Lett.*, 35, 3, L03503, doi:10.1029/2007GL031572.

Gille, S.T. **2008**. Decadal-Scale Temperature Trends in the Southern Hemisphere Ocean, *Journal of Climate*, 21, 18, pp. 4749-4765, doi:dx.doi.org/10.1175/2008JCLI2131.1.

Gordon, A.L., Huber, B.A., Hellmer, H.H and Ffield, A. **1993**. Deep and Bottom Water of the Weddell Sea's Western Rim. *Science,* 262, 5130, pp. 95-97.

Gough, A.J. **2012**. *Sea Ice near an Ice Shelf*. PhD Thesis, University of Otago, Dunedin.

Gough, A.J., Mahoney, A.R., Langhorne, P.J., Williams, M.J.M., Robinson, N.J and Haskell, T.G. **2012.** Signatures of supercooling: McMurdo Sound platelet ice. *Journal of Glaciology*, 58, 207, pp. 38-50, doi:dx.doi.org/10.3189/2012JoG10J218.

Gow, A.J., Ackley, S.F., Govoni, J.W and Weeks, W.F. **1998**. Physical and structural properties of land-fast sea ice in McMurdo Sound, Antarctica. *Antarctic Sea Ice: Physical processes, interactions and variability, Antarctic Research Series, AGU.*, vol. 74, pp. 355-374, doi: 10.1029/AR074p0355.

Grafarend, E.W. 1994. What is the Geoid?, in P. Vanicek and N.T Christou (eds), *Geoid and its Geophysical Interpretations*, CRC Press, USA.

Griggs, J.A and **Bamber**, J.L. **2011**. Antarctic ice-shelf thickness from satellite radar altimetry. *Journal of Glaciology*, 57, 203, pp. 485-498.

Haas, C., Rack, W and Langhorne, P.J. in prep. EM induction assessment of sea ice thickness in McMurdo Sound. in prep.

Haas, C. **2010**. Dynamics versus Thermodynamics: The Sea Ice Thickness Distribution, in D. Thomas & G.S Dieckmann (eds), *Sea Ice*, 2nd ed, Wiley-Blackwell, Oxford.

Haas, C., Hendricks, S., Eicken, H and Herber, A. **2010**. Synoptic airborne thickness surveys reveal state of Arctic sea ice cover. *Geophys. Res. Lett.*, 37, L09501, doi: 10.1029/2010GL042652.

Haas and **Druckenmiller**. **2009**. Ice thickness and Roughness Measurements, in H. Eicken (eds), *Sea-Ice Handbook*, University of Alaska Press.

Haas, C., Lobach, J., Hendricks, S., Rabenstein, L and Pfaffling, A. **2009**. Helicopter-borne measurements of sea ice thickness, using small and lightweight, digital EM system. *Journal of Applied Geophysics*, 67, 3, pp. 234-241.

Hallikainen, M.T., Ulaby, F and Abdelrazik, M. **1986**. Dielectric properties of snow in the 3 to 37 GHz range. *Antennas and Propagation, IEEE Trans.on Geo. and Rem. Sens*, 34, 11, pp. 1329-1340.

Heine, A.J. **1963**. Ice breakout around the Southern end of Ross Island, Antarctica, *New Zealand Journal of Geology and Geophysics*, 6:3, pp. 395-401.

Helm, V., Humbert, A and Miller, H. **2014**. Elevation and elevation change of Greenland and Antarctica derived from CryoSat-2. *The Cryosphere*, 8, 1539-1559, doi: 10.5194/tc-8-1539-2014.

Hellmer, H.H. 2004. Impact of Antarctic ice shelf basal melting on sea ice and deep ocean properties. *Geophys. Res. Lett.*, 31, L10307, doi:10.1029/2004GL019506.

Hendricks, S., Stenseng, L., Helm, V and Haas, C. **2010**. Effects of surface roughness on sea ice freeboard retrieval with an Airborne *Ku*-Band SAR radar altimeter, *Geoscience and Remote Sensing Symposium (IGARSS), 2010 IEEE International*, pp. 3126-3129.

Hofer, R and Mätzler, C. **1980**. Investigations on snow parameters by radiometry in the 3- to 60-mm wavelength region. *J. Geophys. Res*, 85(C1), pp. 453-460, doi: 10.1029/JC085iC01p00453.

Holland, P.R., Bruneau, N., Enright, C., Losch, M., Kurtz, N.T and Kwok, R. **2014**. Modelled trends in Antarctic sea ice thickness. *Journal of Climate*, 27, 3784-3801, doi: dx.doi.org/10.1175/JCLI-D-13-00301.1.

Holland, P.R and Kwok, R. **2012**. Wind-driven trends in Antarctic sea-ice drift. *Nature Geosci,* 5, pp. 872-875, doi:10.1038/ngeo1627.

Hudson, S.R. **2011**. Estimating the global radiative impact of the sea ice–albedo feedback in the Arctic. *J. Geophys. Res*, 116, D16102, doi:10.1029/2011JD015804.

Hughes, K.G., Langhorne, P.J., Leonard, G.H and Stevens, C.L. **Submitted**. Extension of an Ice Shelf Water plume model beneath sea ice with application in McMurdo Sound, Antarctica. *J. Geophys. Res.*

Hutchings, J., Heil, P., Lecomte, O., Stevens, R., Steer, A and Lieser, J.L. **2014**. Comparing methods of measuring sea ice density in the East Antarctic. *Annals of Glaciology*, 56, 69.

Iliffe, J and Lott, R. **2008**. *Datums and Map Projections For Remote Sensing, GIS and Surveying*, 2nd ed, Whittles Publishing, Dunbeath.

Jacobs, S.S., Giulivi, C.F and Mele, P.A. **2002**. Freshening of the Ross Sea During the Late 20th Century. *Science*, 297, 5580, pp. 386-389, doi:10.1126/science.1069574.

Jacobs, S.S., Amos, A.F and Bruchhausen, P.M. **1970**. Ross sea oceanography and antarctic bottom water formation. *Deep Sea Research and Oceanographic Abstracts*, 17, 6, pp. 935-962.

Jeffries, M.O., Weeks, W.F., Shaw, R and Morris, K. **1993**. Structural Characteristics of Congelation and Platelet Ice and Their Role in the Development of Antarctic Land-Fast Sea-Ice. *Journal of Glaciology,* 39, 132, pp. 223-238.

Jensen, J.R. **2000**. *Remote Sensing of the Environment: An Earth Resource Perspective*, Prentice-Hall Inc, USA.

Jensen, J.R. **1999**. Radar altimeter gate tracking: theory and extension. *IEEE Trans.on Geo. and Rem. Sens,* 37, 2, pp. 651-658, doi:10.1109/36.752182.

Johnson, G.C. **2008**. Quantifying Antarctic Bottom Water and North Atlantic Deep Water volumes. *J. Geophys. Res,*113, C05027, doi:10.1029/2007JC004477.

Joughin, I., Smith, B.E and Medley, B. **2014**. Marine Ice Sheet Collapse Potentially Under Way for the Thwaites Glacier Basin, West Antarctica. *Science,* 344, 6185, pp. 735-738, doi: 10.1126/science.1249055.

Joughin, I., Alley, R.B and Holland, D.M. **2012**. Ice-Sheet Response to Oceanic Forcing. *Science,* 338, 6111, pp. 1172-1176, doi:10.1126/science.1226481.

Kern, S and Spreen, G. **2015**. Uncertainties in Antarctic sea-ice thickness retrieval from ICESat. *Annals of Glaciology,* 56(59), pp. 107-119, doi:10.3189/2015AoG69A736.

Kohout, A.L., Williams, M.J.M., Dean, S.M and Meylan, M.H. **2014**. Storm-induced sea-ice breakup and the implications for ice extent. *Nature,* 509, 7502, pp. 604-607, doi: 10.1038/nature13262.

Kruetzmann, N.C., Rack, R., McDonald, A.J and George, S.E. **2011**. Snow accumulation and compaction derived from GPR data near Ross Island, Antarctica. *The Cryosphere,* 5, pp. 391-404, doi:10.5194/tc-5-391-2011.

Kurtz, N.T., Galin, N and Studinger, M. **2014**. An improved CryoSat-2 sea ice freeboard retrieval algorithm through the use of waveform fitting. *The Cryosphere,* 8, 4, pp. 1217-1237, doi:10.5194/tc-8-1217-2014.

Kurtz, N.T and Markus, T. **2012**. Satellite observations of Antarctic sea ice thickness and volume. *J. Geophys. Res*, 117, C08025, doi:10.1029/2012JC008141.

Kurtz, N.T., Markus, T., Cavalieri, D.J., Sparling, L.C., Krabill, W.B., Gasiewski, A.J and Sonntag, J.G. **2009**. Estimation of sea ice thickness distributions through the combination of snow depth and satellite laser altimetry data. *J. Geophys. Res*, 114, C10007, doi:10.1029/2009JC005292.

Kwok, R. **2014**. Simulated effects of a snow layer on retrieval of CryoSat-2 sea ice freeboard. *Geophys. Res. Lett*, 41, 5014–5020, doi:10.1002/2014GL060993.

Kwok, R., Cunningham, G.F., Wensnahan, M., Rigor, I., Zwally, H.J and Yi, D. **2009**. Thinning and volume loss of the Arctic Ocean sea ice cover: 2003-2008. *J. Geophys. Res*, 114, C07005, doi:10.1029/2009JC005312.

Kwok, R and **Rothrock**, D.A. **2009**. Decline in Arctic sea ice thickness from submarine and ICESat records: 1958-2008. *Geophys. Res. Lett*, 36, L15501, doi:10.1029/2009GL039035.

Kwok, R and **Cunningham**, G.F. **2008**. ICESat over Arctic sea ice: Estimation of snow depth and ice thickness, *J. Geophys. Res.*, 113, C08010, doi:10.1029/2008JC004753.

Kwok, R., Cunningham, G.F., Zwally, H.J and Yi, D. **2007**. Ice, Cloud, and land Elevation Satellite (ICESat) over Arctic sea ice: Retrieval of freeboard. *J. Geophys. Res*, 112, C12013, doi: 10.1029/2006JC003978.

Kwok, R, Cunningham, G.F., Zwally, H.J & Yi, D. **2006**. ICESat over Arctic sea ice: Interpretation of altimetric and reflectivity profiles. *J. Geophys. Res*, 111, C06006, doi:10.1029/2005JC003175.

Kwok, R., Zwally, H.J and Yi, D. **2004**. ICESat observations of Arctic sea ice: A first look. *Geophys. Res. Lett*, 31, L16401, doi:10.1029/2004GL020309.

Labroue, S., Boy, F., Picot, N., Urvoy, M and Ablain, M. **2012**. First quality assessment of the Cryosat-2 altimetric system over ocean. *Advances in Space Research*, 50, 8, 10.1016/j.asr.2011.11.018.

Lake, R.A and Lewis, E.L. **1970**. Salt rejection by sea ice during growth. *J. Geophys. Res*, 75, 3, *583–597*, doi:10.1029/JC075i003p00583.

Langhorne, P.J., Hughes, K.G., Gough, A. J., Smith, I. J., Leonard, G.H., Williams, M.J.M., Robinson, N.J., Stevens, C.L., Rack, W., Price, D., Mahoney, A.R., Haas, C and Haskell, T.G. *Geophys. Res. Lett.* **Submitted**.

Langhorne, P.J., Purdie, C.R., Smith, I.J., Leonard, G.H., Kempema, E.W., Petrich, C, Gribble, M.A., Bond, P.E and Haskell, T.G. **2006**. Antarctic Landfast Sea Ice: The Role of Platelet Ice, in *IAHR International Symposium on Ice*, ed. H Saeki. Nakanishi Publishing Co. Ltd, Sapporo, Japan.

Laxon, S.W., Giles, K.A., Ridout, A.L., Wingham, D.J., Willatt, R., Cullen, R., Kwok, R., Schweiger, A., Zhang, J., Haas, C., Hendricks, S., Krishfield, R., Kurtz, N., Farrell, S and

Davidson, M. **2013**. CryoSat-2 estimates of Arctic sea ice thickness and volume, *Geophys. Res. Lett*, 40, 732–737, doi:10.1002/grl.50193.

Laxon, S., Peacock, N and Smith, D. **2003**. High interannual variability of sea ice thickness in the Arctic region. *Nature*, 425, 6961, doi:10.1038/nature02050.

Leonard, G.H., Langhorne, P.J., Williams, M.J.M., Vennell, R., Purdie, C.R., Dempsey, D.E., Haskell, T.G and Frew, R.D. **2011**. Evolution of supercooling under coastal Antarctic sea ice during winter. *Antarctic Science*, 23, 4, pp. 399-409, doi: dx.doi.org/10.1017/S0954102011000265.

Leonard, G.H., Purdie, C.R., Langhorne, P.J., Haskell, T.G., Williams, M.J.M and Frew, R.D. **2006**. Observations of platelet ice growth and oceanographic conditions during the winter of 2003 in McMurdo Sound, Antarctica. *J. Geophys.* Res, 111, C04012, doi:10.1029/2005JC002952.

Lowrie, W. **2007**. *Fundamentals of Geophysics*, 2nd ed, Cambridge University Press, Cambridge.

Lubin, D and **Massom**, R. **2006**. *Polar Remote Sensing*, vol. 1, Atmosphere and Oceans, Springer Praxis Books, Chichester, UK, pp. 309-723.

MacAyeal, D.R., Okal, M.H., Thom, E.T., Brunt, K.M., Kim, Y and Bliss, A.K. **2008**. Tabular iceberg collisions within the coastal regime. *Journal of Glaciology*, 54, 185, pp. 371-385.

Mahoney, A.R., Gough, A.J., Langhorne, P.J., Robinson, N.J., Stevens, C.L., Williams, M.J.M and Haskell, T.G. **2011**. The seasonal appearance of ice shelf water in coastal Antarctica and its effect on sea ice growth. *J. Geophys. Res.*, 116, C11032, doi: 10.1029/2011JC007060.

Maksym, T., Stammerjohn, S.E., Ackley, S.F and Massom, R. **2012**. Antarctic sea ice - a polar opposite. *Oceanography*, 25, 3, pp. 140-151, doi:dx.doi.org/10.5670/oceanog.2012.88.

Markus, T., Massom, R., Worby, A., Lytle, V., Kurtz, N.T and Maksym, T. **2011**. Freeboard, snow depth and sea-ice roughness in East Antarctica from in situ and multiple satellite data. *Annals of Glaciology*, 52, 57, pp. 242-248.

Markus, T and **Cavalieri**, D.J. **1998**. Snow depth distribution over sea ice in the Southern Ocean from satellite passive microwave data in *Antarctic Sea Ice: Physical Processes, Interactions and Variability*, 74, AGU, Washington, DC, pp. 19-39.

Martin, S., Drucker, R.S and Kwok, R. **2007**. The areas and ice production of the western and central Ross Sea polynyas, 1992-2002, and their relation to the B-15 and C-19 iceberg events of 2000 and 2002. *Journal of Marine Systems,* 68, 1-2, pp. 201-214.

Martinson, D.G. **1990**. Evolution of the southern ocean winter mixed layer and sea ice: Open ocean deepwater formation and ventilation. *J. Geophys. Res,* 95(C7), 11641-11654, doi:10.1029/JC095iC07p11641.

Massom, R.A., Giles, A.B., Fricker, H.A., Warner, R.C., Legrésy, B., Hyland, G., Young, N and Fraser, A.D. **2010**. Examining the interaction between multi-year landfast sea ice and the Mertz Glacier Tongue, East Antarctica: Another factor in ice sheet stability? *J. Geophys. Res,* 115, C12027, doi:10.1029/2009JC006083.

Massom, R.A., Eicken, H., Hass, C., Jeffries, M.O., Drinkwater, M.R., Sturm, M., Worby, A.P., Wu, X., Lytle, V.I., Ushio, S., Morris, K., Reid, P.A., Warren, S.G and Allison, I. **2001**. Snow on Antarctic sea ice. *Rev. Geophys.,* 39, 3, pp. 413-445.

Massom, R., Harris, P., Michael, K.J and Potter, M. **1998**. The distribution and formative processes of latent-heat polynyas in East Antarctica. *Annals of Glaciology,* 27, pp. 420-426.

Massonnet, F., Mathiot, P., Fichefet, T., Goosse, H., Konig Beatty, C., Vancoppenolle, M and Lavergne, T. **2013**. A model reconstruction of the Antarctic sea ice thickness and volume changes over 1980-2008 using data assimilation. *Ocean Modelling,* 64, doi: 10.1016/j.ocemod.2013.01.003.

Mathiot, P., Jourdain, N., Barnier, B., Gallée, H., Molines, J., Le Sommer, J and Penduff, T. **2012**. Sensitivity of coastal polynyas and high-salinity shelf water production in the Ross Sea, Antarctica, to the atmospheric forcing. *Ocean Dynamics,* 62, 5, pp. 701-723, doi: 10.1007/s10236-012-0531-y.

Mätzler, C. **1987**. Applications of the interaction of microwaves with the natural snow cover. *Remote Sensing Reviews,* 2, 2, pp. 259-387.

McGill, M., Markus, T., Scott, V.S and Neumann, T. **2013**. The Multiple Altimeter Beam ExperimentalLidar (MABEL): An Airborne Simulator for the ICESat-2 Mission. *Journal of Atmospheric and Oceanic Technology,* 30, 2, pp. 345-352

NASA. **2014**. *ICESat-2: Mission Overview*. Accessed August 2014, available at: http://icesat.gsfc.nasa.gov/icesat2/mission_overview.php

NGA. **2014**. *Earth Gravitational Model 2008*. Retrieved 08/08/2013, from http://earth-info.nga.mil/GandG/wgs84/gravitymod/egm2008/

Ohshima, K.I., Fukamachi, Y., Williams, G.D., Nihashi, S., Roquet, F., Kitade, Y., Tamura, T., Hirano, D., Herraiz-Borreguero, L., Field, I., Hindell, M., Aoki, S and Wakatsuchi, M. **2013**. Antarctic Bottom Water production by intense sea-ice formation in the Cape Darnley polynya. *Nature Geosci,* 6, 3, pp. 235-240, doi:10.1038/ngeo1738.

Ozsoy-Cicek, B., Ackley, S., Xie, H., Yi, D and Zwally, J. **2013**. Sea ice thickness retrieval algorithms based on in situ surface elevation and thickness values for application to altimetry. *J. Geophys. Res,* 118, 8, pp. 3807-3822, doi:10.1002/jgrc.20252.

Padman, L., King, M., Goring, D., Corr, H and Coleman, R. **2003**. Ice-shelf elevation changes due to atmospheric pressure variations. *Journal of Glaciology,* 49, 167, pp. 521-526.

Parkinson, C.L and **Cavalieri**, D.J. **2012**. Antarctic sea ice variability and trends, 1979-2010, *The Cryosphere,* 6, pp. 871-880, doi:10.5194/tc-6-871-2012.

Parmentier, F-J.W., Christensen, T.R., Sorensen, L.L., Rysgaard, S., McGuire, A.D., Miller, P.A and Walker, D.A. **2013**. The impact of lower sea-ice extent on Arctic greenhouse-gas exchange. *Nature Clim. Change,* 3, 3, pp. 195-202, doi: 10.1038/nclimate1784.

Pavlis, N.K., Holmes, S.A., Kenyon, S.C and Factor, J.K. **2012**. The development and evaluation of the Earth Gravitational Model 2008 (EGM2008). *J. Geophys. Res*, 117, B04406, doi:10.1029/2011JB008916.

Peacock, N.R and **Laxon**, S. **2004**. Sea surface height determination in the Arctic Ocean from ERS altimetry. *J. Geophys. Res.,* 109, C07001, doi:10.1029/2001JC001026.

Perovich, D.K., Roesler, C.S and Pegau, W.S. **1998**. Variability in Arctic sea ice optical properties. *J. Geophys. Res*, 103(C1), pp. 1193-1208, doi:10.1029/97JC01614.

Polvani, L.M., Waugh, D.W., Correa, G.J.P and Son, S-W. **2010**. Stratospheric Ozone Depletion: The Main Driver of Twentieth-Century Atmospheric Circulation Changes in the Southern Hemisphere. *Journal of Climate*, 24, 3, pp. 795-812, doi: dx.doi.org/10.1175/2010JCLI3772.1.

Price, D., Rack, W., Langhorne, P.J., Haas, C., Leonard, G and Barnsdale, K. **2014**. The sub-ice platelet layer and its influence on freeboard to thickness conversion of Antarctic sea ice. *The Cryosphere*, 8, 3, 1031-1039, doi:10.5194/tc-8-1031-2014.

Price, D., Rack, W., Haas, C., Langhorne, P.J and Marsh, O. **2013**. Sea ice freeboard in McMurdo Sound, Antarctica, derived by surface-validated ICESat laser altimeter data, *J. Geophys. Res*, 118, 3634–3650, doi:10.1002/jgrc.20266.

Purdie, C.R., Langhorne, P.J., Leonard, G.H and Haskell, T.G. **2006**. Growth of first-year landfast Antarctic sea ice determined from winter temperature measurements. *Annals of Glaciology,* 44, pp. 170-176, doi:dx.doi.org/10.3189/172756406781811853.

Rack, W., Haas, C and Langhorne, P.J. **2013**. Airborne thickness and freeboard measurements over the McMurdo Ice Shelf, Antarctica, and implications for ice density. *J. Geophys. Res,* 118, 11, pp. 5899-5907, doi:10.1002/2013JC009084.

Rahmstorf, S. **2006**. Thermohaline Ocean Circulation , in S.A Elias (ed.), *Encyclopedia of Quaternary Sciences*, Elsevier, Amsterdam.

Remy, J.P., Becquevort, S., Haskell, T.G and Tison, J.L. **2008**. Impact of the B-15 iceberg "stranding event" on the physical and biological properties of sea ice in McMurdo Sound, Ross Sea, Antarctica. *Antarctic Science,* 20, 6, pp. 593-604, doi: 10.1017/S0954102008001284.

Ricker, R., Hendricks, S., Helm, V., Skourup, H and Davidson, M. **2014**. Sensitivity of CryoSat-2 Arctic sea-ice freeboard and thickness on radar-waveform interpretation. *The Cryosphere Discuss.*, 8, 1607-1622, doi:10.5194/tc-8-1607-2014.

Rignot, E., Mouginot, J., Morlighem, M., Seroussi, H and Scheuchl, B. **2014**. Widespread, rapid grounding line retreat of Pine Island, Thwaites, Smith, and Kohler glaciers, West Antarctica, from 1992 to 2011. *Geophys. Res. Lett,* 41, 10, pp. 3502-3509, doi: 10.1002/2014GL060140.

Rignot, E., Jacobs, S., Mouginot, J and Scheuchl, B. **2013**. Ice-Shelf Melting Around Antarctica. *Science,* 341, 6143, pp. 266-270, doi:10.1126/science.1235798.

Rintoul, S.R. **1985**. On the Origin and Influence of Adélie Land Bottom Water, in Ocean, Ice, and Atmosphere: Interactions at the Antarctic Continental Margin (eds S. S. Jacobs and R. F. Weiss). *American Geophysical Union*, Washington, D. C, doi: 10.1029/AR075p0151.

Robinson, N.J., Williams, M.J.M., Stevens, C.L., Langhorne, P.J and Haskell, T.G. **2014**. Evolution of a supercooled Ice Shelf Water plume with an actively growing subice platelet matrix. *J. Geophys. Res*, 119, 3425–3446, doi:10.1002/2013JC009399.

Robinson, N.J and **Williams**, M.J.M. **2012**. Iceberg-induced changes to polynya operation and regional oceanography in the southern Ross Sea, Antarctica, from in situ observations. *Antarctic Science*, 24, 5, pp. 514-526, doi:dx.doi.org/10.1017/S0954102012000296.

Robinson, N.J., Williams, M.J.M., Barrett, P.J and Pyne, A.R. **2010**. Observations of flow and ice-ocean interaction beneath the McMurdo Ice Shelf, Antarctica. *J. Geophys. Res*, 115, C03025, doi:10.1029/2008JC005255.

Robinson, N.J. **2004**. *An oceanographic study of the cavity beneath the McMurdo Ice Shelf, Antarctica*. PhD Thesis. Victoria University of Wellington, Wellington.

Rothrock, D.A., Yu, Y and Maykut, G.A. **1999**. Thinning of the Arctic sea-ice cover. *Geophys. Res. Lett*, 26, 23, pp. 3469-3472, doi:10.1029/1999GL010863.

Rutgers van der Loeff, M.M., Cassar, N., Nicolaus, M., Rabe, B and Stimac, I. **2014**. The influence of sea ice cover on air-sea gas exchange estimated with radon-222 profiles, *J. Geophys. Res*, 119, 5, pp. 2735-2751, doi:10.1002/2013JC009321.

Scagliola, M. **2013**. *CryoSat footprints - Aresys Technical Note*. Accessed August 2014, available at: https://wiki.services.eoportal.org/tiki-download_wiki_attachment.php?attId=2592.

Schmidtko, S and **Johnson**, G.C. **2011**. Multidecadal Warming and Shoaling of Antarctic Intermediate Water. *Journal of Climate*, 25, 1, pp. 207-221, doi: dx.doi.org/10.1175/JCLI-D-11-00021.1.

Schutz, B.E., Zwally, H.J., Shuman, C.A., Hancock, D and DiMarzio, J.P. **2005**. Overview of the ICESat Mission. *Geophys. Res. Lett*, 32, L21S01, doi:10.1029/2005GL024009.

Shepherd, A., Wingham, D and Rignot, E. **2004**. Warm ocean is eroding West Antarctic Ice Sheet, *Geophys. Res. Lett*, 31, L23402, doi:10.1029/2004GL021106.

Siedler, G., Griffies, S.M., Gould, J and Church, J. **2013**. *Ocean Circulation and Climate: A 21st Century Perspective*, Academic Press, Oxford.

Sinclair, K.E., Bertler, N.A.N and Van Ommen, T.D. **2012**. Twentieth-Century Surface Temperature Trends in the Western Ross Sea, Antarctica:: Evidence from a High-Resolution Ice Core, *Journal of Climate*, 25, 10, pp. 3629-3636, doi: dx.doi.org/10.1175/JCLI-D-11-00496.1.

Smith, I.J., Langhorne, P.J., Frew, R.D., Vennell, R and Haskell, T.G. **2012**. Sea ice growth rates near ice shelves. *Cold Regions Science and Technology*, 83-84, 57-70, doi: 10.1016/j.coldregions.2012.06.005.

Soltanzedeh, I., Rack., W., Price, D., and Peyman Z-R. **in prep**. The spatial and temporal variability of snow accumulation and distribution in McMurdo Sound, Antarctica.

Spreen, G., Kern, S., Stammer, D., Forsberg, R and Haarpaintner, J. **2006**. Satellite-based estimates of sea-ice volume flux through Fram Strait. *Annals of Glaciology*, 44, pp. 321-328.

Stammerjohn, S.E., Martinson, D.G., Smith, R.C., Yuan, X and Rind, D. **2008**. Trends in Antarctic annual sea ice retreat and advance and their relation to El Nino-Southern Oscillation and Southern Annular Mode variability. *J. Geophys. Res*, 113, C03S90, doi:10.1029/2007JC004269.

Steig, E.J., Schneider, D.P., Rutherford, S.D., Mann, M.E., Comiso, J.C and Shindell, D.T. **2009**. Warming of the Antarctic ice-sheet surface since the 1957 International Geophysical Year. *Nature*, 457, 7228, pp. 459-462, doi:10.1038/nature07669.

Stephens, B.B and **Keeling**, R.F. **2000**. The influence of Antarctic sea ice on glacial-interglacial CO 2 variations. *Nature,* 404, 6774, pp. 171-174, doi:10.1038/35004556.

Stevens, C.L., Robinson, N.J., Williams, M.J.M and Haskell, T.G. **2009**. Observations of turbulence beneath sea ice in southern McMurdo Sound, Antarctica. *Ocean Sci.*, 5, 4, pp. 435-445.

Stiles, W.H and Ulaby, F.T. **1982**. Dielectric properties of snow. *Proc. of Workshop on Properties of Snow, Snowbird, Utah, April 1981. CRREL Special Rep. 82-18, Utah, 91-103*

Stroeve, J., Holland, M.M., Meier, W., Scambos, T and Serreze, M. **2007**. Arctic sea ice decline: Faster than forecast. *Geophys. Res. Lett.*, 34, L09501, doi:10.1029/2007GL029703.

Sturm, M., Morris, K and Massom, R. **1998**. The winter snow cover of the West Antarctic pack ice: its spatial and temporal variability, in M.O Jeffries (ed), *Antarctic Sea Ice Physical Processess, In teractions and Variability*, American Geophysical Union, Washington DC., pp. 1-18.

Swart, N.C and Fyfe, J.C. **2013**. The influence of recent Antarctic ice sheet retreat on simulated sea ice area trends. *Geophys. Res. Lett*, 40, 4328–4332, doi:10.1002/grl.50820.

Timco, G.W and **Frederking**, R.M.W. **1996**. A review of sea ice density. *Cold Reg. Sci.* Technol, 24, 1–6.

Tamura, T., Ohshima, K.I and Nihashi, S. **2008**. Mapping of sea ice production for Antarctic coastal polynyas. *Geophys. Res. Lett*, *35*, L07606, doi:10.1029/2007GL032903.

Thomas, D. **2004**. *Frozen Oceans: The floating world of pack ice*. Natural History Museum, London.

Trodahl, H.J., McGuinness, M.J., Langhorne, P.J., Collins, K., Pantoja, A.E., Smith, I.J and Haskell, T.G. **2000**. Heat transport in McMurdo Sound first-year fast ice. *J. Geophys. Res*, 105(*C5*), 11347–11358, doi:10.1029/1999JC000003.

Turner, J., Barrand, N.E., Bracegirdle, T.J., Convey, P., Hodgson, D.A., Jarvis, M., Jenkins, A., Marshall, G., Meredith, M.P., Roscoe, H., Shanklin, J., French, J., Goosse, H., Guglielmin, M., Gutt, J., Jacobs, S., Kennicutt, M.C.I., Masson-Delmotte, V., Mayewski, P., Navarro, F., Robinson, S., Scambos, T., Sparrow, M., Summerhayes, C., Speer, K and Klepikov, A. **2014**. Antarctic climate change and the environment: an update. *Polar Record,* 50, 03, pp. 237-259, doi:dx.doi.org/10.1017/S0032247413000296.

Turner, J., Colwell, S.R., Marshall, G.J., Lachlan-Cope, T.A., Carleton, A.M., Jones, P.D., Lagun, V., Reid, P.A and Iagovkina, S. **2005**. Antarctic climate change during the last 50 years. *International Journal of Climatology*, 25, 3, pp. 279-294.

Ulaby, F., Moore, R.K amd Fung, A.K. **1986**. *Microwave Remote Sensing: Active and Passive*, Addison-Wesley, Reading, Mass.

Uren, J and **Price**, W. **2010**. *Surveying for Engineers*, 5th ed, Palgrave Macmillan.

Uto, S., Shimoda, H and Ushio, S. **2006**. Characteristics of sea ice thickness and snow depth distributions of the summer landfast ice in Lützow-holm Bay, East Antarctica, *Annals of Glacioliology*, 44, 281–287, doi:10.3189/172756406781811240.

Vaughan, D., Marshall, G., Connolley, W., Parkinson, C., Mulvaney, R., Hodgson, D., King, J., Pudsey, C and Turner, J. **2003**. Recent Rapid Regional Climate Warming on the Antarctic Peninsula. *Climatic Change,* 60, 3, pp. 243-274.

Vaughan, D.G., Comiso, J.C., Allison, I., Carrasco, J., Kaser, G., Kwok, R., Mote, P., Murray, T., Paul, F., Ren, J., Rignot, E., Solomina, O., Steffen, K and Zhang, T. **2013**. *Observation: Cryosphere*, Intergovernmental Panel on Climate Change, Cambridge, United Kingdom and New York, NY, USA.

Vinnikov, K.Y., Robock, A., Stouffer, R.J., Walsh, J.E., Parkinson, C.L., Cavalieri, D.J., Mitchell, J.F.B., Garrett, D and Zakharov, V.F. **1999**. Global Warming and Northern Hemisphere Sea Ice Extent, *Science*, 286, 5446, pp. 1934-1937.

Wang, C.X and **Wang**, K.G. **2012**. Impact of increasing Antarctic ice-shelf melting on Southern Ocean hydrography. *Journal of Glaciology*, 58, 212, pp. 1191-1200.

Weissling, B.P and **Ackley**, S.F. **2011**. Antarctic sea-ice altimetry : scale and resolution effects on derived ice thickness distribution. *Annals of Glaciology*, 52, 57, pp. 225-232.

Whitworth, T and **Orsi**, A.H. **2006**. Antarctic Bottom Water production and export by tides in the Ross Sea. *Geophys. Res. Lett.* 33, L12609, doi:10.1029/2006GL026357.

Willatt, R.C., Laxon, S., Giles, K., Cullen, R., Haas, C and Helm, V. **2011**. *Ku*-band radar penetration into snow covered Arctic sea ice using airborne data. *Annals of Glaciology*, 52, pp. 197-205.

Willatt, R.C., Giles, K.A., Laxon, S.W., Stone-Drake, L and Worby, A.P. **2010**. Field Investigations of *Ku*-Band Radar Penetration Into Snow Cover on Antarctic Sea Ice. *IEEE Trans.on Geo. and Rem. Sens.* 48, 1, pp. 365-372, doi:10.1109/TGRS.2009.2028237.

Williams, G.D., Aoki, S., Jacobs, S.S., Rintoul, S.R., Tamura, T and Bindoff, N.L. **2010**. Antarctic Bottom Water from the Adélie and George V Land coast, East Antarctica (140–149°E). *J. Geophys. Res*, 115, C04027, doi:10.1029/2009JC005812.

Wingham, D.J., Francis, C.R., Baker, S., Bouzinac, C., Brockley, D., Cullen, R., de Chateau-Thierry, P., Laxon, S.W., Mallow, U., Mavrocordatos, C., Phalippou, L., Ratier, G., Rey, L., Rostan, F., Viau, P and Wallis, D.W. **2006**. CryoSat: A mission to determine the fluctuations in Earth's land and marine ice fields. *Advances in Space Research*, 37, 4, pp. 841-871, doi:10.1016/j.asr.2005.07.027.

Wingham, D.J., Phalippou, L., Mavrocordatos, C and Wallis, D. **2004**. The mean echo and echo cross product from a beamforming interferometric altimeter and their application to elevation measurement. *IEEE Trans.on Geo. and Rem. Sens*, 42, 10, pp. 2305-2323, doi: 10.1109/TGRS.2004.834352.

Worby, A., Steer, A., Lieser, J.L., Heil, P., Yi, D., Markus, T., Allison, I., Massom, R., Galin, N and Zwally, H.J. **2011**. Regional-scale sea-ice and snow thickness distributions from in situ and satellite measurements over East Antartica during SIPEX 2007. *Deep-Sea Research II*, 58, pp. 1125-1136, doi:10.1016/j.dsr2.2010.12.001.

Worby, A.P., Geiger, C.A., Paget, M.J., Van Woert, M.L., Ackley, S.F and DeLiberty, T.L. **2008**. Thickness distribution of Antarctic sea ice. *J. Geophys. Res*, 113, C05S92, doi:10.1029/2007JC004254.

Xie, H., Tekeli, A.E., Ackley, S.F., Yi, D and Zwally, H.J. **2013**. Sea ice thickness estimations from ICESat Altimetry over the Bellingshausen and Amundsen Seas, 2003–2009. *J. Geophys. Res*, 118, 2438–2453, doi:10.1002/jgrc.20179.

Xie, H., Ackley, S.F., Yi, D., Zwally, H.J., Wagner, P., Weissling, B., Lewis, M and Ye, K. **2011**. Sea-ice thickness distribution of the Bellingshausen Sea from surface measurements and ICESat altimetry. *Deep-Sea Research II*, 58, pp. 1039-1051, doi: 10.1016/j.dsr2.2010.10.038.

Yi, D., Zwally, H.J and Robbins, J.W. **2011**. ICESat observations of seasonal and interannual variations of sea-ice freeboard and estimated thickness in the Weddell Sea, Antarctica (2003-2009). *Annals of Glaciology*, 52, 57, pp. 43-51.

Zhang, J. **2013**. Modeling the Impact of Wind Intensification on Antarctic Sea Ice Volume. *Journal of Climate*, 27, 1, pp. 202-214, doi: dx.doi.org/10.1175/JCLI-D-12-00139.1.

Zwally, H.J., Yi, D., Kwok, R and Zhao, Y. **2008**. ICESat measurements of sea ice freeboard and estimates of sea ice thickness in the Weddell Sea. *J. Geophys. Res*, 113, C02S15, doi:10.1029/2007jc004284.

Zwally, H.J., Comiso, J.C., Parkinson, C.L., Cavalieri, D.J and Gloersen, P. **2002a**. Variability of Antarctic sea ice 1979-1998. *J. Geophys. Res*, 107(*C*5), doi:10.1029/2000JC000733.

Zwally, H.J., Schutz, B., Abdalati, W., Abshire, J., Bentley, C., Brenner, A., Bufton, J., Dezio, J., Hancock, D., Harding, D., Herring, T., Minster, B., Quinn, K., Palm, S., Spinhirne, J and Thomas, R. **2002b**. ICESat's laser measurements of polar ice, atmosphere, ocean, and land. *Journal of Geodynamics*, 34, 3-4, pp. 405-445, doi: 10.1016/s0264-3707(02)00042-x.

Zwally, H.J., Parkinson, C.L and Comiso, J.C. **1983**. Variability of Antarctic Sea Ice: and Changes in Carbon Dioxide. *Science*, 220, 4601, pp. 1005-1012, doi: 10.1126/science.220.4601.1005.